Hard exclusive QCD processes

Dissertation

zur Erlangung des
Doktorgrades der Naturwissenschaften
(Dr. rer. nat.)
der naturwissenschaftlichen Fakultät II - Physik
der Universität Regensburg

vorgelegt von
Wolfgang Kugler aus Regensburg

Regensburg, Januar 2007

Promotionsgesuch eingereicht am: 22.01.2007

Die Arbeit wurde angeleitet von: Prof. Dr. A. Schäfer

Prüfungsausschuss: Prof. Dr. C. Back

Prof. Dr. A. Schäfer

Dr. M. Diehl

Prof. Dr. M. Grifoni

Contents

1

Introduction

Revealing the structure of matter is one of the most fundamental questions in physics which still has no satisfactory answer. Long time ago people started to think about the structure of matter and one the very first concepts of the microscopic structure occurred in ancient Greek philosophy, when Demokrit proposed the idea that everything consists of small objects, the atoms.

Our knowledge of the structure of matter has improved since then. It was not before the end of the 19th century that science had developed a picture of atomic physics. But only the development of quantum mechanics at the beginning of the 20th century made a thorough understanding of this picture possible. Further on it was observed that atoms themselves have an internal structure due to the scattering experiments of Rutherford at the beginning of the last century. He observed that atoms are composed by a massive atomic nucleus with positive electric charge surrounded by a much larger cloud of electrons with negative charge. The force acting between the nucleus and the electrons is the electromagnetic force, which can be described by the theory of Quantum Electrodynamics (QED). We also know that the nucleus is built up of positively charged protons and neutrally charged neutrons. They were seen for quite some time as point-like particles. A first hint that the nucleons are not point-like came from the experimental measurements of the magnetic moment of the proton in the 1940's [1]. The experimental results were found to be much larger than expected for a point-like particle. Further measurements of the nucleon form factors F_1 and F_2 in the 1960's substantiated the assumption that nucleons have an internal structure. The point-like constituents of the nucleon are found to be fermions of spin 1/2 and were identified with quarks, proposed by Gell-Mann and Zweig [2, 3]. The interaction between quarks is the

strong force and is mediated by gluons.

The underlying theory of strong interactions is called Quantum Chromodynamics (QCD). It describes the interaction of "colored" quarks via the exchange of "colored" gluons. In contrast to QED, QCD is a non-Abelian quantum field theory which allows the self-interaction of the gauge bosons (gluons) due to the fact that gluons carry a color charge. In QED the gauge bosons (photons) are electrically neutral and therefore cannot couple to each other. In nature it is not possible to observe colored quarks and gluons as free particles, but only in color-neutral combinations (e.g. hadrons). The formation of such highly non-trivial bound states is due to one of the central features of QCD: confinement. The theoretical description of hadronic system is a very difficult task. It becomes feasible through another central property of QCD: asymptotic freedom [4, 5]. The strength of the strong interaction is dependent on the momentum transfer of the reaction. In contrast to QED, where the coupling of two interacting particles becomes larger for decreasing distance, the strong coupling constant α_s decreases for smaller distances. Because the decrease of α_s at high energies, QCD becomes amenable for perturbative methods.

The first scattering experiments at high energies were performed at the Stanford Linear Collider (SLAC) in the 1960's where the internal structure of the nucleon was probed in inclusive deep-inelastic scattering (DIS). In these experiments a electron is scattered on a nucleon, $e + N \to e' + X$, and only the rescattered electron is detected. The results for the DIS cross section showed an unexpected weak dependence on the photon virtuality Q^2. It was possible to extract structure functions from the measured cross section, which encode information about the internal structure of nucleon. One of the main observations was the fact that these structure functions are only dependent on a single variable, the Bjorken scaling variable x_B, instead of two (x_B and Q^2) allowed by kinematics. This observation is called Bjorken scaling. A explanation for Bjorken scaling is provided by the asymptotic freedom of QCD: at large energies Q^2 the strong coupling constant α_s is small and the incoming lepton scatters almost incoherently on the constituents of the nucleon. Therefore the structure functions can be expressed in terms of quark and gluon parton distribution functions (PDFs), $q(x, \mu^2)$ and $g(x, \mu^2)$, where x denotes the momentum fraction carried by the different partons. The dependence of the PDFs on the scale μ^2 is based on the violation of Bjorken scaling and is only logarithmic. It represents the physical scale at which the partons are resolved.

A very important step in the description of high energy inelastic scattering processes with the help of perturbative methods was the formulation of factorization theorems [6–11]. They state that in certain kinematical regions the process can be described as a combination of universal "soft" functions, PDFs, which parameterize the distribution of quarks and gluons inside the nucleon, and "hard" partonic functions. The hard functions are process dependent and describe the interaction of quasi-free quarks and gluons emerging from the nucleons. These hard functions can be calculated as a series in α_s within the framework of perturbative QCD. The PDFs on the other hand cannot be calculated with perturbative methods and have to be extracted from experiments or nowadays from lattice calculations. At present,

the PDFs of the unpolarized nucleon are well established [12, 13] and the confirmation of their universality has given some evidence of the validity of the factorization theorems.

One of the most fundamental properties of elementary particles which is essential for the complete understanding of the internal structure and the dynamics of interaction of hadrons is their spin. Information about the spin structure can be obtained in DIS processes with polarized lepton beams scattering on a polarized target or in polarized proton proton collisions. It is possible to extract the polarized structure functions g_1 and g_2 from such experiments. These polarized structure functions can be expressed in terms of the polarized parton distribution functions $\Delta q(x, \mu^2)$ and $\Delta g(x, \mu^2)$ describing the helicity distributions of partons in the nucleon. One of the most interesting questions is how the spin of the proton, S_z, is built up from its constituents. It can be naively expressed by the sum rule

$$S_z = \frac{1}{2} = \frac{1}{2}\Delta\Sigma + \Delta G + L_z^q + L_z^g \,, \tag{1.1}$$

stating that the spin of the proton is given by the sum of the angular momentum $L_z^{q,g}$ of quarks and gluons, the total quark polarization, $\Delta\Sigma = \int_0^1 dx \sum_q \Delta q(x, \mu^2)$ and the total gluon polarization, $\Delta G = \int_0^1 dx\, \Delta g(x, \mu^2)$. The large interest in spin structure arised after the European Muon Collaboration (EMC) published their results for the first moment of the structure function, g_1, of a proton target [14]. These results can be translated into a surprisingly small value for $\Delta\Sigma \simeq 0.1 - 0.2$ which is in clear contradiction to the naive assumption that the spin of the proton is mainly carried by the quarks. From the EMC result it follows that most of the spin has to come from the gluon polarization and/or from the orbital angular momenta. Unfortunately very little is known about them.

Up to now we only discussed inelastic scattering processes where only the rescattered lepton was detected experimentally, so-called inclusive processes. There also exists the possibility that all final states can be detected separately and which will be the topic of this work: *exclusive processes*. In the last ten years the theoretical and experimental interest in exclusive processes has grown rapidly because this processes provide information about the structure of the nucleon which cannot be obtained from inclusive processes. The two most prominent examples of exclusive processes are deeply virtual compton scattering (DVCS) and exclusive meson production. In DVCS the incoming virtual photon scatters on the nucleon and the final states are the nucleon and a (real or virtual) photon which are both detected in the experiment. In exclusive meson production the final states are also a nucleon and, in contrast to DVCS, a meson instead of a photon. As for inclusive processes there exist factorization theorems for both types of exclusive processes [15, 16]. The factorization theorems state that exclusive processes can be described in terms of a combination of soft universal functions and process dependent hard functions. The hard functions can be calculated with perturbative methods and are given by a series in α_s. Calculating the terms of the series is still a challenging task and in comparison to inclusive processes the progress is not very far. The soft, or non-perturbative functions appearing in the description of exclusive processes are not the same as for inclusive processes. They rather provide information about the structure of the nucleon which cannot be accessed by inclusive measurements. Initially

these functions appeared under different names in the literature: non-forward parton distributions, off-forward parton distributions, off-diagonal parton distributions or skewed parton distributions. Nowadays they are called generalized parton distributions (GPDs), which is the term we will use throughout this work.

To our knowledge, one of the first examples of GPDs was introduced by Dittes et al. [17] in the context of an interpolating function between the Dokshitzer-Gribov-Lipatov-Altarelli-Parisi (DGLAP) evolution [18–22] and the Efremov-Radyushkin-Brodsky-Lepage (ERBL) evolution equation [23–26]. A systematic study of GPDs in a physical process was made by Müller et al. [27] where they showed that GPDs contribute to the virtual photon Compton scattering (the same process has been considered much earlier by Watanabe [28]). The large interest in GPDs started in 1996 when the non-forward nature of parton distributions entering DVCS [29–31] and meson production [32] was emphasized by Ji and Radyushkin. In these publications it was shown that GPDs have a connection to the ordinary PDFs and to elastic form factors, which so far provided information on the structure of the nucleon. In [29] it was also shown that GPDs provide access to the total angular momentum carried by the partons. This offered the opportunity to reveal the spin structure of the nucleon and gave rise to the hope to solve the puzzle how the different partons contribute to the spin of the nucleon. Besides the information about the spin structure, the GPDs provide the possibility to study the nucleon in a three dimensional picture. This property has recently been investigated for the first time by Burkardt [33] using the impact-parameter representation of the GPDs. These information can not be accessed in inclusive processes

In this work we will concentrate on the exclusive production of mesons. On the one hand the theoretical understanding of these processes is not as sophisticated as for DVCS, in particular higher-order corrections in the hard function are poorly understood. On the other hand experimental measurements of at least charged exclusive meson production is easier. than for DVCS.

The work is organized as follows: in the next chapter we will give a brief introduction to the theory of GPDs and will discuss the main properties mentioned in the previous paragraph. In Chapter 3 we will calculate the cross sections for various final state mesons at leading order (LO) of the hard function, compare our results with recent experimental data and discuss the impact of exclusive meson production on the semi-inclusive production of mesons. In order to improve the theoretical predictions for exclusive meson production it is necessary to consider the next-to-leading order corrections (NLO) to the hard functions. We will give a systematic investigation of such NLO corrections in Chapter 4. Finally we will summarize and give a brief outlook.

Parts of this work have already been presented in Physical Review D [34].

2

General framework

In this chapter we will discuss the theoretical framework for exclusive processes. As described in the introduction there are two main processes which are relevant for the existing experiments: deeply virtual compton scattering (DVCS) and exclusive meson production. Both processes are described by the same theoretical framework of collinear factorization [15, 16]. We will explain this framework in some detail in Sec. 2.1 and give there the general definition of the GPDs and the kinematics of the process of exclusive meson production. In Sect. 2.2 we will recall the basic properties of the GPDs and give their physical interpretation. For recent reviews on GPDs see [35–39]. The different properties of the GPDs influence also their evolution, which is different from that of the well known PDFs. This issue will be investigated in Section 2.3. In Sect. 2.4 we will discuss some models for the GPDs, especially the model we use to obtain our theoretical predictions shown in Chapter 3 and Chapter 4. Finally in Section 2.5 we will briefly discuss the so-called transition GPDs, which will become important in Chapter 3.

2.1 Kinematics and definition of GPDs

We consider the process of exclusive meson production (see Fig.2.1)

$$\gamma^*(q) + p(p) \to M(q') + B(p')\,, \tag{2.1}$$

where M is a meson and B is a baryon and where the four-momenta are indicated in parentheses. This general form includes also transition process within the baryon octet,e.g.

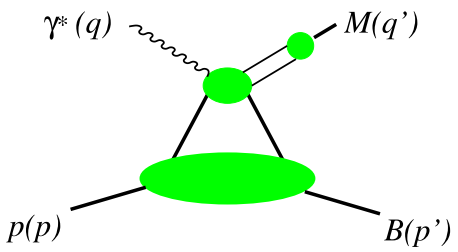

Figure 2.1. Most general graph for the exclusive production of a meson M.

$\gamma^* p \to K^+ \Lambda$. We shall discuss transition processes in a little more detail in Sect. 2.5 and in Chapter 3 we will give a very detailed study of cross sections for such transition processes. For the general process in (2.1) we use the standard kinematic variables

$$Q^2 = -q^2, \qquad W^2 = (p+q)^2, \qquad x_B = \frac{Q^2}{2pq}\,. \tag{2.2}$$

We further define

$$P = \frac{p+p'}{2} \qquad \Delta = p' - p \qquad t = \Delta^2\,. \tag{2.3}$$

Within the framework of collinear factorization [15, 16] the most general diagram for the process in (2.1) is shown in Fig. 2.1. The factorization theorem for exclusive meson production [15] states that the amplitude for the process (2.1) can be written as

$$\mathcal{M} = \int_0^1 dz \int_{-1}^1 dx\, F(x,\xi,t,\mu) T(x,\xi,z,Q^2,\mu)\phi_V(z,\mu) + \text{power suppressed terms}\,. \tag{2.4}$$

Here $F(x,\xi,t,\mu)$ is the generalized parton distribution which is represented in Fig. 2.1 by the large lower blob. The GPDs are non-perturbative objects and cannot be easily determined by first principles. They depend on the three kinematical variables x, the longitudinal momentum fraction of the probed parton, ξ, the longitudinal momentum transfer from the initial to the final state and the Mandelstam variable t. The GPDs are also dependent on the factorization scale μ, representing the physical scale at which the partons are resolved and for which one has an evolution equation, to be discussed in more detail in Sec. 2.3.
The GPDs are defined by the matrix elements (see e.g., [35])

$$\begin{aligned} F^q(x\,\xi,t) &= \frac{1}{2}\int \frac{dz^-}{2\pi} e^{ixP^+z^-} \langle p'|\bar q\left(-\tfrac{z}{2}\right)\gamma^+ q\left(\tfrac{z}{2}\right)|p\rangle\Big|_{z^+=0,z_T=0} \\ &= \frac{1}{2P^+}\left[H^q(x,\xi,t)\,\bar u(p')\,\gamma^+\,u(p) + E^q(x\,\xi,t)\,\bar u(p')\,\frac{i\sigma^{+\alpha}\Delta_\alpha}{2m_N}\,u(p)\right], \end{aligned} \tag{2.5}$$

$$\begin{aligned} \tilde F^q(x\,\xi,t) &= \frac{1}{2}\int \frac{dz^-}{2\pi} e^{ixP^+z^-} \langle p'|\bar q\left(-\tfrac{z}{2}\right)\gamma^+\gamma_5 q\left(\tfrac{z}{2}\right)|p\rangle\Big|_{z^+=0,z_T=0} \\ &= \frac{1}{2P^+}\left[\tilde H^q(x,\xi,t)\,\bar u(p')\,\gamma^+\gamma_5\,u(p) + \tilde E^q(x\,\xi,t)\,\bar u(p')\,\frac{\gamma_5\Delta^+}{2m_N}\,u(p)\right], \end{aligned} \tag{2.6}$$

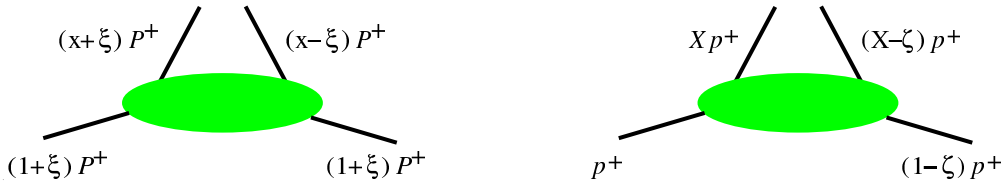

Figure 2.2. Parton and hadron plus-momenta in the parameterization of Ji [35] (left) and Radyushkin [40] (right).

in the case of unpolarized and polarized quark GPDs and for the unpolarized and polarized gluon GPD through

$$\begin{aligned} F^g(x\,\xi,t) &= \frac{1}{P^+}\int \frac{dz^-}{2\pi} e^{ixP^+z^-} \langle p'|G^{+\mu}\left(-\tfrac{z}{2}\right) G_\mu{}^+\left(\tfrac{z}{2}\right)|p\rangle\big|_{z^+=0,z_T=0} \\ &= \frac{1}{2P^+}\left[H^g(x,\xi,t)\,\bar u(p')\,\gamma^+\,u(p) + E^g(x\,\xi,t)\,\bar u(p')\,\frac{i\sigma^{+\alpha}\Delta_\alpha}{2m_N}\,u(p)\right], \end{aligned} \tag{2.7}$$

and

$$\begin{aligned} \tilde F^g(x\,\xi,t) &= \frac{-i}{P^+}\int \frac{dz^-}{2\pi} e^{ixP^+z^-} \langle p'|\tilde G^{+\mu}\left(-\tfrac{z}{2}\right) G_\mu{}^+\left(\tfrac{z}{2}\right)|p\rangle\big|_{z^+=0,z_T=0} \\ &= \frac{1}{2P^+}\left[\tilde H^g(x,\xi,t)\,\bar u(p')\,\gamma^+\gamma_5\,u(p) + \tilde E^g(x\,\xi,t)\,\bar u(p')\,\frac{\gamma_5\Delta^+}{2m_N}\,u(p)\right]. \end{aligned} \tag{2.8}$$

Here the quark fields are denoted with $q(x)$, the gluon field strength by $G^{\mu\nu}(x)$ and the dual field strength by

$$\tilde G^{\mu\nu}(x) = \frac{1}{2}\epsilon^{\mu\nu\alpha\beta}G_{\alpha\beta}(x)\,, \tag{2.9}$$

where the total antisymmetric tensor is defined as

$$\epsilon_{0123} = 1\,. \tag{2.10}$$

For the definition of the GPDs we used light-cone coordinates which are defined by

$$v^\pm = \frac{1}{\sqrt{2}}(v^0 \pm v^3), \qquad v_T = (0, v^1, v^2, 0) \tag{2.11}$$

for any four-vector v. Within this coordinates the light-cone momentum p^+ becomes proportional to the momentum (energy) of a particle in the infinite momentum frame where $p^3 \to \infty$. It is also sometimes useful to introduce two light-like four-vectors n_+ and n_- with the properties

$$n_+^2 = n_-^2 = 0, \qquad n_+n_- = 1\,. \tag{2.12}$$

The GPDs (2.5)−(2.7) depend only on the kinematical variables x, ξ and t because of Lorentz invariance. The skewness variable ξ is defined here by

$$\xi = \frac{p^+ - p'^+}{p^+ + p'^+}\,, \tag{2.13}$$

Figure 2.3. Example graphs for exclusive meson production in the generalized Bjorken limit. The large blob denotes the $p \to B$ transition GPD and the small one the meson distribution amplitude. The left figure shows the quark exchange and the right figure the gluon exchange.

and can be interpreted as the longitudinal momentum transfer from the initial to the final states. In the literature at least two parameterization of the longitudinal momentum transfer exist. They are shown in Fig. 2.2. Their relation is

$$X = \frac{x+\xi}{1+\xi}, \qquad \zeta = \frac{2\xi}{1+\xi}\,. \tag{2.14}$$

Using the symmetric parameterization as in the left diagram in Fig. 2.2 one has the relation

$$\xi \approx \frac{x_B}{2-x_B} \tag{2.15}$$

in the Bjorken limit. We will use the symmetric parameterization throughout of this work and use the relation (2.15) especially to present our results versus x_B.

In the amplitude (2.4) the hard scattering function $T(x, z, Q^2, \mu)$ also appears. This function can be in principal calculated within perturbative QCD up to arbitrary order in the strong coupling constant α_s. Depending on the final state meson, different exchange graphs can appear, as shown in Fig. 2.3 for the leading order in α_s. The left graph in Fig. 2.3 is the quark exchange and probes the different quark GPDs inside the hadron. The right diagram represents the gluon exchange and probes the gluon GPD of the hadron. Which of both graphs contribute to the amplitude is dependent of the final state meson. The gluon contribution to the amplitude can only appear for final state meson with odd C-parity because only for such kind of mesons the C-even gluon scattering kernel gives a non-vanishing contribution to the amplitude. This is due to the fact that the complete process has to preserve C-parity and the incoming virtual photon has odd C-parity. The exact expressions of the hard scattering functions and the amplitude of exclusive meson production will be given in Chapter 3 and Chapter 4.

The last ingredient of the amplitude is the meson distribution amplitude (DA). It is also a non-perturbative object and for a longitudinal polarized meson defined by

$$\langle 0|\bar{q}(y)\gamma_\mu q(-y)|M(q')\rangle_{y^2\to 0} = q'_\mu f_M \int_0^1 dz\, e^{i(2z-1)q'y}\phi_V(z,\mu)\,. \tag{2.16}$$

Here z is a light-cone momentum fraction of one of the quarks and f_M is the meson decay constant.

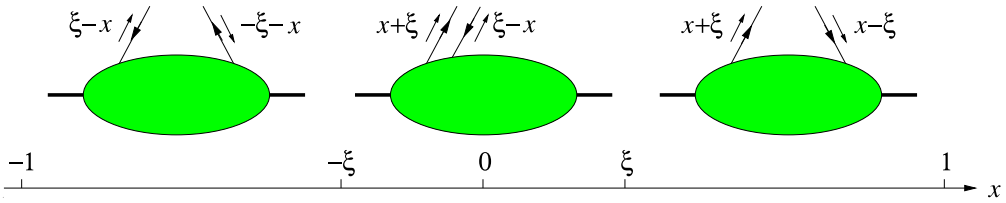

Figure 2.4. The parton interpretation of GPDs in the three intervals $x \in [-1,,-\xi]$, $x \in [-\xi,\xi]$ and $x \in [\xi,1]$. The figure is taken from [38].

The meson DA plays an important role not only in hard exclusive processes but also in the determination of the pion electromagnetic form factor [41], where different models of the DA are used to make quantitative predictions at the level of next-to-leading order in α_s.

2.2 Physical interpretation and properties of GPDs

The quark and gluon GPDs defined in the previous section are functions of three kinematical variables and provide a lot of information about the internal structure of hadrons. Although they have not such a simple interpretation as the PDFs it is nevertheless possible to find a partonic interpretation of the GPDs. As we will see in a few moments they are connected to the ordinary PDFs as well as to the nucleon form factors. Furthermore they can provide a three dimensional picture of the hadron via the dependence on the Mandelstam variable t.

Let us start with the partonic interpretation of GPDs. As it can be seen from the amplitude, the GPDs we defined in (2.5)-(2.8) have support in the region $x \in [-1;1]$, which can be split in three different regions as shown in Fig. 2.4. In the first region, $x \in [\xi,1]$ the two momentum fractions $x+\xi$ and $x-\xi$ are positive and can be interpreted as the emission and absorption of a quark. In the second region, $x \in [-\xi,\xi]$ one has $x+\xi \geq -$ and $x-\xi \leq 0$. One can now interpret the second momentum fraction as an antiquark with the momentum fraction $\xi - x$ which is emitted from the initial proton. Finally in the third region, $x \in [-1,-\xi]$ both momentum fractions are negative and can be seen as the emission and reabsorption of an antiquark. For a detailed discussion of the partonic interpretation of GPDs see Section 3.4 in [38]. The first and third region are also commonly referred to the DGLAP region because the GPDs behave similar to the usual parton distribution functions which obey the DGLAP evolution equation [18–22] (we will discuss the evolution of GPDs in some detail in Sec. 2.3). The second region is referred to the ERBL region because of the meson like behavior of the GPDs and mesons obey the ERBL evolution equation [23–26].

The above parton interpretation is also reflected in the forward limit of GPDs. In the case where $p = p'$ and the initial and final state hadrons have the same helicities the matrix elements in (2.5)-(2.8) reduce to the ones which define the ordinary unpolarized or polarized

parton distribution functions. To be more precise one has the following relations for $\Delta = 0$

$$H^q(x,0,0) = \begin{cases} q(x) & x > 0\,, \\ -\bar{q}(-x) & x < 0\,, \end{cases}$$
$$\tilde{H}^q(x,0,0) = \begin{cases} \Delta q(x) & x > 0\,, \\ \Delta\bar{q}(-x) & x < 0\,, \end{cases} \tag{2.17}$$

for the quark GPDs and

$$\begin{aligned} H^g(x,0,0) &= x\,g(x) \qquad x > 0\,, \\ \tilde{H}^g(x,0,0) &= x\Delta g(x) \quad x > 0\,, \end{aligned} \tag{2.18}$$

for the gluon GPDs. The gluon GPD H^g is an even function x so that for $x < 0$ the GPD H^g has the same forward limit as in (2.18). For the polarized gluon GPD $\tilde{H}^g$ the forward limit for $x < 0$ is given by $-\Delta g(-x)$ because $\tilde{H}^g$ is an odd function in x. For the quark and gluon GPDs E and $\tilde{E}$ exist no such relation as for the GPDs H and $\tilde{H}$ because in their definitions the functions are multiplied with a factor which is proportional to Δ. This does not mean that the functions themselves have no forward limit, but rather carry information about the orbital angular momentum of partons.

As we have seen above, GPDs reduce to the ordinary PDFs in their forward limits. Other physical quantities to which the GPDs are directly connected are the form factors. This connection is give through the moments in the momentum fraction x of the GPDs. If one integrates the matrix elements (2.5)−(2.8) over x one gets matrix elements of local quark-antiquark or gluon operators. To be more precise one has

$$\begin{aligned} \int_{-1}^{1} dx\, H^q(x,\xi,t) &= F_1^q(t), \qquad \int_{-1}^{1} dx\, E^q(x,\xi,t) = F_2^q(t), \\ \int_{-1}^{1} dx\, \tilde{H}^q(x,\xi,t) &= g_A^q(t), \qquad \int_{-1}^{1} dx\, \tilde{E}^q(x,\xi,t) = g_P^q(t), \end{aligned} \tag{2.19}$$

where F_1, F_2, g_p and g_A are the Dirac, Pauli, pseudoscalar and axial form factor, respectively, for each quark flavor separately. The common proton and neutron form factors are given by

$$F_{1,2}^p = e_u F_{1,2}^u + e_d F_{1,2}^d\,, \quad F_{1,2}^n = e_d F_{1,2}^u + e_u F_{1,2}^d\,, \tag{2.20}$$

with the quark charges e_u and e_d in unit of the positron charge.
One of the most remarkable properties of the GPDs is the fact that the integrals in (2.19) are independent of ξ due to Lorentz invariance. A generalization of the above property is the so-called polynomiality: the x-integrals of $x^n H^q$ and $x^n E^q$ (Mellin moments) are polynomials

in ξ of the order $n+1$. To be more precise on has

$$\int_{-1}^{1} dx\, x^n H^q(x,\xi,t) = \sum_{\substack{i=0 \\ \text{even}}}^{n} (2\xi)^i A^q_{n+1,i}(t) + \text{mod}(n,2)\,(2\xi)^{n+1} C^q_{n+1}(t)\,,$$
$$\int_{-1}^{1} dx\, x^n E^q(x,\xi,t) = \sum_{\substack{i=0 \\ \text{even}}}^{n} (2\xi)^i B^q_{n+1,i}(t) - \text{mod}(n,2)\,(2\xi)^{n+1} C^q_{n+1}(t)\,, \qquad (2.21)$$

where $\text{mod}(n,2)$ is 1 for odd n and 0 for even n. The functions A^q, B^q and C^q appear in the form factor decomposition of matrix elements with local twist-two operators (for details see [35, 38]). One finds similar relations for the spin dependent GPDs and for the gluon GPDs. It is remarkable that the terms with the highest power of ξ in (2.21) are of opposite sign, so for the combination of $H^q + E^q$ the x^n-th moment is just a polynomial of degree ξ^n.

A further property of GPDs and their moments is the possibility to get access to the orbital angular momentum of the nucleon. This was for the first time suggested by Ji [29]. It is possible to write a gauge-invariant decomposition of the nucleon spin into quark orbital momentum L^q, quark spin $\Delta\Sigma$ and gluon total angular momentum J^g :

$$\frac{1}{2} = J^q(\mu^2) + J^g(\mu^2) = \frac{1}{2}\Delta\Sigma(\mu^2) + L^q_z(\mu^2) + J^g(\mu^2)\,, \qquad (2.22)$$

where the total quark orbital angular momentum $J^q(\mu^2)$ can be decomposed in a gauge-invariant way into the spin $\Delta\Sigma(\mu^2)$ and the orbital contribution $L^q_z(\mu^2)$. Such a gauge-invariant decomposition does not exist for the gluon orbital angular momentum. The orbital angular momentum of quarks and gluons in the nucleon can be related to the second moment of the GPDs

$$J^q(\mu^2) = \frac{1}{2}\lim_{t\to 0}\int_{-1}^{1} dx\, x\, \left[H^q(x,\xi,t,\mu^2) + E^q(x,\xi,t,\mu^2)\right]\,,$$
$$J^g(\mu^2) = \frac{1}{2}\lim_{t\to 0}\int_{0}^{1} dx\, \left[H^g(x,\xi,t,\mu^2) + E^g(x,\xi,t,\mu^2)\right]\,. \qquad (2.23)$$

The above relation is often referred to as Ji's sum rule [29] and is the only known possibility to access the orbital angular momentum.

All properties discussed so far were related to the longitudinal momentum fractions x and ξ and was done in the momentum space. A further way to find a physical interpretation of GPDs was developed by M. Burkardt [33], by Fourier transforming the GPDs with respect to the transverse momentum transfer but keeping the longitudinal momentum fraction x fixed. This procedure leads to a mixed representation of momentum space and transverse position space and is called impact parameter space. For a detailed review we refer to [42]. The impact parameter representation of GPDs is valid for all values of ξ but for $\xi = 0$ it has

a very intuitive physical interpretation which we now want to discuss briefly. In the impact parameter space representation and at $\xi = 0$ one has

$$q^i(x, \vec{b}_\perp) = \int \frac{d^2\vec{\Delta}_\perp}{(2\pi)^2} e^{i\vec{b}_\perp \vec{\Delta}_\perp} H^i(x, 0, -\vec{\Delta}_\perp^2)\,, \tag{2.24}$$

where now the function $q^i(x, \vec{b}_\perp)$ can be interpreted as the probability density to find a parton with the momentum fraction x at the transverse distance $\vec{b}_\perp$ from the transverse center of momentum, which is defined by $\sum_i x_i \vec{r}_{\perp i}$ (the summation runs over all partons in the hadron and x_i is the momentum fraction carried by the i-th parton). Integrating $q^i(x, \vec{b}_\perp)$ over $\vec{b}_\perp$ leads to the usual quark or gluon PDFs. For the spin dependent GPD $E(x, \xi, t)$ one finds a similar relation

$$e^i(x, \vec{b}_\perp) = \int \frac{d^2\vec{\Delta}_\perp}{(2\pi)^2} e^{i\vec{b}_\perp \vec{\Delta}_\perp} E^i(x, 0, -\vec{\Delta}_\perp^2)\,. \tag{2.25}$$

We have to keep in mind that the GPD $E(x, \xi, t)$ does not contribute to the amplitude when the initial and final state have the same helicity. If we assume to have a state that is a superposition of transversely localized nucleon states with opposite helicities, which we will denote as

$$|X\rangle \equiv \frac{1}{\sqrt{2}} \left(|p^+, \uparrow\rangle + |p^+, \downarrow\rangle\right) \tag{2.26}$$

the impact parameter dependent PDF for this state is given by the following Fourier transformation

$$\begin{aligned} q_X(x, \vec{b}_\perp) =& \int \frac{d^2\vec{\Delta}_\perp}{(2\pi)^2} e^{i\vec{b}_\perp \vec{\Delta}_\perp} \left[H^q(x, 0, -\vec{\Delta}_\perp^2) + i\frac{\Delta_y}{2m_N} E^q(x, 0, -\vec{\Delta}_\perp^2) \right] \\ =& q(x, \vec{b}_\perp) - \frac{1}{2m_N} \frac{\partial}{\partial b_y} e(x, \vec{b}_\perp)\,. \end{aligned} \tag{2.27}$$

Physically, the above equation describes the transverse distortion of the unpolarized impact parameter PDF if the state is polarized in the transverse direction and not in the $\pm z$ direction.

With a appropriate model for the GPDs the above representation of PDFs in the impact parameter space offers for the first time the opportunity to visualize the parton distributions in the transverse plane. Some examples are shown in [42] where one can see that the unpolarized u and d quark distributions are centered around the origin for an unpolarized proton. In the case of a transversely polarized proton, which is described by (2.27) one finds that the two quark distribution are moved away from the origin. The discovery that the quarks are not uniformly distributed in the transverse plain can be a possible explanation for some transverse single spin asymmetries [43].

As mentioned before the impact parameter representation can also be chosen for $\xi \neq 0$ but for this case there exists no simple physical interpretation as for $\xi = 0$. For a detailed discussion of the issue we refer to [42].

2.3 Evolution

The properties described in Sect. 2.2 are all of non-perturbative nature. In this section we want to discuss the most important perturbative property of the GPDs: their evolution.
We want to start with a small review of the theory of the evolution of ordinary parton distribution functions which appear in description of deep-inelastic scattering processes and then turn to the evolution of the GPDs, which is quite different to that of the ordinary PDFs. In deep inelastic scattering a virtual photon with high virtuality Q^2 is exchanged between the lepton and the proton. It acts as a local probe that resolves local distances that are inversely proportional to its virtuality. A change in the resolution scale leads to a more detailed picture of the probed hadron. In other words, the change of the scale Q^2 leads to a different parton number density $q(x, Q^2)$, where x is the usual momentum fraction of the parton.
The change of the PDF $q(x, \mu^2)$ is governed by the well-known Dokshitzer-Gribov-Lipatov-Altarelli-Parisi (DGLAP) equation [18–22]

$$\mu^2 \frac{d}{d\mu^2} q(x, \mu^2) = \int_x^1 \frac{dy}{y} P\left(\frac{x}{y}, \alpha_s(\mu^2)\right) q(y, \mu^2)\,, \tag{2.28}$$

where $P\left(\frac{x}{y}, \alpha_s(\mu^2)\right)$ is the so-called evolution kernel. We can choose a specific combination of cross sections where the gluonic contribution drops out and picks up the so-called non-singlet parton distribution $q_{NS}(x, \mu^2) = q(x, \mu^2) - \bar{q}(x, \mu^2)$. The evolution equation for this combination of PDF is given by (2.28) and the corresponding evolution kernel $P_{NS}(x, \alpha_s(\mu^2)$ is given by an infinite series in α_s

$$P_{NS}(x, \alpha_s(\mu^2)) = \sum_{n=1}^{\infty} \left(\frac{\alpha_s}{2\pi}\right)^n P_{NS}^{(n)}(x)\,. \tag{2.29}$$

For the singlet combination

$$q_S = \sum_q (q + \bar{q})\,, \tag{2.30}$$

the situation is more complicated because the quarks can mix with gluons and the evolution equation has therefore the form

$$\mu^2 \frac{d}{d\mu^2} \begin{pmatrix} q_S \\ g \end{pmatrix} = \int_x^1 \frac{dy}{y} \begin{pmatrix} P^{qq} & P^{qg} \\ P^{gq} & P^{gg} \end{pmatrix} \left(\frac{x}{y}, \alpha_s(\mu^2)\right) \begin{pmatrix} q_S \\ g \end{pmatrix}\,, \tag{2.31}$$

where we the arguments of q_S, g and the evolution kernels P^{ab} are the same as in (2.28). The evolution kernels P^{ab} in (2.31) have similar perturbative expansion as in (2.29).

For the GPDs the situation is different. In contrast to the ordinary PDFs the GPDs have no simple probability interpretation. As explained in Sect. 2.2 there are three different parts in the support region of the GPDs where they have various physical interpretations. In the

regions $x \in [-1, -\xi]$ and $x \in [\xi, 1]$ the GPDs can be treated as ordinary quark or antiquark distribution. Therefore the evolution equation looks similar to the DGLAP equation in this region. In the central region, $x \in [-\xi, \xi]$, the GPDs can be interpreted as the probability to find a meson like quark-antiquark state inside the hadron. In this part of the support region the evolution is related to that of meson distribution amplitudes, which obey the ERBL evolution equation [23–26]. Because of this different behavior of the GPDs the evolution equation also looks different in comparison to the DGLAP equation.
As in the case of the DGLAP evolution one can define for the polarized and unpolarized GPDs singlet and non-singlet combinations given by

$$\begin{aligned} F^q_{NS}(x,\xi,\mu^2) &= F^{q(-)}(x,\xi,\mu^2) = F^q(x,\xi,\mu^2) + F^q(-x,\xi,\mu^2)\,, \\ \tilde{F}^q_{NS}(x,\xi,\mu^2) &= \tilde{F}^{q(-)}(x,\xi,\mu^2) = \tilde{F}^q(x,\xi,\mu^2) - \tilde{F}^q(-x,\xi,\mu^2)\,, \end{aligned} \tag{2.32}$$

and

$$\begin{aligned} F^q_{S}(x,\xi,\mu^2) &= F^{q(+)}(x,\xi,\mu^2) = F^q(x,\xi,\mu^2) - F^q(-x,\xi,\mu^2)\,, \\ \tilde{F}^q_{S}(x,\xi,\mu^2) &= \tilde{F}^{q(+)}(x,\xi,\mu^2) = \tilde{F}^q(x,\xi,\mu^2) + \tilde{F}^q(-x,\xi,\mu^2)\,, \end{aligned} \tag{2.33}$$

where we dropped the t dependence of the GPDs for simplicity. As in the case of DGLAP evolution they obey different evolution equations. For the non-singlet GPDs the evolution equation is given by

$$\mu^2 \frac{d}{d\mu^2} F^{q(-)}(x,\xi,\mu^2) = \int_{-1}^{1} dx' \, \frac{1}{|\xi|} V_{NS}\left(\frac{x}{\xi}, \frac{x'}{\xi}\right) F^{q(-)}(x',\xi,\mu^2)\,. \tag{2.34}$$

An analog equation holds for $\tilde{F}^{q(-)}$. For the singlet GPDs the equation is again somewhat more difficult because one has again a mixing of quark and gluon GPDs. The evolution equation reads therefore

$$\mu^2 \frac{d}{d\mu^2} \begin{pmatrix} F^{(+)}(x,\xi,\mu^2) \\ F^g(x,\xi,\mu^2) \end{pmatrix} = \int_{-1}^{1} dx' \, \frac{1}{|\xi|} \begin{pmatrix} V^{qq}\left(\frac{x}{\xi}, \frac{x'}{\xi}\right) & \frac{1}{\xi} V^{qg}\left(\frac{x}{\xi}, \frac{x'}{\xi}\right) \\ \xi V^{gq}\left(\frac{x}{\xi}, \frac{x'}{\xi}\right) & V^{gg}\left(\frac{x}{\xi}, \frac{x'}{\xi}\right) \end{pmatrix} \begin{pmatrix} F^{(+)}(x',\xi,\mu^2) \\ F^g(x',\xi,\mu^2) \end{pmatrix} \tag{2.35}$$

with

$$F^{(+)}(x,\xi,\mu^2) = \sum_q^{n_f} F^{q(+)}(x,\xi,\mu^2)\,. \tag{2.36}$$

For the polarized singlet GPDs $\tilde{F}^{(+)}$ one has an analog equation (see Appendix D.1).
The exclusive evolution kernels appearing in (2.34) and (2.35) have been calculated for the first time by Gribov et al. [44] but their results contain some mistakes [45]. At the leading order level the evolution kernels have been discussed in detail in [27], and the next-to-leading order kernels have been calculated in [46–50]. In this work we will deal only with the LO

evolution kernels which are given in Appendix D for the polarized and unpolarized singlet and non-singlet GPDs. In the literature there exist different versions of the evolution kernels. In order to be sure to deal with the correct form it is possible to perform some consistency checks. The first opportunity is to see if the evolution kernels have the correct forward limit. For the case $\xi \to 0$ the kernels of (2.34) and (2.35) have to reduce to the ordinary DGLAP evolution kernels of (2.28) and (2.31) (the correct procedure for taking the limit $\xi \to 0$ is described in Appendix D.1). The second possibility to check the correctness of the evolution kernels is to apply the evolution equation to the following sum of moments of the quark and gluon GPDs

$$\int_{-1}^{1} dx \left[x F^{(+)}(x,\xi,t) + F^{g}(x,\xi,t) \right] . \tag{2.37}$$

Using (2.21) it can be shown that this sum corresponds to a special combination of nucleon form factors. Because form factors are physical observables they cannot dependent on the factorization scale μ and therefore we must find

$$\begin{aligned} &\mu^2 \frac{d}{d\mu^2} \int_{-1}^{1} dx \left[x F^{(+)}(x,\xi,\mu^2) + F^{g}(x,\xi,\mu^2) \right] = \\ &= \left\{ \begin{array}{c} \int_{-1}^{1} dx \int_{-1}^{1} dx' F^{(+)}(x',\xi,\mu^2) \left[x V^{qq}\left(\frac{x}{\xi},\frac{x'}{\xi}\right) + \xi V^{gq}\left(\frac{x}{\xi},\frac{x'}{\xi}\right) \right] \\ \int_{-1}^{1} dx \int_{-1}^{1} dx' F^{g}(x',\xi,\mu^2) \left[\frac{x}{\xi} V^{qg}\left(\frac{x}{\xi},\frac{x'}{\xi}\right) + V^{gg}\left(\frac{x}{\xi},\frac{x'}{\xi}\right) \right] \end{array} \right\} \stackrel{!}{=} 0 . \end{aligned} \tag{2.38}$$

A straightforward calculation shows that this relation is indeed fulfilled for the evolution kernels given in Appendix D.1.

In the case of DIS evolution is very important to describe the experimental data in a correct way. This is also true for exclusive processes and we will show in Chapter 3 and Chapter 4 that the amplitude and hence the cross section of exclusive meson production is strongly dependent on the choice of the factorization scale and it is therefore very important to treat the evolution of the GPDs in the right way. Since some time there exists an analytical solution of the evolution equation for the GPDs [51, 52] which also allows a numerical implementation. A second approach is to treat the evolution equation completely numerically [53]. Both approaches are restricted to the leading order evolution but one can find a numerical implementation of the NLO evolution in [54]. In this work we will restrict ourself on the LO evolution because the numerical implementation of the NLO evolution is too time consuming for our purposes and the effects of NLO evolution are small, as we will discuss in some detail in Sect. 4.6.1.

2.4 Modeling the generalized parton distributions

The GPDs are non-perturbative objects and are still essentially unknown. In order to make quantitative predictions for physical observable such as cross sections we therefore need some

kind of model for the GPDs. In the first part of this section we want to give a brief overview of models for the GPDs which are based on dynamics. In the second part we will discuss in some detail the double distributions. They offer an alternative way to parameterize hadronic matrix elements which define the GPDs. For a detailed discussion of the different possible ansätze of GPDs we refer to Chapter 4 of [38].

2.4.1 Model based on dynamics

One possible way to construct models for the GPDs is to use dynamical symmetries of QCD and hence all models and ansätze which we will discuss in the following are based on non-perturbative calculations.

The very first attempt of a dynamical study of quark GPDs was done by Ji et al. [55] and was based on the MIT bag model [56]. Within the MIT bag model the hadron is seen as finite region of space containing quark fields. The curves for the four different GPDs H, E, $\tilde{H}$ and $\tilde{E}$ as a function of x obtained in [55] show a very weak dependence on ξ. The physics reason for this is not understood, nor are the results reliable for $x < \xi$ where one expects that antiquarks play an important role. A further missing piece in this model is the lack of gluonic degrees of freedom, which are known to play play an essential role in scattering processes at small x_B.

A further approach is to model the GPDs with the help of the constituent quark model where the hadron is a simple bound state of a few massive quark constituents. The first study of the connection between the GPDs and and the constituent quark model wave functions was done in [57], where the authors used a non-relativistic quark model to calculate the GPD H^q. The main features of the obtained results are the vanishing of the GPDs at $x = \xi$ and that the GPDs, as a function of x, have a peak whose position shifts to the right with increasing ξ. Treating the ERBL region with this model is problematic because in this region the antiquarks start to become important but they are not covered by the model which is restricted to the region $x > \xi$. In addition the model contains no gluonic degrees of freedom as the MIT bag model.

Another possibility is to make us of chiral symmetry. This is quite natural because the GPDs are low-energy quantities. It is possible to infer some properties of the GPDs from chiral symmetry and chiral perturbation theory. However the GPDs include quark and gluon fields. It is therefore necessary to find a matching procedure to link the low-energy degrees of freedom such as pions to the parton degrees of freedom. The most prominent example of the application of chiral symmetry to the GPDs is the pion exchange contribution to the GPDs $\tilde{E}^q$, mentioned for the first time in [58] and discussed in detail in [59, 60]. Physically this contribution corresponds to the emission of a virtual pion by the initial nucleon. This virtual pion dissociates into a $q\bar{q}$ pair which is probed in the hard scattering process. Because of its physical nature this contribution is present only in ERBL region and contributes only to the isovector combination $\tilde{E}^{u-d}$, due to the quantum numbers. Following [59, 60] this

contribution is given by the limit

$$\lim_{t\to m_\pi^2} \tilde{E}^{u-d}(x,\xi,t) = \frac{\theta(|x|\leq\xi)}{2\xi}\,\phi_\pi\left(\frac{x+\xi}{2\xi}\right)\frac{2m_p f_\pi\, g_{\pi NN}}{m_\pi^2 - t}\,, \tag{2.39}$$

where the meson DA ϕ_π is defined as in (2.16), the coupling constant $g_{\pi NN}$ is given by the Goldberger-Treiman relation and f_π is the pion decay constant. We will use an improved form of this model in Chapter 3 for the calculation of the exclusive production of pions. The pole contribution in (2.39) can be seen as a resonance contribution to the GPDs, although it is questionable that only one single resonance should dominate at small values of t.

Within the chiral quark soliton model, which was detailed studied in [60, 61], one finds corrections to the pole contribution (2.39) that are not negligible at $-t \approx 0.1\,\mathrm{GeV}^2$. In this model the nucleon is seen as a bound state of quarks in a semi-classical pion field. The main ingredients of this model are the spontaneously broken chiral symmetry and the large-N_c limit. A detailed review of this model and references can be found in [37]. Up to now, u and d quark GPDs have been calculated with this model. The analytic results obtained fulfill some of the previous described properties of the GPDs: the forward limit and the reduction of the lowest Mellin moment to the elastic form factors. Further features of the GPDs were found with this model: the GPD H^{u+d} show a rapid variation in x around the point $x = \pm\xi$, the pion pole contribution (2.39) to $\tilde{E}^{u-d}$ can be obtained analytical and even more important the corrections to the pole term can be calculated and parameterized for intermediate values of t. A further very important observation is that the model does not support a factorized t dependence in the form $F(t)f(x,\xi)$ for the GPDs $H(x,\xi,t)$ and $\tilde{H}(x,\xi,t)$. We will use this factorized ansatz in Chapter 3 and we will discuss the impact of this ansatz on our results.

Let us finally mention a further possibility to obtain information about the GPDs, due to lattice calculations. Within this framework, quarks are placed at the interstices of a lattice and interact with each other via the exchange of gluons along the links between the quarks. Unfortunately it is not possible to calculate the GPDs directly on the lattice but rather their Mellin moments, which are related to form factors. For recent progress in this field and references we refer to [62, 63].

2.4.2 Double Distributions

Beside the disadvantages mentioned before (e.g., the lack of gluonic freedom) the most models described in the previous section are not very practicable for phenomenological calculations. The most widely used model for phenomenological calculations is based on the so-called double distributions. They are an alternative way to parameterize the hadronic matrix elements which define the GPDs. The double distributions are defined as the Fourier transform of matrix elements

$$\langle p'|\bar{q}(-\frac{1}{2}z)\not{z}q(\frac{1}{2}z)|p\rangle \tag{2.40}$$

with respect to the two independent variables Pz and Δz,

$$\begin{aligned}\langle p'|\bar{q}(-\frac{1}{2}z)\not{z}q(\frac{1}{2}z)|p\rangle|_{z^2=0} =&\bar{u}(p')\not{z}u(p)\int d\beta\, d\alpha\, e^{-i\beta(Pz)+i\alpha(\Delta z)/2}\, f^q(\beta,\alpha,t)\\ &+\bar{u}(p')\frac{i\sigma^{\mu\alpha}z_\mu\Delta_\alpha}{2m}u(p)\int d\beta\, d\alpha\, e^{-i\beta(Pz)+i\alpha(\Delta z)/2}\, k^q(\beta,\alpha,t)\\ &-\bar{u}(p')\frac{\Delta z}{2m}u(p)\int d\alpha\, e^{i\alpha(\Delta z)/2}\, D^q(\alpha,t)\,. \end{aligned}\tag{2.41}$$

One can find similar expressions for the gluonic matrix element and for the helicity dependent quark and gluon operators. The double distribution have been introduced by Müller at al. [27] and have been rediscovered by Radyushkin, who has given a detailed review in [36]. The last term in (2.41), the so-called D-term was introduced by Polyakov and Weiss [64]. This term does no appear for the helicity dependent quark and gluon matrix element. We will discuss the influence of the D-term on the cross sections of exclusive vector meson production in Sect. 3.3.

The support region of the α and β integration is given by the rhombus $|\alpha|+|\beta|\leq 1$ and the D-term has support for $|\alpha|\leq 1$. For the relation between the GPDs and the double distributions one finds

$$\begin{aligned}H^q(x,\xi,t) &= \int d\beta\, d\alpha\ \delta(x-\beta-\xi\alpha)\, f^q(\beta,\alpha,t) + \mathrm{sgn}(\xi)D^q\Big(\frac{x}{\xi},t\Big),\\ E^q(x,\xi,t) &= \int d\beta\, d\alpha\ \delta(x-\beta-\xi\alpha)\, k^q(\beta,\alpha,t) - \mathrm{sgn}(\xi)D^q\Big(\frac{x}{\xi},t\Big).\end{aligned}\tag{2.42}$$

if one takes a given lightlike z and chooses the frame where $z^+ = z_T = 0$ and the Fourier transform the matrix element (2.40) with respect to z^-. There are analogous expressions for the helicity dependent GPDs $\tilde{H}$ and $\tilde{E}$ and the gluon GPDs there are with the only difference that the D-term is missing for the helicity dependent GPDs.

The forward quark densities can be easily obtained from the functions $f^q(\beta,\alpha,0)$ by the integration over the line $\beta = x$

$$q(x) = \int\limits_{x-1}^{1-x} d\alpha\, f^q(x,\alpha,0)\,.\tag{2.43}$$

This simple connection to the forward densities offers the opportunity to model the GPDs with the well known forward parton densities as input. Following the ansatz in [37, 65] it is possible to write

$$f^q(\beta,\alpha) = q(\beta)h^q(\beta,\alpha)\,,\tag{2.44}$$

where the profile function h^q is normalized to

$$\int\limits_{-1+|\beta|}^{1-|\beta|} d\alpha\, h^q(\alpha,\beta) = 1\tag{2.45}$$

in order to obtain the correct forward limit for the GPDs. This ansatz can of course only made at $t = 0$. For the t dependence of the GPDs the most widely used ansatz is of the factorized form

$$H^q(x,\xi,t) = H^q(x,\xi)\, F_1^p(t) \tag{2.46}$$

where $H^q(x,\xi)$ is determined by (2.42) with (2.44). Within this model the GPDs have automatically the correct forward limit and also the sum rules (2.19) are fulfilled.

All above considerations can be easily transfered to the gluon and polarized GPDs H^g and $\tilde{H}^{q,g}$. The model we will use in this work is specified in detail in Sect. 3.1 where we also briefly discuss the shortcomings of the factorized ansatz (2.46) for the t dependence, and also in Appendix A where we present useful formulas for the convolution of GPDs and the hard scattering kernels.

2.5 Transition GPDs

In contrast to DVCS, where the struck parton is absorbed by the final hadron, in exclusive meson production the final state hadron can have different flavor content from the initial one.

The understanding of transition effects is important, since the reactions with Δ or N^* final states can compete with the usual $p \to p$ reaction in experiments that cannot distinguish between different final baryon states. On the other side if the experimental setup allows a clear detection of the final hadronic system, one can use the transition GPDs to study the different flavor content of the initial state hadron.

For transitions within the ground state baryon octet one has the same spin structure as for the proton GPDs, namely the four GPDs H, E, $\tilde{H}$ and $\tilde{E}$ for each quark flavor transition. In the transition between the baryon octet the gluon GPD cannot contribute because two gluons carry zero isospin and hypercharge. Let us consider for example the $p \to n$ transition. This transition can happen in the process $\gamma^* p \to n\pi^+$ or $\gamma^* p \to \rho^+$ where for the latter process the GPDs are defined by

$$\begin{aligned}
&\frac{1}{2}\int \frac{dz^-}{2\pi}\, e^{ixP^+z^-} \langle n(p')|\, \bar{d}(-\frac{1}{2}z)\, \gamma^+ u(\frac{1}{2}z)\ |p(p)\rangle\Big|_{z^+=0,\, z_T=0} \\
&= \frac{1}{2P^+}\left[H^{du}_{p\to n}(x,\xi,t)\, \bar{u}(p')\gamma^+ u(p) + E^{du}_{p\to n}(x,\xi,t)\, \bar{u}(p')\frac{i\sigma^{+\alpha}\Delta_\alpha}{2m} u(p) \right] .
\end{aligned} \tag{2.47}$$

The problem appearing in the phenomenological description of such process is to find a appropriate model for the transition GPDs like H^{ud}. Unfortunately most of the models discussed in Sect. 2.4 and especially the widely used double distribution model are made for single quark flavors. In [66] it was shown how the transition GPDs are related to the flavor diagonal ones. In the case of the $p \to n$ transition one finds

$$H^{du}_{p\to n} = H^{ud}_{n\to p} = H^u_p - H^d_p\,. \tag{2.48}$$

In Chapter 3 we will also calculate cross sections for the the transitions $p \to \Lambda$ and $p \to \Sigma$ where an explicit exchange of strange quarks take place. The transition GPDs for this processes are defined in (3.9) and can be also related to the flavor diagonal GPDs through SU(3) flavor symmetry [37, 67]. One obtains the following relations

$$\begin{aligned} H^{su}_{p\to\Lambda} &= -\frac{1}{\sqrt{6}}\left[2H^u_p - H^d_p - H^s_p\right] , \\ H^{su}_{p\to\Sigma} &= -\frac{1}{\sqrt{2}}\left[H^d_p - H^s_p\right] , \\ H^{sd}_{p\to\Sigma^+} &= H^s_p - H^d_p . \end{aligned} \tag{2.49}$$

For the GPDs E and $\tilde{H}$ one has analogous expressions. For the GPD $\tilde{E}$ one expects large effects due to flavor SU(3) breaking effects due to the difference of the pion and kaon mass. We will give a list of the most common transition GPDs in Table 3.1.

3

Exclusive processes in semi inclusive reactions

As described in the introduction exclusive processes offer the only opportunity to access the generalized parton distributions. Describing exclusive reaction in the right manner effects also an other type of reactions which are the deep inelastic semi inclusive reactions. In this kind of reactions one observes a single hadron, which carries the momentum fraction z of the photon energy in the target rest frame, in a finale state with large multiplicity. It exist also an QCD factorization theorem for this kind of processes which states that the semi-inclusive cross section can be expressed in terms of the distribution functions of the partons in the targe and of the corresponding fragmentation functions into the observed hadron. The latter functions describe in principle the probability that a single parton of the target hadronizes into a hadron. With this one is able to tag the the active parton via its fragmentation properties which has recently be used for a flavor decomposition of polarized quark and antiquark distributions in the semi-inclusive production of pions and kaons [68]. In addition, measurements of azimuthal asymmetries in semi-inclusive pion or kaon production, such as the Collins and Sievers asymmetries for polarized targets [69], provide interesting informations about the distribution of the spin and transverse momentum carried by quarks and antiquarks in the nucleon.

Although the Bjorken limit for semi-inclusive electroproduction implies a large average of multiplicity of the produced hadronic system there can appear situations in which individual exclusive channels play an important role. Especially in in fixed-target experiments the

limited photon energy restricts the phase space for the quark fragmentation, in particular at large z. And in addition du to the relative low photon virtuality Q^2 the suppression of individual exclusive cross sections, which drop faster with Q^2 in comparison to the semi-inclusive ones, may not be effective. There exists also phenomenological studies which suggest that a large contribution to $\pi^\pm$ production comes from exclusive ρ^0 production, with subsequent decay $\rho^0 \to \pi^+\pi^-$ [70, 71]. The cross sections for exclusive ρ^0 electroproduction have been measured by the HERMES and CLASS experiments, including also the ratio for longitudinal and transverse photons [72–77]. It is natural to ask whether the strange vector mesons ϕ and $K^\star$ play an equally important role in semi-inclusive production of kaons and whether other exclusive channels may be important too. A quantitative answer to these questions will help to delineate the limits of the kinematic region where semi-inclusive data can be analyzed using the factorization theorem.

In this chapter we study the role of exclusive channels in semi-inclusive production on the basis of the factorization theorem for hard exclusive processes. We will do this investigation in two different steps. Firstly we evaluate the longitudinal cross section for exclusive production production of pseudoscalar and vector mesons in the leading-twist approximation and at leading order in the strong coupling. We will focus on π, K and ρ, ϕ, $K^\star$ production using the models described in Sect. 2.4. We explore uncertainties in the obtained cross sections, in particular those du to the generalized part distributions, which are still largely unknown. The uncertainties persist if higher-order and higher-twist corrections are included. We will give a detailed analysis of the higher-order corrections in Chapter 4. Seen from a different perspective, these uncertainties indicate to which extent exclusive meson production is sensitive to GPDs and thus interesting in its own right. It is also known that exclusive meson production at moderate Q^2 is affected by substantial power corrections. For the production of ρ^0, ϕ and π^+ there is data or preliminary data, which we will use to assess the quantitative validity of or calculated cross sections. Secondly, we evaluate the contributions of these exclusive channels to semi-inclusive production of π and K and compare them with the results obtained from leading-twist quark fragmentation. For the exclusive meson production cross sections we rely on experimental data where possible, and only use our leading-twist calculation to estimate the *ratio* of cross sections for measured and unmeasured channels.

We will proceed as following in this chapter. In the first section we will summarize the leading-twist description of exclusive meson production and specify the model we used for the GPDs. In the second and third section we present our analysis of different pseudoscalar and vector meson production channels. In Sect. 3.4 we will discuss the limitations of our leading-order results and give a comparison with experimental data. Finally in Sect. 3.5. we present the contribution of exclusive channels to the semi-inclusive meson production in comparison with the leading-twist quark fragmentation.

3.1 Exclusive meson production in the leading-twist approximation

Let us consider the exclusive electroproduction process

$$e(k) \; + \; p(p) \;\; \rightarrow \;\; e(k') \; + \; M(q') \; + \; B(p'), \tag{3.1}$$

where M is a meson and B a baryon, and where four-momenta are indicated in parentheses. Throughout this work we assume beam and target to be unpolarized. We write $q = k - k'$, $\Delta = p' - p$, and use the standard kinematic variables which we introduced in Sect 2.1

$$t = \Delta^2, \qquad Q^2 = -q^2, \qquad W^2 = (p+q)^2, \qquad x_B = Q^2/(2pq), \qquad y = (pq)/(pk). \tag{3.2}$$

We respectively write m_p, m_B, m_M for the masses of the proton, the baryon B, and the meson M. With Hand's convention [78] for the virtual photon flux, the electroproduction cross section is given by

$$\frac{d\sigma(ep \to eMB)}{dQ^2\, dx_B\, dt} = \frac{\alpha_{em}}{2\pi} \frac{y^2}{1-\epsilon} \frac{1-x_B}{x_B} \frac{1}{Q^2} \left[\frac{d\sigma_T}{dt} + \epsilon \frac{d\sigma_L}{dt} \right] \tag{3.3}$$

in terms of the cross sections $d\sigma_T/dt$ and $d\sigma_L/dt$ of the $\gamma^* p \to MB$ subprocess for transverse and longitudinal γ^*, where

$$\epsilon = \frac{1 - y - (y x_B m_p/Q)^2}{1 - y + y^2/2 + (y x_B m_p/Q)^2} \tag{3.4}$$

is the ratio of longitudinal to transverse photon flux.

In the generalized Bjorken limit of large Q^2 at fixed x_B and fixed t, the process amplitude factorizes into a hard-scattering kernel convoluted with generalized parton distributions for the $p \to B$ transition and with the distribution amplitude of the meson [15]. Example graphs are shown in Fig. 2.3. In this limit the longitudinal cross section can be written as

$$\frac{d\sigma_L}{dt} = \frac{\alpha_{em}}{Q^6} \frac{x_B^2}{1-x_B} \Bigg\{ (1-\xi^2) |\mathcal{H}|^2 - \left[\frac{2\xi(m_B^2 - m_p^2) + t}{(m_B + m_p)^2} + \xi^2 \right] |\mathcal{E}|^2 - \left[\xi + \frac{m_B - m_p}{m_B + m_p} \right] 2\xi \;\; \mathrm{Re}\,(\mathcal{E}^* \mathcal{H}) \Bigg\} \tag{3.5}$$

for vector mesons, and as

$$\frac{d\sigma_L}{dt} = \frac{\alpha_{em}}{Q^6} \frac{x_B^2}{1-x_B} \Bigg\{ (1-\xi^2) |\tilde{\mathcal{H}}|^2 + \frac{(m_B - m_p)^2 - t}{(m_B + m_p)^2} \xi^2 |\tilde{\mathcal{E}}|^2 - \left[\xi + \frac{m_B - m_p}{m_B + m_p} \right] 2\xi \;\; \mathrm{Re}\,(\tilde{\mathcal{E}}^* \tilde{\mathcal{H}}) \Bigg\} \tag{3.6}$$

for pseudoscalar mesons M. The transverse cross section $d\sigma_T/dt$ is power suppressed by $1/Q^2$ compared with $d\sigma_L/dt$. Here we have in addition used the skewness variable

$$\xi = \frac{(p-p')(q+q')}{(p+p')(q+q')} \approx \frac{x_B}{2-x_B}, \tag{3.7}$$

where the approximation holds in the generalized Bjorken limit. Note that the prefactor in (3.5) and (3.6) can be rewritten as $x_B^2/(1-x_B) = 4\xi^2/(1-\xi^2)$. The quantities $\mathcal{H}$, $\mathcal{E}$ and $\tilde{\mathcal{H}}$, $\tilde{\mathcal{E}}$ are specific for each channel. Throughout this work we will take their leading order approximations in α_s. To be specific, we have

$$\begin{aligned}
\mathcal{H}_{K^{*+}\Lambda}(\xi,t) &= \frac{4\pi\alpha_s}{27} f_{K^*} \Bigg[\int_0^1 dz\, \frac{1}{z(1-z)}\, \phi_{K^{*+}}(z) \int_{-1}^1 dx\, \frac{2H_{p\to\Lambda}(x,\xi,t) + H_{p\to\Lambda}(-x,\xi,t)}{\xi - x - i\varepsilon} \\
&\qquad - \int_0^1 dz\, \frac{2z-1}{z(1-z)}\, \phi_{K^{*+}}(z) \int_{-1}^1 dx\, \frac{2H_{p\to\Lambda}(x,\xi,t) - H_{p\to\Lambda}(-x,\xi,t)}{\xi - x - i\varepsilon} \Bigg], \\
\tilde{\mathcal{H}}_{K^{+}\Lambda}(\xi,t) &= \frac{4\pi\alpha_s}{27} f_{K} \Bigg[\int_0^1 dz\, \frac{1}{z(1-z)}\, \phi_{K^{+}}(z) \int_{-1}^1 dx\, \frac{2\tilde{H}_{p\to\Lambda}(x,\xi,t) + \tilde{H}_{p\to\Lambda}(-x,\xi,t)}{\xi - x - i\varepsilon} \\
&\qquad - \int_0^1 dz\, \frac{2z-1}{z(1-z)}\, \phi_{K^{+}}(z) \int_{-1}^1 dx\, \frac{2\tilde{H}_{p\to\Lambda}(x,\xi,t) - \tilde{H}_{p\to\Lambda}(-x,\xi,t)}{\xi - x - i\varepsilon} \Bigg]
\end{aligned} \tag{3.8}$$

for $\gamma^* p \to K^{*+}\Lambda$ and $\gamma^* p \to K^+\Lambda$, respectively, with analogous expressions for $\mathcal{E}_{K^{*+}\Lambda}$ and $\tilde{\mathcal{E}}_{K^+\Lambda}$. The GPDs for the $p \to \Lambda$ transition are defined as

$$\begin{aligned}
&\frac{1}{2}\int \frac{dz^-}{2\pi}\, e^{ixP^+z^-} \langle \Lambda |\, \bar{s}(-\tfrac{1}{2}z)\, \gamma^+ u(\tfrac{1}{2}z)\, |p\rangle \Big|_{z^+=0,\, z_T=0} \\
&\qquad = \frac{1}{2P^+} \left[H_{p\to\Lambda}(x,\xi,t)\, \bar{u}\gamma^+ u + E_{p\to\Lambda}(x,\xi,t)\, \bar{u} \frac{i\sigma^{+\alpha}\Delta_\alpha}{m_\Lambda + m_p} u \right], \\
&\frac{1}{2}\int \frac{dz^-}{2\pi}\, e^{ixP^+z^-} \langle \Lambda |\, \bar{s}(-\tfrac{1}{2}z)\, \gamma^+\gamma_5\, u(\tfrac{1}{2}z)\, |p\rangle \Big|_{z^+=0,\, z_T=0} \\
&\qquad = \frac{1}{2P^+} \left[\tilde{H}_{p\to\Lambda}(x,\xi,t)\, \bar{u}\gamma^+\gamma_5 u + \tilde{E}_{p\to\Lambda}(x,\xi,t)\, \bar{u} \frac{\gamma_5\Delta^+}{m_\Lambda + m_p} u \right],
\end{aligned} \tag{3.9}$$

where we use light-cone coordinates as defined in (2.11) and assume light-cone gauge $A^+ = 0$. For brevity we have not displayed the momentum and polarization dependence of the baryon spinors on the right-hand sides. GPDs for other transitions are defined in full analogy. The integrals over meson distribution amplitudes in (3.8) can be expressed as

$$\int_0^1 dz\, \frac{1}{z(1-z)}\, \phi(z) = 6\Big[1 + \sum_{n=1}^\infty a_{2n}\Big], \qquad \int_0^1 dz\, \frac{2z-1}{z(1-z)}\, \phi(z) = 6 \sum_{n=1}^\infty a_{2n-1} \tag{3.10}$$

Table 3.1. Combinations of proton GPDs to be used for various channels $\gamma p \to MB$ at the place of $2H_{p\to\Lambda}(x,\xi,t) + H_{p\to\Lambda}(-x,\xi,t)$ or $2\tilde{H}_{p\to\Lambda}(x,\xi,t) + \tilde{H}_{p\to\Lambda}(-x,\xi,t)$ in (3.8). All distributions are to be evaluated at arguments x, ξ, t, with H^q, $\tilde{H}^q$ and H^g as defined in [38] and $H^{\bar{q}}$, $\tilde{H}^{\bar{q}}$ given above (3.12).

$\rho^+ n$	$2[H^u - H^d] - [H^{\bar{u}} - H^{\bar{d}}]$
$\rho^0 p$	$\frac{1}{\sqrt{2}}\Big([2H^u + H^d] + [2H^{\bar{u}} + H^{\bar{d}}] + \frac{9}{4}\, x^{-1} H^g \Big)$
ωp	$\frac{1}{\sqrt{2}}\Big([2H^u - H^d] + [2H^{\bar{u}} - H^{\bar{d}}] + \frac{3}{4}\, x^{-1} H^g \Big)$
$K^{*+}\Lambda$	$-\frac{1}{\sqrt{6}}\Big(2[2H^u - H^d - H^s] - [2H^{\bar{u}} - H^{\bar{d}} - H^{\bar{s}}] \Big)$
$K^{*+}\Sigma^0$	$-\frac{1}{\sqrt{2}}\Big(2[H^d - H^s] - [H^{\bar{d}} - H^{\bar{s}}] \Big)$
$K^{*0}\Sigma^+$	$[H^d - H^s] + [H^{\bar{d}} - H^{\bar{s}}]$
ϕp	$-\Big([H^s + H^{\bar{s}}] + \frac{3}{4}\, x^{-1} H^g \Big)$
$\pi^+ n$	$2[\tilde{H}^u - \tilde{H}^d] + [\tilde{H}^{\bar{u}} - \tilde{H}^{\bar{d}}]$
$\pi^0 p$	$\frac{1}{\sqrt{2}}\Big([2\tilde{H}^u + \tilde{H}^d] - [2\tilde{H}^{\bar{u}} + \tilde{H}^{\bar{d}}] \Big)$
$K^+\Lambda$	$-\frac{1}{\sqrt{6}}\Big(2[2\tilde{H}^u - \tilde{H}^d - \tilde{H}^s] + [2\tilde{H}^{\bar{u}} - \tilde{H}^{\bar{d}} - \tilde{H}^{\bar{s}}] \Big)$
$K^+\Sigma^0$	$-\frac{1}{\sqrt{2}}\Big(2[\tilde{H}^d - \tilde{H}^s] + [\tilde{H}^{\bar{d}} - \tilde{H}^{\bar{s}}] \Big)$
$K^0\Sigma^+$	$[\tilde{H}^d - \tilde{H}^s] - [\tilde{H}^{\bar{d}} - \tilde{H}^{\bar{s}}]$

through their coefficients in the expansion

$$\phi(z) = 6z(1-z)\Big[1 + \sum_{n=1}^{\infty} a_n\, C_n^{3/2}(2z-1)\Big] \tag{3.11}$$

on Gegenbauer polynomials, where z is the light-cone momentum fraction carried by the quark in the meson. Note that odd Gegenbauer coefficients a_{2n-1} describe an asymmetry in the momentum distribution of the quark and antiquark in the meson. They can be nonzero for K and K^* due to flavor SU(3) breaking. In (3.8) to (3.11) we have not displayed the logarithmic dependence on the renormalization scale in α_s and on the factorization scale in the GPDs and the distribution amplitudes.

Using flavor SU(3) symmetry one can relate the transition GPDs from the proton to a hyperon to the distributions $H^q(x,\xi,t)$ for quark flavor q in the proton [37, 39]. This gives in particular $H_{p\to\Lambda} = -[2H^u - H^d - H^s]/\sqrt{6}$ and an analogous relation for $\tilde{H}_{p\to\Lambda}$. We use these relations throughout, except for $\tilde{E}$, where there are large effects of SU(3) breaking as

we shall see below. Results analogous to (3.8) hold for all meson channels we consider, see e.g. [37,38,79], and we have collected the relevant combinations of GPDs in Table 3.1. There we have introduced $H^{\bar q}(x,\xi,t) = -H^q(-x,\xi,t)$ and $\tilde H^{\bar q}(x,\xi,t) = \tilde H^q(-x,\xi,t)$, so that for $x > 0$ we have simple forward limits

$$H^q(x,0,0) = q(x), \quad H^{\bar q}(x,0,0) = \bar q(x), \quad \tilde H^q(x,0,0) = \Delta q(x), \quad \tilde H^{\bar q}(x,0,0) = \Delta\bar q(x) \tag{3.12}$$

in terms of the unpolarized and polarized quark and antiquark densities in the proton. For gluons we have $H^g(x,0,0) = xg(x)$, which is the origin of the additional factors x^{-1} in the entries for ρ^0, ω, ϕ. In addition to the replacements in Table 3.1 one has of course to take the appropriate meson distribution amplitude and meson decay constants in (3.8). For the latter we will take $f_\pi = 131\,\text{MeV}$, $f_K = 160\,\text{MeV}$, and

$$f_\rho = 209\,\text{MeV}, \quad f_\omega = 187\,\text{MeV}, \quad f_\phi = 221\,\text{MeV}, \quad f_{K^*} = 218\,\text{MeV} \tag{3.13}$$

from [80].

For α_s in (3.8) we will take the one-loop running coupling at the scale Q^2, with three active quark flavors and $\Lambda_{\text{QCD}} = 200\,\text{MeV}$. This gives $\alpha_s = 0.34$ at $Q^2 = 2.5\,\text{GeV}^2$, where we will show most of our numerical results. We will not attempt more refined choices of renormalization scale, as were for instance explored in [81], since our principal use of the leading-order calculation will be to describe the *relative* size of cross sections for different exclusive channels.

For the calculation of exclusive cross sections we use simple models of GPDs based one the double distribution ansatz as described in Sect. 2.4. As explained there the models have been developed in [37,65] and been used in most phenomenological analyses so far. Our aim here is not to improve on these models, but instead to see by how much predictions can vary *within* the given framework. We take a factorizing t dependence for H and $\tilde H$ described in Sect. 2.4

$$\begin{aligned} H^q(x,\xi,t) &= H^q(x,\xi)\,F_1^p(t), & H^g(x,\xi,t) &= H^g(x,\xi)\,F_1^p(t), \\ \tilde H^q(x,\xi,t) &= \tilde H^q(x,\xi)\,G_A(t)/G_A(0), \end{aligned} \tag{3.14}$$

where $F_1^p(t)$ is the electromagnetic Dirac form factor of the proton and $G_A(t)$ the isovector axial form factor of the nucleon. A more refined version of the model would take different combinations of the proton and neutron form factors for H^u and H^d, but for the low values of t dominating integrated cross sections, $F_1^n(t)$ is much smaller than $F_1^p(t)$ and we simply neglect it. In this sense (3.14) is consistent with the sum rule for the first moment $\int dx\, H^q(x,\xi,t)$. The ansatz for $\tilde H^q$ is consistent with the sum rule for $\int dx\, \tilde H^q(x,\xi,t)$ to the extent that the (unknown) isoscalar axial form factor has the same t dependence as the isovector one. In our numerical evaluations we take the familiar parameterizations

$$F_1^p(t) = \frac{4m_p^2 - 2.8t}{4m_p^2 - t}\,\frac{1}{[1 - t/(0.71\,\text{GeV}^2)]^2}\,, \qquad \frac{G_A(t)}{G_A(0)} = \frac{1}{[1 - t/(1.05\,\text{GeV}^2)]^2}\,. \tag{3.15}$$

We note that for the gluon distribution H^g there is no reason a priori to take the electromagnetic form factor $F_1^p(t)$ in the ansatz (3.14). It turns out, however, that $F_1^p(t)$ is well approximated by a dipole form $F_1^p(t) = [1 - t/(0.98\,\mathrm{GeV}^2)]^{-2}$ for t up to about $3\,\mathrm{GeV}^2$ [82] and thus close to the two-gluon form factor advocated in [83].

It is rather certain that the ansatz (3.14) is too simple and can at best reflect the correct t dependence in a limited range of x and ξ [37,82,84]. For x and ξ in the valence region, say above 0.2, the decrease of GPDs with t is most likely less steep than the one of $F_1^p(t)$ and $G_A(t)$. Whereas there are phenomenological constraints of the t behavior of valence quark GPDs [82] and for gluons at small x [83], the behavior for sea quarks is largely unknown, and sea quarks are important for the x_B region around 0.1 we will be mostly concerned with. Furthermore, the t dependence of meson production at moderate Q^2 is strongly affected by power corrections, as is for instance seen in the Q^2 dependence of the logarithmic slope $B = (\partial/\partial t) \log(d\sigma/dt)|_{t=0}$ for ρ^0 production at very high energies [85]. We note that our ansatz (3.14) gives a slope parameter $B \approx 4\,\mathrm{GeV}^2$, which may be quite realistic for x_B around 0.1. Furthermore, cross section ratios should be less affected by the insufficiency of our ansatz, since they are sensitive only to the relative t dependence of the contributions from different quark flavors and from gluons.

For the t independent functions in (3.14) we use the double distribution based ansatz of [65], whose ingredients are the usual parton densities at a given factorization scale μ and a so-called profile parameter b, where μ and b are to be regarded as free parameters of the model. Explicit expressions are given in App. A. We will not take into account the evolution of GPDs, which should not be too problematic since our numerical applications will stay within a rather narrow range of Q^2.

The modeling of the nucleon helicity-flip distributions E^q and E^g is still at an early stage of development, with the most advanced considerations focused on the valence quark domain [37, 82]. Fortunately, contributions from E enter the unpolarized meson production cross section (3.5) with prefactors that are quite small in the kinematics we are most interested in. Following the argumentation of [86] that E is not much larger than H for a given parton species, we hence neglect E altogether in our cross section estimates.

The distributions $\tilde{E}$ cannot be neglected since they receive contributions proportional to ξ^{-1} that compensate the kinematic prefactors in the cross section (3.6). We model them as described in Sect. 2.4 as

$$\begin{aligned}
\tilde{E}_{p\to n}(x,\xi,t) &= \frac{\theta(|x|\leq\xi)}{2\xi}\,\phi_\pi\left(\frac{x+\xi}{2\xi}\right)\frac{2m_p f_\pi\, g_{\pi NN}}{m_\pi^2 - t}\,\frac{\Lambda^2 - m_\pi^2}{\Lambda^2 - t}, \\
\tilde{E}_{p\to \Lambda}(x,\xi,t) &= \frac{\theta(|x|\leq\xi)}{2\xi}\,\phi_K\left(\frac{x+\xi}{2\xi}\right)\frac{(m_p + m_\Lambda) f_K\, g_{KN\Lambda}}{m_K^2 - t}\,\frac{\Lambda^2 - m_K^2}{\Lambda^2 - t},
\end{aligned} \tag{3.16}$$

where the distribution amplitudes ϕ are the same as those introduced above. For the coupling constants we take the value $g_{\pi NN} = 2m_p G_A(0)/f_\pi \approx 14.7$ from the Goldberger-Treiman relation and $g_{KN\Lambda} \approx -13.3$ from [87]. Continued to the points $t = m_\pi^2$ or $t = m_K^2$ in the unphysical region, the expressions (3.16) become the well-known results from pion or kaon exchange [59, 60, 87]. These can only be expected to be good approximations for t

close to the squared meson masses, and for $-t$ of several $0.1\,\mathrm{GeV}^2$ are to be regarded as extrapolations. In (3.16) we have included form factors that cut off the $1/(m_M^2 - t)$ behavior of the pure pole terms when $-t$ becomes large. As default value for the cut-off mass we will take $\Lambda = 0.8\,\mathrm{GeV}$ [88] and study the sensitivity of results to the precise value of this parameter. We note that for $\Lambda = 0.6\,\mathrm{GeV}$ and $-t \leq 1\,\mathrm{GeV}^2$ the above form of $\tilde{E}_{p\to n}$ differs by less than 15% from the corresponding term calculated in the chiral quark-soliton model as given in Eq. (4.39) of [60].

With this model for $\tilde{E}$ the longitudinal cross section for $\gamma^* p \to \pi^+ n$ takes the form

$$\frac{d\sigma_L}{dt} = \frac{\alpha_{em}}{Q^6}\frac{x_B^2}{1-x_B}\left\{(1-\xi^2)|\tilde{\mathcal{H}}(\xi,t)|^2 - 2m_p\,\xi\ \mathrm{Re}\ \tilde{\mathcal{H}}(\xi,t)\, Q^2 F_\pi(Q^2)\,\frac{g_{\pi NN}}{m_\pi^2 - t}\,\frac{\Lambda^2 - m_\pi^2}{\Lambda^2 - t}\right.$$
$$\left. - \frac{t}{4}\left[Q^2 F_\pi(Q^2)\,\frac{g_{\pi NN}}{m_\pi^2 - t}\,\frac{\Lambda^2 - m_\pi^2}{\Lambda^2 - t}\right]^2\right\}, \tag{3.17}$$

where

$$F_\pi(Q^2) = \frac{2\pi\alpha_s}{9}\frac{f_\pi^2}{Q^2}\left[\int_0^1 dz \frac{1}{z(1-z)}\,\phi_\pi(z)\right]^2 \tag{3.18}$$

is the electromagnetic pion form factor to leading order in α_s and $1/Q^2$. An similar expression involving $F_{K^+}(Q^2)$ is obtained for $\gamma^* p \to K^+\Lambda$ according to (3.6) and (3.16). Note that the the $|\tilde{\mathcal{E}}|^2$ term in $d\sigma_L/dt$ has no x_B dependence other than from the explicit factor $x_B^2/(1-x_B)$. Within our model the $|\tilde{\mathcal{H}}|^2$ term reflects the behavior of the polarized parton distributions at momentum fractions of order ξ, and its contribution to $d\sigma_L/dt$ can very roughly be represented by $[\xi\Delta q(\xi)]^2$.

3.2 Exclusive pseudoscalar meson production

In this and the next section we present numerical results for cross sections of exclusive meson production. Our main focus is to compare the rates for different production channels and to investigate model uncertainties. Comparison with data in Sect. 3.4 will allow us to estimate the shortcomings of the leading approximation in $1/Q^2$ and in α_s, on which our calculations are based.

The factorization theorem for exclusive meson production requires t to be much smaller than Q^2. For definiteness we will give all meson cross sections in this paper integrated over $-t$ from its smallest kinematically allowed value $-t_0$ to an upper limit of $1\,\mathrm{GeV}^2$. In generalized Bjorken kinematics we have

$$-t_0 \approx \frac{2\xi^2(m_B^2 + m_p^2) + 2\xi(m_B^2 - m_p^2)}{1-\xi^2} \tag{3.19}$$

with ξ defined in (3.7). For low enough x_B most of the cross section should be accumulated in this t region, whereas for large x_B our cross sections decrease to the extent that $-t_0$ approaches $1\,\mathrm{GeV}^2$.

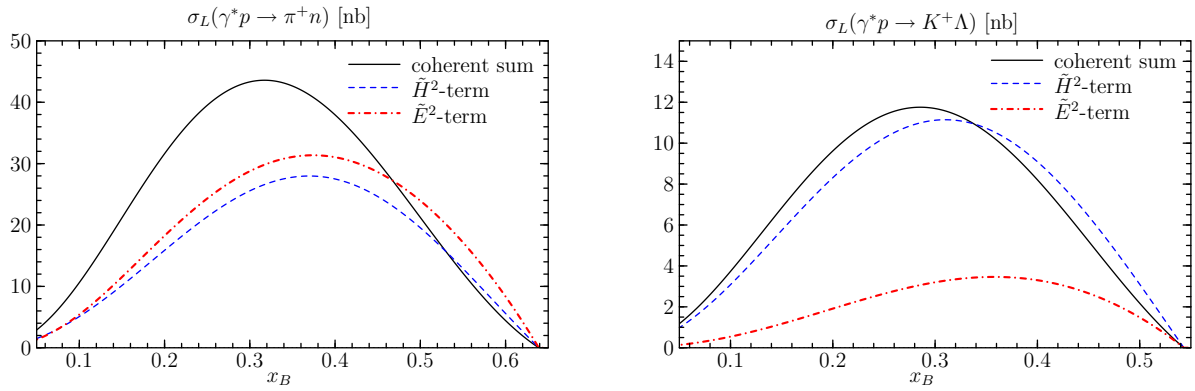

Figure 3.1. Leading-twist cross sections for $\gamma_L^* p \to \pi^+ n$ (left) and $\gamma_L^* p \to K^+ \Lambda$ (right) for $Q^2 = 2.5\,GeV^2$. An upper cut on $-t$ of $1\,GeV^2$ has been applied here and in all further plots of this paper. Shown are the individual contributions from $|\tilde{\mathcal{H}}|^2$ and $|\tilde{\mathcal{E}}|^2$, and their coherent sum according to (3.6).

To begin with, let us investigate the relative importance of the contributions from $\tilde{\mathcal{H}}$ and $\tilde{\mathcal{E}}$ to π^+ and K^+ production with our model assumptions. As is seen in Fig. 3.1, exclusive π^+ production receives comparable contributions from both the $|\tilde{\mathcal{H}}|^2$ and the $|\tilde{\mathcal{E}}|^2$ term in (3.6), as well as from the interference term proportional to $\mathrm{Re}\,(\tilde{\mathcal{E}}^* \tilde{\mathcal{H}})$. Note that the relative weight of the contributions is different for $d\sigma_L/dt$, where it strongly depends on t given the characteristic t dependence of the pion pole term (3.16). In K^+ production the influence of $\tilde{\mathcal{E}}$ is less prominent, since the pole factor $(m_K^2 - t)^{-1}$ gives much less enhancement at small t than $(m_\pi^2 - t)^{-1}$.

To obtain the curves in Fig. 3.1 we have made a number of choices in the non-perturbative input to the cross section, which we now discuss in turn. In Fig. 3.2 we show how the cross section changes when we vary the parameter Λ in our model for $\tilde{E}$, where $\Lambda = 1.3\,\mathrm{GeV}$ represents an upper limit of the values discussed in the phenomenological study [88], and $\Lambda = 0.6\,\mathrm{GeV}$ approximates the form factor dependence obtained for the pion pole contribution in [60], as discussed at the end of Sect. 3.1. Omitting the form factor altogether (tantamount to setting $\Lambda \to \infty$) the π^+ cross section would increase by more than a factor 1.4 and the K^+ cross section by more than a factor 1.7 compared with our default choice $\Lambda = 0.8\,\mathrm{GeV}$. Also, the cross sections would considerably increase when raising the upper cutoff in the $-t$ integration above $1\,\mathrm{GeV}^2$. In other words, the cross section would then receive substantial contributions from values of t far away from the region where the pion or kaon pole term can be regarded as a reasonable approximation of $\tilde{E}$.

For the pion distribution amplitude we have taken the asymptotic form $\phi_\pi(z) = 6z(1-z)$ under scale evolution, which is close to what can be extracted from data on the γ–π transition form factor, see e.g. [89,90]. The study in [90] quotes limits on $a_2 + a_4$ at scale $\mu = 1\,\mathrm{GeV}$ of about ± 0.3 if all other Gegenbauer coefficients are set to zero. This corresponds to a change of the $\gamma^* p \to \pi^+ n$ cross section by a factor $(1 + a_2 + a_4)^2$ between 0.5 and 1.7. For the K^+ distribution amplitude we have taken the asymptotic form as well. Figure 3.3 shows how the

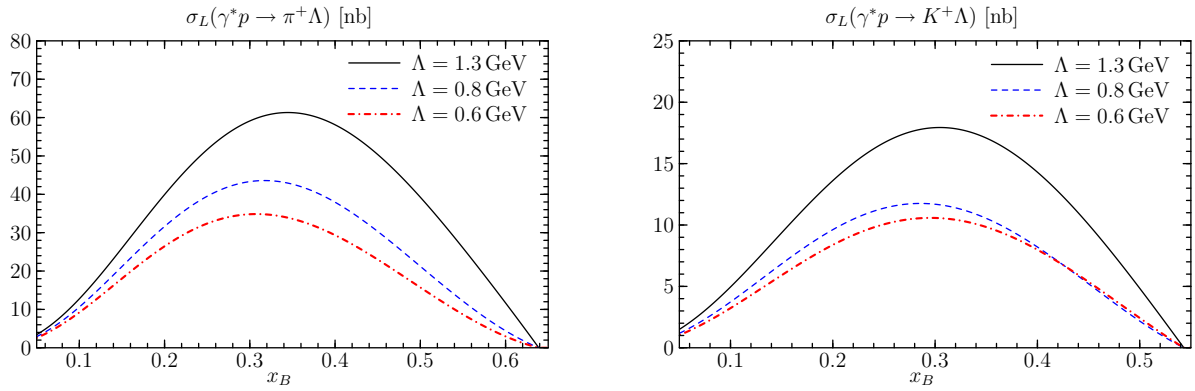

Figure 3.2. Leading-twist cross section for $\gamma_L^* p \to \pi^+ n$ (left) and $\gamma_L^* p \to K^+\Lambda$ (right) at $Q^2 = 2.5\,GeV^2$ obtained with different values of the parameter Λ in the form factor multiplying the pion or kaon pole contribution in (3.16).

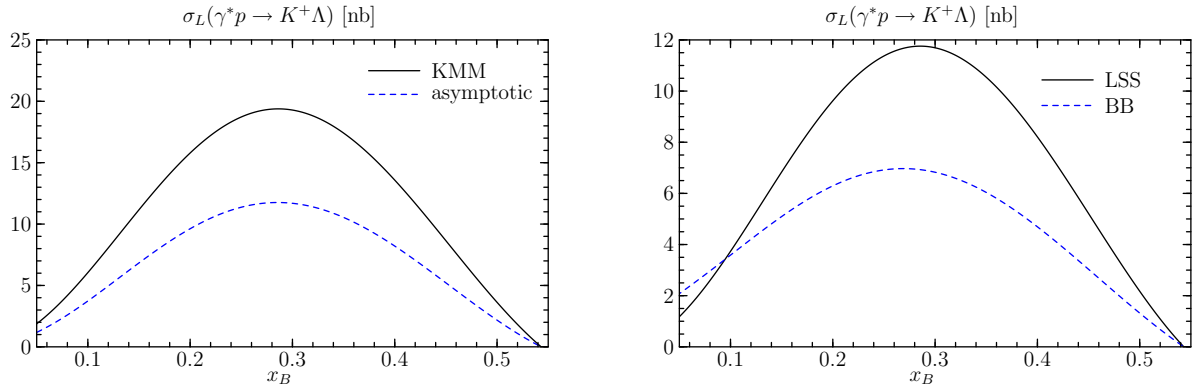

Figure 3.3. Left: Leading-twist cross section for $\gamma_L^* p \to K^+\Lambda$ at $Q^2 = 2.5\,GeV^2$ calculated with the asymptotic kaon distribution amplitude and with the one from Khodjamirian, Mannel and Melcher (KMM) [91]. Right: The same cross section calculated with different parton distributions in the model for $\tilde{H}$. The distributions from Leader, Sidorov and Stamenov (LSS) [93] and from Blümlein and Böttcher (BB) [94] are taken at a scale $\mu = 1\,GeV$.

K^+ cross section changes if instead one takes $a_1 = -0.05$ and $a_2 = 0.27$ at $\mu = 1\,\mathrm{GeV}$ from the QCD sum rule calculation [91]. This value of a_1 is compatible with the findings of [92].

For our model of $\tilde{H}$ we have taken a double distribution ansatz with a profile parameter $b = 1$ (see Sect. 3.1 and App. A). Taking $b = 2$ instead would decrease the K^+ cross section by a factor of approximately 0.6. The pion cross section changes less, because of the relative weight of $\tilde{\mathcal{H}}$ and $\tilde{\mathcal{E}}$. A more important source of uncertainty is however due to the polarized quark densities used as input to model $\tilde{H}$. As a default we have used the LO parameterization from [93] at a scale $\mu = 1\,\mathrm{GeV}$. Using instead the LO parameterization in scenario 1 of [94] at the same scale, the K^+ cross section changes as shown in Fig. 3.3. Note that any uncertainty on parton distributions is amplified in the meson production cross section, where GPDs appear squared.

Let us now comment on other pseudoscalar channels. The cross sections for $\gamma^* p \to K^+\Sigma^0$

is about an order of magnitude smaller than the one for $\gamma^* p \to K^+\Lambda$, as is seen in the numerical study of [87]. For the contribution from $\tilde{\mathcal{H}}$ this can be understood from the flavor structure in Table 3.1, where for a rough estimate one may concentrate on the dominant terms $\tilde{H}^u$ and $\tilde{H}^d$. For current parameterizations of polarized parton densities the combination $[2\tilde{H}^u - \tilde{H}^d]/\sqrt{3}$ for Λ production is clearly larger than $\tilde{H}^d$ in the analogous expression for the Σ^0 channel. Concerning the contribution from $\tilde{\mathcal{E}}$, the coupling $g_{KN\Sigma^0}$ is about three times smaller than $g_{KN\Lambda}$ appearing in (3.16), see [87]. Along the same lines one can see that the cross section for $\gamma^* p \to K^0\Sigma^+$ is of similar size as the one for $\gamma^* p \to K^+\Sigma^0$.

The channel $\gamma^* p \to \pi^0 p$ does not receive contributions from the pion pole term in (3.16) because of charge conjugation invariance, so that in our model it is entirely given by the contribution from $\tilde{\mathcal{H}}$. In Table 3.1 we see that the combination $2\tilde{H}^u + \tilde{H}^d$ for π^0 production is to be compared with $\sqrt{2}[\tilde{H}^u - \tilde{H}^d]$ for $\gamma^* p \to \pi^+ n$, which is of comparable size. One thus expects the π^0 cross section to be similar to the $|\tilde{\mathcal{H}}|^2$ part of the π^+ cross section.

The exclusive channels $\gamma^* p \to \eta p$ and $\gamma^* p \to \eta' p$ involve the combination $2\tilde{H}^u - \tilde{H}^d$ instead of $2\tilde{H}^u + \tilde{H}^d$ in the π^0 case, which is somewhat larger because the polarized distributions Δu and Δd have opposite sign. The strange quark contribution to these channels involves $\tilde{H}^s - \tilde{H}^{\bar{s}}$, which vanishes in our model with polarized parton distributions satisfying $\Delta s(x) = \Delta\bar{s}(x)$. A quantitative analysis requires the appropriate decay constants for the η and η', see for instance [95], but one can in general expect comparable cross sections for the π^0, η and η' channels.

3.3 Exclusive vector meson production

Within our model for the GPDs, the cross section for vector meson production is sensitive to unpolarized quark and gluon densities. To obtain an indication of uncertainties we have compared results with the LO distributions from CTEQ6 [12] and the LO distributions from MRST2001 [96]. For consistency we need LO rather than NLO parton densities, which unfortunately are not available in several of the most recent parton fits. We have checked that the NLO distributions from MRST2001 are in good agreement with those in the MRST2002 and MRST2004 analyses [97] for quark and antiquark densities down to about $x \sim 10^{-2}$ and for the gluon density down to about $x \sim 10^{-1}$. Comparing the LO distributions of CTEQ6 and MRST2001 at a scale $\mu^2 = 1.2\,\mathrm{GeV}^2$ (which is the lowest value accepted by the code for the MRST2001 parameterization) we find that the CTEQ6 gluon is larger for $x \lesssim 10^{-1}$ and smaller for $x \gtrsim 10^{-1}$. The u quark distribution is quite similar in the two sets for $x \gtrsim 10^{-2}$, whereas the s quark is significantly smaller for CTEQ6. The distributions for d, $\bar{u}$, $\bar{d}$ are quite similar for $x \gtrsim 10^{-1}$ and larger for CTEQ6 at smaller x. The LO parameterization of Alekhin [98] has significantly larger u and $\bar{u}$ distributions and a smaller gluon than the two other sets. At $\mu^2 = 1.2\,\mathrm{GeV}^2$ it has however almost no strange quarks in the proton, which we do not consider physically very plausible and which is in clear contrast with the results of CTEQ6, where a dedicated analysis of data constraining the strangeness distribution was performed. Since our study is crucially dependent on the flavor structure of parton

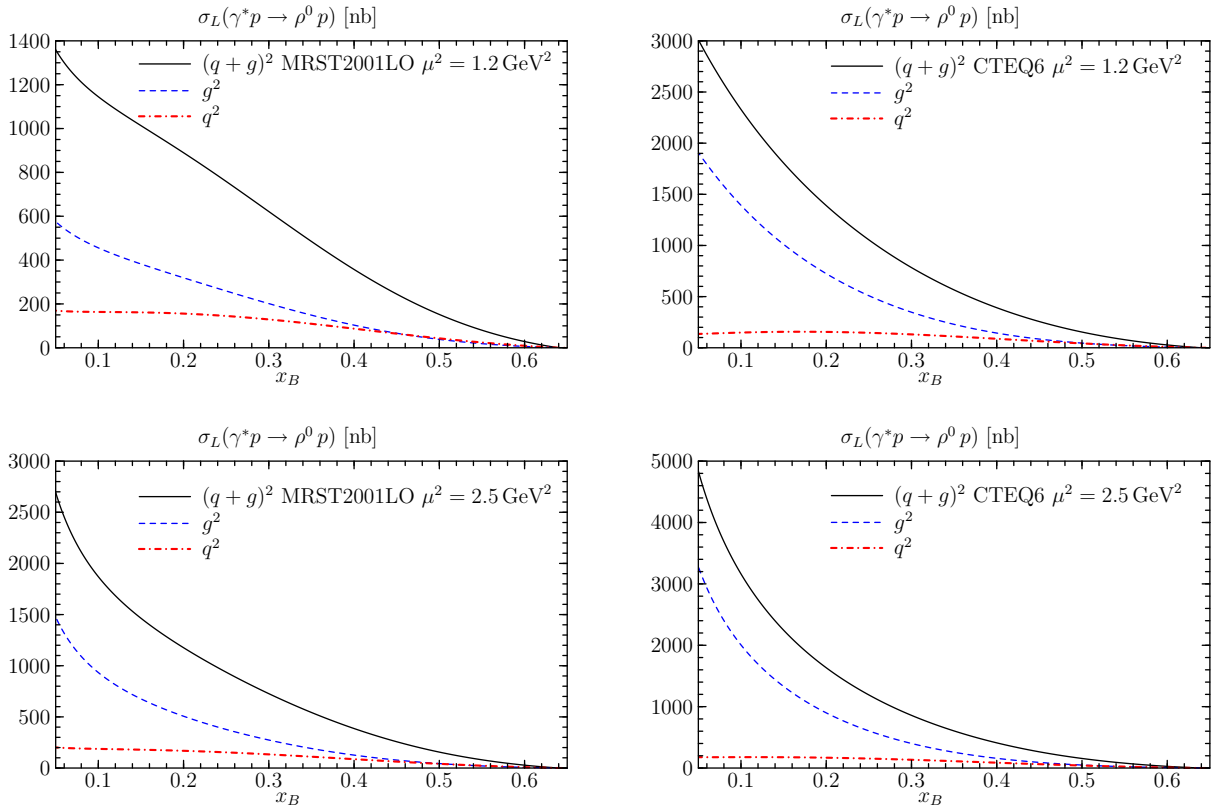

Figure 3.4. Leading-twist cross section for $\gamma_L^* p \to \rho^0 p$ at $Q^2 = 2.5\ GeV^2$. Shown are the individual contributions from quark and gluon distributions and their coherent sum. The parton densities in the double distribution model are taken at scale $\mu^2 = 1.2\ GeV^2$ for the upper and at $\mu^2 = 2.5\ GeV^2$ for the lower plots.

distributions, we have therefore not used [98]. Comparing the different parton sets at the higher scale $\mu^2 = 2.5\,\mathrm{GeV}^2$ we find a very similar picture. In the double distribution model of GPDs we take the profile parameter $b = 2$ for both quark and gluon distributions. For all mesons we take the asymptotic shape of the distribution amplitude, given that no direct experimental information is available for them. Theoretical estimates do not give stronger deviations from the asymptotic form than those we discussed for pseudoscalar mesons, see e.g. the compilation in [80]. In Fig. 3.4 we show the individual contributions from quark and gluon distributions to the ρ^0 cross section as well as their coherent sum. The clear difference between the CTEQ6 and MRST2001 result reflects the current uncertainty on the usual parton densities at low scales in the relevant range of x. A striking feature is the clear dominance of the gluon distribution up to quite high values of x_B. Note that with our model of GPDs the convolutions $\mathcal{H}^q(\xi, t)$ and $\mathcal{H}^g(\xi, t)$ are sensitive to the forward parton distributions in a certain range of momentum fractions around ξ (see App. A). The strong dominance of gluon over quark distributions at small momentum fractions thus still shows its effect at x_B values above 10^{-1}. Note that we have taken the same t dependence for quark and gluon GPDs in our model (3.14), lacking phenomenological evidence to the contrary.

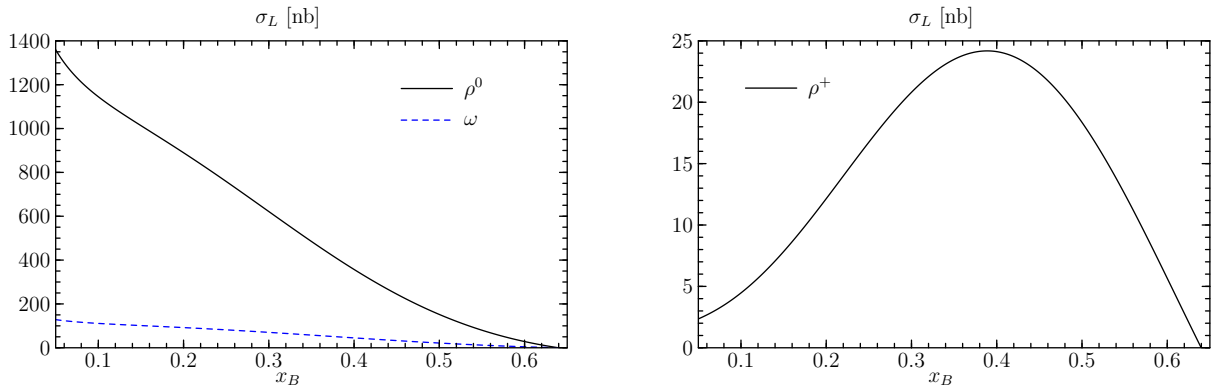

Figure 3.5. Leading-twist cross sections for $\gamma_L^* p \to \rho^0 p$ and $\gamma_L^* p \to \omega p$ (left) and for $\gamma_L^* p \to \rho^+ n$ (right) at $Q^2 = 2.5\ GeV^2$, obtained with the MRST2001 parton densities taken at $\mu^2 = 1.2\ GeV^2$.

Comparison of the t dependence e.g. for ρ^0 and ρ^+ production in equal kinematics could be of help here.

In our numerical calculations we have calculated the integrals (A.5) and (A.6) for the meson production amplitude with a lower cutoff at momentum fractions $x = 10^{-4}$. The cross section for $x_B = 0.05$ changes by less than 2% if we cut off at 10^{-5} or at 10^{-3}. It is diminished by about 10% with a cutoff at 0.005, which gives an indication of the relevance of momentum fractions which are an order of magnitude smaller than the x_B of the process in this model. Similar changes are observed for the individual quark and gluon distributions. We note that if we take a profile parameter $b = 1$ for quarks, the quark contribution to the cross section at $x_B = 0.05$ decreases by 10% when moving the cutoff on x from $x = 10^{-4}$ to $x = 10^{-3}$ and by 35% when moving it from $x = 10^{-4}$ to 0.005. Such a strong dependence on momentum fractions well below x_B seems difficult to understand in physical terms. We note that in the sea quark sector there are no strong theoretical arguments for taking $b = 1$, see Sect. 4.4 of [38].

In Fig. 3.4 we also observe a significant change of the gluon contribution to the cross section when changing the scale of the parton distributions in the double distribution ansatz (A.1). In contrast, the quark contribution changes by at most a factor of 1.3, reflecting the relatively weak scale evolution of quark and antiquark distributions compared with gluons in the relevant kinematic region. Changing the scale of the forward distributions in the double distribution model (A.1) gives a rough indication of how the actual GPDs evolve with μ^2 [65], so that the strong increase with μ^2 seen in Fig. 3.4 reflects a strong scale uncertainty of the leading-order approximation in α_s for channels involving gluon exchange. A full NLO analysis of meson production is possible using the results of [99] but beyond the scope of this work. We will use the smaller scale $\mu^2 = 1.2\,\mathrm{GeV}^2$ in our further studies, because the internal virtualities in the hard-scattering graphs of Fig. 2.3 are typically smaller than Q^2 (see also the study [100] of relevant scales in the small-x limit). Furthermore, the MRST2001 set gives a better description for the ratio of ϕ and ρ^0 production with our model (see below) and will hence be our default choice in the following.

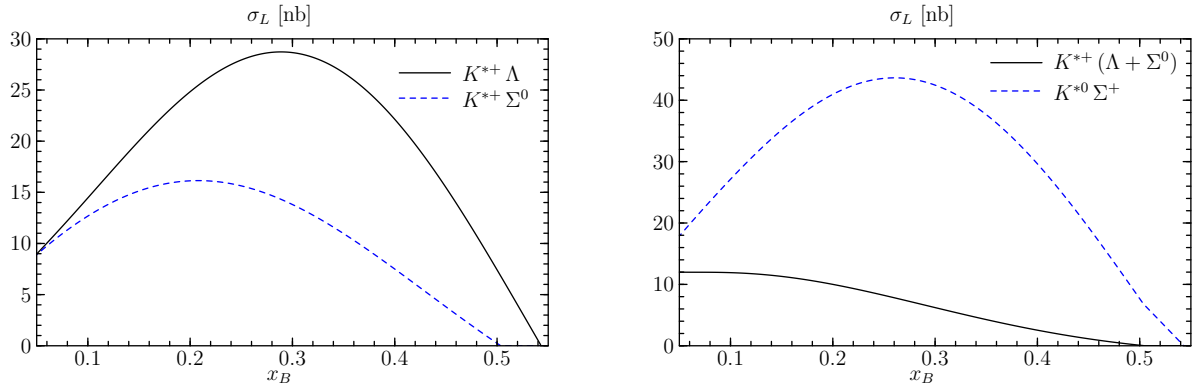

Figure 3.6. Leading-twist cross sections for $\gamma_L^* p \to K^{*+}\Lambda$, $K^{*+}\Sigma^0$, $K^{*0}\Sigma^+$ at $Q^2 = 2.5\,GeV^2$, obtained with the MRST2001 parton densities taken at $\mu^2 = 1.2\,GeV^2$.

In Fig. 3.5 we show the production cross sections for ρ^+, ρ^0 and ω. The x_B behavior of the ρ^+ cross section roughly follows the one of $\xi^2\,[u(\xi) - d(\xi) + \bar{u}(\xi) - \bar{d}(\xi)]^2$, which is a flavor nonsinglet combination and hence does not display the strong rise of sea quarks or gluons at small x. The clear suppression of ω production compared with the ρ^0 is a consequence of the relative factor in the gluon contribution (see Table 3.1) and at large x_B of the relative size of the flavor combination $2H^u - H^d$ compared with $2H^u + H^d$. We remark that the exclusive channel $\gamma^* p \to f_2\, p$ also contributes to semi-inclusive production of π^+, π^- and π^0. It involves the combination $2H^u + H^d - [2H^{\bar{u}} + H^{\bar{d}}]$, where sea quarks drop out, so that one may expect a cross section of similar size as for ρ^+ production. A numerical estimate would however require knowledge of quark and gluon distribution amplitudes of the f_2, see [101], and is beyond the scope of this work.

Figure 3.6 shows our results for K^{*+} and K^{*0} production. In contrast to K^+ production, the cross section for the Λ channel is not much larger than for the Σ^0 channel. Consulting Table 3.1 we see that this is because the contributions from u and d quarks partially cancel in $2H^u - H^d$ whereas they add in $2\tilde{H}^u - \tilde{H}^d$. We remark that the results for K^{*+} and K^{*0} production decrease by less than 25% when instead of MRST2001 we take the CTEQ6 parameterization. The uncertainty due to knowledge of the parton distributions is hence much less than for the gluon dominated channels.

Results for ϕ production are shown in Fig. 3.7. The dominance of the gluon over the strange quark contribution is clearly seen, although strange quarks are not entirely negligible with the MRST2001 parameterization.[1] Since gluons dominate for most x_B, we see the same trend concerning differences between the parameterizations and the choice of scale as for ρ^0 production. The ratio of σ_L for ϕ and ρ^0 production is shown in Fig. 3.8, where the dependence on μ^2 is seen to be much milder since it partially cancels in the ratio. The difference between CTEQ6 and MRST2001 is still significant and mainly due to the difference in the gluon distributions.

Preliminary data from HERMES [73, 76] give a ratio of about 0.08 for the cross sections

[1] In the study [86] strange quarks were neglected based on inspection of the CTEQ6 parameterization.

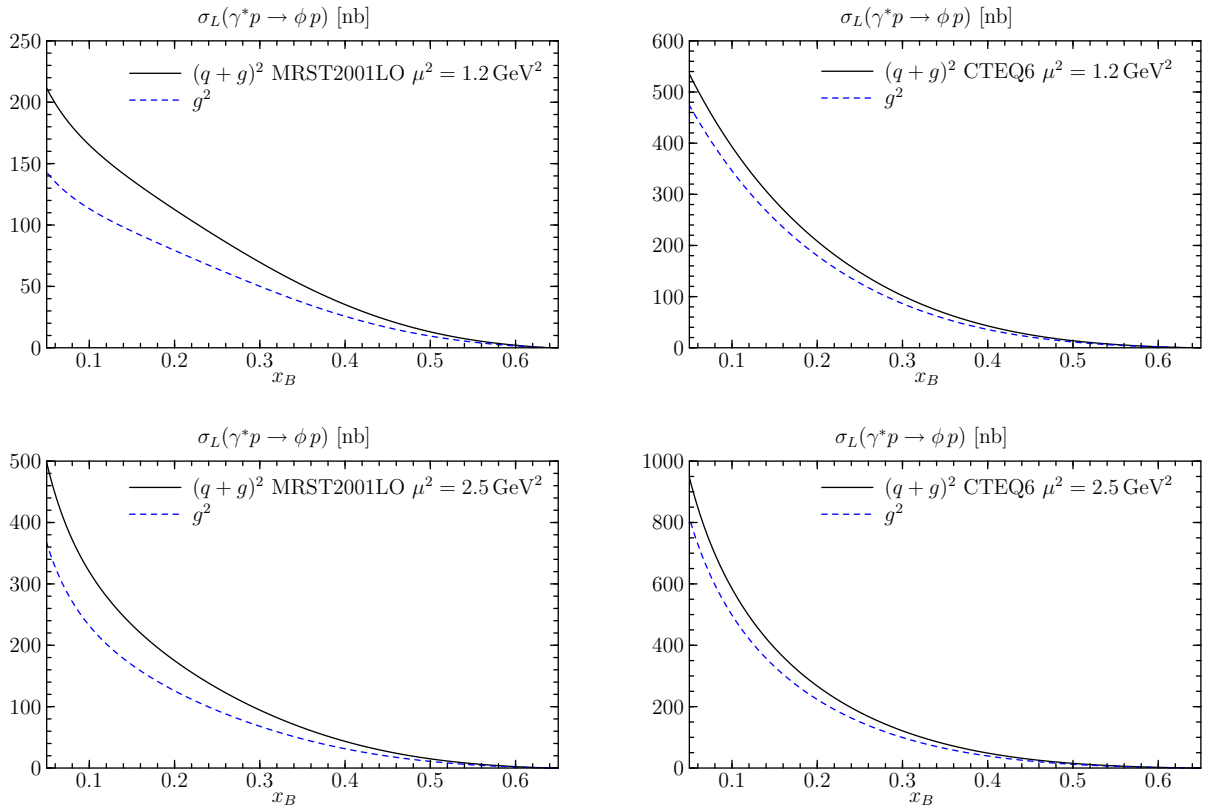

Figure 3.7. Leading-twist cross section for $\gamma_L^* p \to \phi p$ at $Q^2 = 2.5\ GeV^2$. Shown are the individual contributions from gluons and the coherent sum of gluons and strange quarks. The upper plots are for parton densities taken at scale $\mu^2 = 1.2\ GeV^2$ in the double distribution model, and the lower plots for parton densities taken at $\mu^2 = 2.5\ GeV^2$.

of ϕ and ρ^0 production for $x_B = 0.09$ and $Q^2 = 2.46\,\mathrm{GeV}^2$ and for $x_B = 0.13$ and $Q^2 = 3.5\,\mathrm{GeV}^2$. These data contain a significant contribution from σ_T, and preliminary HERMES data [73,75,76] suggest that $R = \sigma_L/\sigma_T$ may be slightly smaller for ϕ than for ρ^0 production at the same Q^2. The ϕ to ρ^0 ratio for σ_L would then be somewhat larger than 0.08. In addition, one can expect that a narrower shape of the distribution amplitude and power corrections due to the strange quark mass would decrease the estimates in Fig. 3.8 [86].

A complete representation of GPDs includes in addition to the double distribution the so-called D-term [64]. It vanishes in the forward limit $\xi = 0$ and does not affect the double distribution ansatz we are using. Its contribution to the GPDs can be expanded in Gegenbauer polynomials as

$$\begin{aligned} H_D^q(x,\xi,t) &= \theta(|x| \le \xi)\left(1 - \frac{x^2}{\xi^2}\right) \sum_{n=0}^{\infty} d_{2n+1}^q(t)\, C_{2n+1}^{3/2}\!\left(\frac{x}{\xi}\right), \\ H_D^g(x,\xi,t) &= \theta(|x| \le \xi)\,\frac{3\xi}{2}\left(1 - \frac{x^2}{\xi^2}\right)^2 \sum_{n=0}^{\infty} d_{2n+1}^g(t)\, C_{2n}^{5/3}\!\left(\frac{x}{\xi}\right) \end{aligned} \tag{3.20}$$

for $\xi > 0$. Such terms contribute to the real part of the convolution integrals needed in the

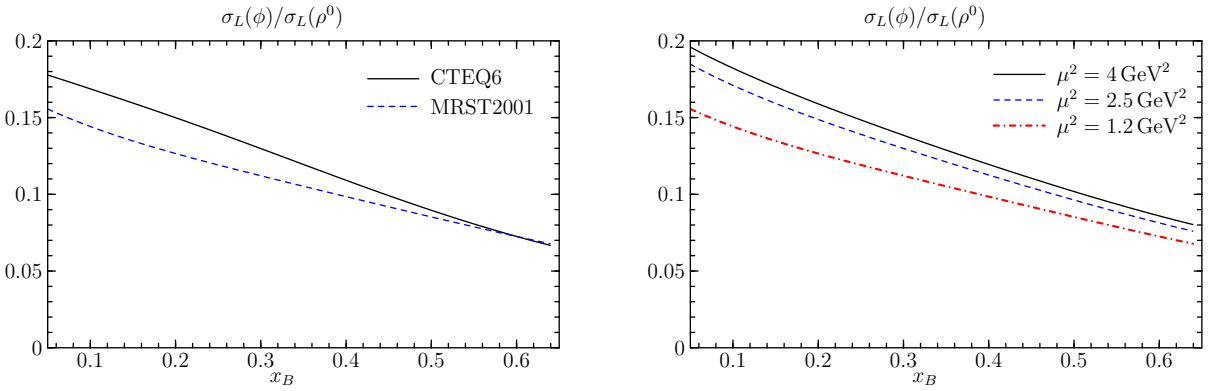

Figure 3.8. Ratio of leading-twist longitudinal cross sections for ϕ and ρ^0 production, obtained with different parton distributions taken at $\mu^2 = 1.2\,GeV^2$ (left) and with the MRST2001 distribution taken at different μ^2 (right).

meson production amplitudes as

$$
\begin{aligned}
I_D^q &= \int_{-1}^{1} dx\, \frac{H_D^q(x,\xi,t)}{\xi - x - i\epsilon} = \int_{-1}^{1} dx\, \frac{H_D^{\bar{q}}(x,\xi,t)}{\xi - x - i\epsilon} = 2\sum_{n=0}^{\infty} d_{2n+1}^q(t)\,, \\
I_D^g &= \int_{-1}^{1} dx\, \frac{H_D^g(x,\xi,t)}{x}\, \frac{1}{\xi - x - i\epsilon} = 2\sum_{n=0}^{\infty} d_{2n+1}^g(t)\,.
\end{aligned}
\tag{3.21}
$$

These terms give a ξ independent contribution to $\mathcal{H}(\xi,t)$, in contrast to the contributions from the double distribution part, which very roughly follow the behavior of $\xi q(\xi)$, $\xi\bar{q}(\xi)$ or $\xi g(\xi)$ and hence grow as ξ becomes smaller. In [102] the first three coefficients in the quark D-term at $t = 0$ have been extracted from a calculation in the chiral quark-soliton model of the nucleon, giving $d_1^u(0) \approx -2.0$, $d_3^u(0) \approx -0.6$, $d_5^u(0) \approx -0.2$ and equal values for d quarks, referring to a scale μ of a few GeV [103]. The gluon D-term is parametrically subleading at the low scale intrinsic to the model, but evolution to μ of a few GeV can give values similar in size to those for quarks. The values $I_D^u = I_D^d = -5.6$ turn out to be similar in size and opposite in sign to the real parts of the corresponding integrals from the double distribution part in our model. The effect of such a D-term is however much weaker on the square $|\mathcal{H}|^2$ appearing the cross section, which is dominated by the imaginary parts of the integrals in a large region of x_B. Taking the above values for the quark D-term and $I_D^g = -11.2$ as an order-of-magnitude estimate, we find that the change of the various vector meson cross sections is at the 10% level for $x_B = 0.1$ and not more than a factor 1.5 in either direction for x_B below 0.3, where for definiteness we have taken the MRST2001 distributions at $\mu^2 = 1.2\,\mathrm{GeV}^2$.

3.4 Comparison with data and discussion of power corrections

Our calculation of meson production cross sections is based on the leading-twist approximation. It is known that corrections in $1/Q^2$ to leading-twist meson cross sections can be substantial for Q^2 of a few GeV^2. A systematic treatment of such power corrections remains an unsolved problem. There is however a number of approaches that allow one to model particular sources of power corrections, see e.g. [38] for a discussion and references. For vector meson production, a considerable suppression of the leading-twist result at moderate Q^2 is found when including in the hard-scattering kernel the transverse momentum of the quarks in the meson [100, 104, 105]. This means that the transverse resolution power of the virtual photon cannot be neglected compared with the transverse size of the meson. Similarly, the finite transverse momentum of the partons coming from the proton gives rise to power corrections, when it is included in the hard-scattering kernel. Estimating both effects in a calculation considering only quark GPDs [104], a suppression of the leading-twist cross section for ρ^0 production by factors of 3.3, 4.9 and 9.2 was found at $Q^2 = 5\,\mathrm{GeV}^2$ for $x_B = 0.3$, 0.45 and 0.6, respectively. The recent study [105] for small x_B, where only gluon GPDs were retained and only the transverse quark momentum in the meson was taken into account, found corresponding suppression factors of 4.6 and 6.6 for respective values of $x_B = 2.95 \times 10^{-3}$ and 10^{-4} at $Q^2 = 4.8\,\mathrm{GeV}^2$. For $Q^2 = 10.9\,\mathrm{GeV}^2$ and $x_B = 4.3 \times 10^{-3}$ this factor decreases to 1.9. The discrepancy of the calculation including power suppression and experimental data is less than 35% in all three cases.[2]

In Table 3.2 we compare our leading-oder results for ρ^0 and ϕ production with data from HERMES [72,73,76,106]. The discrepancy between our calculation and the ρ^0 data is well in the range of what can be explained by suppression from quark transverse momentum (considering in addition the uncertainties of our model for the GPDs). The stronger discrepancy with the ϕ data corresponds to our overestimating the ϕ to ρ^0 production ratio, discussed in the previous subsection.

The CLAS collaboration has published results for ρ^0 production at $x_B = 0.31$ and at $x_B = 0.38$, with Q^2 values between 1.5 and $2.3\,\mathrm{GeV}^2$ [77], and for ϕ production at $x_B = 0.29$ and $Q^2 = 1.7\,\mathrm{GeV}^2$ [107]. We consider that this kinematics, where the hadronic invariant mass W is below 2.3 GeV, is too close to threshold for comparison with a leading-twist calculation. A recent CLAS measurement [108] of ω production at higher energies, with Q^2 up to $5.1\,\mathrm{GeV}^2$ and W up to 2.8 GeV, found that helicity conservation between the γ^* and the ω is strongly violated, in contrast with the predicted behavior in the large-Q^2 limit. This prevented the extraction of σ_L and was ascribed to a strong contribution from π^0 exchange (which is absent in the ρ^0 and ϕ channels).

Let us now turn to π^+ production, where the situation is quite different. For the contri-

[2]The leading-order formula (90) in [105] with which we obtained the suppression factors just quoted contains in addition an approximation for small x_B, which should however not be the dominant effect comparing to the full calculation.

Table 3.2. Experimental values $\sigma_L^{\rm exp}$ of the longitudinal cross section for the production of ρ^0 [72] and ϕ [73, 76, 106] from HERMES, and the ratio between our leading-twist results $\sigma_L^{\rm thy}$ (obtained with the MRST2001 distributions taken at $\mu^2 = 1.2\ GeV^2$) and the data. The data for ϕ production is preliminary.

$\gamma^* p \to \rho^0 p$			
$Q^2[\,\mathrm{GeV}^2]$	x_B	$\sigma_L^{\rm exp}[\mu\mathrm{b}]$	$\sigma_L^{\rm thy}/\sigma_L^{\rm exp}$
2.3	0.1	0.21 ± 0.04	7.1
2.3	0.075	0.21 ± 0.04	7.6
4.0	0.16	0.09 ± 0.02	2.1
4.0	0.12	0.06 ± 0.01	3.5

$\gamma^* p \to \phi p$ (preliminary data)			
$Q^2[\,\mathrm{GeV}^2]$	x_B	$\sigma_L^{\rm exp}[\mathrm{nb}]$	$\sigma_L^{\rm thy}/\sigma_L^{\rm exp}$
2.3	0.087	15.6 ± 3.1	14.9
3.8	0.136	6.2 ± 1.24	5.5

bution from $\tilde{\mathcal{H}}$ one expects a similar suppression from quark transverse momentum as in the case of $\mathcal{H}$ in vector meson production, which was indeed found in the numerical study [104]. The pion exchange contribution from $\tilde{\mathcal{E}}$ is described in terms of the pion form factor according to (3.17), and this relation persists beyond the leading approximation in $1/Q^2$ to the extent that the pion emitted from the nucleon is not too far from off-shell. The power corrections for $\tilde{\mathcal{E}}$ are then the same as those for the pion form factor. The leading-twist expression (3.18) for $F_\pi(Q^2)$, with our choice of α_s specified after (3.13), undershoots the data of [109] by a factor 0.53 at $Q^2 = 1\,\mathrm{GeV}^2$ and a factor 0.41 at $Q^2 = 1.6\,\mathrm{GeV}^2$. For $Q^2 = 3.3\,\mathrm{GeV}^2$ we find this factor to be between 0.34 and 0.77 within the large error bars in [110]. We will not attempt here to summarize the detailed theoretical and phenomenological work on the pion form factor, but remark that in addition to the leading-twist perturbative contribution there is a contribution from the Feynman mechanism, where the photon hits a quark carrying almost all of the pion momentum. This leads to a considerable enhancement over the leading-twist approximation. The calculations of $F_\pi(Q^2)$ in [111], which take this effect into account using different methods, give for instance results larger than our leading-twist value by factors between 2 and 4, even at $Q^2 = 10\,\mathrm{GeV}^2$. Note that these factors are to be squared in the contribution of $|\tilde{\mathcal{E}}|^2$ to the π^+ production cross section. For the production of the neutral pseudoscalars π^0, η, η', where there is no pion exchange contribution, one expects that power corrections will decrease the cross section, similarly to the case of vector meson production.

We have further compared our leading-twist calculation of $\epsilon\sigma_L$ for $\gamma^* p \to \pi^+ n$ with preliminary data on $\sigma_T + \epsilon\sigma_L$ from HERMES [112]. The HERMES data are presented for three different bins in x_B, with the average values of Q^2 and x_B for individual data points ranging from $1.5\,\mathrm{GeV}^2$ and 0.1 to $4.2\,\mathrm{GeV}^2$ and 0.17 in the first bin, from $2.5\,\mathrm{GeV}^2$ and 0.21 to $6.3\,\mathrm{GeV}^2$ and 0.25 in the second bin, and from $4.5\,\mathrm{GeV}^2$ and 0.34 to $10.5\,\mathrm{GeV}^2$ and 0.45 in

the third bin [113]. Averaging the ratio between theoretical and experimental cross sections for the data points in each bin, we find ratios of 0.42, 0.19 and 0.12 in the first, second and third bin, respectively. The large discrepancy at large Q^2 and large x_B (which are strongly correlated in the data) is striking, but not too surprising given the size of corrections just estimated for the pion form factor. The much better agreement at smaller Q^2 and x_B might be accidental, given that we expect comparable contributions from $\tilde{\mathcal{H}}$ and $\tilde{\mathcal{E}}$, for with the power corrections go in different directions. Help in clarifying this issue could come from the spin asymmetry for transverse target polarization, which gives access to the relative size of $\tilde{\mathcal{H}}$ and $\tilde{\mathcal{E}}$ [37].

The case of π^+ production (and also the findings in the ω channel mentioned above) show that there are specific power corrections which will not cancel in cross section ratios for different processes. The situation is however better for channels that are sufficiently similar, as the example of ρ^0 and ϕ production shows. Corrections due to quark transverse momentum (as well as the overall normalization uncertainty from the scale of α_s in our leading-order calculation) will tend to cancel in that case. We hence expect that the overall pattern of differences between various meson cross sections we estimated at leading order will not be overturned in a more realistic treatment, given that these differences are largely controlled by the relevant combinations of quark and gluon distributions.

3.5 Exclusive channels in semi-inclusive pion and kaon production

In semi-inclusive hadron production one considers processes of the type

$$e(k) \; + \; p(p) \;\; \to \;\; e(k') \; + \; h(q_h) \; + \; X, \tag{3.22}$$

where h is a specified hadron and X an unspecified inclusive final state. A basic observable is the distribution of the produced hadron over the variable

$$z = \frac{q_h p}{qp}, \tag{3.23}$$

which measures the fraction of the virtual photon energy carried by the produced hadron in the target rest frame. In the Bjorken limit of large Q^2 at fixed x_B and fixed z, semi-inclusive hadron production can be treated within a QCD factorization approach. The differential cross section factorizes into the distribution of partons of type i in the target, the cross section for the virtual photon scattering off this parton, and the fragmentation function $D^{i\to h}(z)$ describing the fragmentation of the struck parton into the hadron h, which carries a fraction z of its longitudinal momentum. To leading order in α_s one has

$$\frac{d\sigma}{dQ^2\, dx_B\, dz} = 2\pi\alpha_{em}\, \frac{y^2}{1-\epsilon}\, \frac{1}{x_B\, Q^4} \sum_q e_q^2 \Big[q(x_B) D^{q\to h}(z) + \bar{q}(x_B) D^{\bar{q}\to h}(z) \Big], \tag{3.24}$$

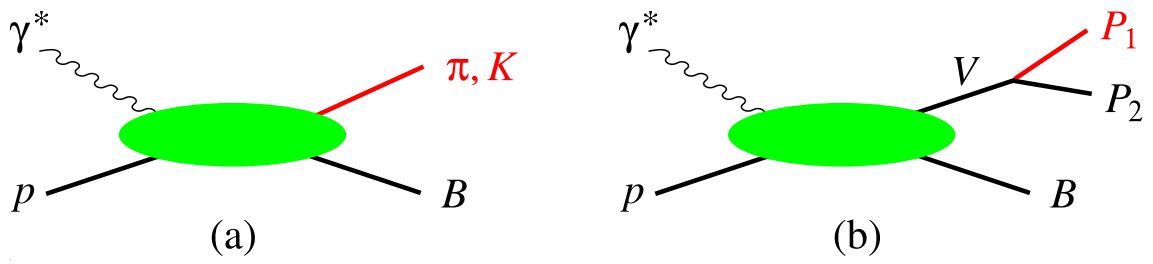

Figure 3.9. Contributions of exclusive channels to semi-inclusive pion and kaon production, calculated at leading order. (a) Direct exclusive production of pseudoscalar mesons. (b) Exclusive production of a vector meson with subsequent decay into pseudoscalars.

where the sum is over quark flavors. Note that (3.24) has the same Q^2-dependence as the inclusive DIS cross section in the Bjorken regime. The fragmentation functions are process-independent and describe not only semi-inclusive DIS but also e^+e^- annihilation into hadrons and the distribution of leading hadrons in high-p_T jets. Their scale evolution is governed by evolution equations analogous to the DGLAP equations for the parton distribution functions. Various parameterizations of the fragmentation functions have been presented in the literature, which fit e^+e^- annihilation and semi-inclusive DIS data at higher scales.

The derivation of semi-inclusive factorization relies on the fact that in the Bjorken limit the inclusive final state X has a large invariant mass

$$m_X^2 = Q^2 \frac{1-z}{x_B} + m_p^2 - (q - q_h)^2, \tag{3.25}$$

and thus a large average multiplicity (note that the squared momentum transfer $(q-q_h)^2$ is always negative). The semi-inclusive cross section is thus obtained by summing over many individual channels. In practice m_X^2 is not very large for Q^2 values of a few GeV^2 typical of fixed-target experiments, for instance at Jefferson Lab or HERMES, especially at high z. At the same time, for moderate Q^2 the suppression of the cross sections for exclusive channels relative to the semi-inclusive cross section (see below) may not yet be effective. One thus can reach a situation in which the cross sections of individual exclusive channels becomes comparable to the semi-inclusive one. It is interesting to compare the semi-inclusive cross section (3.24) with the cross sections of exclusive channels contributing to semi-inclusive production. In the following we investigate the role of exclusive channels in semi-inclusive π and K production on a proton target. We study two types of exclusive channels (see Fig. 3.9) at a quantitative level:

i) direct exclusive production of pseudoscalar mesons, $\gamma^* p \to \pi^+ n$ and $\gamma^* p \to K^+ \Lambda$,

ii) exclusive production of neutral or charged vector mesons ρ, ϕ, K^* with subsequent decay into pseudoscalars.

In the direct production of pseudoscalar mesons (Fig. 3.9a), the energy fraction z carried by the produced meson is related to the invariant momentum transfer to the nucleon t by

$$1 - z = x_B \frac{m_B^2 - m_p^2 - t}{Q^2} \tag{3.26}$$

according to (3.25). Exclusive production in the limit of large Q^2 at fixed x_B and fixed t thus corresponds to values of z very close to 1. For example, π^+ and K^+ production corresponds to $z > 0.94$ in typical HERMES kinematics of $x_B = 0.1$ and $Q^2 = 2.5\,\mathrm{GeV}^2$ with a maximum momentum transfer $|t| = 1\ \mathrm{GeV}^2$ (since the cross section drops rapidly with t, most events have z values yet closer to unity). Such exclusive contributions can usually be separated experimentally from the semi-inclusive events at smaller values of z.

The situation is different for the contribution to semi-inclusive production resulting from the decay of exclusively produced vector mesons (Fig. 3.9b). Since the decay products share the energy of the vector meson, such contributions result in an extended z distribution for the pion or kaon, even in the Bjorken limit. With the approximations described in Appendix B, the z spectrum of the pseudoscalar meson P_1 from the decay $V \to P_1 P_2$ can be written as

$$\frac{d\sigma(ep \to P_1 + P_2\, B)}{dQ^2\, dx_B\, dz} = \frac{\alpha_{em}}{2\pi}\, \frac{y^2}{1-\epsilon}\, \frac{1-x_B}{x_B Q^2} \Big[\, \epsilon \sigma_L(\gamma^* p \to VB)\, D_L(z) + \sigma_T(\gamma^* p \to VB)\, D_T(z) \Big] \tag{3.27}$$

with

$$D_L(z) = \frac{3}{2\zeta^3}\,(z - z_0)^2, \qquad D_T(z) = \frac{3}{4\zeta^3}\,(z - z_1)(z_2 - z). \tag{3.28}$$

Here $z_1 \le z \le z_2$ with

$$z_0 = \frac{E_{P1}}{m_V}\,, \qquad z_1 = z_0 - \zeta\,, \qquad z_2 = z_0 + \zeta\,, \qquad \zeta = \frac{|\boldsymbol{q}_{P1}|}{m_V} \tag{3.29}$$

up to corrections of order $x_B\, m_p^2/Q^2$. For brevity we have not explicitly indicated the dependence of D_L and D_T on x_B and Q^2 due to these corrections. The energy and three-momentum of P_1 in the rest frame of the vector meson

$$\begin{aligned} E_{P1} &= \frac{m_V^2 + m_{P1}^2 - m_{P2}^2}{2m_V}, \\ |\boldsymbol{q}_{P1}| &= \frac{\sqrt{m_V^4 + m_{P1}^4 + m_{P2}^4 - 2\,(m_V^2 m_{P1}^2 + m_V^2 m_{P2}^2 + m_{P1}^2 m_{P2}^2)}}{2m_V} \end{aligned} \tag{3.30}$$

depend only on the meson masses, and so do z_0, z_1 and z_2 in the limit of large Q^2. In particular, the smallest and largest possible values of z for pions from the decay $\rho \to \pi\pi$ are $z_1 = 0.04$ and $z_2 = 0.96$ in that limit. The corresponding values for kaons from $\phi \to KK$ are $z_1 = 0.37$ and $z_2 = 0.63$. For the kaon from K^* decay one has $z_1 = 0.32$ and $z_2 = 0.96$, and for the pion from K^* decay one has $z_1 = 0.04$ and $z_2 = 0.68$.

According to (3.5), (3.6) and (3.27), the contribution of exclusive vector meson production to the cross section $d\sigma/(dQ^2\, dx_B\, dz)$ asymptotically scales as $1/Q^8$ at fixed x_B and z and is thus suppressed by $1/Q^4$ compared with the leading behavior (3.24) of the semi-inclusive cross section. Notice that (3.24) corresponds to transverse photon polarization, with contributions to the longitudinal cross arising at the level of α_s and of $1/Q^2$ corrections, just as in the familiar case of inclusive DIS. The situation is opposite for hard exclusive meson production, where σ_L dominates over σ_T in the large-Q^2 limit. Measurements show however

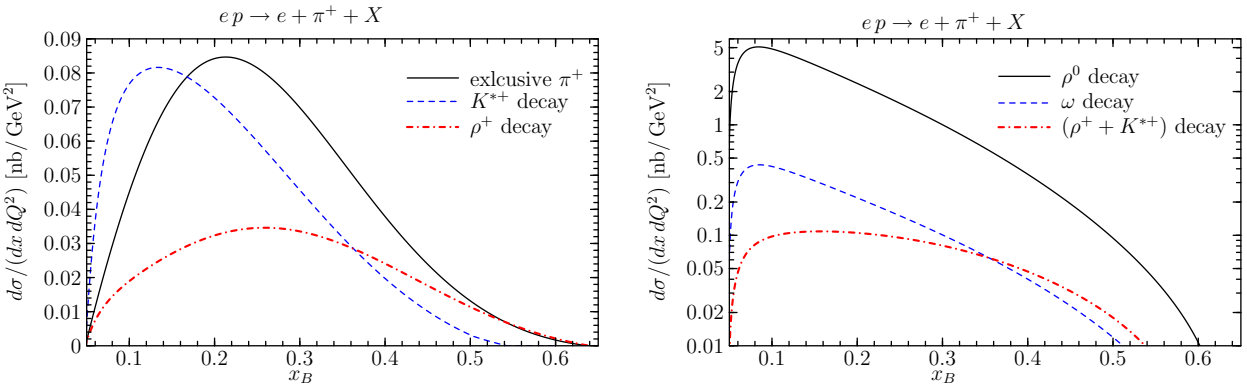

Figure 3.10. Exclusive contributions to the π^+ electroproduction cross section ($e\,p \to e + \pi^+ + X$) at $Q^2 = 2.5\,GeV^2$, obtained from our leading-twist calculation of σ_L. This and the following plots are for a lepton beam energy of 27.5 GeV in the target rest frame. Left: direct exclusive production, and contributions from K^{*+} and ρ^+ decay. Right: sum of contributions from K^{*+} and ρ^+ decay compared with contributions from ω and ρ^0 decay.

that at Q^2 in the few GeV^2 region the ratio $R = \sigma_L/\sigma_T$ is still of order 1 in ρ^0 and ϕ production [73, 75, 76].

We first consider the semi-inclusive production of pions. Depending on the pion charge, exclusive channels contributing here are direct production $ep \to e\pi^+ n$ and the production and decay of ρ and $K^*(892)$. The ρ decays to almost 100% as $\rho^0 \to \pi^+\pi^-$ and $\rho^+ \to \pi^+\pi^0$, and the $K^*(892)$ decays to almost 100% into $K\pi$, with branching fractions

$$\begin{aligned} B(K^{*+} \to K^+\pi^0) &= \tfrac{1}{3}, & B(K^{*+} \to K^0\pi^+) &= \tfrac{2}{3}, \\ B(K^{*0} \to K^+\pi^-) &= \tfrac{2}{3}, & B(K^{*0} \to K^0\pi^0) &= \tfrac{1}{3} \end{aligned} \qquad (3.31)$$

following from isospin symmetry. Note that in quark fragmentation one has $\sigma(\pi^0) = \frac{1}{2}[\sigma(\pi^+) + \sigma(\pi^-)]$, which follows directly from the isospin relations between the pion fragmentation functions. This relation also holds for the contributions from K^* decay, but it is strongly violated for ρ decay. For the ρ^0 this effect was investigated in Ref. [70] in connection with the separation of $\bar{u}$ and $\bar{d}$ distributions in the proton using semi-inclusive DIS.

In Fig. 3.10 we show the result of our leading-twist calculation from Sects. 3.2 and 3.3 for the ep cross section of π^+ production. We give all ep cross section for a lepton beam energy of 27.5 GeV in the target rest frame, corresponding to the HERMES experiment, and recall that all our exclusive cross sections are calculated with an upper cutoff of 1 GeV^2 on $|t|$. We see that the ρ^0 channel is clearly dominating. The ω, which decays to almost 100% into $\pi^+\pi^-\pi^0$, is much less prominent. According to our discussion in Sects. 3.2 and 3.4 one expects that the contribution from $ep \to e\pi^0 p$ to π^0 production is smaller than in the case of direct π^+ production. The same holds for the production and decay of η and η', which have several three-body decays contributing to all three pion channels. As we argued in Sect. 3.3 the production of $f_2(1270)$, which predominantly decays into $\pi^+\pi^-$ and $\pi^0\pi^0$, may contribute at a similar or lower level as ρ^+ decays. In Fig. 3.11 we show the z spectrum arising from different vector meson decays. Whereas ρ decays contribute in almost

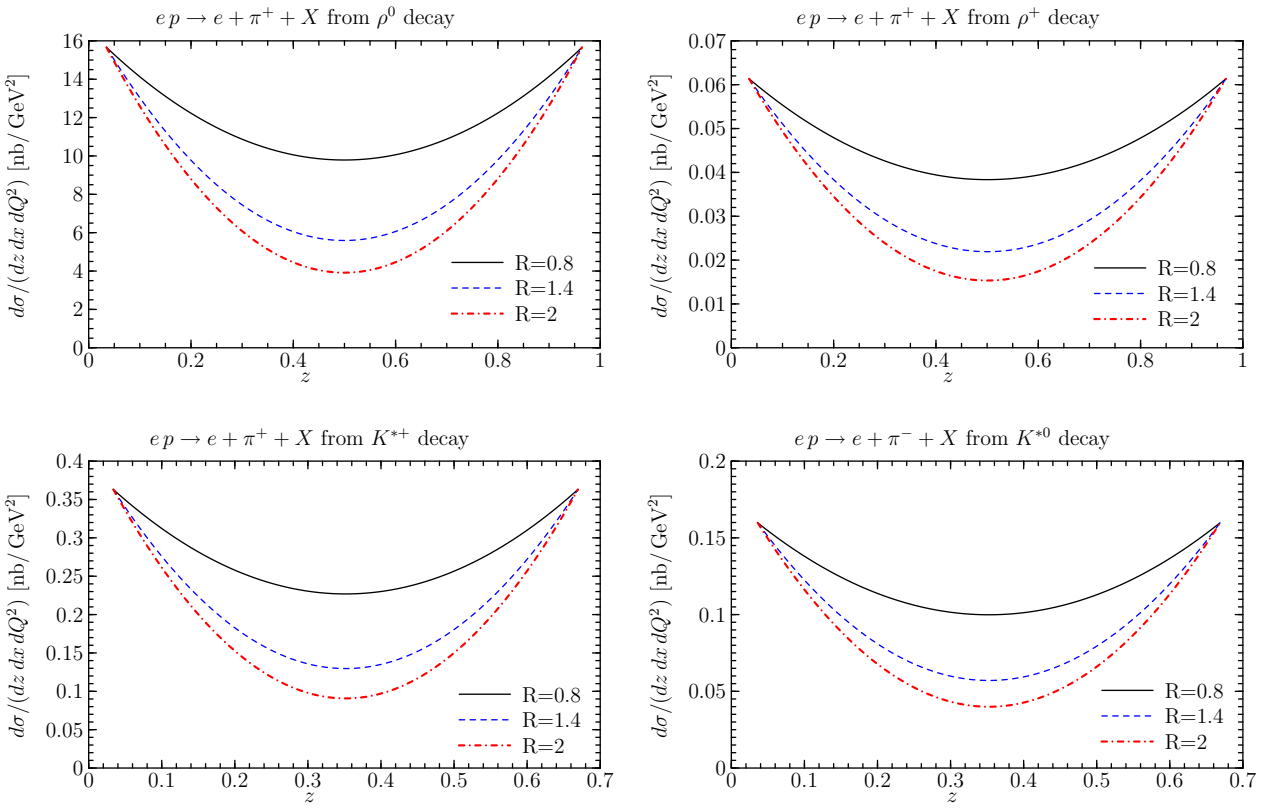

Figure 3.11. Contributions to the semi-inclusive pion electroproduction cross section from decays of exclusively produced vector mesons, for $Q^2 = 2.5\,GeV^2$ and $x_B = 0.1$. Shown are the results corresponding to our leading-twist calculation of σ_L for vector meson production, and a value of $R = \sigma_L/\sigma_T$ chosen as indicated in the figure. Top left: π^+ from ρ^0 decay. Top right: π^+ from ρ^+ decay. Bottom left: π^+ from K^{*+} decay. Bottom right: π^- from K^{*0} decay. The contribution to π^0 production from K^{*+} and K^{*0} decays is given by the average of the corresponding curves in the two lower plots, according to (3.31).

the entire z range, pions from K^* decays are limited to z values below 0.7. Note that due to charge conjugation invariance the z spectrum from ρ^0 decays is identical for the π^+ and π^-, and by isospin invariance the same holds for the π^+ and π^0 spectra from the decay of ρ^+. To illustrate the dependence of the z spectrum on the ratio R of longitudinal and transverse meson production cross sections we have taken values which correspond to the range measured in ρ^0 and ϕ production at $Q^2 = 2.5\,\mathrm{GeV}^2$ [73, 75–77].

We now compare the contribution from exclusive channels with the semi-inclusive cross section obtained from the leading-order expression (3.24) for quark fragmentation. We use the LO parton densities from MRST2001 and the LO fragmentation functions of Kretzer [114], both at a scale $Q^2 = 2.5\,\mathrm{GeV}^2$. Let us first take a look at the high-z tail of the spectrum, where direct exclusive production contributes. Integrating the semi-inclusive cross section for π^+ production for $z > 0.9$ at $Q^2 = 2.5\,\mathrm{GeV}^2$ and $x_B = 0.1$, we obtain $d\sigma/(dQ^2\,dx_B) = 0.19\,\mathrm{nb\,GeV}^{-2}$ from (3.24). This number should be understood as a naive extrapolation: the fragmentation functions are not well known for z close to 1, and in the above kinematics

$z > 0.9$ corresponds to an invariant mass $m_X < 1.84\,\mathrm{GeV}$ according to (3.25), where leading-twist fragmentation can be just marginally valid. Our leading-twist result for $ep \to e\pi^+ n$ gives $d\sigma/(dQ^2\,dx_B) = 0.045\,\mathrm{nb\,GeV}^{-2}$, which according to our comparison with preliminary HERMES data (Sect. 3.4) undershoots the actual cross section by a factor of about 0.4. We thus find that for $z > 0.9$ direct exclusive pion production may be a substantial part of the semi-inclusive cross section, but cannot be more quantitative given the uncertainties just discussed.

For a realistic estimate of exclusive vector meson production we divide our leading-twist results for σ_L by a factor 7, except for ϕ production. According to Table 3.2 this brings us close to the HERMES measurement for ρ^0 production at $Q^2 = 2.3\,\mathrm{GeV}^2$ and $x_B = 0.1$, and according to our arguments in Sect. 3.4 it should give a reasonable estimate for the other channels. In other words, we assume that the ratio of vector meson channels is sufficiently well described by our leading-twist calculation. Only for ϕ production do we divide our leading-twist results by a different factor, namely by 15, following our comparison in Table 3.2 with preliminary HERMES data in this channel. One might argue that for the production of a K^*, which has one light and one strange quark, power corrections are between those for the ρ^0 and for the ϕ, but we refrain from such refinements here. Possible changes by a factor of 2 would in fact not change our conclusions regarding the role of K^* decays. For a prediction of σ_T we divide σ_L obtained as just described by the value $R = \sigma_L/\sigma_T = 1.2$ from preliminary HERMES data for ρ^0 production in the relevant kinematics [73,75], except for the ϕ channel, where instead we take $R = 0.8$ from the parameterization of preliminary HERMES data in [73, 76]. Variation of R as shown in Fig. 3.11 would not affect the conclusions we shall draw.

Integrating the ρ^0 decay contribution to π^+ production for $z > 0.9$ at $Q^2 = 2.5\,\mathrm{GeV}^2$ and $x_B = 0.1$, we find $d\sigma/(dQ^2\,dx_B) = 0.13\,\mathrm{nb\,GeV}^{-2}$, which is surprisingly close to the extrapolation of the fragmentation result given above. The fragmentation formula for π^- production gives $d\sigma/(dQ^2\,dx_B) = 0.07\,\mathrm{nb\,GeV}^{-2}$ when integrated over $z > 0.9$, so that in this case the ρ^0 contribution slightly overshoots the naive fragmentation result. In Fig. 3.12 we show the z spectrum of semi-inclusive π^+ and π^- production, comparing the fragmentation result with the contributions from vector meson decays. Following our above discussion we do not show the cross section from fragmentation for z above 0.9. We see that ρ^0 production gives a sizable contribution to semi-inclusive production for z greater than about 0.8. According to our estimate, ρ^+ production is suppressed relative to ρ^0 by two orders of magnitude and cannot compete with the cross section from quark fragmentation even at large z. The K^* decay contribution is somewhat larger in size but limited to z below 0.7. The fragmentation result for π^0 production is just the average of π^+ and π^- because of isospin invariance. With ρ^0 decay being absent and the contributions from other vector mesons being comparatively small, we find no exclusive channel that is prominent in semi-inclusive π^0 production for the kinematics discussed here. We expect direct exclusive production $ep \to e\pi^0 p$ to be much less important at high z than in the case of π^+ production, to the extent that power corrections enhance the π^+ but suppress the π^0 compared with the leading

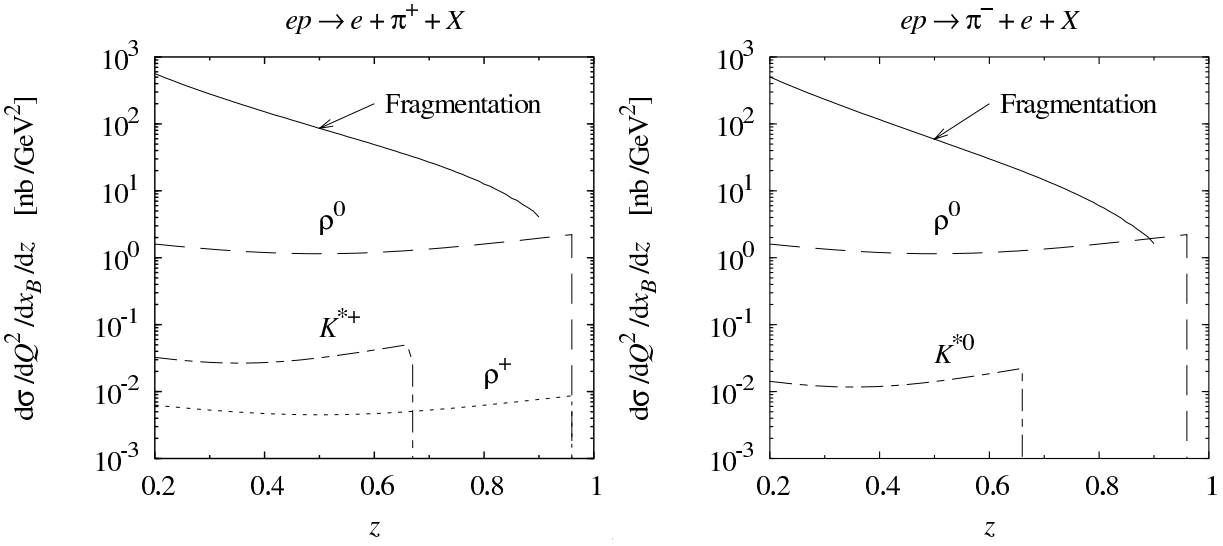

Figure 3.12. The cross section for semi-inclusive electroproduction of π^+ (left) and π^- (right), as a function of z, at $x_B = 0.1$ and $Q^2 = 2.5\,GeV^2$. The cross sections from quark fragmentation were calculated using the LO fragmentation functions of Kretzer [114] and the MRST 2001 LO parton distributions. The contributions from vector meson decays were obtained by adjusting our leading–twist results for the vector meson production cross sections, as explained in the text. The value taken for the ρ^0 cross section matches the HERMES measurement [72]. This plots are taken from [34].

approximation in $1/Q^2$. Given the relative size of cross sections in Fig. 3.10 it is clear that pions from ω production are significantly smaller than the fragmentation result for all z, and we shall not analyze the kinematics of the corresponding three-body decay here.

Turning to semi-inclusive K^+ and K^- production, we show in Fig. 3.13 the contributions of the relevant exclusive channels to the ep cross section, obtained from our leading-twist calculation in Sect. 3.3. The production of ϕ, which decays to approximately 50% into K^+K^-, is clearly dominant for K^+ production, and it is the only channel contributing to K^- production. As is seen in the z-spectra of Fig. 3.14, it is however only the K^+ from K^* decays that extends to z values above 0.65.

Integrating the leading-order fragmentation formula (3.24) for K^+ production for $z > 0.9$ at $Q^2 = 2.5\,\mathrm{GeV}^2$ and $x_B = 0.1$, we obtain $d\sigma/(dQ^2\,dx_B) = 0.048\,\mathrm{nb\,GeV}^{-2}$, which is to be understood as an extrapolation as in the pion case discussed above. Our leading-twist estimate for direct exclusive K^+ production in Sect. 3.2 gives $d\sigma/(dQ^2\,dx_B) = 0.016\,\mathrm{nb/\,GeV}^2$. Following our discussion in Sect. 3.4 one expects that power corrections will lead to weaker enhancement than in the case of $ep \to e\pi^+ n$ (or possibly even to a suppression), because $\tilde{\mathcal{H}}$ is more important in the leading-twist cross section for K^+ production than $\tilde{\mathcal{E}}$. Nevertheless, the above numbers suggest that direct exclusive K^+ production may be of some significance at the high-z end of the spectrum.

If we integrate the K^+ spectrum from K^{*+} and K^{*0} decays for $z > 0.9$, dividing our leading-twist result by 7 and accounting for the transverse cross section as described above, we obtain $d\sigma/(dQ^2\,dx_B) = 0.0021\,\mathrm{nb\,GeV}^{-2}$, which is well below our extrapolation from

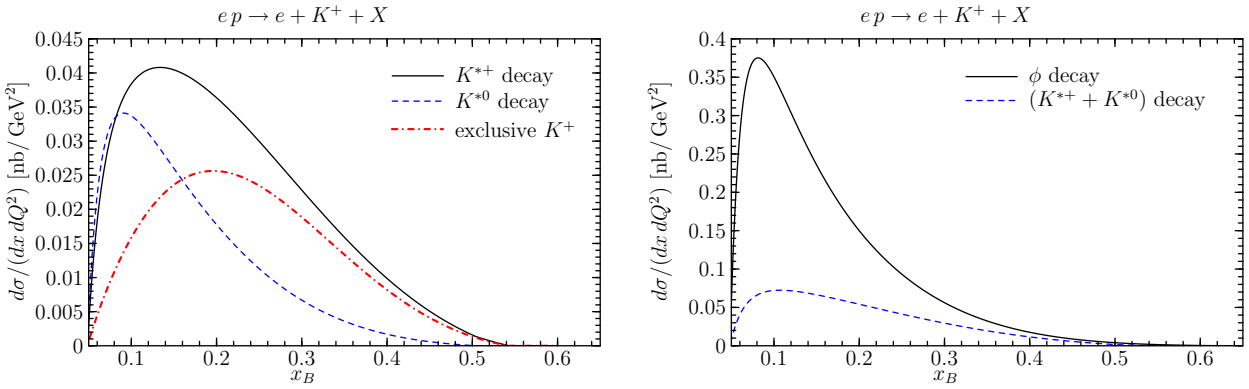

Figure 3.13. Same as Fig. 3.10, but for electroproduction of K^+.

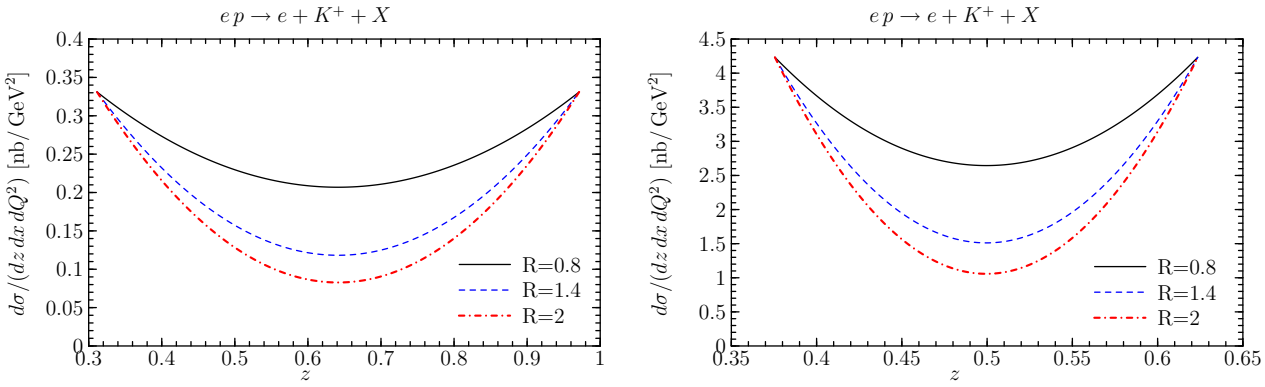

Figure 3.14. Same as Fig. 3.11, but for the contribution from K^{*+} and K^{*0} decays to K^+ production (left) and for the contribution of ϕ decay to K^+ or K^- production (right).

leading-twist fragmentation. In Fig. 3.15 we compare the fragmentation result for semi-inclusive K^+ and K^- production with the individual contributions from K^* and ϕ decays. We conclude that, even within the uncertainties of our estimates, contributions from K^* production are only a fraction of the fragmentation result at any z, and that ϕ production, despite its larger cross section, is always well below the semi-inclusive cross section. Our finding concerning the ϕ contribution agrees with a recent study of measured kaon multiplicities in [115]. On one hand, kaon production by quark fragmentation is less suppressed compared with pion production than is exclusive ϕ production compared with production of ρ^0, and on the other hand ϕ decays only contribute in a z-range where the fragmentation functions are still large. Apart possibly from direct K^+ production at z close to 1, we thus find no exclusive channel dominating K^+ or K^- production in typical HERMES kinematics.

So far we have compared exclusive channels with quark fragmentation at $x_B = 0.1$ and $Q^2 = 2.5\,\mathrm{GeV}^2$. We have also performed the comparison of Figs. 3.12 and 3.15 for $x_B = 0.3$ at the same Q^2. For the vector meson cross sections we used the same values of R and the same correction factors as for $x_B = 0.1$, dividing our leading-twist cross sections by 7 for

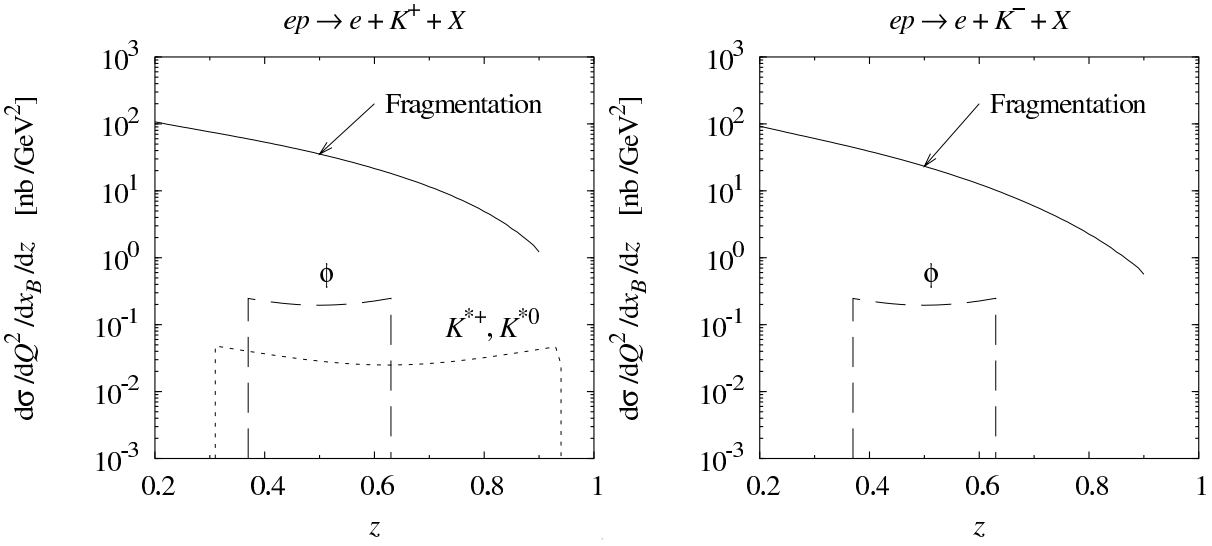

Figure 3.15. Same as Fig. 3.12, but for semi-inclusive production of K^+ (left) and K^- (right). As discussed in the text, the ϕ production cross section used in this plot matches the preliminary results of a HERMES measurement [73, 76]. This plots are taken from [34].

all vector mesons except the ϕ, where we divide by 15. In doing this, we assume that the leading-twist approximation gives a realistic description of the x_B dependence in this region. We find that our qualitative conclusions do not change when going to the larger value of x_B.

A comment is in order concerning the treatment of exclusive channels in the analysis of semi-inclusive DIS data when extracting quark fragmentation or distribution functions. It is by no means clear that by subtracting contributions of individual exclusive channels from the total yield one obtains an observable more suitable for comparison with the quark fragmentation formulae. In fact, the derivation of factorization theorems relies on the sum over all channels X in (3.22) to be complete. At sufficiently large Q^2, each individual exclusive channel by itself is a power correction which may or may not be included in the leading-twist analysis. This situation is similar to the one with the contribution from individual nucleon resonances to the cross section of inclusive DIS. A way to think about the relation of exclusive channels to the leading-twist cross section is quark-hadron duality. It remains a challenge to formulate the problem of quark-hadron duality for semi-inclusive DIS in a quantitative fashion.

Symmetry properties like $\sigma(\pi^0) = \frac{1}{2}[\sigma(\pi^+) + \sigma(\pi^-)]$ can emerge from summing over many channels which do not fulfill this relation individually. If however a single channel like ρ^0 production dominates the semi-inclusive cross section, it clearly becomes more and more difficult for the remaining channels to compensate the missing symmetry between charged and neutral pion production. In such a situation, parton-hadron duality must cease to work. The outcome of our study is that indeed the only channel whose contribution can become dangerously large in HERMES kinematics, is the ρ^0 contribution to π^+ and π^- production.

4

Higher order corrections to exclusive meson production

In the previous chapter we found that treating the exclusive production of mesons at the leading order level in α_s and at leading twist is not sufficient for describing the available experimental data in a satisfying way. One way to decrease the discrapency is to include higher twist corrections to the amplitude. This approach was used in the limit of high energies which are important for experiments like H1 and ZEUS at HERA and at leading order in the strong coupling constant. In a recent work [116] the calculation of power corrections was extended to low energies which are important for fixed target experiments like HERMES. In this work the authors found a large suppression of the leading-twist cross section due to the power corrections. The question that arises now is the how large the influence of next-to-leading order corrections is on the leading-twist amplitude at different energies.
Taking into the consideration the NLO effects is important also to discuss the applicability of the perturbative expansion at leading twist. Up to now this question remains unanswered for exclusive meson production. In the case of DVCS there are first hints of a convergence of the perturbation series. In that case, the NLO corrections can be quite large [117, 118], but the next-to-next-to-leading order (NNLO) corrections, recently calculated in [119, 120], are much smaller. This suggests that for DVCS one could assume the validity of the perturbative approach. In the case of exclusive meson production the situation is less clear. Up to these days there are no detailed studies about the size of NLO corrections. The first attempt to include NLO corrections was done in [121]. In this work the authors focused on the

exclusive production of π^+. For this process the calculation is directly related to that of the pion electromagnetic form factor [41]. This is due to the fact that for exclusive production of π^+ only the quark exchange diagram contributes to the amplitude. The effect of the next-to-leading order corrections which was found in [121] was quite substantial and led to a large change of the cross sections. For heavy and light neutral vector mesons the situation is somewhat different. In this production channels not only the quark exchange contributes to the amplitude, but also the gluon exchange channel. The calculation of the gluonic hard scattering kernel was done in [122] for photoproduction of heavy vector mesons and in [99] for electroproduction of light mesons. In these two works just mentioned the authors did some first numerical calculations of the NLO corrections. They did this investigation for high energies and in this regime they found large corrections to the amplitude in the case of heavy meson production and also in the case of light meson production. The large corrections found in [99, 122] could be an indication of the failing of the leading twist and fixed order in α_s approach at high energies.
In this chapter we want to give a systematic analysis of NLO corrections for exclusive meson production. We do not restrict ourselves to a special kinematical regime, in order to obtain quantitative predictions for the most important experiments. We will present our results for single parts of the amplitude focusing mainly on the results for the unpolarized GPD $H(x, \xi, t)$ which is the most important one in the case of neutral vector meson production. We will also present the results for the unpolarized helicity-flip GPD $E(x, \xi, t)$ using a specific model. And we present results for the polarized GPDs, which are the ingredients for the exclusive production of pions and kaons. Finally, we will also present some results for exclusive cross sections that can be compared with available experimental data and we will discuss the validity of the collinear factorization approach.

4.1 The amplitude of exclusive meson production at next-to-leading order

As in the case of DVCS where the gluon contribution just starts at next-to-leading order one has for the exclusive meson production a new term appearing in the amplitude. In addition to the quark and gluon contribution which appear at the leading order in α_s this new term is the pure singlet contribution coming from a special class of diagrams. We have shown three example diagrams for the exclusive meson production at NLO in Fig. 4.1, where the first one is the known quark exchange part of the amplitude, the second one is the new contribution starting at NLO and finally the third diagram representing the gluonic part of the amplitude.

We split the amplitude into three different parts: the gluon and singlet contribution, which mix under evolution and the flavor non-singlet part which does not mix with the other two parts under evolution. The first two parts appear only in the production of neutral vector mesons on which we will mainly concentrate. The non-singlet contribution appears in any process and is the only term for exclusive production of charged mesons.

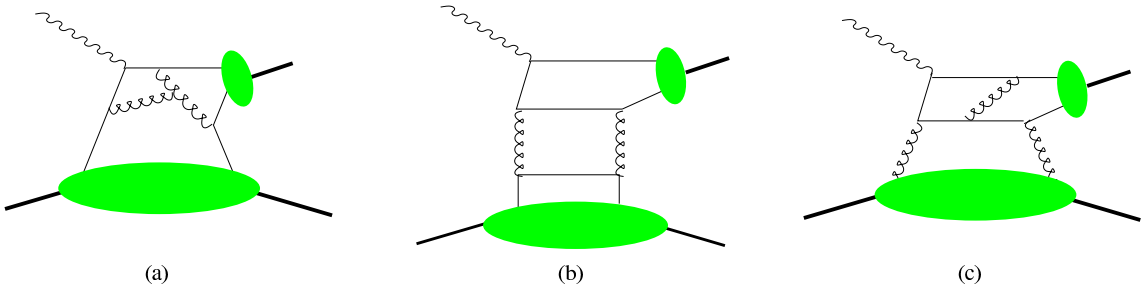

Figure 4.1. Example diagrams for exclusive meson production at next-to-leading order. Diagram (a) corresponds to the quark exchange, diagram (b) is the new singlet contribution and diagram (c) is the gluon exchange.

With these three contributions the amplitude of the exclusive production of neutral vector mesons reads

$$\begin{aligned}\mathcal{M}_{\gamma_L^\star \to V_L N} = &\frac{2\pi\sqrt{4\pi\alpha} f_V}{N_c\, Q\, \xi} Q_V \int_0^1 dz\, \phi_V(z) \\ &\times \int_{-1}^1 dx \left[T_g(z,x) F^g(x,\xi,t) + F^{(+)}(x,\xi,t) \left(T_{(+)}(z,x) + \frac{1}{N_f} T_q(z,x) \right) \right. \\ &\left. + T_q(z,x) \left(e^V_{u-d} F^{u-d}(x,\xi,t) + e^V_{d-s} F^{d-s}(x,\xi,t) \right) \right] , \end{aligned} \tag{4.1}$$

where we have suppressed the factorization and renormalization scale dependence of the meson DA, the hard scattering kernels and the GPDs for simplicity. The GPDs $F^g(x,\xi,t)$ and $F^{(+)}(x,\xi,t)$ are defined as in (2.7) and (2.36). The two flavor non-singlet GPDs $F^{u-d}(x,\xi,t)$ and $F^{d-s}(x,\xi,t)$ are defined as

$$\begin{aligned} F^{u-d}(x,\xi,t) =& (F^u(x,\xi,t) - F^u(-x,\xi,t)) - (F^d(x,\xi,t) - F^d(-x,\xi,t)) , \\ F^{d-s}(x,\xi,t) =& (F^d(x,\xi,t) - F^d(-x,\xi,t)) - (F^s(x,\xi,t) - F^s(-x,\xi,t)) . \end{aligned} \tag{4.2}$$

In contrast to the calculations in Chapter 3 we followed here the convention of [122] for the definition of the amplitude which allows a clear distinction of the different exchange channels and the leading and next-to-leading contributions. At the LO level the definition (4.1) is equivalent to the definition used in Chapter 3 .

We introduced in (4.1) the three different scattering kernels $T_g(z,x)$, $T_{(+)}(z,x)$ and $T_q(z,x)$ which correspond to the gluon, singlet and quark exchange diagrams respectively. The kernels are again functions of the two variables x and z as in Sect. 3.1. The explicit expressions for the full NLO scattering kernels are given in [122] and we do not want to repeat them at this point but give the formulas in Appendix C. One of the results of this work are the analytical expressions of the convolution of scattering kernels and the meson DA which we will present in Appendix C because the results are too long to show them here.

In (4.1) we also introduced the three process dependent charges Q_V, e_{u-d} and e_{d-s}. If one

assumes that the flavor content of the mesons is given by $\frac{1}{\sqrt{2}}(|u\bar{u}\rangle - |d\bar{d}\rangle)$, $\frac{1}{\sqrt{2}}(|u\bar{u}\rangle + |d\bar{d}\rangle)$ and $|s\bar{s}\rangle$ for ρ, ω and ϕ respectively then the charge factors are defined as

$$Q_\rho = \frac{1}{\sqrt{2}}\,, \qquad Q_\omega = \frac{1}{3\sqrt{2}}\,, \qquad Q_\phi = \frac{-1}{3}\,, \tag{4.3}$$

and

$$e^\rho_{u-d} = e^\rho_{d-s} = e^\omega_{d-s} = -e^\phi_{u-d} = \frac{1}{3}\,, \quad e^\omega_{u-d} = \frac{5}{3}\,, \quad e^\phi_{d-s} = -\frac{2}{3}\,. \tag{4.4}$$

4.2 Scale dependence of the amplitude

We have skipped the scale dependence of the meson DA, the GPDs and the hard scattering kernel in the previous section for shortness and now want to give a brief discussion of the different scales appearing in the amplitude of exclusive meson production.
As in leading order the GPDs and the meson DA are dependent on the factorization scale μ_F. Throughout Chapter 3 we have neglected the scale dependence of the meson DA completely because we were not interested in the evolution of the Gegenbauer coefficients a_n. We also used no special evolution procedure in the previous chapter and just took our choice of the factorization scale to obtain the forward PDFs which we then used as input for the double distribution ansatz to model the GPDs.
Now the situation is different: at NLO not only the GPDs and the meson DA but also the scattering kernels have an explicit scale dependence of the form

$$\ln\left(\frac{Q^2}{\mu_F^2}\right) \quad \text{and} \quad \ln\left(\frac{Q^2}{\mu_R^2}\right)\,. \tag{4.5}$$

This is a consequence of the evolution of the amplitude: the derivative of the amplitude with respect to the factorization or renormalization scale has to vanish at fixed order of $\alpha_s(\mu_R)$. This property can also be used to check the correctness of the scattering kernels. To be more precise one has

$$\mu^2 \frac{d}{d\mu^2}\mathcal{M} = 0\,, \tag{4.6}$$

for fixed order in the strong coupling. We will demonstrate in Appendix D.2 in detail that the above relation is fulfilled using the hard scattering and evolution kernels given in Appendix C.1 and Appendix D.1.
With the help of the above equation it is also possible to distinguish the parts in the scattering kernels which correspond to the factorization scale of the GPDs and the factorization scale of the meson DA which not necessarily have to be the same. For the rest of this work the two abbreviations μ_F and $\mu_{F(GPD)}$ are equivalent and denote the factorization scale of the GPDs. If necessary we will call the factorization scale of the meson DA $\mu_{F(DA)}$, to avoid confusions.
The scale dependence of the hard scattering kernels are purely determined by the evolution

equation and the renormalization group equation (RGE). We want to explain this, using for example the pure singlet scattering kernel (C.20). This scattering kernel appears at the NLO level and hence is proportional to $\alpha_s^2(\mu_R^2)$ and has no logarithmic dependence on the renormalization scale. This issue can be easily understood if we apply the RGE, which is given

$$\mu_R^2 \frac{d\alpha_s(\mu_R^2)}{d\mu_R^2} = -\beta_0 \alpha_s^2(\mu_R^2) - \beta_1 \alpha_s^3(\mu_R^2) + \mathcal{O}(\alpha_s^4)\,, \tag{4.7}$$

with

$$\begin{aligned} \beta_0 &= \frac{11}{3} N_c - \frac{2}{3} n_f\,, \\ \beta_1 &= \frac{51}{3} N_c - \frac{19}{3} n_f \end{aligned} \tag{4.8}$$

to the singlet scattering kernel. Taking the derivative with respect to μ_R of the singlet kernel the lowest term is of the power α_s^3. Because we are just considering terms up to the power α_s^2 it is obvious that at this power of α_s we cannot have an explicit logarithmic dependence of the singlet scattering kernel on μ_R. There is also a very intuitive picture of the fact that the singlet kernel cannot depend logarithmically on μ_R: terms containing logarithms of μ_R are always proportional to β_0 because they correspond to Feynman diagrams containing quark loops. Because quark loops in a digram give an additional power of α_s, the singlet scattering kernel cannot depend on terms proportional to β_0 at the order α_s^2. Term proportional to β_0 will appear for the singlet scattering kernel at the order α_s^3.
On can use similar arguments for the dependence on the two factorization scales $\mu_{F(GPD)}$ and $\mu_{F(DA)}$ and we will show this explicit in Appendix D.2, where we take the derivative of the amplitude with respect to the factorization scale.

4.3 Numerical treatment of the NLO amplitude

As for the leading order amplitude, where we developed a semi-analytic approach to calculate the real and imaginary part of the amplitude (cf. Appendix A) we want to calculate this two parts for the amplitude at NLO level. But now the situation is more difficult due to the fact that the scattering kernels are much more complicate functions. Furthermore we want to include the evolution of the GPDs and want to use a more realistic ansatz for the t dependence of the GPDs. This makes it impossible to find similar expressions for the real and imaginary part of the convolution of the GPDs and the hard scattering kernel as in the case of the LO amplitude. We have

$$\int_{-1}^{1} dx\, f(x,\xi,t) \frac{1}{\xi - x - i\epsilon} = \fint_{-1}^{1} dx \frac{f(x,\xi,t)}{\xi - x}) + i\pi f(\xi,\xi,t)\,. \tag{4.9}$$

We want to mention that the sign of the $i\epsilon$ cannot be chosen arbitrarily. The correct sign for the $i\epsilon$-prescription is given by the replacement $\xi \to \xi - i\epsilon$. Taking the correct sign for the

$i\epsilon$-prescription is not only important for the pole structure of the amplitude. As one sees in the Appendix C.1 the NLO scattering kernel contain terms proportional to logarithms and polylogarithms. These functions have a branch cut in the regions $x \in [-1, -\xi]$ and $x \in [\xi, 1]$ and the sign of $i\epsilon$ specifies the branch of the logarithms.
For the numerical evaluation of the amplitude it is easier to use the variable

$$y = \frac{\xi - x}{2\xi} - i\epsilon\,, \tag{4.10}$$

which is also defined in Appendix C.1. Using this variable the remaining x-integration can be written as

$$\mathcal{M}_{\gamma_L^\star \to V_L N} \sim \int\limits_{-1}^{1} dx F(x,\xi,t) T\left(\frac{\xi - x}{2\xi}\right) = 2\xi \int\limits_{-\frac{1-\xi}{2\xi}}^{\frac{1+\xi}{2\xi}} F(\xi(1-2y),\xi,t) T(y)\,. \tag{4.11}$$

In comparison to the LO amplitude the imaginary part is now not only given by $F(\xi,\xi,t)$ but by an integral in the two regions where the logarithmic and polylogarithmic functions of the scattering kernels have their branch cut.
For the computation of the amplitude it is sufficient to consider only the region $x \in [0,1]$ or $y \in [-(1-\xi)/2\xi, 1/2]$ because of the symmetry properties of the GPDs and the scattering kernels as discussed in Sect. 2.2 and Appendix C.1. As mentioned at the beginning of this section it was possible to find an analytical expression for the convolution of the GPDs and the scattering kernels within the double distribution ansatz. This is not possible for the NLO scattering kernels and we need a possibility to treat the poles of the scattering kernels in the right way. For this purpose we will use the subtraction method which we will explain at a short example: considering the singular integral of the type

$$\int\limits_{-1/2}^{1/2} dy \frac{f(y)}{(1-y)(y-i\epsilon)}\,, \tag{4.12}$$

which appear in the convolution of hard scattering kernels and the GPDs. It can be rewritten as

$$\int\limits_{-1/2}^{1/2} dy \frac{f(y)}{(1-y)(y-i\epsilon)} = \int\limits_{-1/2}^{1/2} dy \frac{f(y)-f(0)}{(1-y)y} + f(0) \int\limits_{-1/2}^{1/2} dy \frac{1}{(1-y)(y-i\epsilon)}\,. \tag{4.13}$$

With this rewriting we have removed the original singularity and the last term in (4.13) can be integrated in the complex plane.We finally obtain

$$\int\limits_{-1/2}^{1/2} dy \frac{f(y)}{(1-y)(y-i\epsilon)} = \int\limits_{-1/2}^{1/2} dy \frac{f(y)-f(0)}{(1-y)y} + f(0)(i\pi + \ln(3))\,. \tag{4.14}$$

With this procedure we obtain automatically the correct sign for the imaginary part. The constant term $f(0)\ln(3)$ is the subtraction term and can be calculated also for the NLO scattering kernels. The numerical values for the subtraction terms and an example of how to separate the real and imaginary part for the NLO amplitude are given in App. C.2. Using the above method makes the final integration much easier because we only have to compute logarithmic singular integrals which can be treated with programs like *MATHEMATICA*.

4.4 High energy behavior of the amplitude

The high energy regime of hard processes is very interesting because it has been experimentally quite extensively tested at the HERA experiments H1 and ZEUS. This experiments have probed the production of light vector mesons like ρ^0, ϕ and ω but also the heavy vector mesons J/Ψ and Υ in the x_B range from 10^{-2} to 10^{-4}. For a review of the experimental situation see [123,124]. In this region of small x_B the process of exclusive vector meson production is clearly dominated by the imaginary part of the gluon contribution to the amplitude. The dominance of the gluon contribution was found already at values of $x_B \equiv 0.05$ as shown in our results for the cross section of ρ^0 and ϕ production in Sect. 3.3. In our physical picture this means that the process is dominated by the two-gluon exchange. Being dominated by the gluon contribution the choice of the factorization is very important because the scale violation in the gluon density is quite strong for small x_B.
The choice of the factorization scale and Q^2 in the previous chapter was quite arbitrary because at LO both scales appear independently. For the amplitude at NLO this is not the case because we have now an explicit logarithmic dependence of the scattering kernel on the factorization scale. This terms should diminish the dependence of the amplitude on the factorization scale at fixed Q^2. In order to get a first impression of the size of the NLO correction at small x_B we will expand our hard scattering kernels in powers of $1/y$, which corresponds to small values of ξ. We will not focus only on the gluon scattering kernel $T_g(x)$ but we will also include the scattering kernel for the pure singlet contribution $T_{(+)}$.

Expanding the real and imaginary part of the gluon scattering kernel in powers of $1/y$ we obtain

$$\begin{aligned}\mathrm{Re}\,\mathcal{I}_{g,0}(y) = \ln\left(\frac{Q^2}{\mu_F^2}\right)\left[-4(c_1-c_2)+(4c_2-3c_1)\ln|y|\right] - \frac{3}{4}c_1(4-\pi^2) \\ + \frac{\beta_0}{2}\ln\left(\frac{\mu_R^2}{\mu_{F(GPD)}^2}\right) + \ln^2|y|\left(2c_2 - c_1\frac{3}{2}\right) - \pi^2 c_2 + \mathcal{O}\left(\frac{1}{y}\right),\end{aligned} \tag{4.15}$$

for the real part and

$$\mathrm{Im}\,\mathcal{I}_{g,0}(y) = 4y(c_1-c_2)\left[\ln\left(\frac{Q^2}{\mu_F^2}\right) - 2\right] + \mathcal{O}(1)\,, \tag{4.16}$$

for the imaginary part. To obtain this expansion we used the formulas given in Appendix C.3. We have to combine the above results with the LO scattering kernel $1/(y\bar{y})$ to obtain the

complete NLO scattering kernel. We obtain the following result for the NLO gluon scattering kernel in powers of $1/y$

$$\begin{aligned}\mathrm{Re}\, T_{g,NLO}(y) = \frac{1}{y\bar{y}}\Bigg(&\ln\left(\frac{Q^2}{\mu_F^2}\right)\left[-4(c_1-c_2)+(4c_2-3c_1)\ln|y|\right]-\frac{3}{4}c_1(4-\pi^2) \\ &+\frac{\beta_0}{2}\ln\left(\frac{\mu_R^2}{\mu_{F(GPD)}^2}\right)+\ln^2|y|\left(2c_2-c_1\frac{3}{2}\right)-\pi^2 c_2\Bigg)+\mathcal{O}\left(\frac{1}{y^2\bar{y}}\right),\end{aligned} \tag{4.17}$$

for the real part and for the imaginary part we obtain

$$\mathrm{Im}\, T_{g,NLO}(y) = \frac{4}{\bar{y}}(c_1-c_2)\left[\ln\left(\frac{Q^2}{\mu_F^2}\right)-2\right]+\mathcal{O}\left(\frac{1}{y\bar{y}}\right). \tag{4.18}$$

It is obvious that the above expansion fits not for the whole integration region $y \in \left[-\frac{1-\xi}{2\xi}, \frac{1}{2}\right]$. Nevertheless we can make a first rough estimate about the size of the NLO corrections. Under the assumption that the main contribution to the integral comes from the integration region $-\frac{1-\xi}{2\xi} \ll y \ll -\frac{1}{2}$ (which is corresponding to the interval $2\xi \ll x \ll 1$ in the original variable x) we can neglect the terms of our prescription of the real and imaginary part in App. C.2 containing the integrals in the region $y \in [-1/2, 1/2]$. For the imaginary part of the gluon contribution to the amplitude we get

$$\mathrm{Im}\,\mathcal{M} \sim \frac{\pi\alpha_s}{Q}\left(F^g(\xi,\xi,t)+\frac{\alpha_s}{\pi}N_c\left[\ln\left(\frac{Q^2}{\mu_F^2}\right)-2\right]\int\limits_{-\frac{1-\xi}{2\xi}}^{-\frac{1}{2}} dy\,\frac{F^g(\xi(1-2y),\xi,t)}{\bar{y}}\right). \tag{4.19}$$

If we now assume the behavior of the gluon GPD at small values of x to be $F^g(x,\xi,t) \sim const.$ and of the order $F^g(\xi,\xi,t)$ we find

$$\mathrm{Im}\,\mathcal{M} \sim \frac{\pi\alpha_s}{Q}\left(F^g(\xi,\xi,t)+\frac{\alpha_s}{\pi}N_c\left[\ln\left(\frac{Q^2}{\mu_F^2}\right)-2\right]\ln\left(\frac{1}{\xi}\right)F^g(\xi,\xi,t)\right). \tag{4.20}$$

This result indicates that the NLO corrections to the imaginary part are parametrically large, $\sim \ln(1/\xi)$ and of opposite sign to the LO part unless we choose $\mu_F < \frac{Q}{e}$. This result was originally obtained in [99, 122]. We can also immediately see that the NLO corrections for the real part do not show a similar behavior because the expansion just starts at the order $1/(y\bar{y})$. The question now arises, is how good our approximation is. We have checked our approximation of the scattering kernel as well as the simplification of the gluon GPD at small x numerically. We find that our result with the expanded scattering kernel and the exact gluon GPD the deviation from the exact result is at the 5-10% level for $x_B < 5 \cdot 10^{-3}$. If we also use the approximation for the GPD we found a strong discrepancy with the exact result. But for a first rough estimate of the size of the NLO corrections our approximation is sufficient and we will see in Sect. 4.6 that our exact results show the similar behavior we obtained here.

Let us now turn to the pure singlet part of the amplitude. We restrict ourself now only on the imaginary part and expand the scattering kernel again in powers of $1/y$. Using again the expressions in App. C.3 we obtain

$$\mathrm{Im}\,\mathcal{I}_q(y) = 2\left[3 - \ln\left(\frac{Q^2}{\mu^2_{F(GPD)}}\right)\right] + \mathcal{O}\left(\frac{1}{y}\right) . \tag{4.21}$$

For the real part of the singlet scattering kernel (C.20) we find one additional power more in $1/y$ as for the gluon scattering kernel. Assuming that the behavior of the singlet GPD at small x is given by $F^{(+)}(x,\xi,t) \sim 1/x$ we find again that the imaginary part has a logarithmic enhanced contribution $\ln(1/\xi)$ as for the NLO gluon contribution of the amplitude. Because the singlet scattering kernel appears at order α_s^2 we have no comparison to a LO contribution as for the gluon part of the amplitude. To keep the corrections through the pure singlet part of the amplitude small at small x we have to choose the factorization scale to be $\mu_{F(GPD)} \approx Q/e^{3/2}$ which is much smaller than for the gluon case. This leads now to the situation where we are not able to keep the NLO contributions of the gluon and the pure singlet part simultaneously small.

Let us finally mention that we find no similar behavior for the NLO quark scattering kernel at small x. For the imaginary part of the quark kernel we find the leading power is given by $1/y$. Therefore we find no logarithmically enhanced contributions for the NLO quark scattering kernel at small x.

4.5 Modeling of $E(x,\xi,t)$

In Chapter 3 we have neglected the contributions to the cross section proportional $|\mathcal{E}|^2$ because it has a kinematical factor ξ^2 in front and thus gives only a small contribution. In this chapter we are mainly interested in the amplitude of exclusive meson production and therefore we also want to determine the size of the contributions arising from the GPD $E(x,\xi,t)$.

To obtain a model for the helicity flip GPD $E(x,\xi,t)$ we follow the ansatz of [82] which is based on the extraction of GPDs from experimental data of different from factors. Because of Lorentz invariance the ξ-dependence drops out in the sum rule for the form factors (2.19) and the ansatz concentrates on the correlation between the variables x and t.
For our purpose we need the GPDs at $\xi \neq 0$, so we use the ξ-independent ansatz of [82] and take this as "forward" input for the double distribution model (2.44). For the valence distribution we took the following ansatz for $\xi = 0$

$$E^q_v(x,t,\mu^2) = E^q(x,t,\mu^2) + E^q(-x,t,\mu^2) = e^q_v(x)\exp[t g_q(x)] \tag{4.22}$$

with

$$g_q(x) = \alpha'(1-x)^3 \log\frac{1}{x} + D_q(1-x)^3 + C_q x(1-x)^2 \tag{4.23}$$

u_v	$2\bar{u}$	d_v	$2\bar{d}$	$E_v^u(x,t=0)$	$E_v^d(x,t=0)$
0.289	0.055	0.118	0.071	0.138	-0.13

Table 4.1. Second moments of forward PDFs for CTEQ6M parameterization at $\mu_F = 2\,GeV$ and for $E_v^q(x,t=0)$ according to the model of [82].

with $\alpha' = 0.9\,\mathrm{GeV}^{-2}$ and

$$e_v^q(x) = N_q \kappa_q x^{-\alpha_q}(1-x)^{\beta_q}\,.$$

κ_q is the contribution of a quark flavor q to the anomalous magnetic moment of the proton. For the free parameters in (4.23) we take the default choice of [82]

$$\begin{aligned} &\beta_u = 3.99, && \beta_d = 5.59 \\ &C_u = 1.22\,\mathrm{GeV}^{-2}, && C_d = 2.59\,\mathrm{GeV}^{-2} \\ &D_u = 0.38\,\mathrm{GeV}^{-2}, && D_d = -0.75\,\mathrm{GeV}^{-2}\,, \end{aligned} \tag{4.24}$$

and take $\alpha_u = \alpha_d = 0.55$ according to [82]. The correct normalization is ensured by the factor

$$N_q = \frac{\Gamma(2-\alpha_q+\beta_q)}{\Gamma(1-\alpha_q)\Gamma(1+\beta_q)}\,, \tag{4.25}$$

which guarantees the right contribution of the quark flavor q to the anomalous magnetic moment of the proton.
Besides of the valence distribution we also need the antiquark distribution $E^{\bar{q}}(x,\xi,t)$. We use a similar ansatz as for the valence distribution

$$E^{\bar{q}}(x\,t,\mu^2) = e^{\bar{q}}(x)\exp[t g_{\bar{q}}(x)]\,. \tag{4.26}$$

For $g_{\bar{q}}(x)$ we use the form of 4.23 and for the general shape we use the ansatz

$$e^{\bar{q}}(x) = N_{\bar{q}} x^{-\alpha_{\bar{q}}}(1-x)^{\beta_{\bar{q}}}\,.$$

For the normalization there is no corresponding equation as for $E_v^q(x,t)$. As a guess we use the second moments of the forward PDFs, and extract from the ratio of the valence quark contribution to the anti-quark contribution. For u-quarks one finds roughly a factor 1/10 for the ratio of anti-quarks to valence quarks and for d-quarks we find a factor 1/3 for the same ratio, where we used the CTEQ6M parameterization at the scale $\mu = 2\,\mathrm{GeV}$. So we have for the normalization

$$\frac{\int_0^1 dx\, x E^{\bar{q}}(x,t=0)}{\int_0^1 dx\, x E_v^q(x,t=0)} = \frac{\int_0^1 dx\, x\bar{q}(x)}{\int_0^1 dx\, x q_v(x)}\,. \tag{4.27}$$

One finds for the second moments of the forward PDFs the values listed in Tab. 4.1. The

normalization factors $N_{\bar{q}}$ are therefore given by

$$N_{\bar{u}} = \frac{0.1381}{10}\frac{\Gamma(3-\alpha_{\bar{u}}+\beta_{\bar{u}})}{\Gamma(2-\alpha_{\bar{u}})\Gamma(1+\beta_{\bar{u}})}\,,$$
$$N_{\bar{d}} = -\frac{0.13}{3}\frac{\Gamma(3-\alpha_{\bar{d}}+\beta_{\bar{d}})}{\Gamma(2-\alpha_{\bar{d}})\Gamma(1+\beta_{\bar{d}})}\,. \tag{4.28}$$

The low-x behavior of $e^{\bar{q}}(x)$ is given by the exponent $\alpha_{\bar{q}}$ which we fitted in the range $x \in [10^{-4}; 10^{-3}]$ to the forward PDFs. We obtain the following values

$$\alpha_{\bar{u}} = \alpha_{\bar{d}} = 1.25\,. \tag{4.29}$$

The parameter $\beta_{\bar{q}}$ was also fitted to the forward PDFs and then tuned in such way that the positivity condition

$$|e^{\bar{q}}| \leq 2m_p \left(\frac{g(x)}{f(x)}\right)^{3/2} \sqrt{f(x)-g(x)}\,\bar{q}(x)\,e^{\frac{1}{2}(1+\ln 2)} \tag{4.30}$$

is fulfilled in the range $x \leq 0.9$. In order to satisfy the condition (4.30) we have to set

$$\beta_{\bar{u}} = 9.6 \qquad \text{and} \qquad \beta_{\bar{d}} = 9.2\,. \tag{4.31}$$

We also need the helicity flip GPD for gluons for which we use the ansatz

$$E^g(x,\xi=0,t) = N_g x^{-\alpha_g}(1-x)^{\beta_g} e^{t g_g(x)} \tag{4.32}$$

with

$$g_g(x) = \alpha'_g(1-x)^2 \log\frac{1}{x} + B(1-x)^2\,. \tag{4.33}$$

The parameter α' and B are obtained from exclusive J/ψ photoproduction at ZEUS and H1 [125, 126]. We use the average of their results for our two parameters, which are then given by

$$\alpha'_g = 0.140\,\mathrm{GeV}^{-2}\,, \qquad B = 2.195\,\mathrm{GeV}^{-2}\,. \tag{4.34}$$

As condition for the normalization of $E^g(x,t)$ one can use the sum rule

$$\sum_q \int_0^1 dx\, x\,[E^q_v(x,0) + 2E^{\bar{q}}(x,0)] + \int_0^1 dx\, E^g(x,0) = 0\,. \tag{4.35}$$

So the normalization factor N_g is given by

$$N_g = 0.0505\frac{\Gamma(2-\alpha_g+\beta_g)}{\Gamma(1-\alpha_g)\Gamma(1+\beta_g)}\,. \tag{4.36}$$

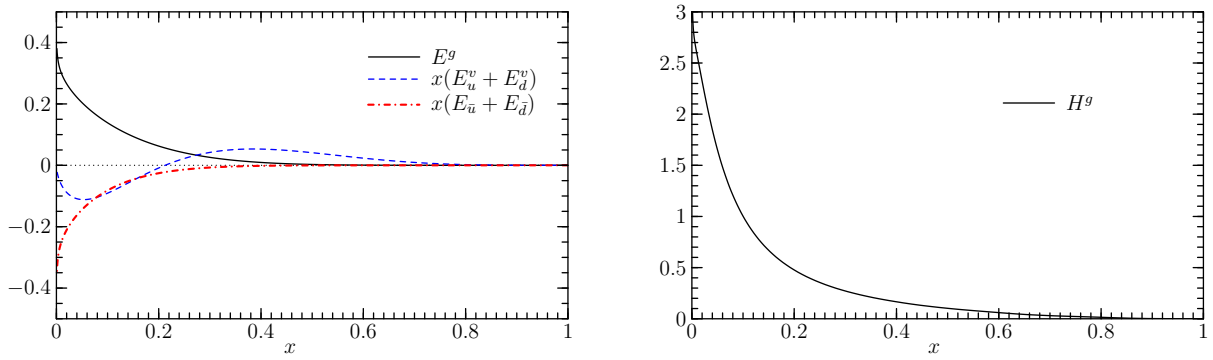

Figure 4.2. Comparison of the helicity dependent GPD $E(x,\xi,t)$ and the gluon GPD $H^g(x,\xi,t)$ at $\xi = 0$, $t = -0.15\,GeV^2$ and $\mu_F = 2\,GeV$.

The parameter α_g and β_g in (4.32) are fitted in the same way as the parameter for the anti-quark GPD and β_g is changed in that way that the positivity condition (4.30) is fulfilled in the range $x \in [10^{-4}; 0.9]$. The numerical values for the parameters are

$$\alpha_g = 0.102\,, \qquad \beta_g = 6.7\,. \tag{4.37}$$

In Fig. 4.2 we show the results for the valence, sea and gluon helicity dependent GPDs for $\xi = 0$, $t = -0.15\,\mathrm{GeV}^2$ and at the initial scale $\mu_F = 2\,\mathrm{GeV}$. Form this figure it is immediately clear that the contribution coming from $E^g(x,\xi,t)$ will be much smaller than the corresponding contribution form $H^g(x,\xi,t)$. An additional information one gains from Fig. 4.2 is the sign of the contribution from $E^q(x,\xi,t)$. It will be opposite to that of the contributions from $H^q(x,\xi,t)$ because of the negative valued GPDs $E_v^u + E_v^d$ and $E_{\bar{u}} + E_{\bar{d}}$.

All our parameterizations are still independent functions of ξ. Because we do not want to restrict ourself on the case $\xi = 0$, we use our ansatz as input distribution for the double distribution which is discussed in some detail in Sect. 2.4. According to (A.1) the ξ dependence of the GPDs $E^q(x,\xi,t)$ and $E^g(x,\xi,t)$ is generated by

$$\begin{aligned}
E^q(x,\xi,t) &= \int_{-1}^{1} d\beta \int_{-1+|\beta|}^{1-|\beta|} d\alpha\; \delta(x-\beta-\xi\alpha)\, h(\beta,\alpha) \Big[\theta(\beta)\, E_q(\beta,t) \;- \theta(-\beta)\, E_{\bar{q}}(-\beta,t)\Big]\,, \\
E^g(x,\xi,t) &= \int_{-1}^{1} d\beta \int_{-1+|\beta|}^{1-|\beta|} d\alpha\; \delta(x-\beta-\xi\alpha)\, h(\beta,\alpha)\, \beta \Big[\theta(\beta)\, E^g(\beta,t) \;- \theta(-\beta)\, E^g(\beta,t)\Big]\,,
\end{aligned} \tag{4.38}$$

where $E^q(x,t)$ is given by

$$E_q(x,t) = E_v^q(x,t) + 2E_{\bar{q}}(x,t)\,. \tag{4.39}$$

We will use the discussed parameterization for the t dependence in the following section also for the GPDs $H(x,\xi,t)$ and $\tilde{H}(x,\xi,t)$. For the gluon GPD $H^g(x,\xi,t)$ we will use the

same parameters (4.34) and (4.37) as for $E^g(x,\xi,t)$. For the u and d quark GPDs $H^u(x,\xi,t)$ and $H^d(x,\xi,t)$ we used the following ansatz at $\xi = 0$

$$H^q(x,t) = q(x)\exp[t f_q(x)]\,, \tag{4.40}$$

where

$$f_q(x) = \alpha'(1-x)^3 \log\frac{1}{x} + B_q(1-x)^3 + A_q x(1-x)^2 \tag{4.41}$$

and we choose $\alpha' = 0.9\,\mathrm{GeV}^2$. For the parameters B_q and A_q we choose the following values from [82]

$$\begin{aligned} A_u &= 1.26\,\mathrm{GeV}^{-2}, \quad & A_d &= 3.82\,\mathrm{GeV}^{-2} \\ B_u &= 0.59\,\mathrm{GeV}^{-2}, \quad & B_d &= 0.32\,\mathrm{GeV}^{-2}\,, \end{aligned} \tag{4.42}$$

where we make no distinction for the valence and sea quarks as we did for $E(x,\xi,t)$. For the polarized quark GPDs $\tilde{H}^u(x,\xi,t)$ and $\tilde{H}^d(x,\xi,t)$ we use the same parameters (4.42) as for the unpolarized GPDs for simplicity. For a detailed discussion of the polarized GPDs see [82].

4.6 Numerical results

In this section we want to present our numerical results for the amplitude of exclusive meson production at NLO. We will again use the double distribution model for the GPDs. But now we will use the numerical implementation of [53] for the evolution of the GPDs where we take the analytic parameterization of the CTEQ6M forward parton densities [12] at the starting scale $\mu_F = 1.3\,\mathrm{GeV}$ as input. Instead of the factorized ansatz of the t-dependence of the GPDs we will now use the parameterization of [82] which we discussed in some detail in the previous section at the example for the helicity-flip GPD $E(x,\xi,t)$.
For the determination of the strong coupling constant $\alpha_s(\mu_R)$ we use the two loop result with fixed $N_f = 3$. This is due to the fact that we do not want to consider the production of charm quarks and also the numerical difference is at the level of two % for range of μ_R we want to consider.
We present our result for the real and imaginary part of the amplitude in the following form where we have neglected the prefactors of (4.1):

$$\mathcal{H}^g(\xi,t) = \int_{-1}^{1} dx\, T_g(x) H^g(x,\xi,t)\,, \tag{4.43}$$

$$\mathcal{H}^{S(a)}(\xi,t) = \int_{-1}^{1} dx\, \frac{1}{N_f} T_{q,V}(x) H^{(+)}(x,\xi,t)\,, \quad \mathcal{H}^{S(b)}(\xi,t) = \int_{-1}^{1} dx\, T_{(+)}(x) H^{(+)}(x,\xi,t)\,, \tag{4.44}$$

$$\mathcal{H}^{u-d}(\xi,t) = \int_{-1}^{1} dx\, T_{q,V}(x) H^{u-d}(x,\xi,t)\,, \quad \mathcal{H}^{d-s}(\xi,t) = \int_{-1}^{1} dx\, T_{q,V}(x) H^{d-s}(x,\xi,t)\,. \quad (4.45)$$

For the helicity-flip GPD $E(x,\xi,t)$ we have defined analog expression.
We want to present our results for two different regions of x_B, the small-x_B region given by $x_B \in [10^{-4}, 10^{-1}]$ which will correspond to high energies achieved by H1 and ZEUS. The second region is for fixed target experiments like HERMES and is given by $x_B \in [0.1, 0.3]$. For this two sector we choose fixed values for Q^2, the factorization and renormalization scale. We will discuss the scale dependence of our results separately at fixed values of x_B.

4.6.1 Results for $\mathcal{H}$

We want to start with the results for the convolution of the GPD $H(x,\xi,t)$ with the different scattering kernels because one expects that this is the largest contribution to the amplitude. In this and the following section the abbreviation NLO refer to the part of the amplitude which are proportional to α_s^2 and LO referred to the part of the amplitude proportional to α_s. The sum of both we will explicitly denote by LO+NLO. We also like to mention that the presented results are always for the asymptotic scattering kernel and will be marked explicitly if we consider scattering kernels obtained from the higher Gegenbauer coefficients in the expansion of the meson DA.
Let us first discuss the case of $x_B \in [10^{-4}, 10^{-1}]$ and $t = 0\,\text{GeV}$. An interesting question arising is the magnitude of the different terms in the NLO scattering kernels. The results are presented in Fig 4.3 where we have chosen $Q = \mu_R = \mu_F = 4\,\text{GeV}$ and split the different scattering kernels in scale dependent and scale independent terms. The upper two plots show the results for real and imaginary part of the gluon contribution to the amplitude. One clearly sees the strong rise of the constant term of the imaginary part as described in Sect. 4.4. The sign of the constant term is opposite to that proportional to $\ln(Q^2/\mu_F^2)$. For the choice $Q = \mu_F$ this term is equivalent to zero and one is only left with the large contribution of the constant term. And one is left with a large contribution form the constant term. The same situation shows up for the real part of the NLO gluon term but there the rise of the constant term is not as strong for small x_B as for the imaginary part. It is also clear from the upper two plots in Fig. 4.3 that one has to choose $\mu_R \ll \mu_F$ or $\mu_R \gg \mu_F$ to obtain sizable contributions form the term proportional to $\ln(\mu_R^2/\mu_F^2)$. And especially for the widely use choice $\mu_R = \mu_F$ this term is exact zero.
Let us now turn the pure singlet contribution of the amplitude. The single parts are shown in the two middle plots of Fig. 4.3. For this contribution one has no term dependent on the renormalization scale but only one proportional to $\ln(Q^2/\mu_F^2)$. This term is again of opposite sign in comparison to the constant term as in the case of the gluon contributions. In comparison to the gluon results the absolute magnitude of the contributions is much smaller. As explained in Sect. 4.4 it is not possible to find a scale setting for Q and μ_F for which the corrections of the gluon and the pure singlet contribution become small.
The situation is different for the convolution of the singlet GPD with the quark scattering

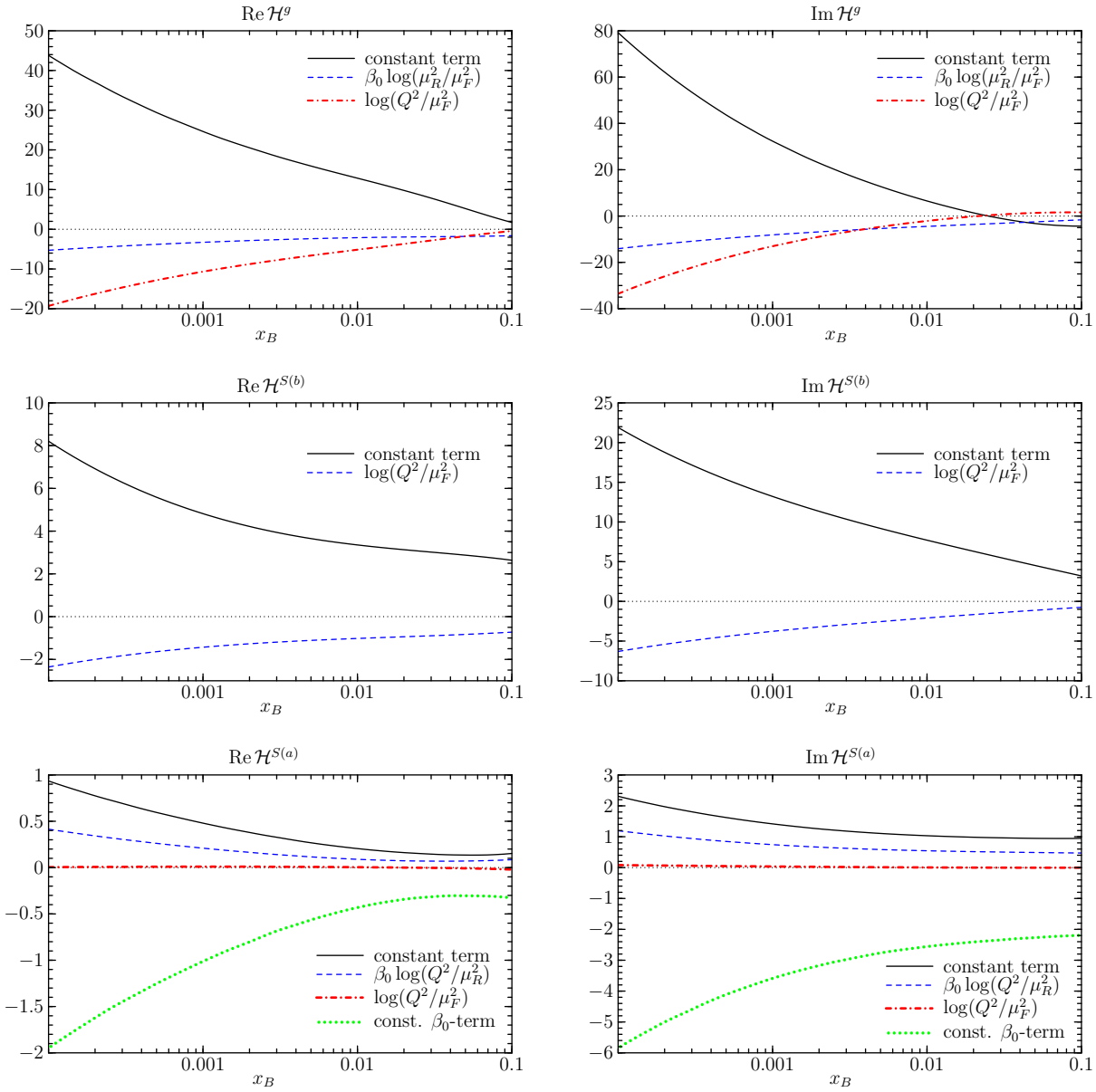

Figure 4.3. Single contributions to the pure NLO part of the real and imaginary part for the amplitude with the specific choice $\mu_F = \mu_R = 4\,GeV$. The upper left and upper right figure correspond to the real and imaginary part for the gluon contribution to the amplitude. The two figures in the middle are the real and imaginary part of the singlet term, $T_{(+)}$, of the amplitude and the lower two plots are for the singlet GPD convoluted with the quark scattering kernel.

kernel. In the lower two plots of Fig. 4.3 one sees that for this case the contributions coming from the term proportional to μ_F are negligible small compared to the other ones. A new feature is the appearance of two constant terms, the first one is analog to the constant terms of the previous two parts of the amplitude. The second one is proportional to β_0 and therefore directly related to the term proportional to the renormalization scale. The two constant terms have opposite sign and for $Q = \mu_R$ they show a cancellation which leads to a small correction to the LO contribution as we will see. The term proportional to μ_R is positive and therefore can lead to cancellations with the constant β_0-term. This is used in the BLM scale setting prescription [127]. Within this prescription the renormalization scale is chosen in such a way that the higher order corrections proportional to β_0 vanish. For our case that means that the constant β_0 term and the term proportional to μ_R cancel each other. We will discuss the BLM scale setting in detail later in this section.

Let us turn now to the comparison of LO and NLO parts of the amplitude. The results are shown in Fig. 4.4 for the small-x_B region. We choose again $Q = \mu_R = \mu_F$ and in addition $Q = \mu_{F(DA)}$ because we also want to investigate the influence of the higher Gegenbauer coefficients. With this specific choice all scale dependent terms of the scattering kernels are identical to zero and we are just left with the constant terms. The upper two plots of Fig. 4.4 show again the gluon contribution of the amplitude. We find that with setting all scales equal the NLO corrections are of the same magnitude but of opposite sign as expected from the high energy expansion in Sect. 4.4. This happens for the real as well as for the imaginary part. The sum of LO and NLO parts would therefore lead to a almost complete cancellation of the real and imaginary part of the gluon contribution of the amplitude. This would lead to an approximately flat energy behavior of the cross section (if one neglects the contributions coming from the quark terms). This is a clear contrast to the experimental observations [123] which support a rising of the cross section with energy for fixed Q^2. We will see later in this section when discussing the scale dependence of our results for fixed x_B that the situation changes. Nevertheless this observation does not support the naive scale setting procedure at high energies.
The situation is similar for the contributions coming from the singlet GPD $H^{(+)}(x, \xi, t)$ as shown in the two middle plots of Fig. 4.4. There we plotted the NLO part coming from the convolution with the singlet and quark kernel in comparison to the LO contribution of the convolution with the quark kernel. Again the scales are all identical and one finds that the new contribution from the singlet kernel is of opposite sign and is even larger than the LO contribution from the quark kernel. This would again lead to cancellation of both contributions. A pleasant observation is that the NLO corrections to the quark scattering kernel are small in comparison to the LO ones and hence give only a small correction to the amplitude. In the last two plots of Fig. 4.4 we compared the sum of all above LO and NLO contributions and show also the results one obtains for the scattering kernels proportional to the higher Gegenbauer coefficients. For a better comparison of the different terms we set $a_2 = a_4 = 1$. As stated in the discussion of the single terms one now clearly sees that for the sum of them one finds a nearly complete cancellation of the LO and asymptotic

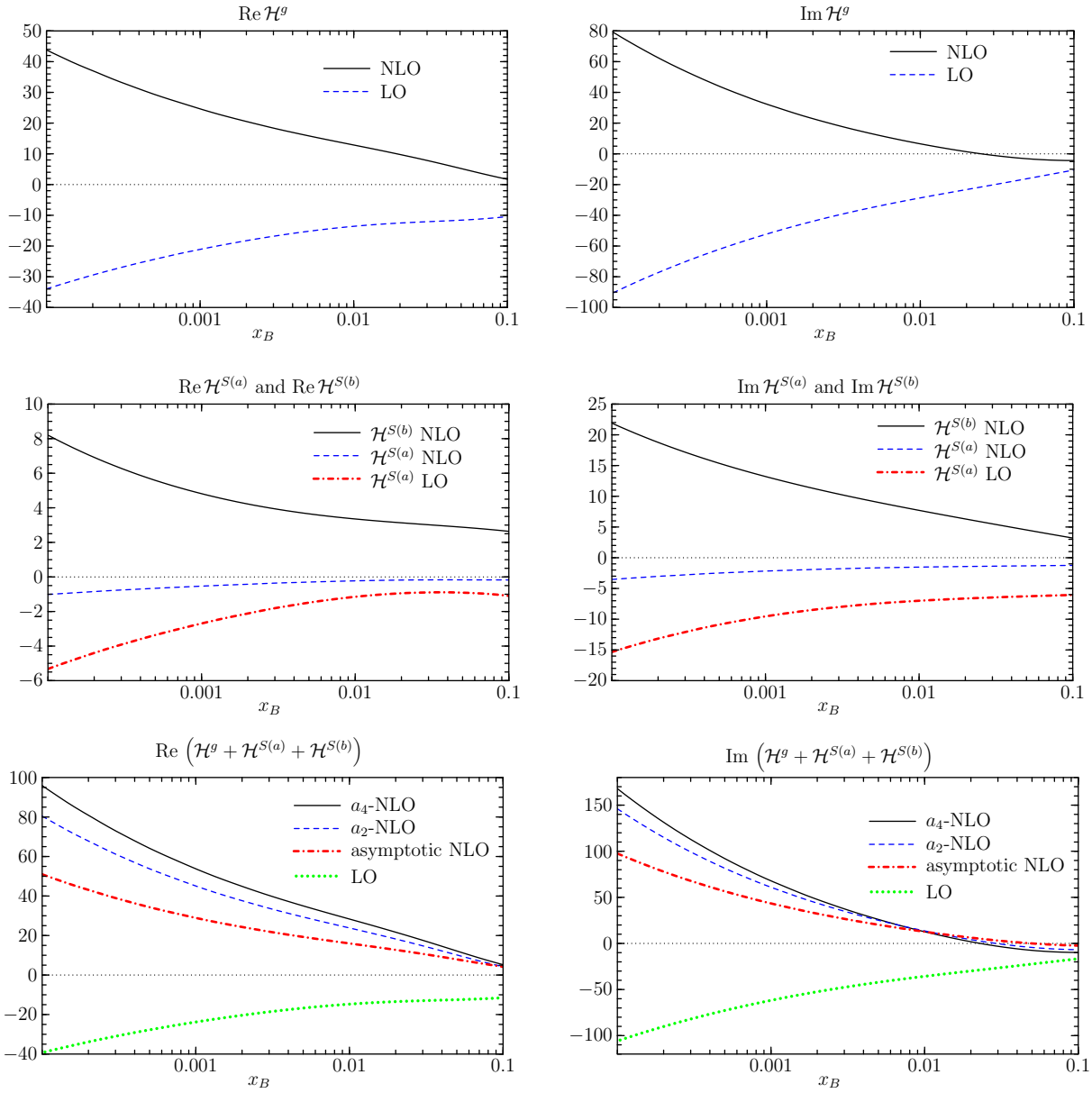

Figure 4.4. Comparison of pure LO and NLO parts for $\mathcal{H}^g$ (upper two plots), $\mathcal{H}^{S(a)}$ and $\mathcal{H}^{S(b)}$ (middle plots) and the sum of all three (lower figures) at the scales $\mu_{F(GPD)} = \mu_{F(DA)} = \mu_R = Q = 4\,GeV$. The label a_2-NLO (a_4-NLO) corresponds to the result for the convolution with the scattering kernel obtained from the second (fourth) term in the Gegenbauer expansion of the meson distribution amplitude, where we set $a_2 = a_4 = 1$.

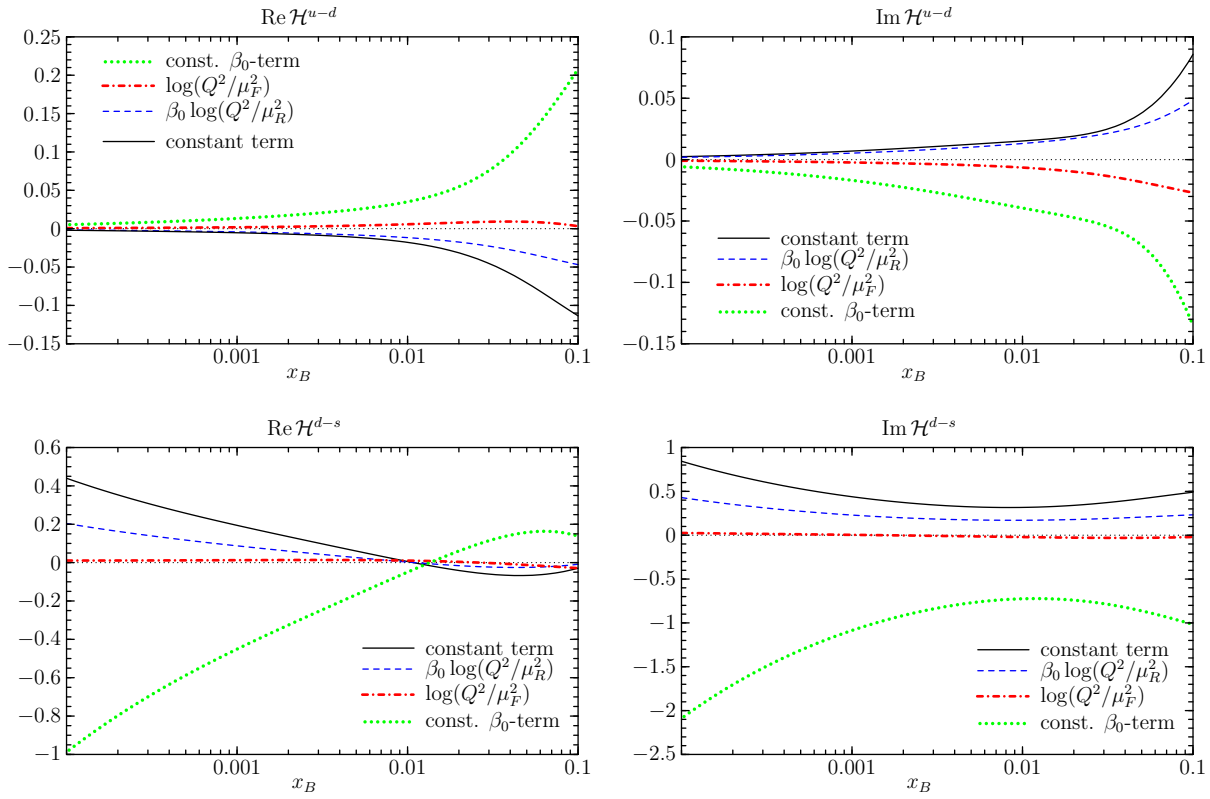

Figure 4.5. Single contributions to the pure NLO part of flavor non-singlet combinations $H^{u-d}(x,\xi,t)$ and $H^{d-s}(x,\xi,t)$ with the specific choice $\mu_F = \mu_R = 4\,GeV$.

NLO contribution. The results for the NLO contributions from the higher Gegenbauer coefficients have the same sign as the asymptotic correction but they are larger by its absolute value. One also sees that the change from the asymptotic scattering kernel to the scattering kernel proportional to a_2 is much bigger than the change from a_2 to a_4. This supports the assumption that the expansion of the meson DA in terms of Gegenbauer polynomials is a converging series.

For completeness we present the results for the two flavor non-singlet GPDs $H^{u-d}(x,\xi,t)$ and $H^{d-s}(x,\xi,t)$ in the small-x_B region. Figure 4.5 shows again the different contributions to the pure asymptotic NLO part for $Q = \mu_R = \mu_F = 4\,\text{GeV}$. One finds a different behavior for the $u-d$ and the $d-s$ combination. In the case of $u-d$ the single contributions almost vanish at very small x_B. This is due to the fact that for the u and d quark distribution are quite identical at this values of x_B and one has a complete cancellation of both contributions. For $d-s$ this is not the case because the d quark distribution is still larger than the strange quark distribution. But both combinations give results of the same order of magnitude as the gluon and singlet terms in the region $x_B \sim 0.1$. In Fig. 4.6 we compare the LO and the sum of LO and NLO contributions for the two non-singlet combinations. For all scales being equal we find only small correction to the LO part. This is due to the partial cancellation of the two constant terms of the scattering kernel as for the convolution of the singlet GPD

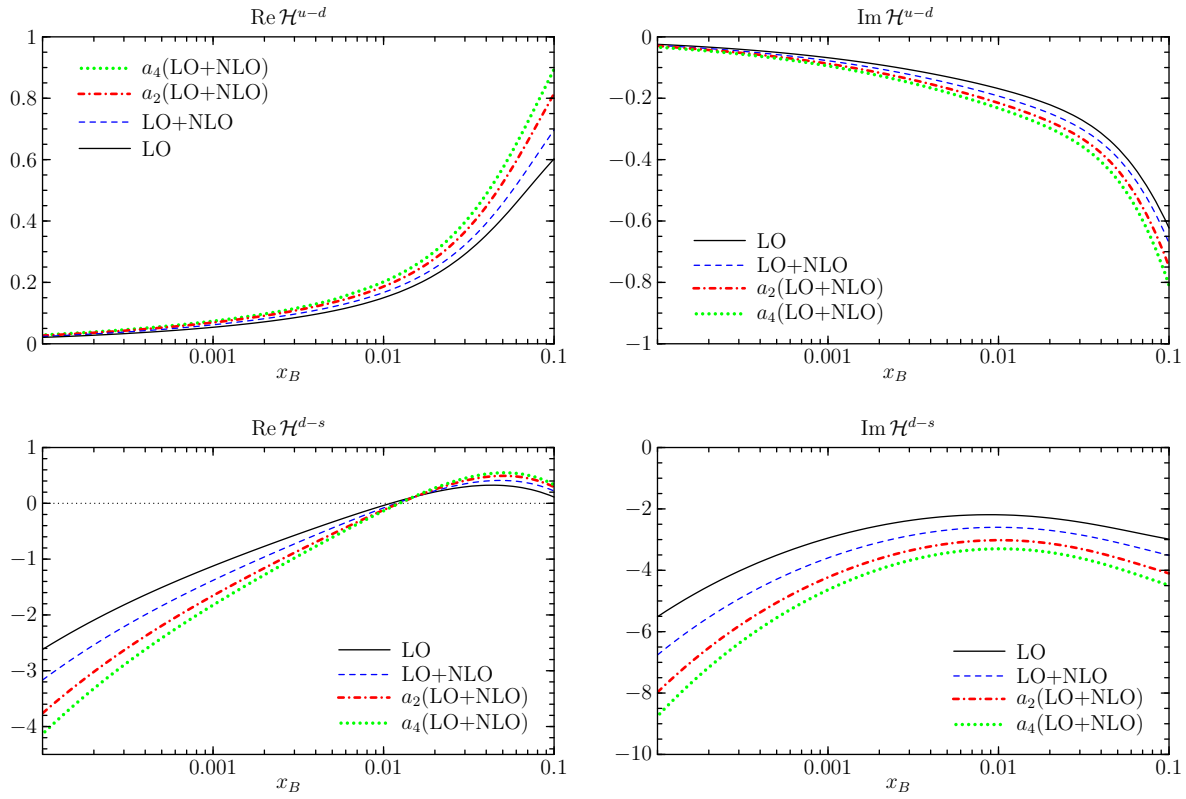

Figure 4.6. Comparison of LO sum of LO and NLO terms of the two GPDs $H^{u-d}(x,\xi,t)$ and $H^{d-s}(x,\xi,t)$ with the scale set to be $\mu_{F(GPD)} = \mu_{F(DA)} = \mu_R = 4\,GeV$.

with the quark scattering kernel.

After the discussion of the small-x_B we now want to turn to the region where $x_B \in [0.1, 0.3]$ which is of interest in fixed target experiments. We will proceed as before and want to start with the different contributions to the NLO parts of the gluon and singlet terms of the amplitude. Because of the limited energy range of fixed target experiments we will choose now $Q = \mu_R = \mu_F = 2\,\text{GeV}$. In Fig. 4.7 we show our results for the individual terms of the gluon and singlet terms. The plots look quite similar to Fig. 4.3 but as expected the gluon and two singlet contributions are of the same order of magnitude. For the gluon we find again the different signs of the constant term and the μ_F dependent term but now also the term proportional to the renormalization scale can give sizeable contributions. For the pure singlet part, shown in the two middle plots of Fig. 4.3, we find the same picture as in the small-x_B region. It is also obvious that for our special choice of the scale the constant terms of the pure singlet and gluon part will cancel each other in the imaginary part because they have opposite sign. This will lead to a small correction to the LO contribution for the sum of both terms. For the real part it is vice versa. Here the two constant parts have the same sign and one can expect large NLO corrections. The single terms of the convolution of singlet GPD and quark scattering kernel show the same behavior as in the small-x_B region and because now the amplitude is no longer purely dominated by the gluon part one will

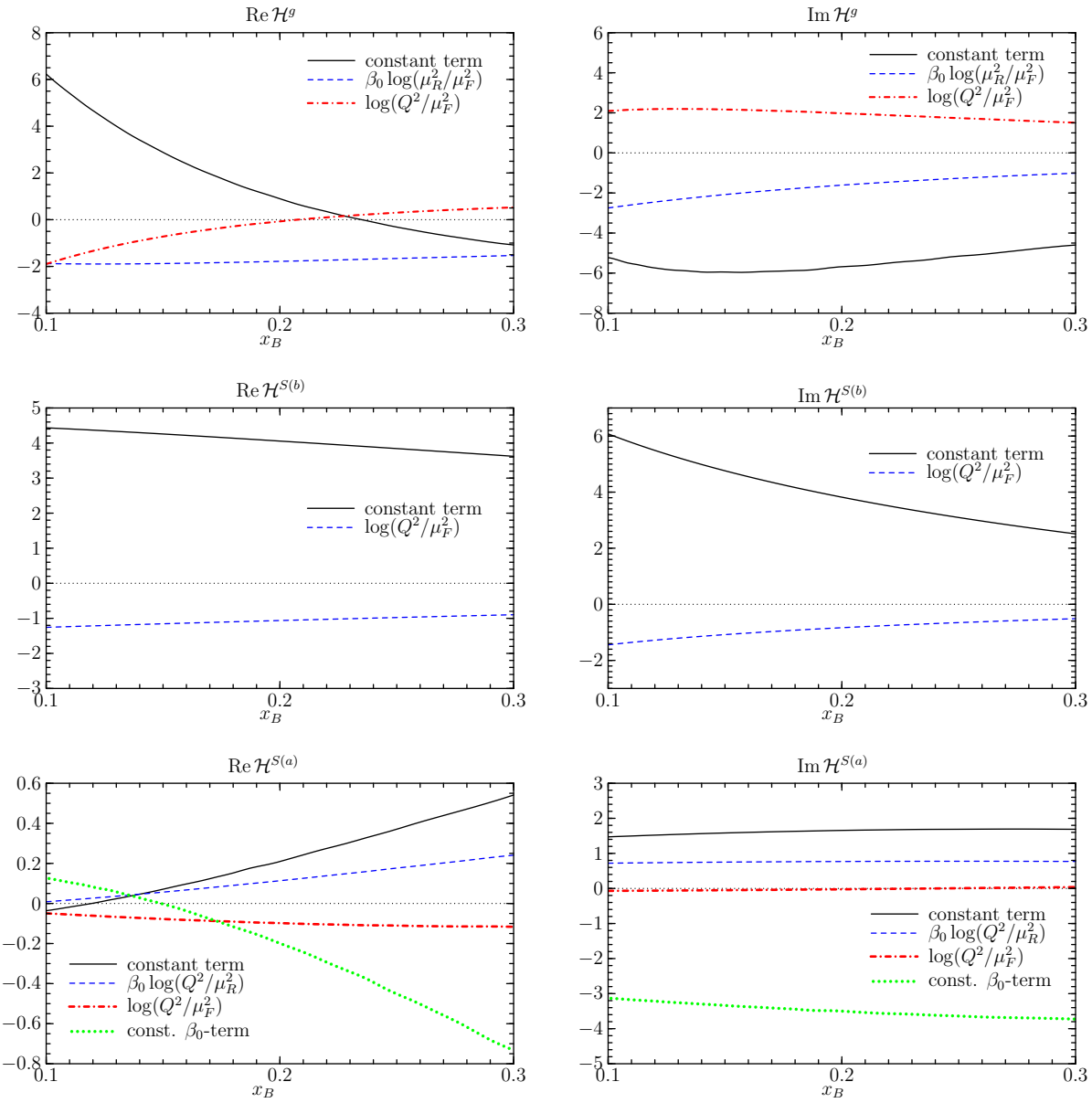

Figure 4.7. Single contributions to the pure NLO part of the real and imaginary part for the amplitude with the specific choice $\mu_F = \mu_R = 2\,GeV$. The upper left and upper right figure correspond to the real and imaginary part for the gluon contribution to the amplitude. The two figures in the middle are the real and imaginary part of the singlet term, $T_{(+)}$, of the amplitude and the lower two plots are for the singlet GPD convoluted with the quark scattering kernel.

find a bigger influence of these contributions.
If we compare now the LO and NLO contributions to the previous three terms we find in Fig 4.8 that for the gluon term one has again strong cancellations for the real and imaginary part. For imaginary part of the gluon the NLO corrections are of the same sign as the LO ones. For $x_B \approx 0.1$ they are relative small but become larger for increasing x_B. The comparison of the singlet terms shows that for the real part one has very small correction coming from the quark kernel. The real part is in this situation and for our scale setting mainly dominated by the pure singlet NLO contribution. For the imaginary part it is different. Here again the correction from the NLO quark kernel is small but the LO contribution from the quark scattering kernel and the NLO term from the singlet kernel have the same size and different sign. Adding all three contributions together (as done in the lower two plots of Fig. 4.8) we find for the real part very large corrections which are of opposite sign and only become small at $x_B \sim 0.3$. The results for the higher Gegenbauer coefficient are again larger from their absolute value than the results of the asymptotic meson DA, but one again finds a converging behavior of this series. For the imaginary part the situation looks better. Because of the cancellation between the gluon and pure singlet NLO terms the corrections are very small for the asymptotic meson DA because they are determined by the small corrections from the convolution of quark scattering kernel and singlet GPD.

We now turn to the discussion of the results for the non-singlet combinations $H^{u-d}(x,\xi,t)$ and $H^{d-s}(x,\xi,t)$ in the large-x_B regime. The single contributions to the NLO part are shown in Fig. 4.9. We find a similar picture for both combinations as in the small-x_B region. Again we choose $Q = \mu_R = \mu_F = 2\,\mathrm{GeV}$ as for the gluon and singlet terms of the amplitude. The absolute size of the different contributions are now of the same order as for the gluon and singlet contributions and one expects that the non-singlet combinations give a noticeable contribution to the amplitude. The single contributions to the NLO part of the non-singlet combinations show the same behavior as in the small-x_B regime. Especially the compensation of the two constant terms remains. This will lead again to small corrections to the LO part in the case of the naive scale setting where all scales are equal. But for the BLM scale setting procedure, described above, one will find large NLO corrections. This was already observed in [121] were the authors computed the NLO corrections to exclusive π^+ production and found the correction being much larger for the BLM scale setting then for the naive setting. Now this can be easily understood through the knowledge of the size of the different contributions to the NLO part of the scattering kernel. The absolute size of the corrections for the naive scale setting is shown in Fig. 4.10. As expected the corrections are small and we show the results in the form of sum of LO and NLO. The corrections are at the level of 10% for the real and imaginary part. Also the NLO corrections from the higher Gegenbauer coefficients do not change this conclusion.

Finally, concluding the discussion of the x_B behavior of the amplitude, one can say that for small values of x_B we find large corrections to the gluon and pure singlet part as well for the real and the imaginary part with the naive scale setting. This observation is in full agreement with the results of [122] where the authors computed the NLO corrections to photoproduction

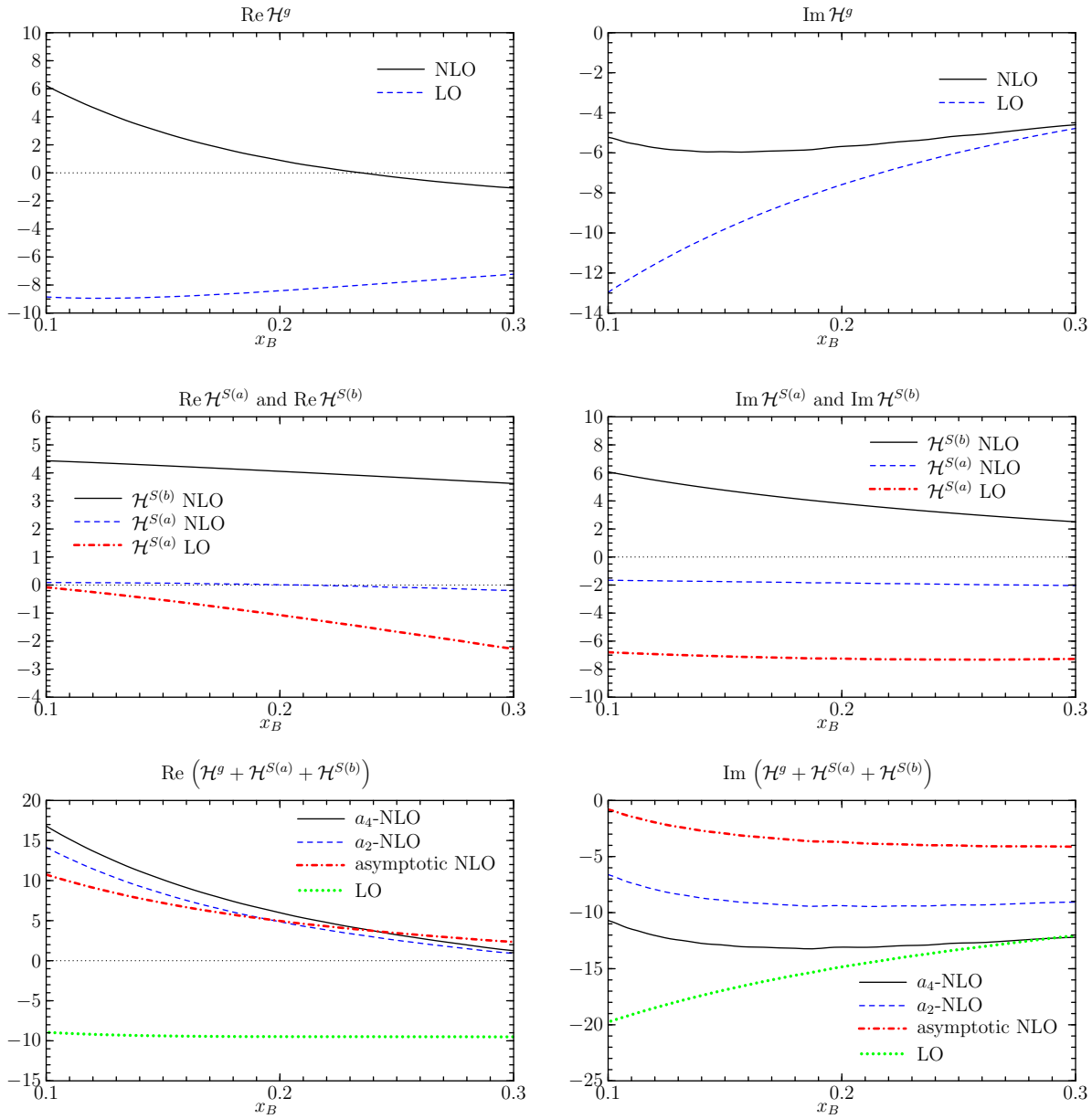

Figure 4.8. Comparison of pure LO and NLO parts for $\mathcal{H}^g$ (upper two plots), $\mathcal{H}^{S(a)}$ and $\mathcal{H}^{S(b)}$ (middle plots) and the sum of all three (lower figures) at the scales $\mu_{F(GPD)} = \mu_{F(DA)} = \mu_R = Q = 2\,GeV$. The label a_2-NLO (a_4-NLO) corresponds to the result for the convolution with the scattering kernel obtained from the second (fourth) term in the Gegenbauer expansion of the meson distribution amplitude.

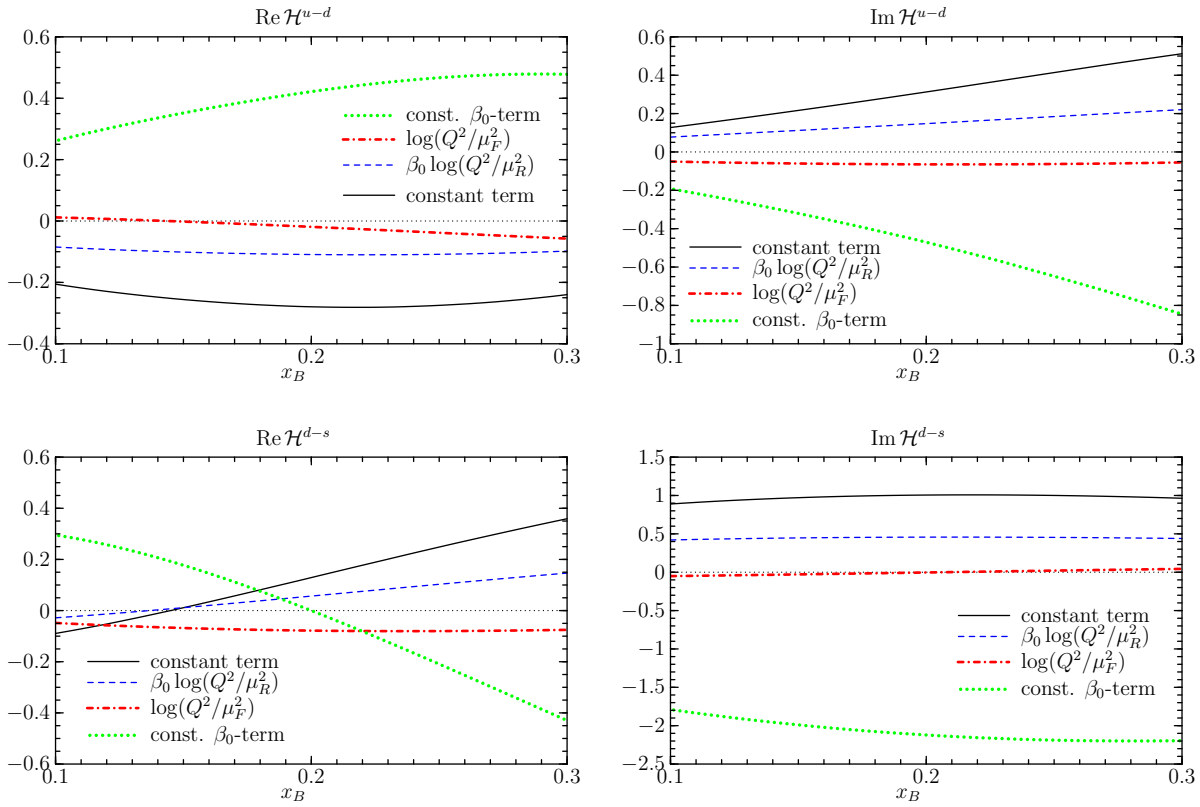

Figure 4.9. Single contributions to the pure NLO part of the real and imaginary part for the amplitude with the specific choice $\mu_F = \mu_R = 2$ GeV.

of J/Ψ at high energies. Especially for the imaginary part the corrections show a strong rise for small values of x_B and they are roughly proportional to $\ln\left(\frac{1}{\xi}\right)$ as expected from the high energy expansion of the amplitude in Sect. 4.4. For processes like exclusive ρ^0 production which are dominated at high energies by the gluon exchange contribution this situation is very unsatisfying. For the today available values of Q^2 only very small values of the factorization scale would lead to small corrections. The situation for the pure singlet contribution is similar to that of the gluon contribution. But one needs even smaller values for μ_F than for the gluon contribution to obtain small NLO corrections. The other possibility keeping the NLO corrections for the pure singlet and gluon part of the amplitude small is to go to extreme large values of Q^2. We will discuss this issue in detail in the next part of this section when discussing the scale dependence of the amplitude at fixed x_B. For the part of the amplitude containing the convolution of singlet GPD and quark scattering kernel and the two non-singlet combinations the situation is different. For the naive scale setting we found only small corrections at the order of 10-20% to the LO part. This is due to the cancellation of the two constant terms of the scattering kernel which have opposite sign. On the other hand assuming the BLM scale setting prescription would lead to much larger correction because the complete term proportional to β_0 will vanish within this prescription and one is left with only one constant term which is of opposite sign to the LO contribution. This

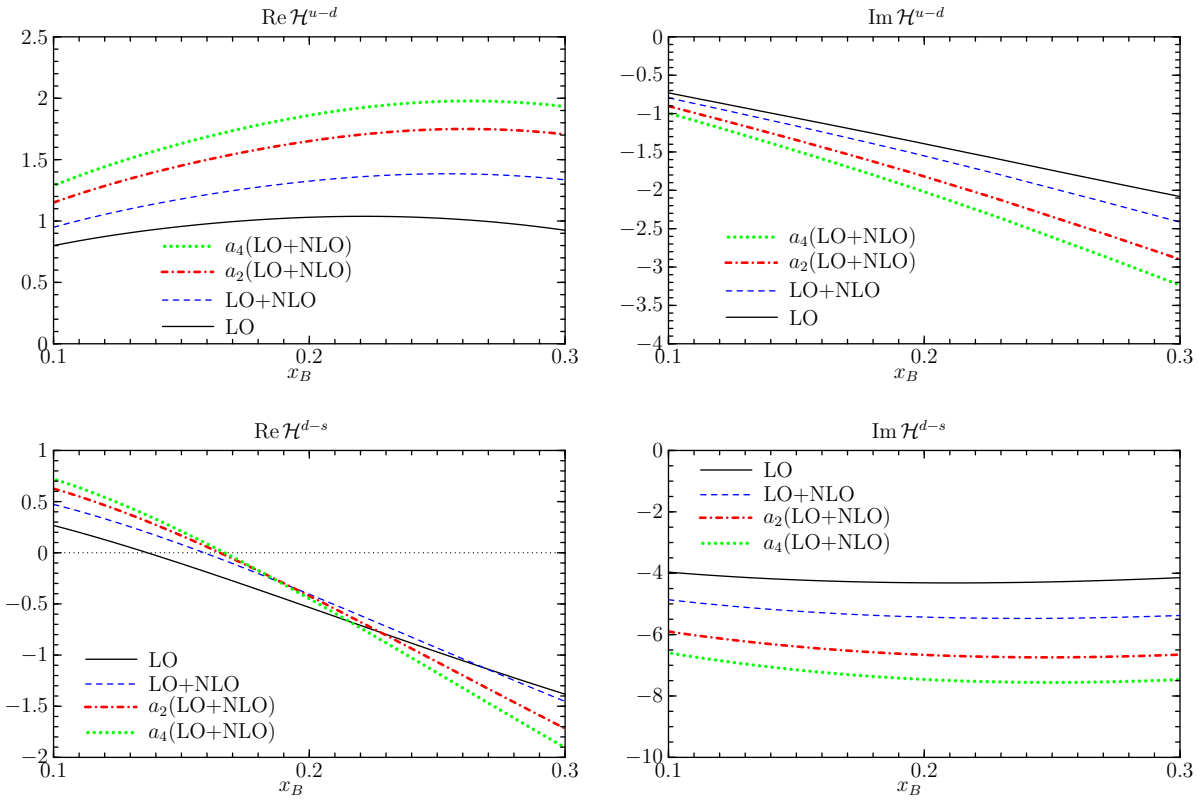

Figure 4.10. Comparison of pure LO and sum of LO and NLO parts for $\mathcal{H}^{u-d}$ (upper two plots) and $\mathcal{H}^{d-s)}$ (lower plots) at the scales $\mu_{F(GPD)} = \mu_{F(DA)} = \mu_R = Q = 2\,GeV$. The label a_2-NLO (a_4-NLO) corresponds to the results for the convolution with the scattering kernel obtained from the second (fourth) term in the Gegenbauer expansion of the meson DA.

observation causes the conclusion that for processes like exclusive ρ^+ or π^+ production the BLM scale setting prescription will lead to very large corrections to the cross sections as it was found in [121]. Concerning our results for the scattering kernel of the higher Gegenbauer coefficients one has to conclude that their contribution to the complete amplitude will be important, especially for small values of x_B and the naive choice of scales. Because then one has the above described cancellation of the LO and NLO part of the pure singlet and gluon contribution. For larger values of x_B and for the non-singlet contribution the effect of the higher Gegenbauer coefficients on the amplitude is much weaker and they can only be seen as small corrections to the asymptotic result. The second observation is the fact that the absolute size of the contributions coming from the different coefficients becomes smaller if one goes to the higher Gegenbauer coefficients. This indicates again the convergence of the series in the expansion of the meson distribution amplitude.

Scale dependence of the amplitude

We want now turn to the discussion of the scale dependence of our results. The investigation of the scale dependence of the amplitude at NLO level is of great interest because under consideration of the NLO corrections the dependence of the amplitude on the factor-

ization and renormalization should be improved in comparison to the pure LO amplitude. For example we studied in Sect. 3.3 the dependence of the cross section for exclusive vector meson production on the factorization scale μ_F. We found a large uncertainty for the cross section by changing the scale by a factor two. Through the higher order corrections this large uncertainty should be reduced and even considering only the level of amplitude this effect should be clearly visible.

As for the previous discussion we present our results for $t = 0\,\text{GeV}$. For the purpose of our scale studies we fix the values at three different values of ξ and Q corresponding to three different experimental situations: for high energy experiments like H1 or ZEUS we choose $\xi = 10^{-3}$ and $Q = 4\,\text{GeV}$. This value of ξ corresponds to $x_B \approx 2 \cdot 10^{-3}$. For fixed target experiments like HERMES we take $\xi = 0.1$, which gives approximately $x_B \approx 0.18$ and $Q = 2\,\text{GeV}$. For the upcoming 12 GeV JLAB upgrade, which hopefully gives us the possibility to probe the large-x_B region together with high values of Q^2, we take $\xi = 0.4$ ($x_B \approx 0.6$) and $Q = 3\,\text{GeV}$. We present our results for the two different contribution of the amplitude: the sum of the gluon and the singlet contributions and the non-singlet contributions. To present the results in this form is important for the investigation of th factorization scale dependence because the non-singlet contributions do not mix with the others under evolution and hence can be treated separately. The gluon and singlet GPD on the other hand mix with each other under evolution and so only the sum of both parts can describe the correct dependence on the factorization scale. Additionally we want to mention that the following results are for the asymptotic scattering kernels. For the higher Gegenbauer moments the main interesting property is the dependence on the factorization scale of the meson DA. We will discuss this issue in this section separately.

We want to start with the dependence on the renormalization scale μ_R where we keep the above described separation of the amplitude into the two contributions for simplicity. In order to discuss only the μ_R dependence we fix the remaining scale to be equal, $Q = \mu_F$. We choose the range $\mu_R \in [1\,\text{GeV}, 10\,\text{GeV}]$ which covers the most interesting region. Beginning with the results for the singlet and gluon part of the amplitude the results are shown in Fig. 4.11. The first two plots are for the real and imaginary part in the high energy region where the amplitude is dominated by the gluon contribution. For the pure LO part the results just follow the running of α_s. For our range of the renormalization scale the strong coupling is given by $\alpha_s(1\,\text{GeV}) = 0.51$ and $\alpha_s(10\,\text{GeV}) = 0.16$. So the LO part changes by a factor of three for the real and imaginary part. The sum of LO and NLO corrections show a different behavior especially for low values of μ_R. The shape is much steeper because in that region of small renormalization scale the term proportional to $\ln\left(\frac{\mu_R^2}{\mu_F^2}\right)$ is numerically large and negative. So it adds up to the positive constant term of the NLO and due to the large value of α_s this effect is amplified and leads to that large correction. For this small value of ξ it has to be stated that a stable theoretical prediction can only be made for $\mu_R > 4\,\text{GeV}$ for real and imaginary part. Especially for $\mu_R < 2\,\text{GeV}$ there is no numerical stability in the results. The situation does not become better for larger values as shown it the two middle plots of Fig. 4.11. There we applied the typical kinematics of the HERMES experiment. For

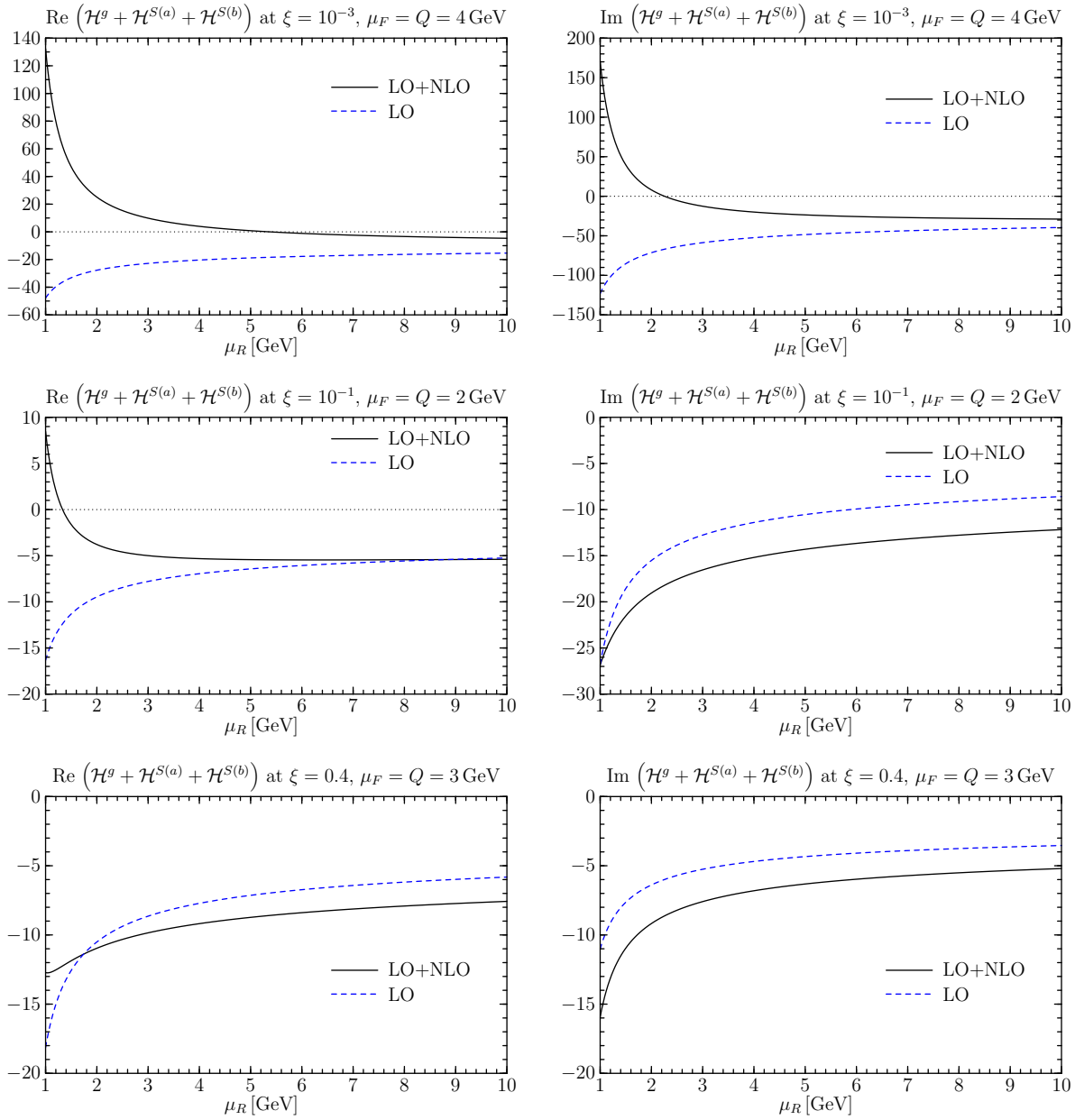

Figure 4.11. Real and imaginary part of the sum of $\mathcal{H}^g$, $\mathcal{H}^{S(a)}$ and $\mathcal{H}^{S(b)}$ for different values of μ_R and three different kinematical regions.

the real part we find again the change of sign at very low values of μ_R. The corrections to the imaginary part are now of the same sign and the shape is not as steep as in the small-x_B region but the results anyhow become stable only for $\mu_R > 3\,\text{GeV}$. In this region of x_B the gluon part is not anymore the dominant one. So one can think about applying the BLM scale setting prescription. But this prescription would shift the renormalization scale in the infrared region as found in [121]. The author found that within their model, which also is based on the double distribution ansatz, for the BLM scale setting $\mu_R \approx 0.3Q$. Applying this result to our situation would lead to $\mu_R \sim 0.6\,\text{GeV}$. In this region the strong coupling is so large that one cannot talk seriously about perturbation theory. For the kinematical region achieved with 12 GeV upgrade at JLAB the situation changes not too much as shown in the last two plots of Fig. 4.11. For the real part it looks like that for the high values of x_B and Q lead to a stabilization of the result for a wide range of μ_R but for the imaginary part we find no improvement in comparison to the LO amplitude. And again the BLM scale setting is not applicable in this kinematical region.

Let us now briefly discuss the size of the corrections due to the NLO terms of the amplitude. We found that the corrections are quite large and especially at very low x_B and small μ_R they are significantly big. For the kinematical regions of high x_B and small Q the NLO terms lead to corrections about 25−50% of the LO amplitude for the whole range of μ_R we considered. We can conclude that for fixed $Q = \mu_F$ and fixed values of x_B the dependence of the amplitude with respect to the renormalization scale shows no improvement by taking the NLO corrections into account. We only find that the numerical results for the sum of LO and NLO contribution show a much steeper behavior than the pure LO results at very small values of μ_R. This happens due to an accidental addition of different NLO terms in the amplitude. But this strong dependence on the renormalization scale happens in a region of μ_R which we will not consider in the further discussion because the values of α_s becomes very large.

So far we discussed the renormalization scale dependence of the sum of gluon and singlet parts of the amplitude. Now we want turn to the two non-singlet combinations $u - d$ and $d - s$. The results for them are presented in Fig. 4.12 for the combination $u - d$ and in Fig. 4.13 for the combination $d - s$. The results we found are quite the same for both combination of flavors and are similar to the results we found for the sum of gluon and singlet terms of the amplitude. For very small values of the renormalization scale there is no stability of the results when we choose μ_R in the range 1-3 GeV. This induces again that the BLM scale prescription cannot be applied. In addition we find, as for the gluon and the singlet parts, that the corrections to the LO part are large at small values of μ_R. It is also obvious from the obtained results that in comparison to the gluon and singlet parts of the amplitude the absolute magnitude non-singlet contributions can only compete for the large values of ξ.

After the discussion of the renormalization scale dependence of the different parts of the amplitude where we found no significant improvement by consideration of the NLO corrections we want now turn to the factorization scale dependence. As we found in the LO

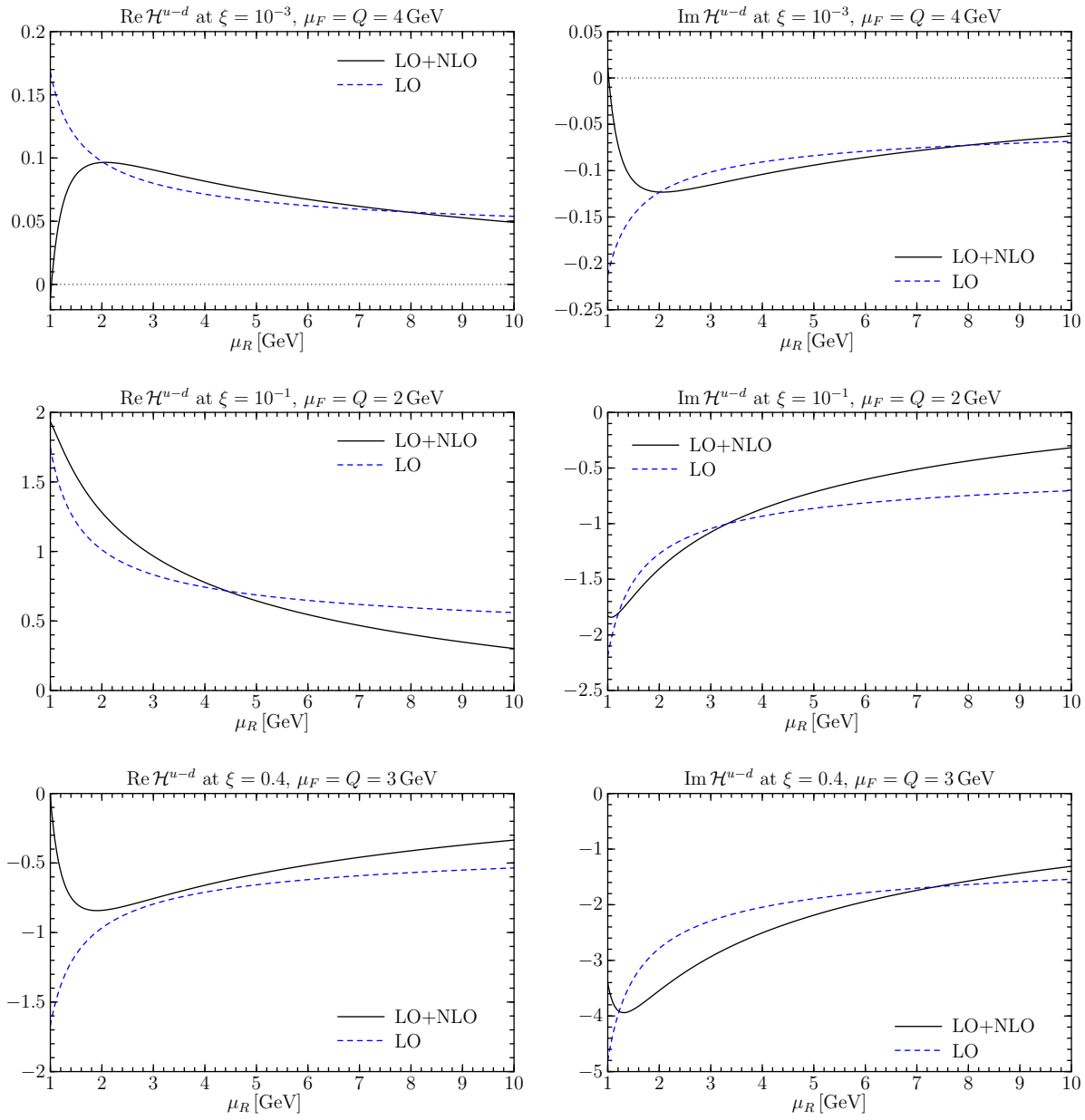

Figure 4.12. Real and imaginary part of the non-singlet combination H^{u-d} and H^{d-s} for different values of μ_R and fixed values of ξ and $Q = \mu_F$.

description of the exclusive vector meson production in Sect. 3.3 the choice of the factorization scale has a large influence on the cross section and is the main source of uncertainty at the LO level. Within the model we used in Sect. 3.3 we did not consider the evolution of the GPDs but rather used the evolved forward parton densities in the double distribution model. Now we want to use the numerical procedure of [53] for LO evolution in order to treat the evolution of the GPDs in the correct way. This is important because due to the mixing of gluon and singlet parts of the amplitude under evolution both parts get contributions from each other when evolving them to higher scales. As mentioned in Sect. 2.3 there

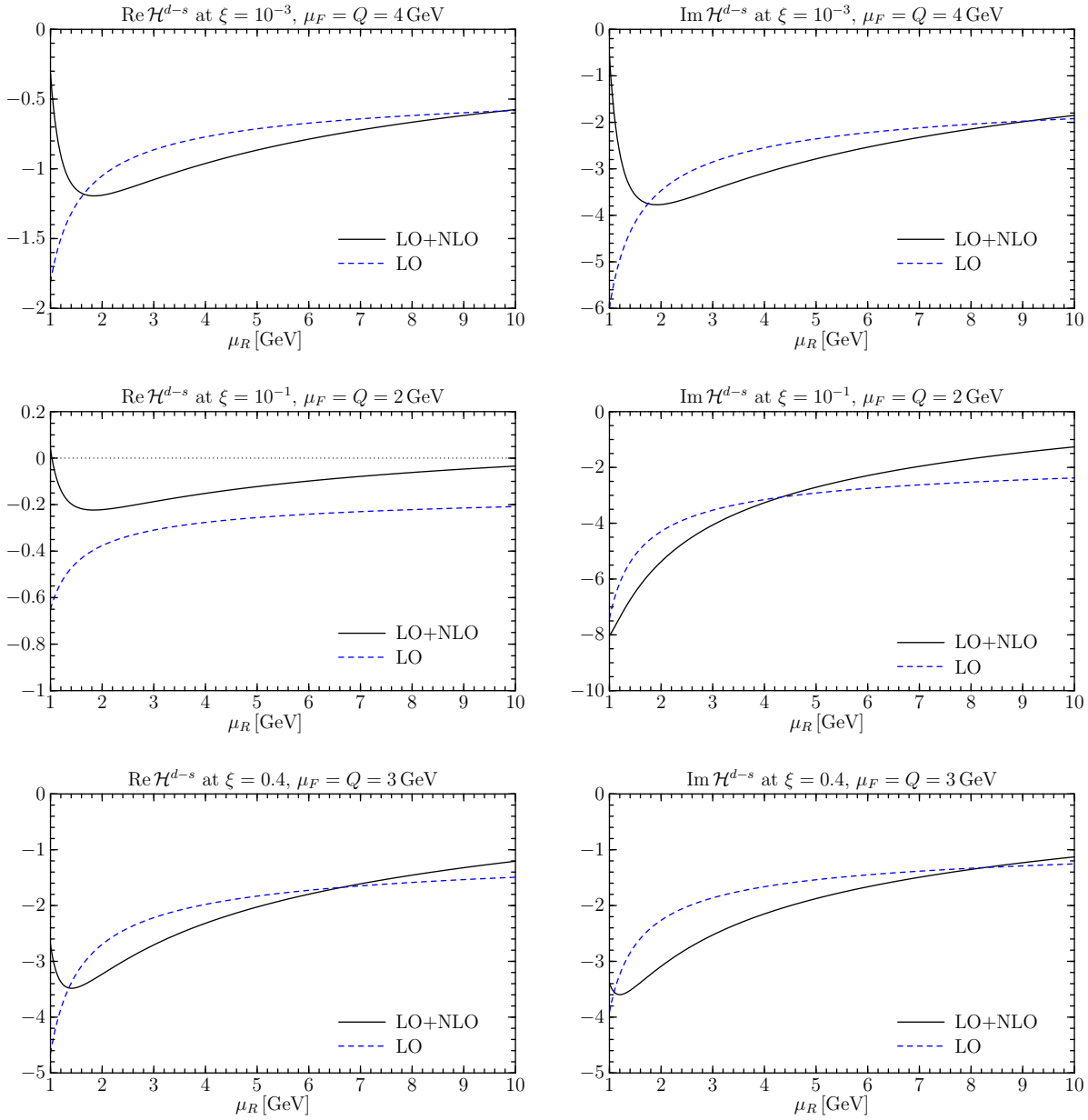

Figure 4.13. Real and imaginary part of the non-singlet combination H^{d-s} for different values of μ_R and fixed values of ξ and $Q = \mu_F$.

exists also an analytical solution of the evolution equation [51, 52] but this solution and its numerical implementation is too time consuming for our purposes. We restrict ourself to the LO evolution although there is a numerical code for NLO evolution available, but this is also not applicable for our studies. In addition a detailed discussion on the influence of LO and NLO evolution [128] shows that the difference is between 5-10% by going from LO to NLO evolution. The effect is much larger for very small values of ξ and if the evolution range runs through a large interval.

We want to start again with the presentation of our results for the sum of the gluon and singlet parts of the amplitude which are mixing under evolution. For the three kinematical regions also used for the discussion of the renormalization scale dependence the results are shown in Fig. 4.14. For our discussion of the factorization scale dependence we set $Q = \mu_R$. As it can be seen from Fig. 4.14 we find for the $\xi = 10^{-3}$ a strong increase of the LO part of the amplitude for μ_F becoming larger. Because the amplitude is at this value of ξ clearly dominated by the gluon distribution that rising is a consequence of the large evolution effects of the gluon GPD. For the sum of LO and NLO parts we find a change in the sign of the real part and the size of the corrections is growing with larger values of μ_F. In addition we find that the scale dependence reduces for the sum of LO and NLO part in comparison to the pure LO result. For the imaginary part the situation looks similar but there we find no sign change. But again the corrections are becoming bigger when increasing the factorization scale. This can be understood if we remind the single contributions to the gluonic NLO part in Fig. 4.3. The constant part starts to become larger for higher values of μ_F as the term proportional to $\ln\left(\frac{Q^2}{\mu_F^2}\right)$ and both terms have opposite sign. For our choice $Q = 4\,\mathrm{GeV}$ one only finds a cancellation of both terms and hence a small NLO correction for very small values of μ_F. For the imaginary part we find also that the sum of LO and NLO contribution seems to bee quite stable over a wide range of μ_F. For the kinematical region with $\xi = 0.1$ and $Q = 2\,\mathrm{GeV}$ the situation looks a little bit different. Here we find that the imaginary part of the pure LO contribution is not as strong dependent on μ_F as for the low x_B region. This is due to the fact that the gluon and singlet GPDs do not show such a strong evolution behavior at this moderate value of ξ. Also the LO real part shows a weaker scale dependence in this region. For the sum of LO and NLO contributions we find that the corrections are smaller than for the small value of ξ. And additionally one finds that the difference of LO and sum of LO and NLO contributions diverges much slower in this kinematical region. For the JLAB kinematics with $\xi = 0.4$ and $Q = 3\,\mathrm{GeV}$ the situation for the real part look very promising. The corrections due to the NLO contributions are small and the result changes not much over the whole range of μ_F we considered. For the imaginary part we find also a stable result over the range of the factorization scale but the corrections are larger as for the real part. The second observation is that the difference of LO and sum of LO and NLO stays constant in the complete interval of μ_F.

So for the factorization scale dependence of the sum of gluon and singlet parts one has the two different conclusions: for the high energy region one finds an weaker dependence of the amplitude for the sum of LO and NLO contribution but for our typical choice of

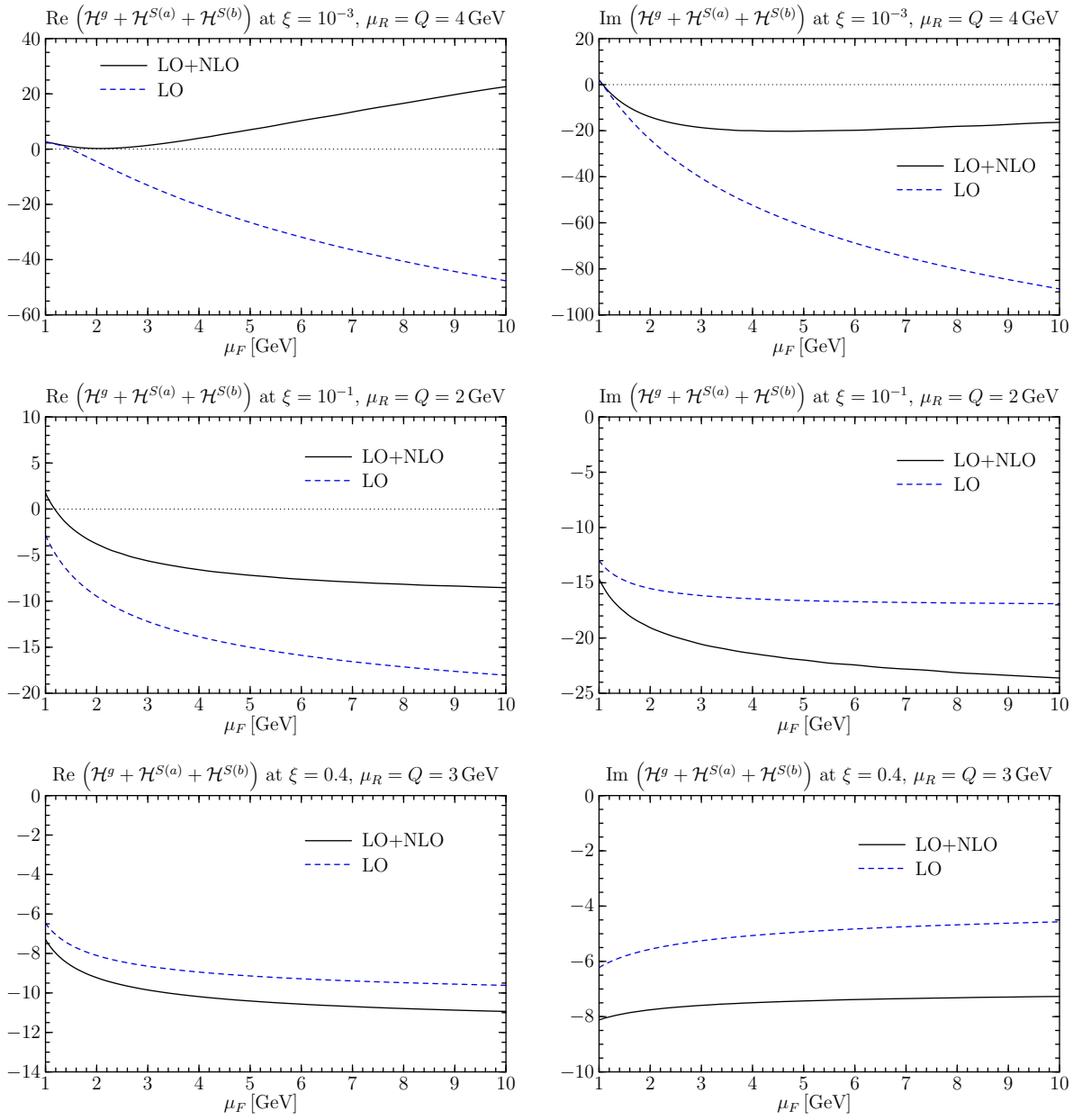

Figure 4.14. Real and imaginary part for different values of μ_F and three different kinematical situations for the sum of gluon and singlet parts of the amplitude.

Q one has large corrections to the LO amplitude. The size of the corrections is strongly dependent on the choice of Q as we will demonstrate in the next paragraph. On the other hand for moderate and large values we also find a weaker μ_F dependence and in addition the corrections are much smaller than in the high energy regime.

The results obtained for the factorization scale dependence rises the question how predictive the theoretical results for the NLO amplitude can be. Especially for high energies where we found very large corrections to the LO amplitude. We want to explore if one finds for small values of ξ a kinematical setup where the result of the amplitude is stable and where

the corrections are small. We show this on the example of the imaginary part in Fig. 4.15. In this figure we show the imaginary part of the sum of gluon and singlet parts of the amplitude for different values of ξ and two different choices of $Q = \mu_R$. In the upper two plots the results are presented for $\xi = 10^{-2}$ with $Q = \mu_R = 4\,\mathrm{GeV}$ in the left plot, which corresponds to the kinematical region achieved at the COMPASS experiment, and $Q = \mu_R = 7\,\mathrm{GeV}$ in the right plot. One finds that for the first choice of Q and μ_R neither the LO nor the sum of LO and NLO contributions show flat behavior. But the difference of both curves diverges only slowly and the size of the corrections are quite acceptable. The situation becomes even better if we take $Q = \mu_R = 7\,\mathrm{GeV}$. The dependence on μ_F becomes somewhat weaker and more important, the corrections are quite small over the whole interval of the factorization scale. So for a different choice of the factorization and renormalization scale with $\mu_R = Q$ the corrections become stable and small at $Q = 7\,\mathrm{GeV}$. This value of Q is unfortunately too large to be achieved in todays experiments. But even the results for $Q = 4\,\mathrm{GeV}$ see to be promising, because the corrections are not too large and the difference of LO and sum of LO and NLO increases slowly over our range of μ_F. Turning to smaller values of ξ (and hence x_B) we find that $Q = \mu_R = 7\,\mathrm{GeV}$ is not sufficient to keep the corrections small as seen in the middle plots of Fig. 4.15. The left middle plot shows the same as in Fig. 4.14 where we set $Q = \mu_R = 4\,\mathrm{GeV}$. The corrections for the larger values of Q and μ_R are only small in the region $\mu_F \approx 1\,\mathrm{GeV} - 2\,\mathrm{GeV}$ and than starting to diverge. The result for the sum of LO and NLO has a quiet flat behavior for the large value of Q but the large corrections makes it not easy to make clear theoretical predictions. In order to keep the corrections small for this value of ξ we would need a much larger value of $Q = \mu_R$ which is far away to bee reached in experiments. The situation becomes even worse if we assume ξ to be $\xi = 10^{-4}$. The results are shown in the lower two plots of Fig. 4.15. There we find that even for $Q = \mu_R = 7\,\mathrm{GeV}$ the correction are very large and the difference starts to diverge from $\mu_F > 4\,\mathrm{GeV}$. For such a small value of ξ the corrections can only be kept under control for Q much bigger than $10\,\mathrm{GeV}$ and hence can be not compared with experimental data.
To conclude this discussion we have to state that for small ξ and the choice $Q = \mu_R$ and different values of the factorization scale μ_F we can only find small corrections for extremely large values of Q. The results imply that the smaller the value of ξ the larger Q and μ_R have to be, to keep the corrections small. For ξ of the order 10^{-2} or larger we find that the NLO corrections are of reasonable size and are not diverging,even at moderate values of Q.

To complete the discussion of the factorization scale dependence of the amplitude with fixed and equal Q and μ_R we briefly discuss the two non-singlet combinations of the amplitude. We will keep this discussion of our results quite short because it is widle known that evolution effects for non-singlet combinations are not as strong as for the singlet or gluon contribution of the amplitude. We show our results for the imaginary part of both combinations in Fig. 4.16. We concentrate on the results for the imaginary part because for the real part they look very similar and offer no deeper insight. We only show the results at the point $\xi = 0.1$ because as we have seen from the previous discussions of our results the non-singlet combinations do not contribute to the amplitude in a significant way for smaller

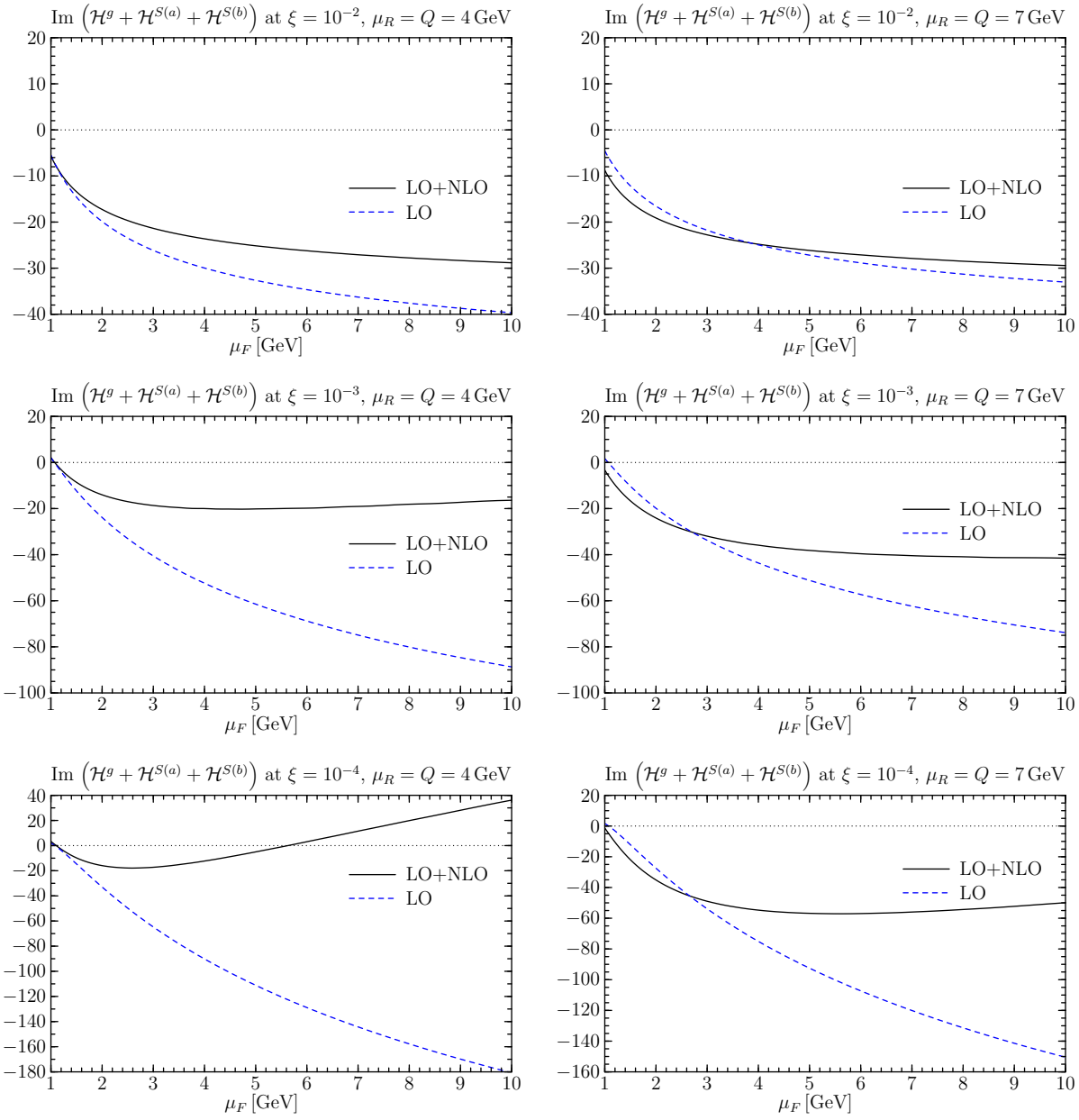

Figure 4.15. Imaginary part for the sum of gluon and singlet parts of the amplitude for different values of μ_F. The upper two plots are at $\xi = 10^{-2}$ and $Q = \mu_R = 4$ GeV (left plot) and $Q = \mu_R = 7$ GeV (right plot). The two middle plots are for $\xi = 10^{-3}$ and the lower two plots for $\xi = 10^{-4}$ with the same choices for Q and μ_R for the left and right plot as in the first two plots.

values of ξ in comparison to the gluon and singlet parts. As one can see in Fig. 4.16 the imaginary part for the combination $u - d$ is more sensitive to the choice of the factorization scale than the combination $d - s$. But the change is not as large as for the sum of gluon and singlet parts. The size of the corrections is over the complete range of μ_F between 10% and 20% and the difference between LO and sum of LO and NLO does not start to diverge as it was the case before. For the combination of $d - s$ quarks the scale dependence is very weak even at the LO level. The size of the correction is as for the combination $u - d$ about

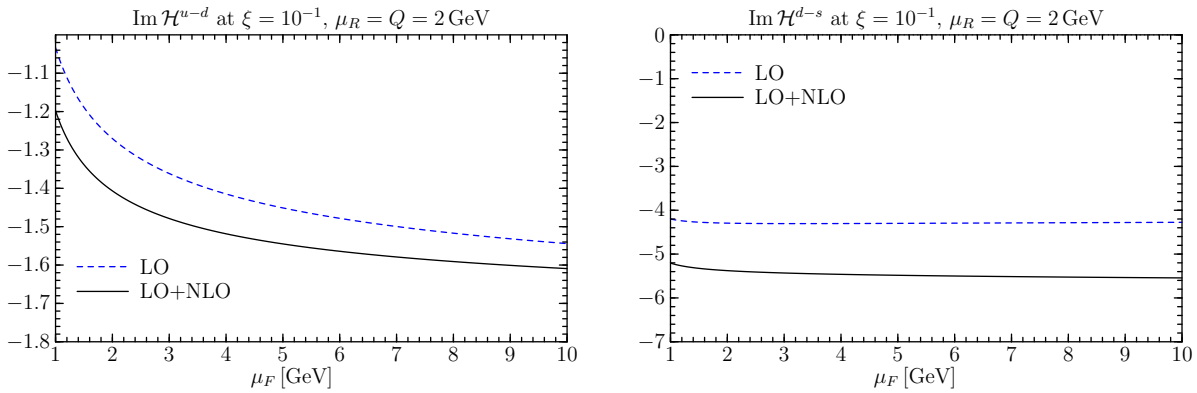

Figure 4.16. Imaginary part of H^{u-d} and H^{d-s} at $\xi = 10^{-1}$ for different values of μ_F and fixed $Q = \mu_R = 2$ GeV.

20% for the complete interval of μ_F and does not start to drift apart. So the situation for the non-singlet combinations is quite more suitable than for the sum of gluon and singlet parts of the amplitude. The corrections to the leading order amplitude are moderate and numerical stable for a wide range of the factorization scale. If we assume $\xi = 0.4$ which can be relevant for the JLAB upgrade the situation is similar but the corrections become even smaller. This implies that the framework of collinear factorization we used for our theoretical prescription of exclusive meson production seems to be applicable for the kinematics of fixed target experiments. For high energy experiments on the other hand one has very large corrections to the amplitude even at high values of Q and μ_R which are still growing for higher values of the factorization scale.

So far we have treated the factorization and renormalization scale separately. A widely used way in the literature is to set both scales equal, $\mu_R = \mu_F$. We will also use this procedure of scale setting and want to discuss our results. We would like to start again with the results for the sum of gluon and singlet parts of the amplitude which are shown in Fig. 4.17 where we again plotted the three different kinematical configurations. For the scale setting $\mu_R = \mu_F$ we also show the results for the higher Gegenbauer coefficients scattering kernels for which we set $\mu_R = \mu_{F(GPD)} = \mu_{F(DA)}$. For the $\xi = 10^{-3}$ we find that the pure LO amplitude has a strong dependence on μ. The falling of the α_s for higher scales cannot compensate the strong rising of the gluon contribution. We also find that the corrections are large over the complete range of scales. The results for the higher Gegenbauer coefficients, where we set $a_2 = a_4 = 1$, are larger from their absolute value but show the same quantitative behavior. The strong rise of our results for small scale can be explained by the small size of α_s in that region. This enhances the NLO contributions for small scales. The situation becomes better for higher values of ξ as we see in the two middle and lower plots in Fig. 4.17. We find, except for small scales, only small corrections to the LO amplitude. The results show also a flat behavior over a wide range of μ. This also hints that our approach suites better for higher values of x_B then for smaller ones. But we also can conclude thaht the results become more stable when treating the factorization and renormalization scale in the same

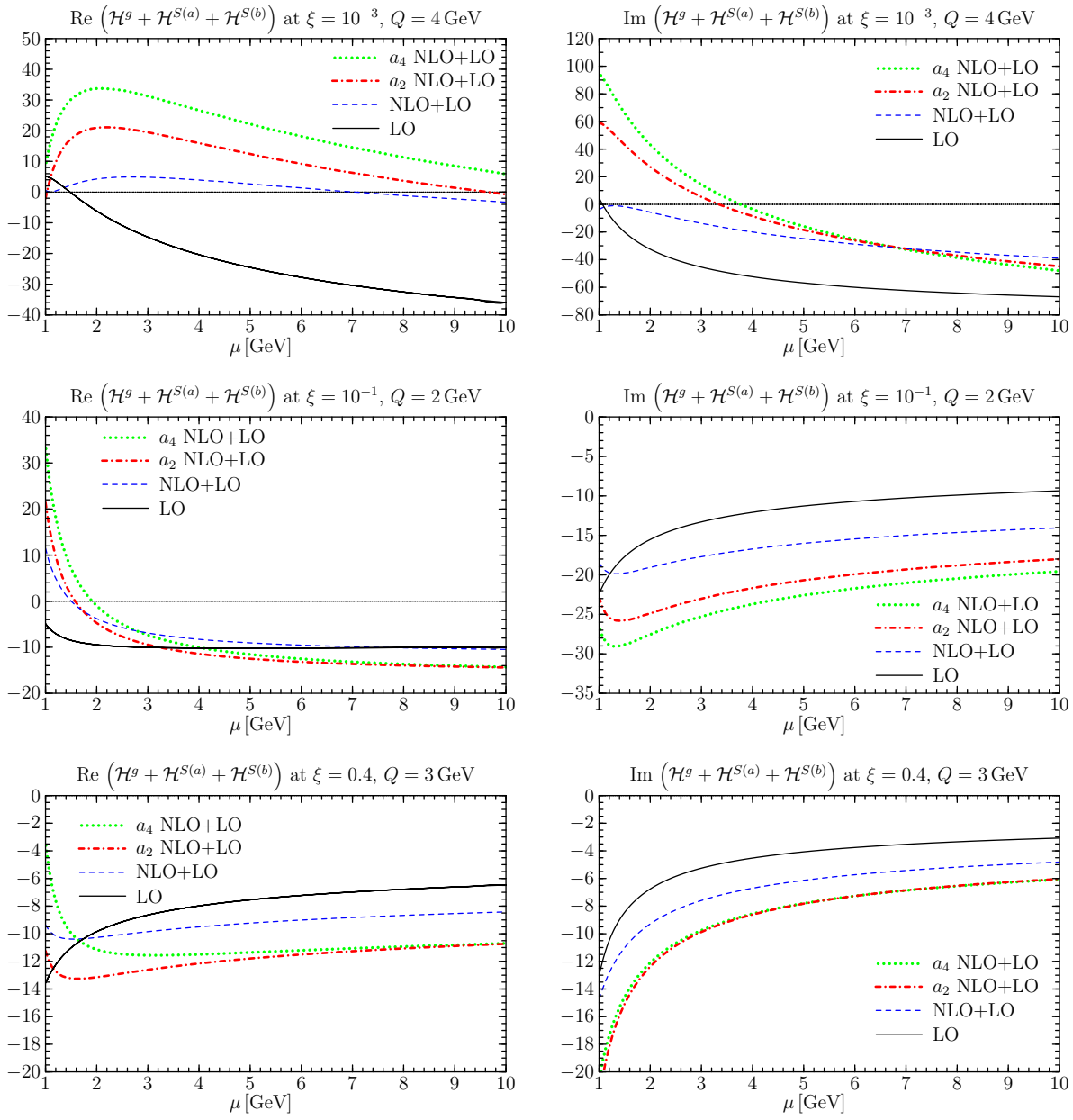

Figure 4.17. Real and imaginary part for different values of $\mu_{F(GPD)} = \mu_{F(DA)} = \mu_R$.

way. This becomes clearer if we redo our analysis of Fig. 4.15 for $\mu_R = \mu_F$. The results are shown in Fig. 4.18 where we only used the asymptotic scattering kernel. We find that for $\xi = 10^{-2}$ and $Q = 4\,\mathrm{GeV}$ the corrections to the LO amplitude are becoming small if one considers only the region $\mu > 2\,\mathrm{GeV}$ and do not diverge for large scales as it happens if one fixes $Q = \mu_R$. For a higher value of Q the corrections become even smaller and also the shape is approximately flat over nearly the complete range of μ. If we turn to smaller values of ξ, as shown in the middle and lower plots of Fig. 4.18 we find that the corrections are larger and for the low value of Q they also start to diverge. But the divergence is not as strong as for the case $Q = \mu_R$. The situation improves when we choose $Q = 7\,\mathrm{GeV}$. Beside

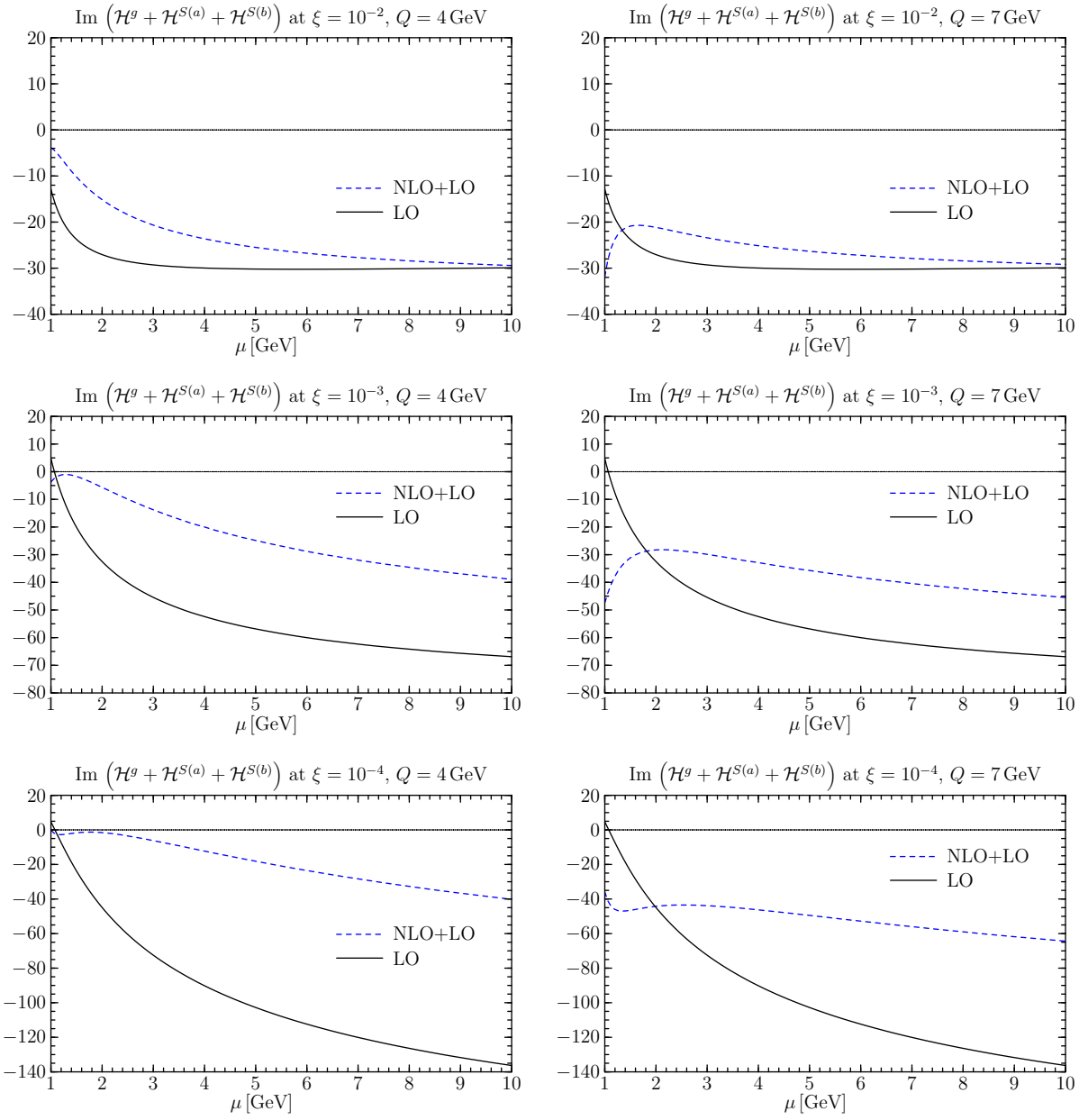

Figure 4.18. Imaginary part for the sum of gluon and singlet parts of the amplitude for different values of $\mu_F = \mu_R$. The upper two plots are at $\xi = 10^{-2}$ and $Q = 4\,GeV$ (left plot) and $Q = 7\,GeV$ (right plot). The two middle plots are for $\xi = 10^{-3}$ and the lower two plots for $\xi = 10^{-4}$ with the same choices for Q for the left and right plot as in the first two plots.

that the corrections are large and the results show no flat scale dependence. The results of Fig. 4.18 support the assumption to choose the factorization and renormalization scale even at small values of x_B.

Let us now briefly discuss the same scenario of scale setting for the two non-singlet combinations of the amplitude. The results are shown in Fig. 4.19 where we again only show the imaginary part of both contribution. We also concentrate only on the kinematical region where $\xi = 0.1$ and $Q = 2\,\mathrm{GeV}$. For the smaller values of ξ the non-singlet contribution

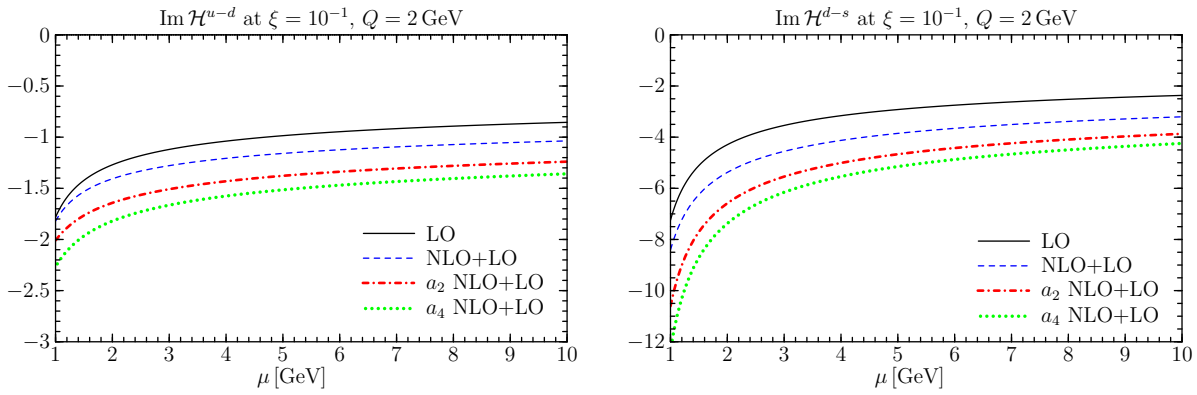

Figure 4.19. Imaginary part of H^{u-d} and H^{d-s} for different values of $\mu = \mu_{F(GPD)} = \mu_{F(DA)} = \mu_R$ at $\xi = 0.1$ and $Q = 2$ GeV.

do not contribute to the amplitude in a significant way, as stated before. The situation does also not change if we assume ξ to be in the region of the JLAB upgrade kinematics. If we look at Fig. 4.19 we find a flat behavior of the results for the sum of LO and NLO contributions. The situation is for $u-d$ somewhat better than for $d-s$ especially for small scales. We find also that the corrections from the NLO part are small and the difference of LO and sum of LO and NLO stays constant over the whole interval. The results for the higher Gegenbauer coefficients (we used again $a_2 = a_4$) are larger than result for the asymptotic scattering kernel. But one again finds the nice behavior of convergence of the results. For the non-singlet contributions we can also conclude that choosing μ_F equal to μ_R does not improve the situation very much in comparison to the situation where one treats both scales different. This is of course only true as long we choose them in a reasonable way which means choosing it not to small.

We discussed in the previous paragraphs only the scale dependence of the results for the asymptotic scattering kernels. We also presented results for the higher Gegenbauer coefficients but did not investigate the dependence of our results on the factorization scale of the meson DA ($\mu_{F(DA)}$). This scale appears only in the scattering kernel of the higher Gegenbauer coefficients. The Gegenbauer coefficients a_n are not fixed parameter but evolve at leading-logarithmic accuracy according to

$$a_n(\mu_{F(DA)}) = a_n(\mu_0) \left(\frac{\alpha_s(\mu_{F(DA)})}{\alpha_s(\mu_0)} \right)^{\gamma_n^{(0)}/(2\beta_0)} , \tag{4.46}$$

where we choose $\mu_0 = 2\,\mathrm{GeV}$ and the anomalous dimension $\gamma_n^{(0)}$ is given by

$$\gamma_n^{(0)} = 8 C_F \left(\psi(n+2) + \gamma_E - \frac{3}{4} - \frac{1}{2(n+1)(n+2)} \right) \tag{4.47}$$

with $C_F = 4/3$. The dependence of the scattering on $\mu_{F(DA)}$ should compensate the evolution of the Gegenbauer coefficients a_n. In order to see that this is really the case we present our results in the following form: we multiply the LO and NLO results with the prefactor of

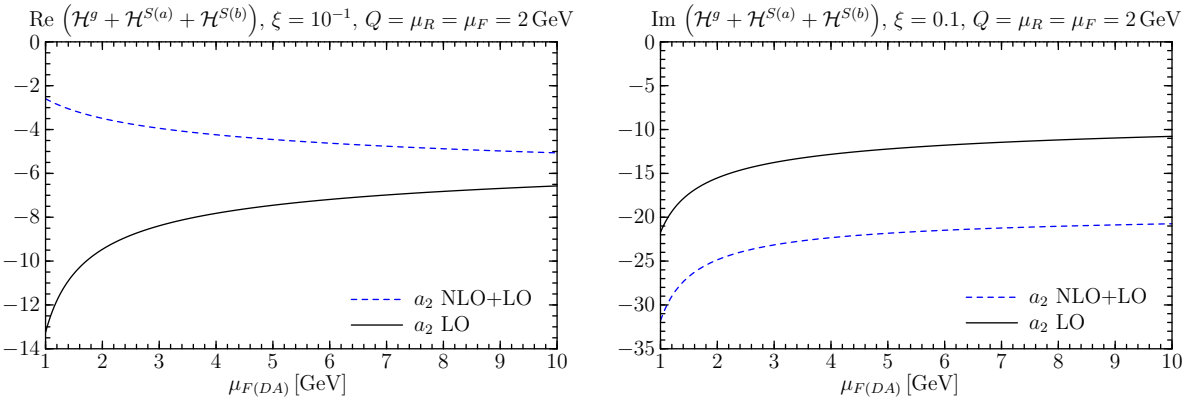

Figure 4.20. Real and imaginary part for the sum $\mathcal{H}^g + \mathcal{H}^{S(a)} + \mathcal{H}^{S(b)}$ for different values of $\mu_{F(DA)}$ with $Q = \mu_{F(GPD)} = \mu_R = 2$ GeV.

$a_n(\mu_0)$ in (4.46) and vary the factorization scale $\mu_{F(DA)}$. The results for the contribution of the Gegenbauer coefficient a_2 are shown in Fig. 4.20. We present only the results for the low energy region and for the sum of gluon and singlet parts of the amplitude because the results do not change qualitatively for the non-singlet contributions and at smaller values of ξ. We see in Fig. 4.20 that there is no improvement on the scale dependence when including the NLO terms. For the real part the situation looks better and we found a more flat dependence on the factorization scale of the meson DA. The corrections due to the NLO terms are again quite large but we find no change in the overall sign as we did for the high energy region. For the next higher coefficient a_4 the results look similar and we also find no large improvement on the scale dependence.

Finite values of t

All our previous results were obtained for $t = 0\,\mathrm{GeV}^2$. Now we want to investigate how a finite value of t influences our results. The t-dependence of our model for the GPDs is discussed in some detail in Sect. 4.5 where we explained how we model the GPD $E(x, \xi, t)$. Our ansatz for the t-dependence follows the ansatz of [82] and has the general form

$$H^{q,g}(x, \xi = 0, t) \sim \exp(t\, f_{q,g}(x))\,. \tag{4.48}$$

Because t is negative we expect that the results are smaller in comparison to the results obtained for $t = 0\,\mathrm{GeV}^2$. We do not want to repeat the complete analysis of the case of t equal zero but give some example plots. We start with the x_B behavior of the sum of gluon and singlet parts of the amplitude for a fixed value of t. The results for the pure LO and NLO parts are shown in Fig. 4.21 versus x_B. As expected we find a suppression of our results for $t = 0\,\mathrm{GeV}^2$ as seen in Fig. 4.21. The suppression factor is about 40% at very small values of x_B as well for the LO and NLO part and also for real and imaginary part. The factor of suppression reduces for larger values of x_B. This can be understood, taking a closer look at

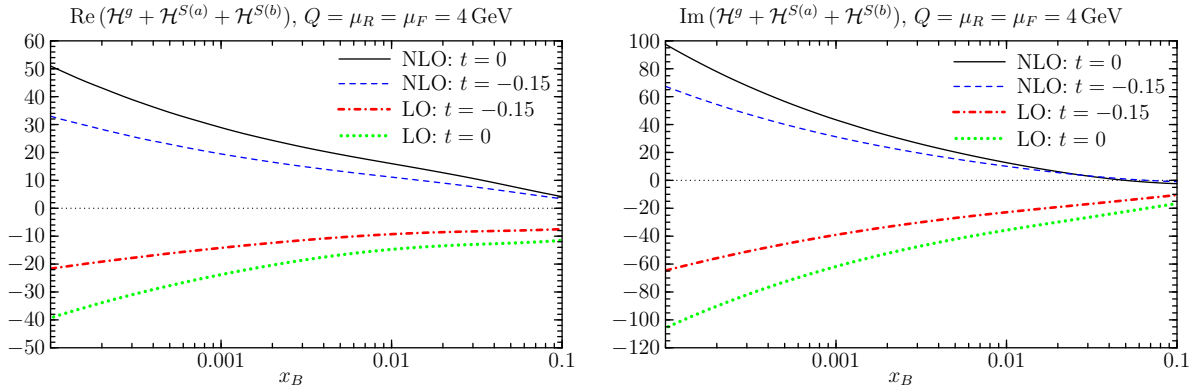

Figure 4.21. Real and imaginary part for the sum of gluon and singlet contributions of the amplitude vs. x_B for $t = 0\,GeV$ and $t = -0.15\,GeV$. We choose the scales to be $Q = \mu_R = \mu_F = 4\,GeV$.

the function $f(x)$ in (4.48). The functions for the quark and gluon GPD are given by

$$f_q(x) = \alpha'_q(1-x)^3 \log\frac{1}{x} + D_q(1-x)^3 + C_q x(1-x)^2\,,$$
$$f_g(x) = \alpha'_g(1-x)^3 \log\frac{1}{x} + B(1-x)^2\,. \tag{4.49}$$

Due to the different values of $\alpha'_q = 0.9\,\mathrm{GeV}^{-2}$ and $\alpha'_g = 0.14\,\mathrm{GeV}^{-2}$ we expect that the suppression at small values of x is for the quark GPDs larger than for the gluon GPD. For our choice $Q = \mu_R = \mu_F = 4\,\mathrm{GeV}$ in Fig. 4.21 we find that the suppression factor becomes larger at small x_B as we expected for the quark GPDs. On the other side we might expect that at very small values of x_B the gluon GPD gives the dominant contribution to the amplitude and hence the suppression factor should not increase in the way we found in Fig. 4.21. But for our choice of the scale the gluon contribution is very small because the LO and NLO contributions of the gluon term nearly compensate as seen in Fig. 4.4. Therefore it is not surprising that we find an increasing suppression factor for small values of x_B.

If we now want to investigate the dependence of the amplitude on t it is obvious that the suppression should become larger for increasing t for the quark contribution. This behavior is shown in Fig. 4.22 where we plotted the sum of LO and NLO contributions of the sum of gluon and singlet parts of the amplitude at two different kinematical setups. In the left plot we choose the high energy situation with $\xi = 10^{-3}$ and $Q = \mu_R = \mu_F = 4\,\mathrm{GeV}$. We find that the imaginary part is much more sensitive on t than the real part. One can understand this if one keeps in mind that at LO the imaginary part of the amplitude is just given by the point $H(\xi, \xi, t)$ and hence is much more sensitive than the real part which is determined by the convolution of the GPDs and the hard scattering kernel. If we turn to the kinematical situation where $\xi = 10^{-1}$ and $Q = \mu_R = \mu_F = 2\,\mathrm{GeV}$, which is shown in the right plot of Fig. 4.22, we find for the real part a stronger dependence on t as for the high energy kinematics. Additionally we find that the real part changes sign at $t \approx -0.35\,\mathrm{GeV}^2$. For this phenomenon we have no physical explanation because as said before the real part is given by principal value integrals of the GPDs and the hard scattering kernels. For the imaginary

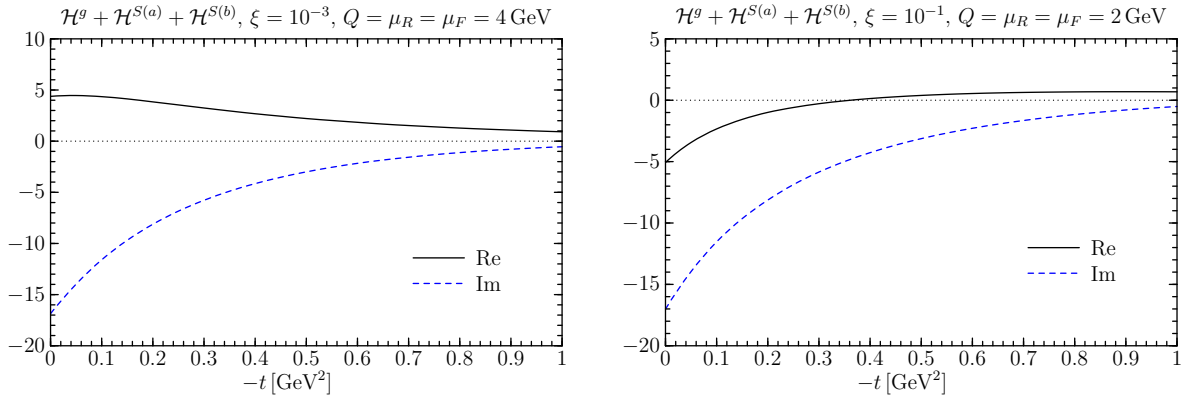

Figure 4.22. Real and imaginary part for the sum of gluon and singlet contributions of the amplitude vs. t. We plotted the sum of LO and NLO contributions. The left figure shows the high energy region with $\xi = 10^{-3}$ and $Q = \mu_R = \mu_F = 4$ GeV, the right plot is for the low energy regime with $\xi = 10^{-1}$ and $Q = \mu_R = \mu_F = 2$ GeV.

part the plot looks almost identical as for the high energy kinematics.

Let us now turn briefly to the non-singlet parts H^{u-d} and H^{d-s} of the amplitude and their t-dependence. For simplicity we only want to present the results for the sum of LO and NLO contributions because we found in the results before that the NLO terms give only small corrections to the LO part. We also show our results for the region $x_B \in [0.1, 0.3]$ because there the non-singlet terms start to give sizeable contributions to the amplitude. For the real and imaginary part of both non-singlet combinations the results are shown in Fig. 4.23. For the real part we cannot make the statement that for finite value of t our results are smaller than for $t = 0\,\mathrm{GeV}^2$. This is again due to the fact that the real part is given by a principal value integral and hence one cannot easily argue as for the imaginary part. For the imaginary part we find on the other hand a clear reduction of our results for $t = -0.15\,\mathrm{GeV}^2$ in comparison to the results for vanishing t. The factor of reduction is quite the same for both combinations is roughly 40% and stays nearly constant of the range of x_B. Finally we want to show the dependence of the real and imaginary part of the two non-singlet combinations for various values of t. The left plot of Fig. 4.24 shows the sum of the LO and NLO contributions for the real and imaginary part of the combination $u - d$. We find again that the t-dependence is much weaker for the real than for the imaginary part. For the combination $d - s$ we find a change of sign for the real part for increasing values of t whereas the imaginary part shows the same strong falling behavior than for the combination $u - d$. One can explain this again by the different structure of the real and imaginary part. More over, since the corrections form the NLO contributions are relative small in comparison to the gluon and singlet parts of the amplitude the imaginary part is widely dominated by the LO contributions which is, as stated before, just given by the GPDs at the point $x = \xi$. This leads to the fact that the imaginary part shows a stronger dependence on t.

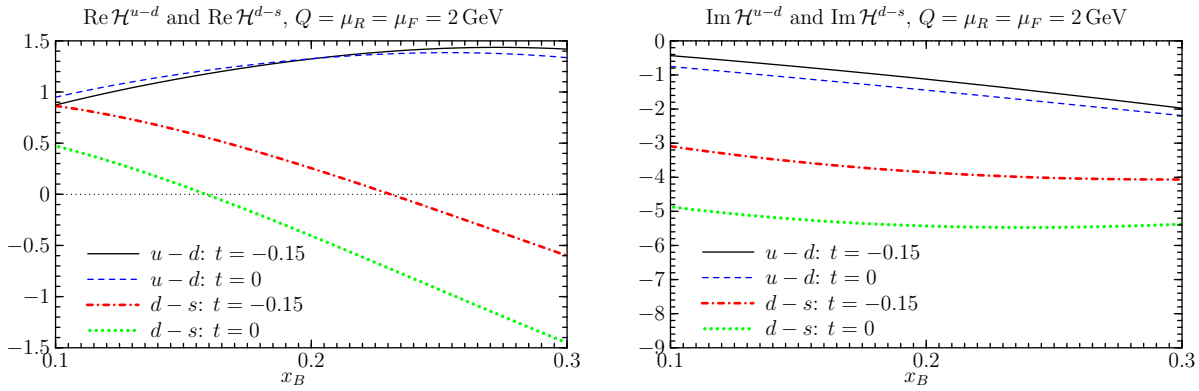

Figure 4.23. Real and imaginary part for the non-singlet combinations H^{u-d} and H^{d-s} vs. x_B with $Q = \mu_R = \mu_F = 2$ GeV. The plots show the sum of LO and NLO contributions.

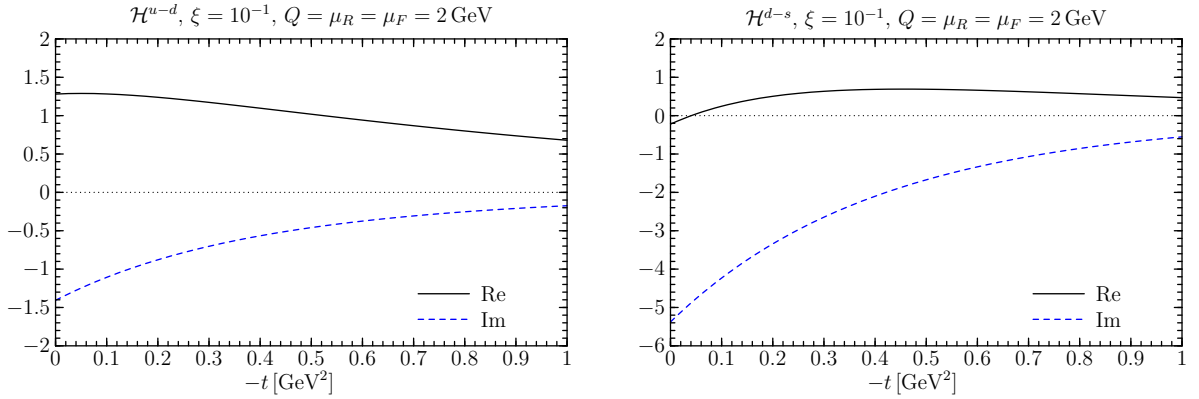

Figure 4.24. Real and imaginary part for the non-singlet combinations H^{u-d} and H^{d-s} vs. t with $\xi = 10^{-1}$ and $Q = \mu_R = \mu_F = 2$ GeV. The plots show the sum of LO and NLO contributions.

4.6.2 Results for $\mathcal{E}$

In the previous section we have discussed in great detail the NLO corrections to the part of the amplitude containing the GPD $H(x,\xi,t)$. The contributions coming from that part give the largest contributions to physical observable like cross sections. This can be seen in (3.5) where we give the formula for the cross section of exclusive vector meson production. One can see from this equation that the contributions proportional to $E(x,\xi,t)$ are suppressed with at least a factor of ξ or $t/(4m^2)$ in comparison to the term proportional to $H(x,\xi,t)$. In addition to the cross section there is a second observable which involves leading-twist amplitudes and can be expressed using the factorization theorem, namely the single spin asymmetry (SSA) for a transversely polarized target. The SSA have been discussed the first time for pseudoscalar meson production in [67] and the analog for vector meson production was given in [37]. The SSA is directly proportional to the imaginary part of the product $\mathcal{H}\mathcal{E}^*$

$$SSA \sim \mathrm{Im}\,(\mathcal{H}\mathcal{E}^*)\,, \tag{4.50}$$

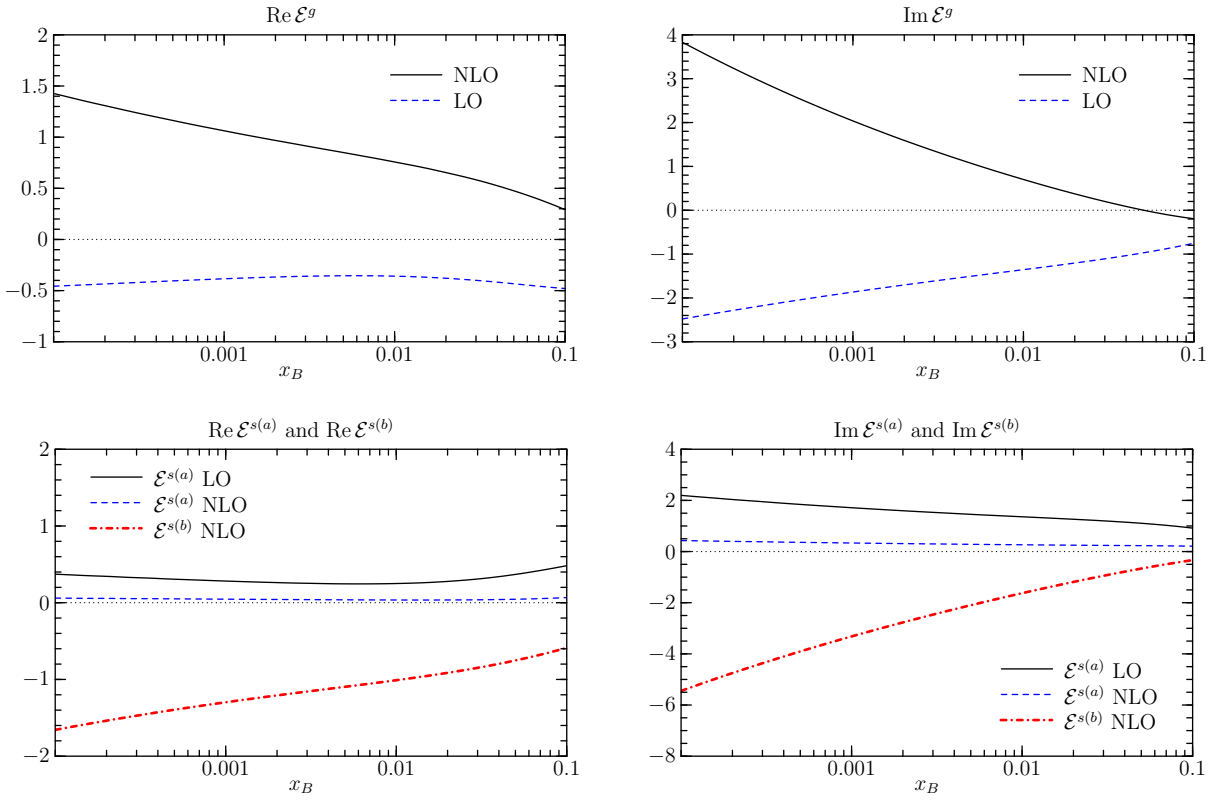

Figure 4.25. Comparison of pure LO and NLO parts for $\mathcal{E}^g$ (upper two plots), $\mathcal{E}^{S(a)}$ and $\mathcal{E}^{S(b)}$ (lower plots) at the scales $\mu_F = \mu_R = Q = 4\,GeV$ and $t = -0.15\,GeV^2$.

where $\mathcal{H}$ and $\mathcal{E}$ denotes the convolution of the GPDs $H(x,\xi,t)$ and $E(x,\xi,t)$ with the scattering kernels.
First numerical estimates [37, 67] found that the asymmetries for both pseudoscalar and vector meson production can be sizable. Therefore it is clear that we also need numerical calculations for the convolution of scattering kernels and $E(x,\xi,t)$ to obtain a theoretical prediction for the SSA.

We described in Sect. 4.5 how one may obtain a model for the GPD $E(x,\xi,t)$ and we will use this model to calculate numerical values for the convolution of the GPD and the scattering kernels. We do not want to repeat the complete analysis of the previous section but want to give only these results where we find a qualitative change of our results. We also show our results for the fixed value $t = -0.15\,\mathrm{GeV}^2$ because our model is based on the correlation between the x and t-dependence of the GPDs.

We want to start with the discussion of the x_B behavior of our results. In Fig. 4.25 we show the pure LO and NLO contributions to the gluon and the both singlet parts of the amplitude at $\mu_F = \mu_R = Q = 4\,\mathrm{GeV}$. In comparison to the results obtained for the GPD $H(x,\xi,t)$ the main difference is in the absolute value of the contributions. They are much smaller than for $H(x,\xi,t)$ but the qualitative behavior is the same with the exception that for the singlet terms the sign changes. This is due the fact that for our model the d quark

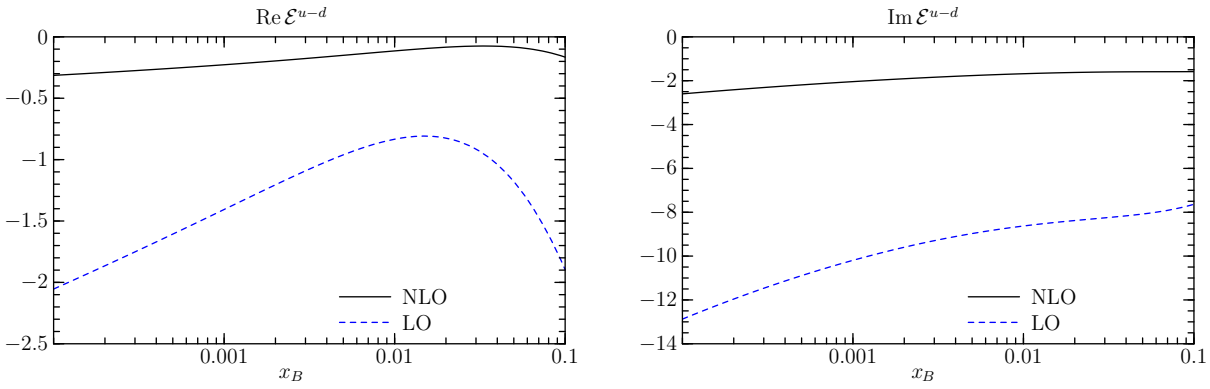

Figure 4.26. Comparison of pure LO and NLO parts for $\mathcal{E}^{u-d}$ for the scales $\mu_F = \mu_R = Q = 4\ GeV$ and $t = -0.15\ GeV^2$.

GPDs is negative and much larger than the u quark GPD as shown in Fig. 4.2. We again find that the NLO contribution of the pure singlet term $\mathcal{E}^{s(b)}$ is much larger than the LO contribution of the convolution of the singlet GPD and the quark scattering kernel as for the GPD $H(x,\xi,t)$. If we turn now to the non-singlet combination $u-d$ we find that their contributions are large even for small values of x_B. The results are shown in Fig. 4.26 for the real and imaginary part. The absolute size is even bigger than the contributions of the gluon and singlet parts. This is due to the fact that u and d quark GPDs are of opposite sign and the d quark GPD is much larger than the u quark GPD. This leads to the situation that for the combination $u-d$ there is an enhancement of the GPD instead of a cancellation. Therefore we find that large contributions of the non-singlet GPD even at that small values of x_B. The size of the corrections for the non-singlet GPD is small in comparison to the LO part as for the non-singlet GPD H^{u-d} in Sect. 4.6.1.

Now we want briefly discuss the large x_B-behavior, starting again with gluon and singlet terms of the amplitude. We have chosen in Fig. 4.27 again $\mu_F = \mu_R = 2\,\text{GeV}$ as in Sect. 4.6.1 for direct comparison with the results for the GPD $H(x,\xi,t)$. We can see from Fig. 4.27 that the absolute size of the different contributions is much smaller than for the GPD $H(x,\xi,t)$ (see Fig. 4.8 for direct comparison). The qualitative behavior is the same as for the non-flip GPD. The main difference is the change of sign for the singlet contributions of the amplitude in comparison to the results obtained for $H(x,\xi,t)$ in Sect. 4.6.1. But this effect has been observed also for the small-x_B region. The reason is again the different sign and absolute size of the u and d quark GPDs. For the non-singlet combination the results for the large x_B-region are shown in Fig. 4.28. We find again a large contribution to the real and imaginary part of the amplitude coming from the non-singlet term. Im comparison to the gluon and singlet parts the contributions are much larger by their absolute size. As before we also find that for the specific choice of scales the NLO corrections are small in comparison with the LO contribution. We can conclude that for the large-x_B region the amplitude is clearly dominated by the non-singlet term. This was not so clear for the results of the GPD $H(x,\xi,t)$ where the non-singlet terms give a sizeable contribution to the amplitude but are

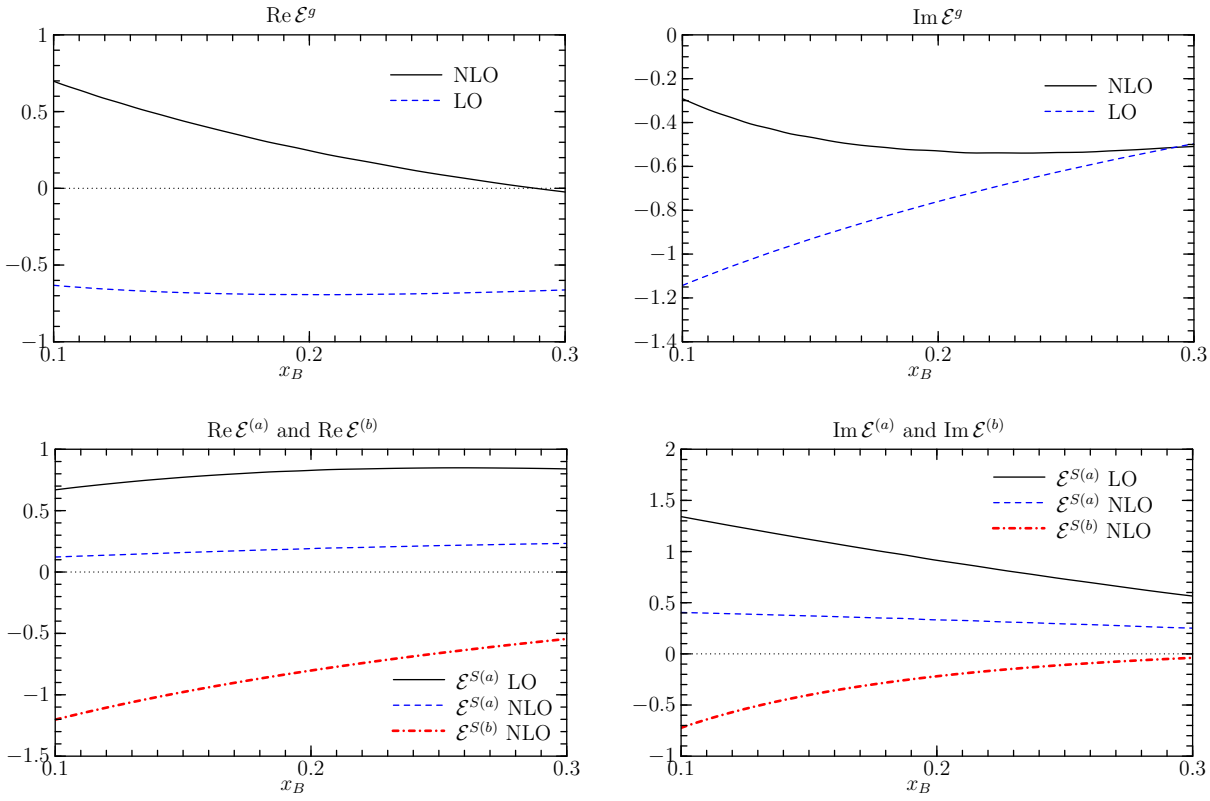

Figure 4.27. Comparison of pure LO and NLO parts for $\mathcal{E}^g$ (upper two plots), $\mathcal{E}^{S(a)}$ and $\mathcal{E}^{S(b)}$ (lower plots) at the scales $\mu_F = \mu_R = Q = 2\ GeV$ and $t = -0.15\ GeV^2$.

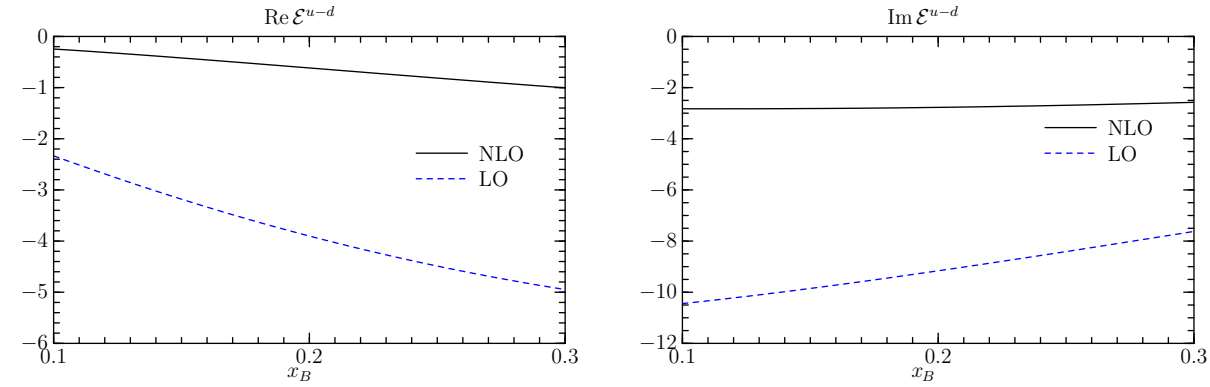

Figure 4.28. Comparison of pure LO and NLO parts for $\mathcal{E}^{u-d}$ for the scales $\mu_F = \mu_R = Q = 2\ GeV$ and $t = -0.15\ GeV^2$.

not as dominant as for the GPD $E(x, \xi, t)$.

We do not want to repeat the analysis for the higher Gegenbauer coefficients because the results show the same qualitative features as the results for the GPD $H(x, \xi, t)$. For the higher coefficients we also find an enhancement of the NLO corrections but for higher and higher coefficients the results converge.

Let us now turn to the scale dependence of the results for the GPD $E(x, \xi, t)$. For the

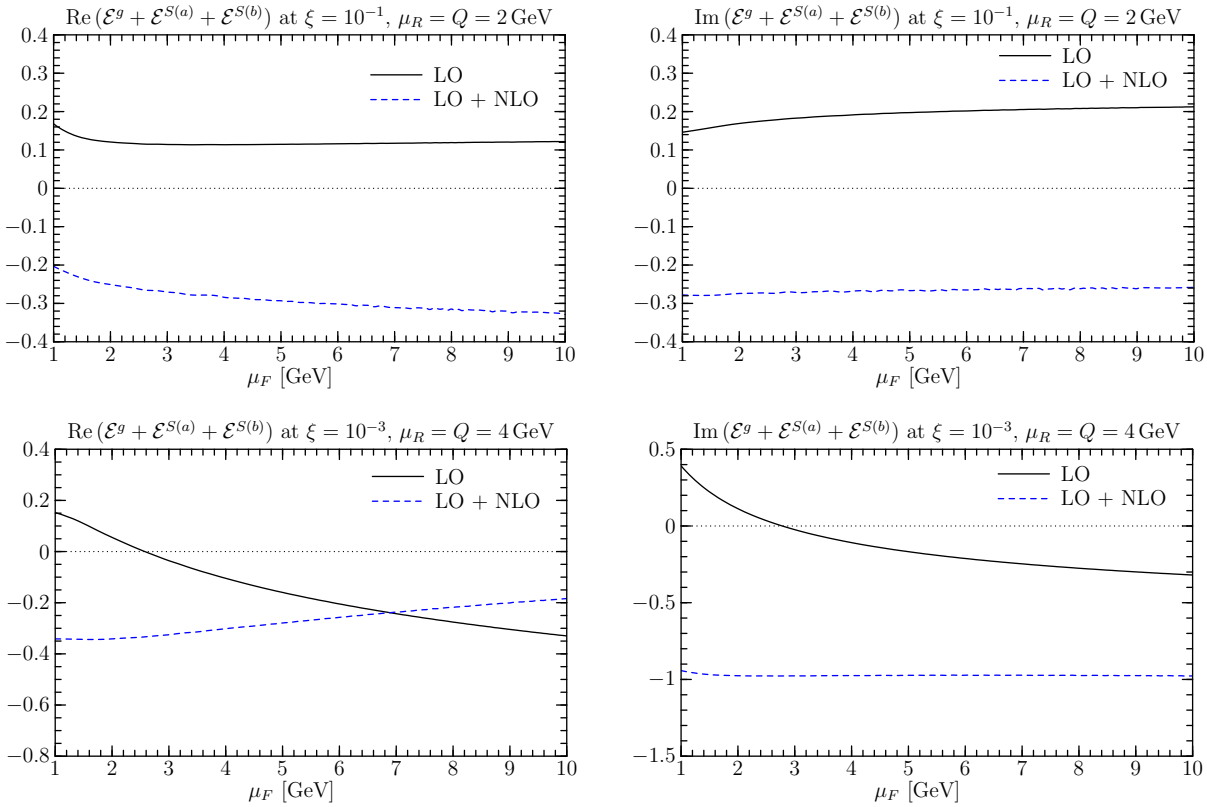

Figure 4.29. Comparison of pure LO and sum of LO and NLO parts for different values of μ_F. The upper two plots show the real and imaginary part for xi $= 10^{-1}$ and $\mu_R = Q = 2\,GeV$. The lower tow plots the real and imaginary part for xi $= 10^{-3}$ and $\mu_R = Q = 4\,GeV$. All results are obtained for $t = -0.15\,GeV^2$.

renormalization scale dependence at fixed $\mu_F = Q$ we find the same qualitative results as for the GPD $H(x, \xi, t)$: the pure LO part follows directly the falling of the strong coupling at higher values of μ_R. For the sum of LO and NLO contributions we find again a strong dependence on the renormalization scale for very low values of $\mu_R \sim 1 - 3\,\mathrm{GeV}$. The results become more stable for higher values of μ_R. This observation was done not only in the high energy region ($\xi = 10^{-3}$, $\mu_F = Q = 4\,\mathrm{GeV}$) but also in the low energy region ($\xi = 10^{-1}$, $\mu_F = Q = 2\,\mathrm{GeV}$). These results are not only restricted to the gluon and singlet parts of the amplitude but they are also valid for the non-singlet part of the amplitude. The more interesting case is the dependence on the factorization scale μ_F. We present our results again for the two different kinematical regions $\xi = 10^{-3}$ with $\mu_R = Q = 4\,\mathrm{GeV}$ and $\xi = 10^{-1}$ with $\mu_R = Q = 2\,\mathrm{GeV}$. We would like to start to discuss our results for the sum of gluon and singlet parts of the amplitude because they mix under evolution and hence cannot be treated separately. Our results for the real and imaginary part are shown in Fig. 4.29 for both kinematical setups. For the low energy region and high energy region we find that the correction due to the NLO contributions are large. Similar results we also found for the GPD $H(x, \xi, t)$ but in that case the corrections for the low energy region were not as large as they are for $E(x, \xi, t)$. In contrast to the non-flip GPD we found that the scale dependence

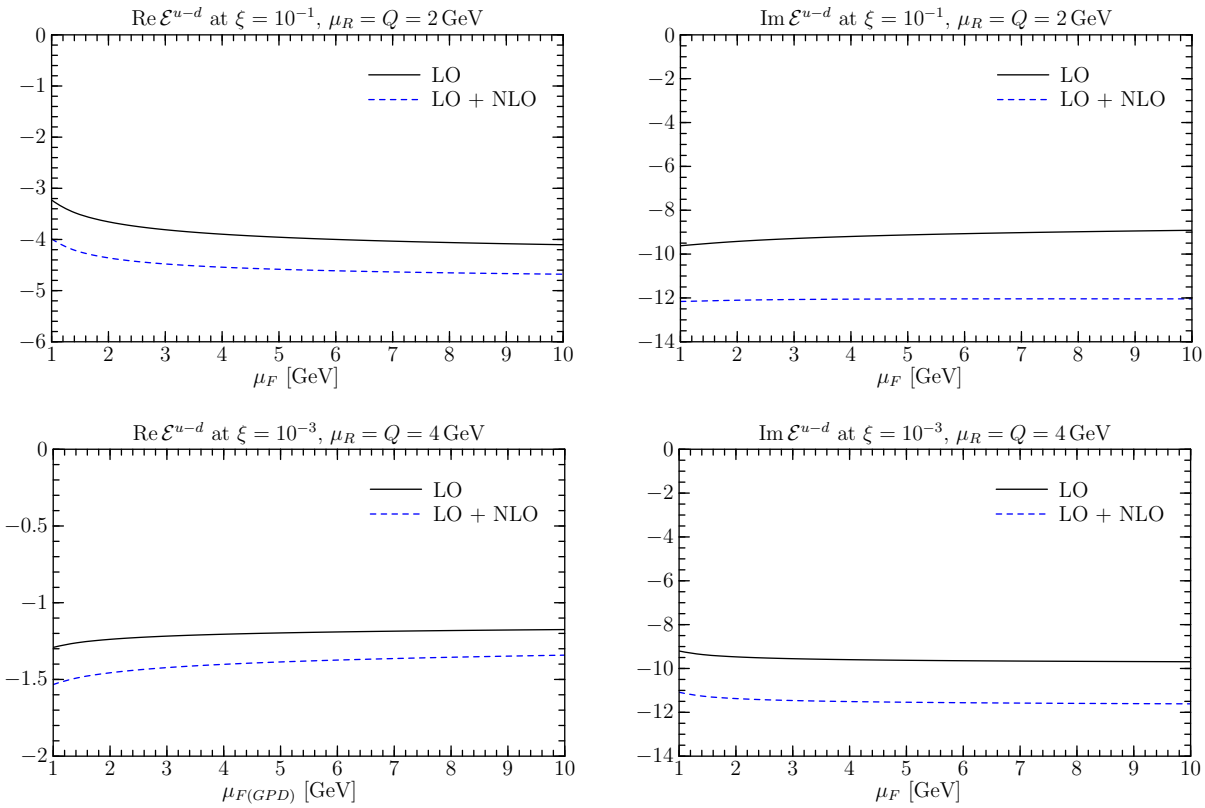

Figure 4.30. Comparison of pure LO and sum of LO and NLO parts of the non-singlet combination $\mathcal{E}^{u-d}$ for different values of μ_F. The upper two plots show the real and imaginary part for $xi = 10^{-1}$ and $\mu_R = Q = 2\,GeV$. The lower tow plots the real and imaginary part for $xi = 10^{-3}$ and $\mu_R = Q = 4\,GeV$. All results are obtained for $t = -0.15\,GeV^2$.

is not so strong, even at LO level. This is due to the fact that the gluon GPD $E^g(x,\xi,t)$ does not evolve as strong as the corresponding non-flip GPD $H^g(x,\xi,t)$. The evolution of $H^g(x,\xi,t)$ was the main source of the strong factorization scale dependence in Sect. 4.6.1. Now the dependence is much weaker and shape is approximately flat if we add the NLO terms. The very large corrections in the low energy region are somewhat surprising but as stated above, the amplitude is clearly dominated by the non-singlet part and hence the large corrections play no important role for the complete amplitude. For the non-singlet part our results are shown in Fig. 4.30. The factorization scale dependence is very flat for the LO and the sum of LO and NLO terms. This result we also obtained for the non-singlet combination of GPD $H(x,\xi,t)$. The corrections are small in comparison to the gluon and singlet part of the amplitude and the absolute size of the contribution is much larger than the contributions from the sum of gluon and singlet.

Our results show that the contributions to the amplitude coming from the GPD $E(x,\xi,t)$ are small in comparison to the contributions from $H(x,\xi,t)$, especially at high energies. For lower energies the contributions from the helicity-flip GPD can affect the amplitude because the dominant non-singlet contributions are of the same order of magnitude as the contributions of the non-flip GPD $H(x,\xi,t)$. Also the additional suppression due to the

extra factor ξ in front of the terms containing the GPD $E(x,\xi,t)$ is not pronounced at low energies. We have not discussed in detail the renormalization scale dependence of our results and we also have not shown the results for the higher Gegenbauer coefficients. The results are qualitatively the same as for the GPD $H(x,\xi,t)$. And also the t dependence of our results is similar to that for $H(x,\xi,t)$ because we used an analog parameterization for the function $f(x)$ to model the t dependence (4.23).

4.6.3 Results for the polarized GPDs $\tilde{H}(x,\xi,t)$ and $\tilde{E}(x,\xi,t)$

In the previous sections we discussed our results for the unpolarized GPDs $H(x,\xi,t)$ and $E(x,\xi,t)$. In this section we want to discuss the polarized GPDs $\tilde{H}(x,\xi,t)$ and $\tilde{E}(x,\xi,t)$. These GPDs are necessary to describe the exclusive production of pseudoscalar mesons like pions and kaons. We have discussed the cross sections for pseudoscalar meson production in detail in Sect. 3.2 at the LO level. The first NLO calculation for the exclusive production of pions was done in [121] where the authors found large corrections to the cross section for a specific choice of Q, the factorization and the renormalization scale. We are in this section also only interested in the exclusive production of charged pions. Therefore we show our results only for the non-singlet combination $u-d$. The flavor singlet combination $u+d$ appears only in the exclusive production of π^0 which we do not want to consider. The polarized gluon GPD $\tilde{H}^g$ appears for example in the production of h_1 and there only at NLO level.

To obtain numerical results we need a model for the GPDs $\tilde{H}$ and $\tilde{E}$. For $\tilde{E}$ we use the same model as in Sect. 3.1 given by

$$\tilde{E}(x,\xi,t) = \frac{\theta(|x|\leq\xi)}{2\xi}\,\phi_\pi\left(\frac{x+\xi}{2\xi}\right)\frac{2m_p f_\pi\, g_{\pi NN}}{m_\pi^2-t}\,\frac{\Lambda^2-m_\pi^2}{\Lambda^2-t}\,. \tag{4.51}$$

In this section we are not interested in cross sections or other observables but only in the amplitude and hence we can omit to specify the value for the additional parameter Λ. The pion distribution amplitude is defined in the same way as in (3.11) given by

$$\phi_\pi(z) = 6z(1-z)\Big[1+\sum_{n=1}^{\infty} a_n\, C_n^{3/2}(2z-1)\Big]\,. \tag{4.52}$$

For the GPD $\tilde{H}$ we also use again the double distribution ansatz of Sect. 3.1. Instead of the factorized ansatz for the (x,ξ) and t-dependence we use the ansatz described in Sect. 4.5 where we also specified the parameters of our model.

We want to start with our results for $\tilde{E}$. For exclusive π^+ production the convolution of GPD and the hard scattering kernel is given by

$$\int_{-1}^{1} dx\,\tilde{E}(x,\xi,t)\left[Q_u T_q\left(\frac{\xi-x}{2\xi}\right)-Q_d T_q\left(\frac{\xi+x}{2\xi}\right)\right]\,, \tag{4.53}$$

where the scattering kernel T_q is given by (C.25) and Q_u and Q_d are the u and d quark charge. Because the support region of $\tilde{E}(x,\xi,t)$ is restricted to the ERBL region the result of the convolution (4.53) is purely real and at LO we find

$$\mathcal{N}\alpha_s(\mu_R^2)\,(1+a_2+a_4) \tag{4.54}$$

where

$$\mathcal{N} = \frac{1}{2\xi}\frac{2m_p f_\pi g_{\pi NN}}{m_\pi^2 - t}\frac{\Lambda^2 - m_\pi^2}{\Lambda^2 - t}\frac{9}{4}C_F\,. \tag{4.55}$$

For the NLO scattering kernel we obtain the result

$$\begin{aligned}\mathcal{N}\alpha_s^2(\mu_R^2)\frac{1}{12\pi}\Bigg\{&39.5 + 149.964a_2 + 196.851a_4 + 320.242a_2a_4 + 128.581a_2^2 + 195.313a_4^2\\ &- \frac{27}{2}(1+a_2+a_4)^2\ln\left(\frac{Q^2}{\mu_R^2}\right)\\ &- \left(\frac{25}{3}a_2(1+a_2) + \frac{182}{15}a_4(1+a_4) - \frac{50}{3}a_2a_4\right)\ln\left(\frac{Q^2}{\mu_{F(DA)}^2}\right)\\ &- \left(\frac{25}{3}a_2(1+a_2) + \frac{182}{15}a_4(1+a_4) - \frac{364}{15}a_2a_4\right)\ln\left(\frac{Q^2}{\mu_{F(GPD)}^2}\right)\Bigg\}\end{aligned} \tag{4.56}$$

It is not surprising that the $\mu_{F(GPD)}$ dependence vanishes for the asymptotic term of the meson DA (4.52) because the coefficient of $\ln(Q^2/\mu_{F(GPD)}^2)$ is the LO evolution kernel and the asymptotic DA is its eigenfunction with zero eigenvalue. To get an impression of the absolute size of the corrections we need an estimate of the size of the different Gegenbauer coefficients. For the value of a_2 exists a new lattice result [129]

$$a_2^\pi(\mu = 2\,\mathrm{GeV}) = 0.201(114)\,. \tag{4.57}$$

Unfortunately there exists no value for a_4 from lattice calculations. But in the work [130] the authors give the value

$$a_4^\pi(\mu = 2\,\mathrm{GeV}) = -0.10(5)\,. \tag{4.58}$$

Using these values for the higher Gegenbauer coefficients we can estimate the size of the NLO corrections. For simplicity we choose all scales to be equal ($Q = \mu_R = \mu_{F(GPD)} = \mu_{F(DA)}$) and obtain for the sum of LO and NLO contribution

$$\mathrm{LO} + \mathrm{NLO} = \mathcal{N}\alpha_s(\mu_R^2)\left[1.101 + \frac{\alpha_s(\mu_R^2)}{\pi}4.22\right]\,. \tag{4.59}$$

For the arbitrary choice $\mu_R = 2\,\mathrm{GeV}$ the corrections due to the NLO terms are of the order 30%. From (4.56) it is obvious that the main corrections are due to the asymptotic term of the Gegenbauer expansion of the meson DA. But also the terms proportional to a_2 and a_4 give sizeable corrections with our choice for the coefficients (4.57) and (4.58). On the other side the terms in (4.56) proportional to higher powers of the Gegenbauer coefficients give

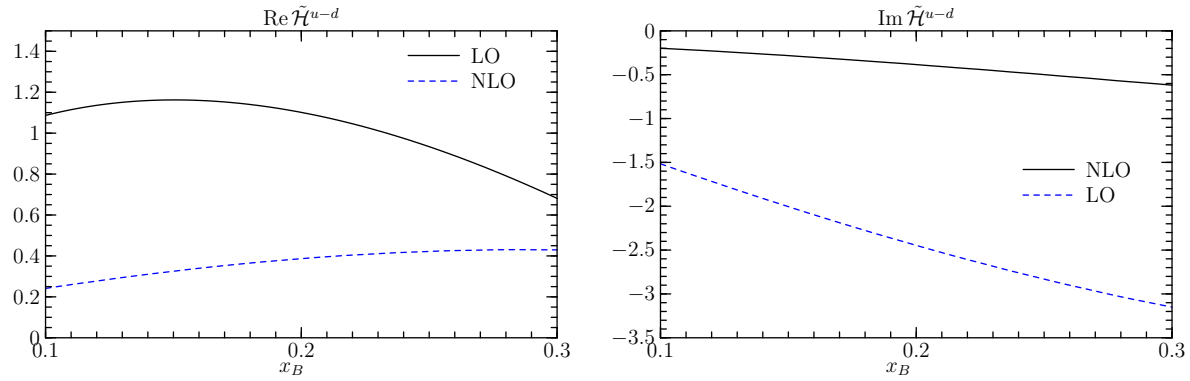

Figure 4.31. Comparison of pure LO and NLO parts for $\tilde{\mathcal{H}}^{u-d}$ at the scales $\mu_F = \mu_R = Q = 2$ GeV.

only a very small contribution to the NLO corrections in comparison to the term depending linear on them.

Let us turn to the discussion of the results for the GPD $\tilde{H}(x,\xi,t)$. As mentioned at the beginning of this section we used the double distribution model with the improved t dependence described in Sect. 4.5. As forward parton distribution we used the analytic parameterization of Blümlein et al. [94] at the initial scale $Q_0^2 = 4\,\mathrm{GeV}^2$ and at NLO (`ISET` 3). The main feature of that parameterization is the equal treatment of the different sea quarks. For our non-singlet combination the contribution of the sea quarks is therefore exactly zero and we obtain for small values of x_B a vanishing result and so we concentrate only on the large-x_B region. We keep the discussion of the results very short because they show the same qualitative behavior as the result for the unpolarized non-singlet GPD $H^{u-d}(x,\xi,t)$.
In Fig. 4.31 we show the comparison of the pure LO and NLO parts at $Q = \mu_F = \mu_R = 2\,\mathrm{GeV}$ for the large-x_B region. We find as for the unpolarized case that the corrections are small and of the same sign as the LO contributions. This would lead to an increase of the cross section with our naive scale setting. This result was observed for the first time in [121] where the authors also applied the BLM scale setting procedure and found a strong decrease of the cross section. This result is not surprising and we discussed this issue in detail in Sect. 4.6.1. The results for the higher Gegenbauer coefficients show the same behavior as in the case of the unpolarized GPDs and also the renormalization scale dependence of our results for fixed $Q = \mu_F$ are similar to that of the unpolarized case. More interesting is the factorization scale dependence at fixed $Q = \mu_R$. The results for $\xi = 10^{-1}$ and $Q = \mu_R = 2\,\mathrm{GeV}$ are shown in Fig. 4.32. We find that the unpolarized GPDs do not evolve as strong as the unpolarized ones even if we take only the LO contribution into account. For the sum of LO and NLO contribution the situation becomes somewhat better, especially for the real part. The corrections we found are moderate and reach the 50% level only for the real part at very high values of μ_F which seem to be an unrealistic choice for the kinematical region of fixed target experiments.

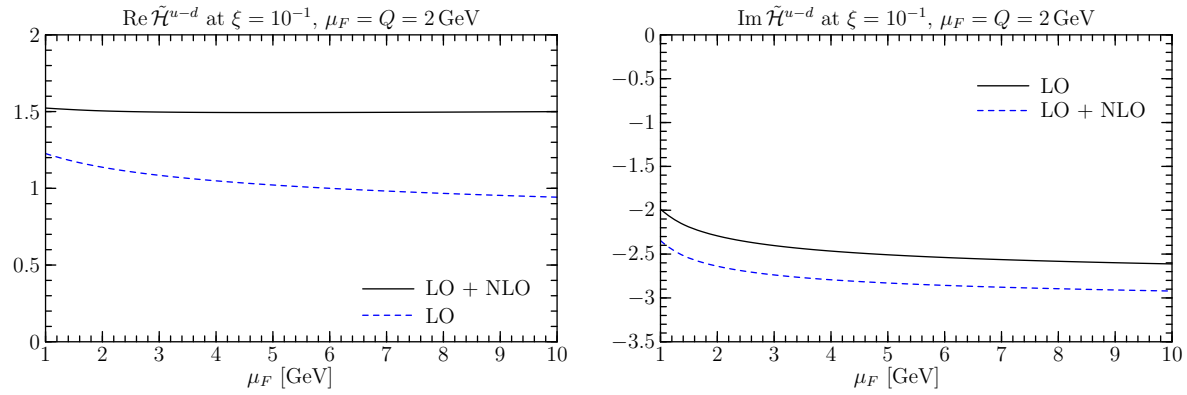

Figure 4.32. Real and imaginary part of the LO and sum of LO and NLO parts of $\tilde{\mathcal{H}}^{u-d}$ for different values of μ_F at $\xi = 10^{-1}$ and $Q = \mu_R = 2$ GeV.

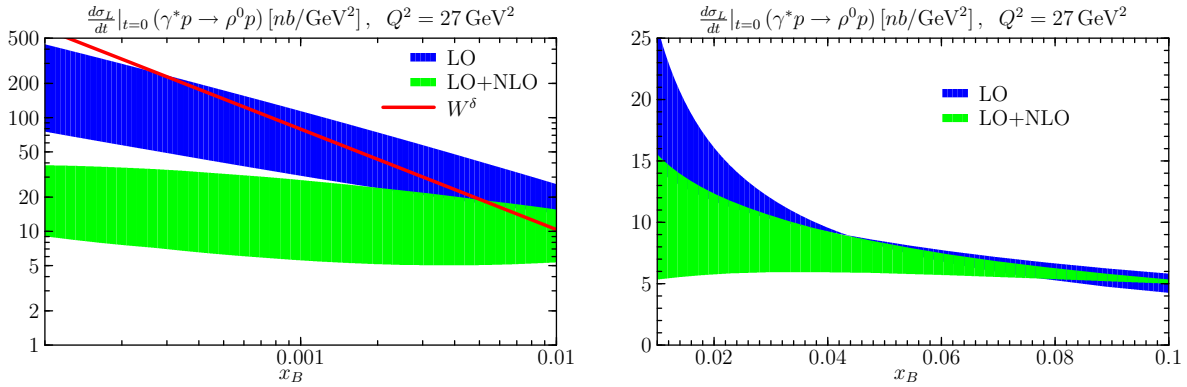

Figure 4.33. Differential cross section for exclusive ρ^0-production at $Q^2 = 27$ GeV^2. The bands are obtained by the two different choices $\mu_F = \mu_R = Q/2$ and $\mu_F = \mu_R = 2Q$. The red curve in the left plot shows the measured W dependence of the cross section [131], $\sigma(\gamma^* p \to \rho^0 p) \propto W^\delta$ with $\delta = 0.88$ at $Q^2 = 27$ GeV^2. The renormalization of this curve is chosen arbitrarily in order to fit into the plotted range.

4.6.4 Cross section for exclusive ρ^0-production

At the end of this chapter let us briefly discuss the consequences of our previous results for the cross section of exclusive ρ^0-production. Because we are here mainly interested in the x_B-dependence of the cross section we calculate the differential forward cross section

$$\frac{d\sigma_L}{dt}|_{t=0}\,. \tag{4.60}$$

For a first estimate of the cross section we neglect the term proportional to $|\mathcal{E}|^2$ and $\mathrm{Re}\,(\mathcal{H}\mathcal{E}^*)$ because these terms have at least one additional kinematical factor ξ in front and do therefore give no big contribution to the cross section for the region of x_B we are interested in. We present our result for the cross section in Fig. 4.33. We have chosen the value of $Q^2 = 27\,\mathrm{GeV}^2$ because we want to avoid effects from higher twist contributions. The bands in Fig. 4.33 are obtained by varying the renormalization and factorization scale in the following way: in order to cover a broad range of possibilities we choose $\mu_F = \mu_R = Q/2$ and $\mu_F = \mu_R = 2Q$.

In the left plot of Fig. 4.33 we show the results for the very low-x_B region as achieved at H1 or ZEUS. We find that the corrections to the cross section are very large and even more problematic: the sum of LO and NLO does not show the correct energy behavior. From experimental measurements at the H1 [85] and ZEUS experiment [132] we know that the cross section increases for higher energies. For our result of LO and NLO terms we find in contrast to the experimental results a approximately flat energy behavior for small values of x_B for both choices of μ_F and μ_R. We show in Fig. 4.33 also the measured W dependence of the cross section (red curve in the left plot). The cross section is roughly proportional to $W^{0.88}$ at $Q = 27\,\mathrm{GeV}^2$ [131] and we have chosen the normalization in such a way that the curve fits into the plot range. We see that the measured energy is much more steeper than the behavior we find for our full result. From this result we can conclude that the leading twist at fixed order α_s approach fails at such high energies even for our large value of Q^2. The situation becomes better if we turn to higher values of x_B as shown in the right plot of Fig. 4.33. There we show our result for the same value of Q^2 and the same choices of the renormalization and factorization scale. The region of x_B can be achieved by the COMPASS and HERMES experiment even if our value of Q^2 is to large for these experiments. We observe that the corrections due to the NLO terms in the amplitude start to converge for higher and higher values of x_B. This is caused by the fact that at this values of x_B the gluon and singlet contribution start to lose their dominance in the amplitude and the non-singlet contributions (which have small NLO corrections) give a sizable contribution to the amplitude. From this result one can assume that for even higher values of x_B and moderate values of Q^2 the NLO corrections to the cross sections are not too large.

We finally can conclude that the leading twist and fixed order α_s approach we used for the calculation of the amplitude is insufficient for high energy processes where we found very large corrections even on the amplitude level. The corrections amplify on the level of cross sections and lead to an unstable theoretical prediction. At low energies the situation is more under control. The correction can nevertheless be quite large as it was shown for exclusive pion production in [121] but they are not as sensitive on specific choices of Q, μ_F and μ_R as in the high energy regime.

5

Summary and outlook

In this work we have investigated some new aspects of the exclusive production of mesons. These processes offer the opportunity to get access to the GPDs, which contain rich information about the structure of the nucleon. After a general introduction and a brief review of the theoretical framework of GPDs and their properties in Chapter 1 and 2, we have evaluated the cross section for a variety of exclusive meson production channels for moderate to large x_B at leading order in $1/Q^2$ and in α_s. Cross sections change significantly when varying the non-perturbative input, generalized parton distributions and meson distribution amplitudes, within plausible limits of current model building. On one hand this implies an uncertainty in predicting these cross sections, but on the other hand it implies that their measurement can ultimately help to constrain the non-perturbative functions, provided theoretical control over corrections to the leading-order formulae. We find the largest cross section uncertainties for ρ^0, ω and ϕ production, which is sensitive to the gluon GPD over a large range of x_B, reflecting the current uncertainty of the unpolarized gluon density at low scales. Comparing our leading-twist cross section with experimental data, we confirm that for Q^2 of a few GeV^2 power corrections are substantial. In particular, the suppression of vector meson cross sections we find is consistent with what has been estimated in the literature from the effects of parton transverse momentum in the hard-scattering subprocess. As it is seen for the ratio of ϕ and ρ^0 production, the most serious theoretical uncertainties cancel in cross section ratios for sufficiently similar channels (the main distinction being between channels with and without t-channel pion exchange).

Rescaling our leading-twist cross sections in order to be consistent with experimental data for ρ^0 and ϕ production, we have compared their contribution to semi-inclusive pion or

kaon production with the result of leading-twist quark fragmentation, focusing on the typical kinematics of HERMES measurements, where $Q^2 \sim 2.5\,\mathrm{GeV}^2$ and $x_B \sim 0.1$. Within large uncertainties, direct exclusive production of π^+ and possibly K^+ appears to be comparable to the fragmentation result extrapolated to the bin $0.9 < z < 1$. Through their decays, exclusively produced ρ, ϕ and K^* contribute in a wide range of z. Pions from K^* decay and kaons from ϕ decay are however limited to z below 0.7. With this and the relative size of cross sections, our estimates indicate that in typical HERMES kinematics the only exclusive channel whose cross section can compete with quark fragmentation is the ρ^0. The ρ^0 saturates the quark fragmentation result for semi-inclusive π^+ and π^- production at large z. Since the ρ^0 does not contribute to π^0 and to kaon production, there is no corresponding "dangerous" vector channel in these cases.

The large discrepancy of our leading order results and the experimental measurements and the strong dependence on the factorization scale found in Chapter 3 motivated the systematic investigation of next-to-leading order corrections in Chapter 4. Our results for the different parts of the amplitude lead to different conclusions for high and low energies. At high energies we found huge corrections to the gluon part of the amplitude and large contributions from the singlet part, which arises for the first time at next-to-leading order. The scale dependence of the NLO corrections of the gluon and singlet part strongly disfavors the naive scale setting procedure, widely used in the literature. The overall dependence on the factorization scale has improved by considering the sum of LO and NLO part of the amplitude for both contributions. But at small values of x_B they are not under theoretical control even at very large values of Q^2. These results make use of the leading-twist and fixed-order approach highly questionable. It manifests itself in our result for the cross section for exclusive ρ^0 production, where we found that by inclusion of the NLO corrections the cross section shows an approximately flat energy behavior which is in clear contrast to the experimental measurements even when varying the factorization scale over a huge range. A rough estimate of the size of the NLO corrections in the high energy regime indicates that they are parametrically of the size $\alpha_s \ln(1/\xi)$ for the gluon and the singlet part of the amplitude. It would be of great interest to see if the results improve and become more stable when resumming such logarithms to all orders. To calculate the resummation, which will have roughly the form $(\alpha_s \ln(1/\xi))^n$, is a challenging task for future projects.

The situation changes when we consider the low energy regime and moderate values of Q^2. In this kinematical region, which is of interest for experiments like COMPASS or HERMES, the corrections to the LO amplitude are of the order of 10-30% for the gluon and singlet part. Even more important, the corrections are approximately constant over a broad range of the factorization and renormalization scales for fixed values of Q^2. In this energy region the contributions from the non-singlet part of the amplitude start to play an important role. For this part the NLO corrections are of the order of $20-30\%$. The size of the corrections for the non-singlet parts becomes very large if we apply the BLM scale setting procedure due to a cancellation of different terms in the NLO scattering kernel. The BLM scale setting procedure also favors a very low renormalization scale, where the

applicability of perturbation theory is questionable. The large corrections and the small size of μ_R lead to the conclusion that the BLM scale setting is not the correct way to choose the renormalization scale. The BLM scale setting gives further no constraints on the choice of the factorization scale. From our results it follows that choosing $\mu_R = \mu_F$ leads to more reliable results for the non-singlet part of the amplitude. The size of the corrections and the stability gives hope that the theoretical predictions for physical observables like cross sections and especially for single-spin asymmetries show a substantial improvement in this kinematical region. The calculation of cross sections and single-spin asymmetries for different final state mesons is under progress and we hope to present some results in the near future.

Finally we investigated for the first time the impact of the GPD $E(x, \xi, t)$ on the scattering amplitude. Our results showed the same qualitative features described above. The main difference is the absolute size of the different contributions in comparison to the results for the GPD $H(x, \xi, t)$. For our specific model we found the gluon and singlet contribution being much smaller for $E(x, \xi, t)$ than for $H(x, \xi, t)$. On the other hand the non-singlet contribution plays an important role, even at small values of x_B. This is due to the fact that the u and d quark GPDs have opposite sign and the d quark GPD is much larger. Therefore the two contributions do not cancel each other as in the case of $H(x, \xi, t)$ where both GPDs are of the same sign. It remains to be studied in future analyses how a different model for $E(x, \xi, t)$ affects our results. Such an investigation will be of great interest, especially for the calculation of single-spin asymmetries, which are the only way to directly access the GPD $E(x, \xi, t)$ in exclusive meson production.

A

Integrals over GPDs within the double distribution model

The t independent functions in the ansatz (3.14) for quark and gluon GPDs are modeled as described in Sect. 2.4

$$
\begin{aligned}
H^q(x,\xi) &= \int_{-1}^{1} d\beta \int_{-1+|\beta|}^{1-|\beta|} d\alpha\; \delta(x-\beta-\xi\alpha)\, h(\beta,\alpha) \Big[\theta(\beta)\, q(\beta) \;-\theta(-\beta)\, \bar{q}(-\beta)\Big], \\
H^g(x,\xi) &= \int_{-1}^{1} d\beta \int_{-1+|\beta|}^{1-|\beta|} d\alpha\; \delta(x-\beta-\xi\alpha)\, h(\beta,\alpha)\, \beta \Big[\theta(\beta)\, g(\beta) \;-\theta(-\beta)\, g(-\beta)\Big], \\
\tilde{H}^q(x,\xi) &= \int_{-1}^{1} d\beta \int_{-1+|\beta|}^{1-|\beta|} d\alpha\; \delta(x-\beta-\xi\alpha)\, h(\beta,\alpha) \Big[\theta(\beta)\, \Delta q(\beta) + \theta(-\beta)\, \Delta\bar{q}(-\beta)\Big],
\end{aligned}
\tag{A.1}
$$

where θ denotes the usual step function, q, $\bar{q}$, Δq, $\Delta\bar{q}$ the unpolarized and polarized quark and antiquark distributions, and g the unpolarized gluon distribution. The profile function

$$
h(\beta,\alpha) = \frac{\Gamma(2b+2)}{2^{2b+1}\Gamma^2(b+1)} \frac{[(1-|\beta|)^2-\alpha^2]^b}{(1-|\beta|)^{2b+1}} \tag{A.2}
$$

depends on a parameter b, which we chose to be either $b=1$ or $b=2$ in this work.

For meson production amplitudes at leading order in α_s we need the integrals

$$\begin{aligned} I^q(\xi) &= \int_{-1}^{1} dx\, \frac{H^q(x,\xi)}{\xi - x - i\epsilon}\,, \qquad I^{\bar q}(\xi) = \int_{-1}^{1} dx\, \frac{H^{\bar q}(x,\xi)}{\xi - x - i\epsilon} = [I^q(-\xi)]^*, \\ \tilde I^q(\xi) &= \int_{-1}^{1} dx\, \frac{\tilde H^q(x,\xi)}{\xi - x - i\epsilon}\,, \qquad \tilde I^{\bar q}(\xi) = \int_{-1}^{1} dx\, \frac{\tilde H^{\bar q}(x,\xi)}{\xi - x - i\epsilon} = -[\tilde I^q(-\xi)]^*, \end{aligned} \tag{A.3}$$

where we used the definitions $H^{\bar q}(x,\xi) = -H^q(-x,\xi)$ and $\tilde H^{\bar q}(x,\xi) = \tilde H^q(-x,\xi)$ together with the fact that these functions are even in ξ. The required integral for gluons can be brought into the same form as $I^q(\xi)$ by rewriting

$$I^g(\xi) = \int_{-1}^{1} dx\, \frac{H^g(x,\xi)}{x}\, \frac{1}{\xi - x - i\epsilon} = \frac{1}{\xi} \int_{-1}^{1} dx\, \frac{H^g(x,\xi)}{\xi - x - i\epsilon}\,, \tag{A.4}$$

where we used that $H^g(x,\xi)$ is even in x. The imaginary parts of these integrals are readily converted into integrals over β, with

$$\begin{aligned} \text{Im } I^q(\xi) &= \int_0^{\frac{2\xi}{1+\xi}} d\beta\, I(\beta,\xi)\, q(\beta), \\ I(\beta,\xi) &= \frac{\pi\Gamma(2b+2)}{2^{2b+1}\Gamma^2(b+1)}\, \frac{(1-\xi^2)^b}{\xi^{2b+1}}\, \frac{1}{(1-\beta)^{2b+1}} \Big(\frac{2\xi}{1+\xi} - \beta\Big)^b \beta^b \end{aligned} \tag{A.5}$$

for $\xi > 0$. The function $I(\beta,\xi)$ vanishes at the endpoints of the integration region, which in particular ensures the convergence of the integral at $\beta = 0$ for common parameterizations of quark densities. To obtain the analogous expressions for $I^{\bar q}$, $\tilde I^q$, $\tilde I^{\bar q}$ and I^g one has to replace $q(\beta)$ with $\bar q(\beta)$, $\Delta q(\beta)$, $\Delta\bar q(\beta)$ and $\beta g(\beta)$, respectively.

The real parts of the amplitudes involve principal value integrals, whose numerical evaluation requires some care, especially for small ξ. For our choices of profile parameters $b = 1$ and $b = 2$ one can explicitly perform the α integral after inserting (A.1) into (A.3) and (A.4). The result is

$$\begin{aligned} \text{Re } I^q(\xi) &= \int_0^1 d\beta \Big[R(\beta,\xi)\, q(\beta) + R(\beta,-\xi)\, \bar q(\beta) \Big] \\ &= \int_0^1 d\beta \left\{ R(\beta,\xi) \Big[q(\beta) - \bar q(\beta) \Big] + \Big[R(\beta,\xi) + R(\beta,-\xi) \Big]\, \bar q(\beta) \right\}, \\ \text{Re } I^g(\xi) &= \int_0^1 d\beta \Big[R(\beta,\xi) + R(\beta,-\xi) \Big] \beta g(\beta)\,, \end{aligned}$$

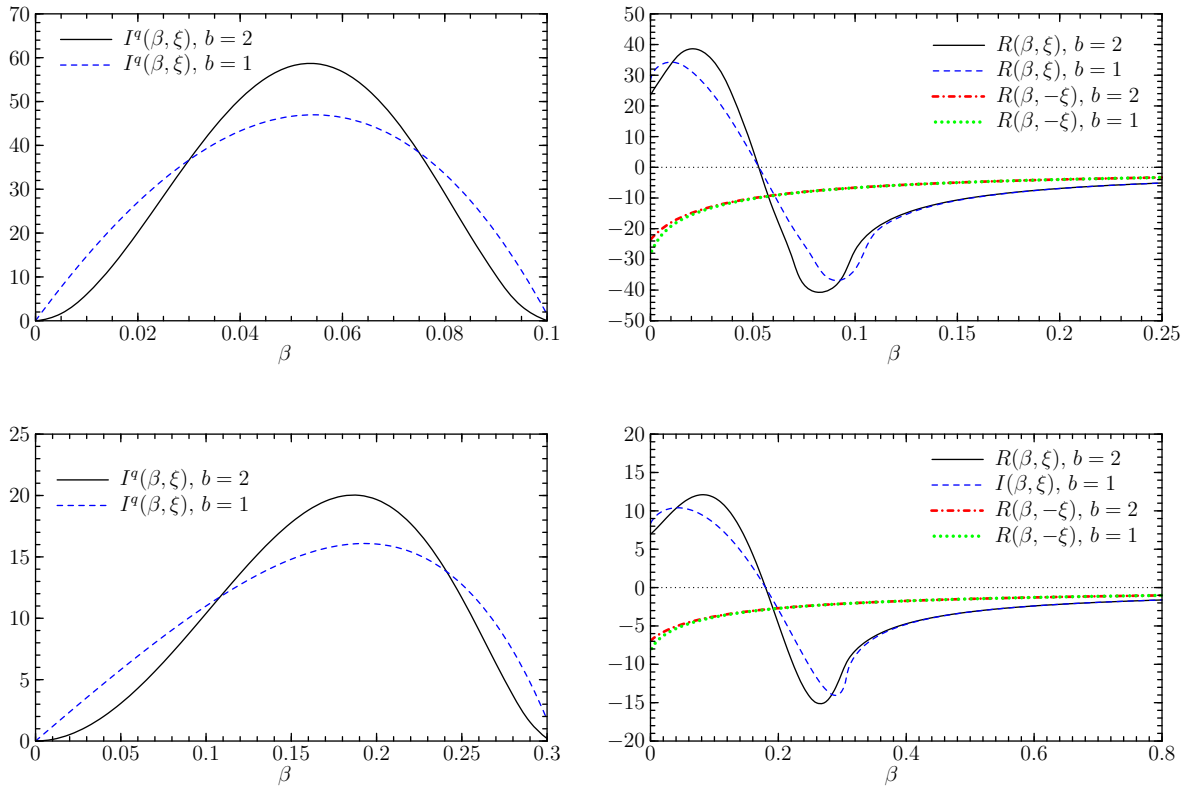

Figure A.1. The functions appearing in the integrals (A.5) and (A.6) for the meson production amplitude for $\xi = 0.053$ (top) and $\xi = 0.18$ (bottom), which respectively correspond to $x_B = 0.1$ and $x_B = 0.3$. Note the different ranges for β in the plots.

$$\text{Re}\ \tilde{I}^q(\xi) \;=\; \int_0^1 d\beta \left[R(\beta,\xi)\,\Delta q(\beta) - R(\beta,-\xi)\,\Delta\bar{q}(\beta) \right], \tag{A.6}$$

with

$$\begin{aligned} R(\beta,\xi) \;&\overset{b=1}{=}\; -\frac{3}{4\xi^3(1-\beta)^3}\left(2\xi(1-\beta)(\beta-\xi) \right. \\ &\qquad \left. + \beta(1-\xi)\Big[\beta(1+\xi)-2\xi\Big] \log\frac{|\beta(1+\xi)-2\xi|}{\beta(1-\xi)} \right), \\ R(\beta,\xi) \;&\overset{b=2}{=}\; \frac{5}{16\xi^5(1-\beta)^5}\left(2\xi(1-\beta)(\beta-\xi)\Big[3(\beta-\xi)^2 - 5\xi^2(1-\beta)^2\Big] \right. \\ &\qquad \left. + 3\beta^2(1-\xi)^2\Big[\beta(1+\xi)-2\xi\Big]^2 \log\frac{|\beta(1+\xi)-2\xi|}{\beta(1-\xi)} \right). \end{aligned} \tag{A.7}$$

For both $b = 1$ and $b = 2$, the function $R(\beta,\xi)$ is continuous in the full interval of integration, with finite limits at $\beta = 0$ and $\beta = 1$. If $\xi > 0$ it is positive for $\beta < \xi$ and negative for

$\beta > \xi$, and if $\xi < 0$ it is negative in the entire interval. Convergence of the integral for polarized quark distributions requires that $\Delta q(\beta)$ and $\Delta\bar{q}(\beta)$ have integrable singularities at $\beta = 0$, which is the case for the parton densities we use in this study. The unpolarized quark distributions have a steeper behavior at small β, but since $R(\beta,\xi) + R(\beta,-\xi) \sim \beta$ for $\beta \to 0$ it is sufficient to have integrable singularities for $q(\beta) - \bar{q}(\beta)$ and for $\beta\bar{q}(\beta)$.

In Fig. A.1 we illustrate the behavior of the functions multiplying the parton distributions in the integrals (A.5) and (A.6). The imaginary part of the amplitude involves momentum fractions in the parton densities between 0 and $2\xi/(1+\xi) = x_B$, with a maximum of the shape function $I(\beta,\xi)$ for β around ξ. In contrast, the real part is sensitive to higher momentum fractions, with a partial cancellation from values above and below ξ. One also clearly sees the stronger sensitivity to small β if $b = 1$. Note that the functions shown in the figure will be multiplied in the amplitude with functions showing a strong rise towards $\beta = 0$.

B

Distribution of pions or kaons from vector meson decay

In this appendix we discuss the decay of a vector meson into two pseudoscalar mesons and derive the z distribution given in (3.27). Consider the contribution of $ep \to VB$ with subsequent decay $V \to P_1 P_2$ to semi-inclusive production $ep \to P_1 + X$. A useful set of variables to describe the decay of the vector meson are the polar and azimuthal angles θ and φ of P_1 in the vector meson center-of-mass, as shown in Fig. B.1. The distribution in these angles is connected in a straightforward way with the spin density matrix of the produced vector meson [133], and the phase space element has a factorized form in the variables Q^2, x_B, t and θ, φ. The variable z used for semi-inclusive production of P_1 is then given by

$$z = a + b\cos\theta + c\sin\theta\cos\varphi \tag{B.1}$$

with

$$\begin{aligned}
a &= \frac{E_{P1}}{m_V}\,\frac{r_2\,(1+2x_B\,m_p^2/Q^2) + r_3\sqrt{1+4x_B^2\,m_p^2/Q^2}}{2r_1}\,\Big[1+O(x_B\Delta_T^2/Q^2)\Big] \;\approx\; \frac{E_{P1}}{m_V}\,,\\
b &= \frac{|\boldsymbol{q}_{P1}|}{m_V}\,\frac{r_3\,(1+2x_B\,m_p^2/Q^2) + r_2\sqrt{1+4x_B^2\,m_p^2/Q^2}}{2r_1}\,\Big[1+O(x_B\Delta_T^2/Q^2)\Big] \;\approx\; \frac{|\boldsymbol{q}_{P1}|}{m_V}\,,\\
c &= -\,\frac{|\boldsymbol{q}_{P1}|\Delta_T}{Q^2}\,\frac{2x_B}{1-x_B}\,\frac{\sqrt{1+4x_B^2\,m_p^2/Q^2}}{r_3}\,,
\end{aligned} \tag{B.2}$$

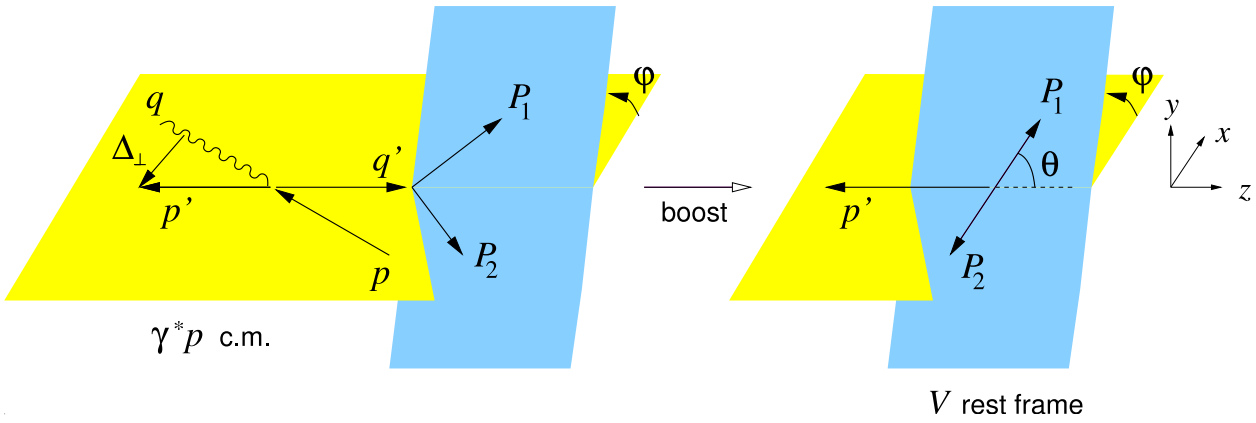

Figure B.1. Kinematic variables for $\gamma^*(q)+p(p)\to V(q')+B(p')$ followed by the decay $V\to P_1P_2$, shown in the $\gamma^* p$ center-of-mass and in the rest frame of V. Here θ and φ are the spherical coordinates of the momentum of P_1 in the depicted coordinate system.

where we abbreviated

$$r_1 = 1+\frac{x_B}{1-x_B}\,\frac{m_p^2}{Q^2}, \qquad r_2 = 1+\frac{x_B}{1-x_B}\,\frac{m_V^2-m_B^2+m_p^2}{Q^2},$$
$$r_3 = \left[\left(1-\frac{x_B}{1-x_B}\,\frac{m_V^2+m_B^2-m_p^2}{Q^2}\right)^2-\left(\frac{x_B}{1-x_B}\,\frac{2m_Vm_B}{Q^2}\right)^2\right]^{1/2}. \tag{B.3}$$

The energy and momentum E_{P1} and $|\boldsymbol{q}_{P1}|$ of P_1 in the rest frame of V have already been given in (3.30), and Δ_T is the transverse momentum of the scattered baryon with respect to the initial proton in the γ^*p center-of-mass (see Fig. B.1). The approximate expressions in (B.2) are valid up to relative corrections of order $x_B m_p^2/Q^2$ and $x_B\Delta_T^2/Q^2$, and to the same accuracy one has $\Delta_T^2=(1-x_B)(t_0-t)$. Changing variables from θ to z gives for the cross section

$$\frac{d\sigma(ep\to P_1+P_2B)}{dQ^2\,dx_B\,dt\,d\varphi\,dz}=\frac{1}{b-c\cos\theta\cos\varphi}\,\frac{d\sigma(ep\to P_1+P_2B)}{dQ^2\,dx_B\,dt\,d\varphi\,d\cos\theta}. \tag{B.4}$$

In Bjorken kinematics one has $c\ll b$ and can replace the Jacobian in (B.4) by $1/b$ (except in the small region where $\sin\theta\sim c/b$, which is not relevant for our purposes). Neglecting Δ_T we get $z=a+b\cos\theta$ with a and b evaluated at $\Delta_T=0$, and integration over t and φ gives

$$\frac{d\sigma(ep\to P_1+P_2B)}{dQ^2\,dx_B\,dz}=\frac{3}{4b^3}\left[2(z-a)^2\,\frac{d\sigma(ep\to V_LB)}{dQ^2\,dx_B}+(z-a+b)(a+b-z)\frac{d\sigma(ep\to V_TB)}{dQ^2\,dx_B}\right] \tag{B.5}$$

in terms of the cross sections for the production of longitudinally or transversely polarized vector mesons. Using s-channel helicity conservation, which is experimentally seen to hold at the few 10% level in ρ^0 and ϕ production [73–76], these cross sections respectively correspond to the production from longitudinally or transversely polarized virtual photons, and we finally obtain (3.27). In our numerical applications we have used the exact expressions from (B.2)

and (B.3) at $\Delta_T = 0$, and thus in particular neglected c. Since the integrated cross sections are dominated by small Δ_T, this should be a very good approximation for the values of Q^2 and x_B we focus on in the present study. The inclusion of finite Δ_T effects in the kinematics would considerably complicate any analysis.

C

Scattering kernels and properties of the amplitude

In this appendix we want to give the formulas for the hard scattering kernels introduced in (4.1) in Section 4.1 according to [122]. The original scattering kernels are functions of the two momentum fractions x and z and they enter in the amplitude via the convolutions with the meson DA and the GPDs. We further want to present our results for the convolution of scattering kernel and DA, which can be performed analytically. In the second section we briefly demonstrate how one can separate the real and imaginary part of the NLO amplitude and we show our results for the subtraction terms which appear in the numerical treatment of the convolution of the scattering kernels and the GPDs. Finally we present some useful formulas for the expansion of polylogarithmic functions at large arguments which we used in Sec. 4.4 to obtain the high energy limit of the amplitude.

C.1 Hard scattering kernels

We give the original expressions for the hard scattering kernels $T_g(z,x)$, $T_{(+)}(z,x)$ and $T_q(z,x)$ for the amplitude of exclusive meson production (4.1) and the analytical results for the convolution of the meson DA and the scattering kernels. We start with the scattering kernel for the gluon exchange diagrams $T_g(z,x)$, which is given by

$$T_g(z,x) = \frac{\alpha_s(\mu_R^2)\xi}{z\bar{z}(x+\xi-i\epsilon)(x-\xi+i\epsilon)}\left[1+\frac{\alpha_s(\mu_R^2)}{4\pi}\mathcal{I}_g\left(z,\frac{\xi-x}{2\xi}-i\epsilon\right)\right], \tag{C.1}$$

where

$$\begin{aligned}
\mathcal{I}_g(z,y) = &\ln\left(\frac{Q^2}{\mu^2_{F(GPD)}}\right)\left[2(c_1-c_2)\left(\frac{\bar{y}}{y}+\frac{y}{\bar{y}}\right)[y\ln(y)+\bar{y}\ln(\bar{y})]-\frac{c_1}{2}\left(\frac{y}{\bar{y}}\ln(y)+\frac{\bar{y}}{y}\ln(\bar{y})\right)\right]\\
&+\ln\left(\frac{Q^2}{\mu^2_{F(DA)}}\right)c_1\left(\frac{3}{2}+z\ln(z)+\bar{z}\ln(\bar{z})\right)+\frac{\beta_0}{2}\ln\left(\frac{\mu^2_{F(GPD)}}{\mu^2_R}\right)\\
&-c_1\left[\frac{z\bar{z}}{(z-y)^3}\left\{\left[(-y\bar{y}+(z-y)^2\right]H(z,y)-(z-y)R(z,y)\right\}\right.\\
&\left.-\frac{1}{2}\frac{1}{z-y}\left[y(1-3\bar{y})\ln(yz)-\bar{y}(1-3y)\ln(\bar{y}\bar{z})\right]\right]\\
&-(c_1-c_2)\frac{y-\bar{y}}{(z-y)^2}\left\{\left[(-y\bar{y}+(z-y)^2\right]H(z,y)-(z-y)R(z,y)\right\}\\
&+\frac{c_1}{2}\left[-7+\bar{z}\ln^2(z)+z\ln^2(\bar{z})-\frac{1}{2}\left(\frac{y}{\bar{y}}\ln^2(y)+\frac{\bar{y}}{y}\ln^2(\bar{y})\right)+\frac{3}{2}\ln(z\bar{z})\right.\\
&\left.+\ln(y\bar{y})[\bar{z}\ln(z)+z\ln(\bar{z})]+\left(\frac{1}{\bar{y}}+1+3y\right)\ln(y)+\left(\frac{1}{y}+1+3\bar{y}\right)\ln(\bar{y})\right]\\
&+(c_1-c_2)\left[\left(\frac{1}{\bar{y}}-2y\right)(\ln(y)+\ln(z\bar{z}))\ln(y)\right.\\
&\left.+\left(\frac{1}{y}-2\bar{y}\right)(\ln(\bar{y})+\ln(z\bar{z}))\ln(\bar{y})-2\left(\frac{2}{\bar{y}}-1\right)\ln(y)-2\left(\frac{2}{y}-1\right)\ln(\bar{y})\right]\\
&+\{z\to\bar{z}\}\,, \qquad \text{(C.2)}
\end{aligned}$$

where we introduced the two functions

$$R(z,y) = z\ln(y)+\bar{z}\ln(\bar{y})+z\ln(z)+\bar{z}\ln(\bar{z})\,, \qquad \text{(C.3)}$$

$$H(z,y) = Li_2(\bar{y})-Li_2(y)+Li_2(z)-Li_2(\bar{z})+\ln(y)\ln(\bar{z})-\ln(\bar{y})\ln(z)\,. \qquad \text{(C.4)}$$

The color factors c_1 and c_2 are given by

$$c_1 = C_F = \frac{N_c^2-1}{2N_c}\,, \quad c_2 = C_f - \frac{C_A}{2} = -\frac{1}{2N_c}\,, \qquad \text{(C.5)}$$

and the β-function is defined as

$$\beta_0 = \frac{11}{3}N_c - \frac{2}{3N_f}\,, \qquad \text{(C.6)}$$

where N_f is the effective number of quark flavors.
The plylogarithmic function $Li_2(z)$ appearing in (C.3) and (C.3) is defined through

$$Li_2(z) = -\int_0^z \frac{dt}{t}\ln(1-t)\,, \qquad \text{(C.7)}$$

Above and in the following we also use the shorthand notation

$$\bar{y} = 1 - y\,. \tag{C.8}$$

The scattering kernel $T_{(+)}(z,x)$ for the pure singlet contribution of the amplitude is given by

$$T_{(+)}(z,x) = \frac{\alpha_s^2(\mu_R^2)C_F}{8\pi\, z\bar{z}}\mathcal{I}_q\left(z, \frac{\xi - x}{2\xi} - i\epsilon\right)\,, \tag{C.9}$$

with

$$\begin{aligned}\mathcal{I}_q(z,y) =& \frac{1}{(z-y)^2}\left[\left(-y\bar{y} + (z-y)^2\right)H(z,y) - (z-y)R(z,y)\right] \\ &- \ln\left(\frac{Q^2}{\mu^2_{F(GPD)}}\right)(y-\bar{y})\left(\frac{\ln(y)}{\bar{y}} + \frac{\ln(\bar{y})}{y}\right) + 2\left(\frac{y\ln(y)}{\bar{y}} - \frac{\bar{y}\ln(\bar{y})}{y}\right) \\ &- \ln(z\bar{z})\frac{y-\bar{y}}{2}\left(\frac{\ln(y)}{\bar{y}} + \frac{\ln(\bar{y})}{y}\right) - \frac{y-\bar{y}}{2}\left(\frac{\ln^2(y)}{\bar{y}} + \frac{\ln^2(\bar{y})}{y}\right) + \{z \to \bar{z}\}\,.\end{aligned} \tag{C.10}$$

For the quark scattering kernel $T_q(z,x)$ the situation is different to the previous two kernels because it is process dependent. We give the original definition of $T_q(z,x)$ for the process of a neutral vector meson. In that case $T_q(z,x)$ is defined by

$$T_q(z,x) = \left\{T\left(z, \frac{x+\xi}{2\xi} - i\epsilon\right) - T\left(\bar{z}, \frac{\xi - x}{2\xi} - i\epsilon\right)\right\} + \{z \to \bar{z}\}\,, \tag{C.11}$$

where

$$\begin{aligned}T(v,u) =& \frac{\alpha_S(\mu_R^2)C_F}{4vu}\left(1 + \frac{\alpha_S(\mu_R^2)}{4\pi}\left[\, c_1\left(2\left[\frac{3}{2} + \ln(v)\right]\ln\left(\frac{Q^2}{\mu^2_{F(DA)}}\right)\right.\right.\right. \\ &+2\left[\frac{3}{2} + \ln(u)\right]\ln\left(\frac{Q^2}{\mu^2_{F(GPD)}}\right) + \ln^2(vu) + 6\ln(vu) - \frac{\ln(v)}{\bar{v}} - \frac{\ln(u)}{\bar{u}} - \frac{28}{3}\Bigg) \\ &+ \beta_0\left(\frac{5}{3} - \ln(vu) - \ln\left(\frac{Q^2}{\mu_R^2}\right)\right) + c_2\left(2\frac{(\bar{v}v^2 + \bar{u}u^2)}{(v-u)^3}\left[Li_2(\bar{u}) - Li_2(\bar{v})\right.\right. \\ &+Li_2(v) - Li_2(u) + \ln(\bar{v})\ln(u) - \ln(\bar{u})\ln(v)] + 2\frac{(v+u-2vu)\ln\bar{v}\bar{u}}{(v-u)^2} \\ &+ 2\left[Li_2(\bar{u}) + Li_2(\bar{v}) - Li_2(u) - Li_2(v) + \ln(\bar{v})\ln(u) + \ln(\bar{u})\ln(v)\right] \\ &\left.\left.\left.+4\frac{vu\ln(vu)}{(v-u)^2} - 4\ln(\bar{v})\ln(\bar{u}) - \frac{20}{3}\right)\right]\right)\,.\end{aligned} \tag{C.12}$$

In contrast to the original definition of the scattering kernels in [122] we have split the factorization scale dependence into one which belongs to the scale appearing in the GPD, $\mu_{F(GPD)}$ and one which corresponds to the meson DA, $\mu_{F(DA)}$. This is due to the fact that

the GPDs and the meson DA obey different kind of evolution equations. The calculation which leads to this differentiation is shown in Appendix D. We also want to mention that we changed the definition of y in comparison to the original work [99] in the way

$$y = -y_{\,[99]}\,. \tag{C.13}$$

We now want to present our analytical results for the convolution of the scattering kernels with the meson distribution amplitude. For this calculation one needs to specify a model for the meson distribution amplitude. Throughout this work we use the decomposition of the DA into Gegenbauer polynomials. This kind of choice is based on the fact that the evolution of the DA obeys the ERBL evolution equation. The solution of that equation can be represented within the basis of orthonormal Gegenbauer polynomials. As mentioned in Chapter 3 and Chapter 4 the model for the meson DA reads

$$\phi(z,\mu_{F(DA)}) = 6z(1-z)\Big[1+\sum_{n=1}^{\infty} a_n(\mu_{F(DA)})\, C_n^{3/2}(2z-1)\Big]\,. \tag{C.14}$$

As described before we truncate the series in $C.14$ at $n=4$ because there exist no theoretical estimates for the Gegenbauer coefficients with $n>4$.
After the convolution

$$\int_0^1 dz\,\phi(z,\mu_{F(DA)}) \left\{ \begin{array}{c} T_g(z,x) \\ T_{(+)}(z,x) \\ T_q(z,x) \end{array} \right\} \tag{C.15}$$

the gluon scattering kernel is given by

$$\begin{aligned} T_g(x) =& \frac{6\alpha_s(\mu_R^2)\,\xi}{(x+\xi-i\epsilon)(x-\xi+i\epsilon)}\left[(1+a_2+a_4)+\frac{\alpha_s(\mu_R^2)}{2\pi}\left(\mathcal{I}_{g,0}\left(\frac{\xi-x}{2\xi}-i\epsilon\right)\right.\right. \\ &\left.\left. +a_2\,\mathcal{I}_{g,2}\left(\frac{\xi-x}{2\xi}-i\epsilon\right)+a_4\,\mathcal{I}_{g,4}\left(\frac{\xi-x}{2\xi}-i\epsilon\right)\right)\right]\,, \end{aligned} \tag{C.16}$$

with

$$\begin{aligned} \mathcal{I}_{g,0}(y) =& \ln\left(\frac{Q^2}{\mu_{F(GPD)}^2}\right)\left[2(c_1-c_2)\frac{y^2+\bar{y}^2}{\bar{y}}\ln(y)-\frac{c_1}{2}\frac{y}{\bar{y}}\ln(y)\right]+\frac{\beta_0}{4}\ln\left(\frac{\mu_R^2}{\mu_{F(GPD)}^2}\right) \\ &+\frac{c_1}{2}\left[-\frac{5}{2}+\left(\frac{1}{\bar{y}}+1-4y\right)\ln(y)-\frac{1}{2}\frac{y}{\bar{y}}\ln^2(y)\right] \\ &+(c_1-c_2)\left[\left(8y-\frac{6}{\bar{y}}\right)\ln(y)+\left(\frac{1}{\bar{y}}-2y\right)\ln^2(y)+2(\bar{y}-y)Li_2(\bar{y})\right] \\ &-c_1\left[(\bar{y}-y)Li_2(\bar{y})+2y\bar{y}\left(3Li_3(\bar{y})-\ln(y)Li_2(y)-\frac{\pi^2}{6}\ln(\bar{y})\right)\right] \\ &+\{y\to\bar{y}\}\,, \end{aligned} \tag{C.17}$$

$$\begin{aligned}\mathcal{I}_{g,2}(y) =& \ln\left(\frac{Q^2}{\mu^2_{F(GPD)}}\right)\left[2(c_1-c_2)\frac{y^2+\bar{y}^2}{\bar{y}}\ln(y)\right] - \frac{c_1}{2}\frac{y}{\bar{y}}\ln(y) + \frac{\beta_0}{4}\ln\left(\frac{\mu_R^2}{\mu^2_{F(GPD)}}\right)\\ &- \frac{25}{24}c_1\ln\left(\frac{Q^2}{\mu^2_{F(DA)}}\right) + \frac{c_1}{2}\left[\frac{35}{36}(5-54y\bar{y}) - \frac{y}{2\bar{y}}\ln^2(y)\right.\\ &\left.-7(\bar{y}-y)(1-30y\bar{y})Li_2(\bar{y}) - (3+y(775-14y(281-45y(9-4y))))\frac{\ln(y)}{6\bar{y}}\right]\\ &+ (c_1-c_2)\left[-15\left(\frac{1}{4}-y\bar{y}\right) + \left(-\frac{5}{6}-\frac{23}{3\bar{y}}+2y(29-15y(5-4y))\right)\ln(y)\right.\\ &\left.+\left(\frac{1}{\bar{y}}-2y\right)\ln^2(y) + (\bar{y}-y)(7-60y\bar{y})Li_2(\bar{y})\right]\\ &- 6y\bar{y}\left(5(\bar{y}-y)^2c_2 + (2-15y\bar{y})c_1\right)\left(3Li_3(\bar{y}) - \ln(y)Li_2(y) - \frac{\pi^2}{6}\ln(y)\right)\\ &+ \{y\to\bar{y}\}\,, \end{aligned} \tag{C.18}$$

$$\begin{aligned}\mathcal{I}_{g,4}(y) =& \ln\left(\frac{Q^2}{\mu^2_{F(GPD)}}\right)\left[2(c_1-c_2)\frac{y^2+\bar{y}^2}{\bar{y}}\ln(y)\right] - \frac{c_1}{2}\frac{y}{\bar{y}}\ln(y) + \frac{\beta_0}{4}\ln\left(\frac{\mu_R^2}{\mu^2_{F(GPD)}}\right)\\ &- \frac{91}{60}c_1\ln\left(\frac{Q^2}{\mu^2_{F(DA)}}\right) + \frac{c_1}{2}\left[\frac{27287}{1800} - 35y\bar{y}(17-72y\bar{y}) - \frac{y}{2\bar{y}}\ln^2(y)\right.\\ &\left.+\left(-\frac{5}{2}+\frac{1}{\bar{y}}-\frac{11596}{15}y+9660y^2-24160y^3+45360y^4-20160y^5\right)\ln(y)\right.\\ &\left.+16(\bar{y}-y)(1-105y\bar{y}(1-6y\bar{y}))Li_2(\bar{y})\right] + (c_1-c_2)\left[-\frac{35}{16}(\bar{y}-y)^2(5-72y\bar{y})\right.\\ &\left.+\left(-\frac{77}{60}-\frac{257}{30\bar{y}}+\frac{1741}{5}y-2940y^2+8960y^3-11340y^4+5040y^2\right)\ln(y)\right.\\ &\left.+2(\bar{y}-y)(8-315y\bar{y}(\bar{y}-y)^2)Li_2(\bar{y})\right] - 30y\bar{y}\left[c_1(1+42y\bar{y}(\bar{y}-y)^2)\right.\\ &\left.+7c_2(\bar{y}-y)^2(1-6y\bar{y})\right]\left(3Li_3(\bar{y}) - \ln(y)Li_2(y) - \frac{\pi^2}{6}\ln(y)\right)\\ &+ \{y\to\bar{y}\}\,. \end{aligned} \tag{C.19}$$

For the singlet scattering kernel $T_{(+)}(z,x)$ we obtain

$$\begin{aligned}T_{(+)}(x) = \frac{3\alpha_s^2(\mu_R^2)\,C_F}{2\pi}&\left[\mathcal{I}_{q,0}\left(\frac{\xi-x}{2\xi}-i\epsilon\right) + a_2\,\mathcal{I}_{q,2}\left(\frac{\xi-x}{2\xi}-i\epsilon\right)\right.\\ &\left.+a_4\,\mathcal{I}_{q,4}\left(\frac{\xi-x}{2\xi}-i\epsilon\right)\right]\end{aligned} \tag{C.20}$$

where

$$\begin{aligned}\mathcal{I}_{q,0}(y) =& \ln\left(\frac{Q^2}{\mu^2_{F,(GPD)}}\right)(\bar{y}-y)\left(\frac{\ln(y)}{\bar{y}}+\frac{\ln(\bar{y})}{y}\right)+(y-\bar{y})\left(\frac{\ln(y)}{\bar{y}}+\frac{\ln(\bar{y})}{y}\right)\\ &-\frac{y-\bar{y}}{2}\left(\frac{\ln^2(y)}{\bar{y}}+\frac{\ln^2(\bar{y})}{y}\right)+2\left(\frac{y\ln(y)}{\bar{y}}-\frac{\bar{y}\ln(\bar{y})}{y}\right)\\ &+2\left[Li_2(\bar{y})-Li_2(y)+\ln(\bar{y})-\ln(y)\right], \end{aligned} \tag{C.21}$$

$$\begin{aligned}\mathcal{I}_{q,2}(y) =& \ln\left(\frac{Q^2}{\mu^2_{F,(GPD)}}\right)(\bar{y}-y)\left(\frac{\ln(y)}{\bar{y}}+\frac{\ln(\bar{y})}{y}\right)+\frac{11}{6}(y-\bar{y})\left(\frac{\ln(y)}{\bar{y}}+\frac{\ln(\bar{y})}{y}\right)\\ &-\frac{y-\bar{y}}{2}\left(\frac{\ln^2(y)}{\bar{y}}+\frac{\ln^2(\bar{y})}{y}\right)+2\left(\frac{y\ln(y)}{\bar{y}}-\frac{\bar{y}\ln(\bar{y})}{y}\right)-\frac{15}{2}+15y\\ &+(7-60y\bar{y})(Li_2(\bar{y})-Li_2(y))+\ln(\bar{y})\left(\frac{107}{6}-15y(5-4y)\right)\\ &+\ln(y)\left(-\frac{17}{6}+15y(3-4y)\right)+30y\bar{y}(\bar{y}-y)\left[\ln^2(\bar{y})\ln(y)+3Li_3(\bar{y})\right.\\ &\left.+3Li_3(y)+(\ln(\bar{y})-\ln(y))Li_2(y)-\frac{\pi^2}{6}(2\ln(\bar{y})+\ln(y))\right], \end{aligned} \tag{C.22}$$

$$\begin{aligned}\mathcal{I}_{q,4}(y) =& \ln\left(\frac{Q^2}{\mu^2_{F,(GPD)}}\right)(\bar{y}-y)\left(\frac{\ln(y)}{\bar{y}}+\frac{\ln(\bar{y})}{y}\right)+\frac{137}{60}(y-\bar{y})\left(\frac{\ln(y)}{\bar{y}}+\frac{\ln(\bar{y})}{y}\right)\\ &-\frac{y-\bar{y}}{2}\left(\frac{\ln^2(y)}{\bar{y}}+\frac{\ln^2(\bar{y})}{y}\right)+2\left(\frac{y\ln(y)}{\bar{y}}-\frac{\bar{y}\ln(\bar{y})}{y}\right)\\ &-\frac{35}{8}(\bar{y}-y)(5-72y\bar{y})+(16-630y\bar{y}(\bar{y}-y)^2)(Li_2(\bar{y})-Li2(y))\\ &+\ln(\bar{y})\left(\frac{3347}{60}-\frac{2135}{2}y+4165y^2-5670y^3+2520y^4\right)\\ &+\ln(y)\left(-\frac{197}{60}+\frac{665}{2}y-2275y^2+4410y^3-2520y^4\right)\\ &+210y\bar{y}(\bar{y}-y)(1-6y\bar{y})\left[\ln^2(\bar{y})\ln(y)+3Li_3(\bar{y})+3Li_3(y)\right.\\ &\left.+(\ln(\bar{y})-\ln(y))Li_2(y)-\frac{\pi^2}{6}(2\ln(\bar{y})+\ln(y))\right]. \end{aligned} \tag{C.23}$$

For the analytical integration of polylogarithmic functions very useful formulas can be found in [134].

As it can be seen from the formulas (C.16) and (C.20) the integrated gluon and singlet scattering kernel contain only contributions from the even Gegenbauer coefficients a_2 and a_4. This is caused by the fact that the original kernels are symmetric under the transformation $z \to \bar{z}$. The integrated gluon and singlet kernel also show a special symmetry under the

exchange $y \to \bar{y}$, which corresponds to the transformation $x \to -x$. The gluon scattering kernel is symmetric under this transformation and the singlet kernel antisymmetric. This behavior reflects the symmetry of the corresponding GPDs.
For the quark scattering kernel the situation is somewhat different because the symmetry properties and also the contribution from the higher Gegenbauer coefficients are process dependent. For the most common mesons like the neutral or charged vector mesons or pions the contribution from the odd Gegenbauer coefficient also vanishes. But in case of pseudoscalar production of kaons one obtains terms proportional to a_1 and a_3 due to SU(3) symmetry breaking effects. The symmetry property with respect to the replacement $y \to \bar{y}$ is also process dependent. Because we are mainly interested in the production of neutral vector mesons the quark scattering kernel has to reflect the symmetry of the corresponding quark GPD which is in our case an odd function of x. But because of completeness we give our results only for the convolution

$$\int_0^1 dz\, \phi(z) T(z,x) \tag{C.24}$$

where $T(z,x)$ is given in (C.12). From that result one can easily obtain the expressions for the quark kernel which is symmetric or antisymmetric in $y \to \bar{y}$. As result of the convolution in (C.24) we obtain

$$\begin{aligned} T_q(x) = \frac{3\alpha_s(\mu_R^2) C_F}{4\left(\frac{\xi - x}{2\xi} - i\epsilon\right)} \Bigg[1 - a_1 + a_2 - a_3 + a_4 + \frac{\alpha_s(\mu_R^2)}{4\pi} \Bigg(\mathcal{T}_{(0)}\left(\frac{\xi - x}{2\xi} - i\epsilon\right) \\ + a_1 \mathcal{T}_{(1)}\left(\frac{\xi - x}{2\xi} - i\epsilon\right) + a_2 \mathcal{T}_{(2)}\left(\frac{\xi - x}{2\xi} - i\epsilon\right) \\ + a_3 \mathcal{T}_{(3)}\left(\frac{\xi - x}{2\xi} - i\epsilon\right) + a_4 \mathcal{T}_{(4)}\left(\frac{\xi - x}{2\xi} - i\epsilon\right) \Bigg) \Bigg] \end{aligned} \tag{C.25}$$

with

$$\begin{aligned} \mathcal{T}_{(0)}(y) =& c_1 \left[\ln\left(\frac{Q^2}{\mu_{F,(GPD)}^2}\right) \left(\frac{3}{2} + \ln(y)\right) - \frac{17}{12} + \frac{1}{2}\ln^2(y) - \frac{1}{2}\frac{\ln(y)}{\bar{y}} + \frac{3}{2}\ln(y) \right] \\ &+ \beta_0 \left[\frac{19}{12} - \frac{1}{2}\ln(y) - \frac{1}{2}\ln\left(\frac{Q^2}{\mu_R^2}\right) \right] + c_2 \Bigg\{ -\frac{1}{3} + 4(3y-2)\ln(\bar{y}) \\ &+ 2(1-6y)\ln(y) + 4(1-3y)(Li_2(y) - Li_2(\bar{y})) + 2(1-6y\bar{y}) \Bigg[Li_3(\bar{y}) \\ &+ 3Li_3(y) - \ln(y) Li_2(y) - \ln(\bar{y}) Li_2(\bar{y}) - \frac{\pi^2}{6}(\ln(y) + \ln(\bar{y})) \Bigg] \Bigg\}, \end{aligned} \tag{C.26}$$

$$\begin{aligned}\mathcal{T}_{(1)}(y) =& c_1 \left[\frac{4}{3}\ln\left(\frac{Q^2}{\mu^2_{F,(DA)}}\right) - \ln\left(\frac{Q^2}{\mu^2_{F,(GPD)}}\right)\left(\frac{3}{2}+\ln(y)\right) + \frac{269}{36}\right.\\ &\left. -\frac{1}{2}\ln^2(y) + \frac{1}{2}\frac{\ln(y)}{\bar{y}} - \frac{1}{6}\ln(y)\right] + \beta_0\left[-\frac{9}{4} + \frac{1}{2}\ln(y) + \frac{1}{2}\ln\left(\frac{Q^2}{\mu_R^2}\right)\right]\\ &+ c_2\left\{-\frac{35}{3} + 33y + (39 - 3y(53-44y)))\ln(\bar{y})\right.\\ &+ (-9+3y(31-44y))\ln(y) + 6\,(3-y(21-22y))\,(Li_2(\bar{y}) - Li_2(y))\\ &- 6\,[1-2y(6-y(16-11y))]\left[3(Li_3(\bar{y}) + Li_3(y)) - \ln(y)Li_2(y)\right.\\ &\left.\left. - \ln(\bar{y})Li_2(\bar{y}) - \frac{\pi^2}{6}(\ln(y)+\ln(\bar{y}))\right]\right\}, \end{aligned} \tag{C.27}$$

$$\begin{aligned}\mathcal{T}_{(2)}(y) =& c_1 \left[-\frac{25}{12}\ln\left(\frac{Q^2}{\mu^2_{F,(DA)}}\right) + \ln\left(\frac{Q^2}{\mu^2_{F,(GPD)}}\right)\left(\frac{3}{2}+\ln(y)\right) - \frac{1019}{144} + \frac{1}{2}\ln^2(y)\right.\\ &\left. -\frac{1}{2}\frac{\ln(y)}{\bar{y}} - \frac{7}{12}\ln(y)\right] + \beta_0\left[\frac{21}{8} - \frac{1}{2}\ln(y) - \frac{1}{2}\ln\left(\frac{Q^2}{\mu_R^2}\right)\right]\\ &+ c_2\left\{\frac{401}{12} - 255y + 270y^2 + \ln(\bar{y})\left(-\frac{299}{3} + 867y - 1830y^2 + 1080y^3\right)\right.\\ &+ \ln(y)\left(\frac{56}{3} - 357y + 1290y^2 - 1080y^3\right)\\ &+ (Li_2(\bar{y}) - Li_2(y))\left(-44 + 582y - 1560y^2 + 1080y^3\right)\\ &+ \left[12 - 252y + 1272y^2 - 2100y^3 + 1080y^4\right]\left[3(Li_3(\bar{y}) + Li_3(y))\right.\\ &\left.\left. - \ln(y)Li_2(y) - \ln(\bar{y})Li_2(\bar{y}) - \frac{\pi^2}{6}(\ln(y)+\ln(\bar{y}))\right]\right\}, \end{aligned} \tag{C.28}$$

$$\begin{aligned}\mathcal{T}_{(3)}(y) =& c_1 \left[\frac{157}{60}\ln\left(\frac{Q^2}{\mu^2_{F,(DA)}}\right) - \ln\left(\frac{Q^2}{\mu^2_{F,(GPD)}}\right)\left(\frac{3}{2}+\ln(y)\right) + \frac{23071}{3600} - \frac{1}{2}\ln^2(y)\right.\\ &\left. +\frac{1}{2}\frac{\ln(y)}{\bar{y}} + \frac{67}{60}\ln(y)\right] + \beta_0\left[-\frac{347}{120} + \frac{1}{2}\ln(\bar{y}) + \frac{1}{2}\ln\left(\frac{Q^2}{\mu_R^2}\right)\right]\\ &+ c_2\left\{-70 + \frac{4045}{4}y - 2730y^2 + 1890y^3\right.\\ &+ \ln(\bar{y})\left(\frac{3635}{18} - \frac{18335}{6}y + 11920y^2 - 16590y^3 + 7560y^4\right)\\ &+ \ln(y)\left(-\frac{575}{18} + \frac{5885}{6}y - 6460y^2 + 12810y^3 - 7560y^4\right)\\ &\left.+ (Li_2(\bar{y}) - Li_2(y))\left[\frac{250}{3} - 1820y + 8980y^2 - 14700y^3 + 7560y^4\right]\right. \end{aligned}$$

$$+ 10\left[-2 + 66y - 540y^2 + 1570y^3 - 1848y^4 + 756y^5\right]\Bigg[3(Li_3(\bar{y}) + Li_3(y)) - \ln(y)Li_2(y) - \ln(\bar{y})Li_2(\bar{y}) - \frac{\pi^2}{6}(\ln(y) + \ln(\bar{y}))\Bigg]\Bigg\}\,, \tag{C.29}$$

$$\begin{aligned}\mathcal{T}_{(4)}(y) =& c_1\left[-\frac{91}{30}\ln\left(\frac{Q^2}{\mu^2_{F,(DA)}}\right) + \ln\left(\frac{Q^2}{\mu^2_{F,(GPD)}}\right)\left(\frac{3}{2} + \ln(y)\right) - \frac{10213}{1800} + \frac{1}{2}\ln^2(y)\right.\\ &\left. - \frac{1}{2}\frac{\ln(y)}{\bar{y}} - \frac{23}{15}\ln(y)\right] + \beta_0\left[\frac{31}{10} - \frac{1}{2}\ln(\bar{y}) - \frac{1}{2}\ln\left(\frac{Q^2}{\mu_R^2}\right)\right]\\ &+ c_2\left\{\frac{4903}{40} - \frac{5775}{2}y + \frac{57085}{4}y^2 - 23310y^3 + 11970y^4\right.\\ &+ \ln(\bar{y})\left(-\frac{21109}{60} + \frac{41451}{5}y - \frac{103285}{2}y^2 + 125020y^3 - 129150y^4 + 47880y^5\right)\\ &+ \ln(y)\left(\frac{2899}{60} - \frac{11001}{5}y + \frac{45535}{2}y^2 - 78400y^3 + 105210y^4 - 47880y^5\right)\\ &+ (Li_2(y) - Li_2(\bar{y}))\left[137 - 4506y + 35280y^2 - 100380y^3 + 117180y^4 - 47880y^5\right]\\ &+ 10\left[3 - 144y + 1740y^2 - 7770y^3 + 15498y^4 - 14112y^5 + 4788y^6\right]\\ &\left.\times\left[3(Li_3(\bar{y}) + Li_3(y)) - \ln(y)Li_2(y) - \ln(\bar{y})Li_2(\bar{y}) - \frac{\pi^2}{6}(\ln(y) + \ln(\bar{y}))\right]\right\}\,.\end{aligned} \tag{C.30}$$

Let us mention that for the convolution $\int_0^1 dz\,\phi(z)T(\bar{z},x)$ one obtains the same results as in (C.25) but the overall sign of the odd Gegenbauer coefficients changes. In the case of neutral vector meson production, which picks up the C-even part of the scattering kernels, one obtains the correct quark scattering kernel by the following rule

$$T_{q,V} = 2\left(T_q(x) - T_q(-x)\right)\,. \tag{C.31}$$

The factor two in front of the above equation appears due to the symmetry of the original scattering kernel (C.11) in z.

C.2 Real and imaginary part of the amplitude

For the amplitude of exclusive meson production at NLO it is not as easy to determine the real and imaginary part as in leading order where we have

$$\int\limits_{-1}^{1} dx \frac{F(x,\xi,t)}{\xi - x - i\epsilon} = \fint\limits_{-1}^{1} dx \frac{F(x,\xi,t)}{\xi - x} + i\pi F(\xi,\xi,t)\,. \tag{C.32}$$

Within the factorized ansatz for the GPDs (2.46) and (3.14) which we used to model the GPDs, we have developed a semi-analytical method (App. A) to calculate the real and

imaginary part of the amplitude. The method based on the simplicity of the scattering kernels at LO in α_s. As explained in Sect. 4.3 it is not possible to develop such a method for the NLO scattering kernels. Instead we will use the method of subtraction as explained in Sect. 4.3 to remove the poles from the scattering kernels which make a numerical treatment much more complicated.
In the following we want to show how we split the remaining convolution of scattering kernel and the GPDs into its real and imaginary part using the gluon contribution of the amplitude as an example. With our choice of y and using the symmetry properties of the gluon GPD and the gluon scattering kernel the original integral transforms to

$$\int\limits_{-1}^{1} dx\, T_g(x) F^g(x,\xi,t) \to 4\xi \int\limits_{-\frac{1-\xi}{2\xi}}^{\frac{1}{2}} dy\, T_g\left(y - i\epsilon\right) F^g(\xi(1-2y),\xi,t)\,, \tag{C.33}$$

where $T_g(x)$ is given by (C.16). For the LO term of the scattering kernel it is easy to apply the subtraction procedure of Sect. 4.3 and we obtain

$$\begin{aligned}
&4\xi \int\limits_{-\frac{1-\xi}{2\xi}}^{\frac{1}{2}} dy\, T_{g,LO}(y - i\epsilon) F^g(\xi(1-2y),\xi,t) = \\
&= -\alpha_s 6\left(1 + a_2 + a_4\right) \left[\int\limits_{-\frac{1-\xi}{2\xi}}^{-1/2} dy\, \frac{F^g(\xi(1-2y),\xi,t)}{\bar{y}y} \right. \\
&\qquad \left. + \int\limits_{-1/2}^{1/2} dy\, \frac{F^g(\xi(1-2y),\xi,t) - F^g(\xi,\xi,t)}{\bar{y}y} + F^g(\xi,\xi,t)\left(\ln\left(3\right) + i\pi\right) \right] .
\end{aligned} \tag{C.34}$$

For the pure NLO term of the scattering kernel we use the same method but now the structure of the integrals is more complicated. To obtain separate results for the real and imaginary part we use the following relations for the imaginary part of logarithmic and polylogarithmic functions. For the single logarithm the imaginary part is just given by

$$\mathrm{Im}\left\{\ln(y - i\epsilon)\right\} = -i\pi T(-y)\,, \tag{C.35}$$

where $T(y) = 0$ if $y < 0$ and $T(y) = 1$ if $y > 0$. For the polylogarithmic functions appearing in the scattering kernel we have

$$\begin{aligned}
\mathrm{Im}\left\{Li_2(y - i\epsilon)\right\} &= -i\pi T(y-1)\ln(-y)\,, \\
\mathrm{Im}\left\{Li_3(y - i\epsilon)\right\} &= -i\pi T(y-1)\frac{\ln^2(-y)}{2}\,.
\end{aligned} \tag{C.36}$$

Using this relations we obtain for the real part of the pure NLO gluon contribution

$$
\begin{aligned}
&\mathrm{Re}\left(4\xi \int\limits_{-\frac{1-\xi}{2\xi}}^{\frac{1}{2}} dy\, T_{g,NLO}(y-i\epsilon)F^g(\xi(1-2y),\xi,t)\right) = \\
&= -\frac{3\alpha_s^2}{\pi}\left\{\int\limits_{-\frac{1-\xi}{2\xi}}^{-1/2} dy \frac{F^g(\xi(1-2y),\xi,t)}{y\bar{y}}\mathcal{F}^g_{Re}(y) + \int\limits_{-1/2}^{1/2} du \frac{F^g(\xi(1-2y),\xi,t)-F^g(\xi,\xi,t)}{y\bar{y}}\mathcal{F}^g_{Re}(y)\right. \\
&- \pi^2\left(\int\limits_{-\frac{1-\xi}{2\xi}}^{-1/2} dy\, \frac{F^g(\xi(1-2y),\xi,t)}{y\bar{y}}\mathcal{G}^g_{Re}(y) + \int\limits_{-1/2}^{0} dy\, \frac{F^g(\xi(1-2y),\xi,t)-F^g(\xi,\xi,t)}{y\bar{y}}\mathcal{G}^g_{Re}(y)\right) \\
&\left. + F^g(\xi,\xi,t)\,\mathcal{C}^g_{Re}\right\}. \qquad \text{(C.37)}
\end{aligned}
$$

The functions $\mathcal{F}^g_{Re}(y)$ and $\mathcal{G}^g_{Re}(y)$ are given by

$$
\begin{aligned}
\mathcal{F}^g_{Re}(y) =& \ln\left(\frac{Q^2}{\mu^2_{F(GPD)}}\right)\left[-\frac{c_1}{2}\left(\frac{y}{\bar{y}}\ln|y| + \frac{\bar{y}}{y}\ln(\bar{y})\right) + 2(c_1-c_2)(y^2+\bar{y}^2)\left(\frac{\ln|y|}{\bar{y}} + \frac{\ln(\bar{y})}{y}\right)\right] \\
&+ \frac{\beta_0}{2}\ln\left(\frac{\mu_R^2}{\mu^2_{F(GPD)}}\right) + \frac{c_1}{2}\left[-5 + \ln|y|\left(1+\frac{1}{\bar{y}}-4y\right) + \ln(\bar{y})\left(1+\frac{1}{y}-4\bar{y}\right)\right. \\
&\left. -\frac{1}{2}\left(\frac{y\ln^2|y|}{\bar{y}} + \frac{\bar{y}\ln^2(\bar{y})}{y}\right)\right] + (c_1-c_2)\left[\ln|y|\left(8y-\frac{6}{\bar{y}}\right) + \ln(\bar{y})\left(8\bar{y}-\frac{6}{y}\right)\right. \\
&\left. + \ln^2|y|\left(\frac{1}{\bar{y}}-2y\right) + \ln^2(\bar{y})\left(\frac{1}{y}-2\bar{y}\right) + 2(\bar{y}-y)\left[Re(Li_2(\bar{y})) - Li_2(y)\right]\right] \\
&- c_1\left[(\bar{y}-y)\left(Re(Li_2(\bar{y})) - Li_2(y)\right) + 2y\bar{y}\left(3(Re(Li_3(\bar{y})) + Li_3(y))\right.\right. \\
&\left.\left. - \ln|y|Li_2(y) - \ln(\bar{y})Re(Li_2(\bar{y}))\right) - \frac{\pi^2}{6}\left(\ln|y| + \ln(\bar{y})\right)\right], \qquad \text{(C.38)}
\end{aligned}
$$

and

$$
\mathcal{G}^g_{Re}(y) = -\frac{c_1}{4}\frac{y}{\bar{y}} + (c_1-c_2)\left(\frac{1}{\bar{y}}-2y\right). \qquad \text{(C.39)}
$$

We showed only the result for the asymptotic form of the scattering kernel. For the scattering kernels containing the the higher Gegenbauer coefficients a_2 and a_4 which are given in (C.18) and (C.19) on finds similar but even longer expressions. The subtraction term $\mathcal{C}^g_{Re}$ of (C.37) is not the same for the asymptotic form of the scattering kernel and the parts with the

Table C.1. Subtraction constants $\mathcal{C}^g_{Re}$ and $\mathcal{C}^g_{Im}$ for real and imaginary part of the gluon convolution.

	$\mathcal{C}^g_{Re}$
LO	1.09861
NLO asy.	$21.8017\ln\left(\frac{Q^2}{\mu^2_{F(GPD)}}\right) - 4.9438\ln\left(\frac{Q^2}{\mu^2_R}\right) - 57.5748$
NLO a_2	$21.8017\ln\left(\frac{Q^2}{\mu^2_{F(GPD)}}\right) - 4.9438\ln\left(\frac{Q^2}{\mu^2_R}\right) - 3.0517\ln\left(\frac{Q^2}{\mu^2_{F(DA)}}\right) - 81.4733$
NLO a_4	$21.8017\ln\left(\frac{Q^2}{\mu^2_{F(GPD)}}\right) - 4.9438\ln\left(\frac{Q^2}{\mu^2_R}\right) - 4.4433\ln\left(\frac{Q^2}{\mu^2_{F(DA)}}\right) - 92.4704$
	$\mathcal{C}^g_{Im}$
LO	1
NLO asy.	$0.5258\ln\left(\frac{Q^2}{\mu^2_{F(GPD)}}\right) - 4.5\ln\left(\frac{Q^2}{\mu^2_R}\right) + 7.4319$
NLO a_2	$0.5258\ln\left(\frac{Q^2}{\mu^2_{F(GPD)}}\right) - 4.5\ln\left(\frac{Q^2}{\mu^2_R}\right) - 2.7777\ln\left(\frac{Q^2}{\mu^2_{F(DA)}}\right) + 18.6315$
NLO a_4	$0.5258\ln\left(\frac{Q^2}{\mu^2_{F(GPD)}}\right) - 4.5\ln\left(\frac{Q^2}{\mu^2_R}\right) - 4.0444\ln\left(\frac{Q^2}{\mu^2_{F(DA)}}\right) + 25.9552$

higher Gegenbauer coefficients. In principle one could find an analytical expression for the subtraction terms but the results are very lengthy and not very intuitive. Therefore we give their numerical values for the asymptotic form and the higher Gegenbauer coefficients in Table C.1. In that table we also listed the subtraction terms for the imaginary part which in the case of the NLO terms are no longer given by such a simple term as in the LO case. For the NLO term of the scattering kernel the imaginary part is given by

$$\begin{aligned}
&\frac{1}{\pi}\mathrm{Im}\left(4\xi\int\limits_{-\frac{1-\xi}{2\xi}}^{\frac{1}{2}} dy\, T_{g,NLO}(y-i\epsilon)F^g(\xi(1-2y),\xi,t)\right) = \\
&= -\frac{3\alpha_s^2}{\pi}\left\{\int\limits_{-\frac{1-\xi}{2\xi}}^{-1/2} dy\frac{F^g(\xi(1-2y),\xi,t)}{y\bar{y}}\mathcal{F}^g_{Im}(y)\right. \\
&\left.+\int\limits_{-1/2}^{0} dy\frac{F^g(\xi(1-2y),\xi,t)-F^g(\xi,\xi,t)}{y\bar{y}}\mathcal{F}^g_{Im}(y)+F^g(\xi,\xi,t)\,\mathcal{C}^g_{Im}\right\}. \qquad \text{(C.40)}
\end{aligned}$$

It is worth to mention that in contrast to the real part the integration interval is now $y \in \left[-\frac{1-\xi}{2\xi}, 0\right]$ which corresponds to the DGLAP region. The function $\mathcal{F}^g_{Im}(y)$ is not as

Table C.2. Subtraction constants $\mathcal{C}_{Re}^{(+)}$ and $\mathcal{C}_{Im}^{(+)}$ for real and imaginary part of the singlet convolution.

	$\mathcal{C}_{Re}^{(+)}$	$\mathcal{C}_{Im}^{(+)}$
NLO asy.	$-2.5343 \ln\left(\frac{Q^2}{\mu^2_{F(GPD)}}\right) + 9.6099$	$-0.5945 \ln\left(\frac{Q^2}{\mu^2_{F(GPD)}}\right) + 2.9636$
NLO a_2	$-2.5343 \ln\left(\frac{Q^2}{\mu^2_{F(GPD)}}\right) + 13.7495$	$-0.5945 \ln\left(\frac{Q^2}{\mu^2_{F(GPD)}}\right) + 3.9400$
NLO a_4	$-2.5343 \ln\left(\frac{Q^2}{\mu^2_{F(GPD)}}\right) + 16.0150$	$-0.5945 \ln\left(\frac{Q^2}{\mu^2_{F(GPD)}}\right) + 5.0977$

complicated as for the real part and is given by

$$\begin{aligned}\mathcal{F}^g_{Im}(y) = &\ln\left(\frac{Q^2}{\mu^2_{F(GPD)}}\right)\left[\frac{c_1}{2}\frac{y}{\bar{y}} - 2(c_1-c_2)\frac{y^2+\bar{y}^2}{\bar{y}}\right] - \frac{c_1}{2}\left[1-4y+\frac{1}{\bar{y}} - \frac{y}{\bar{y}}\ln|y|\right] \\ &- (c_1-c_2)\left[8y - \frac{6}{\bar{y}} - 2(1-2y)\ln(\bar{y}) + 2\ln|y|\left(\frac{1}{\bar{y}} - 2y\right)\right] \\ &- c_1\left[(1-2y)\ln(\bar{y}) + 2y\bar{y}\left(\frac{1}{2}\ln^2(\bar{y}) + Li_2(y) + \frac{\pi^2}{6}\right)\right].\end{aligned} \tag{C.41}$$

As mentioned above we show the numerical values for the subtraction term $\mathcal{C}^g_{Im}$ in Table C.1.

We can apply the above procedure also for the singlet and the quark terms of the amplitude. We do not want repeat the previous steps for this contributions because the expressions look similar and with help of the relations (C.35) and (C.36) for the correct imaginary part of the logarithm and the polylogarithms it is very easy to obtain similar expressions as in (C.37) and (C.40). But we want to give the numerical values of the subtraction terms for the real and imaginary part of the singlet and quark scattering kernels. For the singlet scattering kernel the results are shown in Table C.2. For the quark scattering kernel we have the two possibilities: the first is to antisymmetrize the scattering kernel in the x through

$$T_{q,asymm} = T_q(x) - T_q(-x)\,. \tag{C.42}$$

We need this combination for the exclusive production of neutral vector mesons as explained in Sec. C.1. The subtraction terms for the real and imaginary parts are shown in Table C.3. The second possibility is to symmetrize the quark scattering kernel in x by

$$T_{q,asymm} = T_q(x) + T_q(-x)\,. \tag{C.43}$$

The symmetric version of the scattering kernel is necessary to describe the exclusive production of charged mesons because in that case corresponding quark charges are not the same as it can bee seen for example in Table. 3.1. For the symmetric quark scattering kernel the subtraction terms are different to those of the antisymmetric kernel and we show their

Table C.3. Subtraction constants $\mathcal{C}_{Re}^{q(asym)}$ and $\mathcal{C}_{Im}^{q(asym)}$ for real and imaginary part of the antisymmetric quark convolution.

	$\mathcal{C}_{Re}^{q(asym)}$
LO	-1.09861
NLO asy.	$4.5932 \ln\left(\frac{Q^2}{\mu^2_{F(GPD)}}\right) + 4.9438 \ln\left(\frac{Q^2}{\mu^2_R}\right) - 26.0154$
NLO a_2	$4.5932 \ln\left(\frac{Q^2}{\mu^2_{F(GPD)}}\right) + 4.9438 \ln\left(\frac{Q^2}{\mu^2_R}\right) + 3.0517 \ln\left(\frac{Q^2}{\mu^2_{F(DA)}}\right) - 48.0109$
NLO a_4	$4.5932 \ln\left(\frac{Q^2}{\mu^2_{F(GPD)}}\right) + 4.9438 \ln\left(\frac{Q^2}{\mu^2_R}\right) + 4.4432 \ln\left(\frac{Q^2}{\mu^2_{F(DA)}}\right) - 60.9711$
	$\mathcal{C}_{Im}^{q(asym)}$
LO	1
NLO asy.	$1.0758 \ln\left(\frac{Q^2}{\mu^2_{F(GPD)}}\right) - 4.5 \ln\left(\frac{Q^2}{\mu^2_R}\right) + 6.1408$
NLO a_2	$1.0758 \ln\left(\frac{Q^2}{\mu^2_{F(GPD)}}\right) - 4.5 \ln\left(\frac{Q^2}{\mu^2_R}\right) - 2.7777 \ln\left(\frac{Q^2}{\mu^2_{F(DA)}}\right) + 16.0930$
NLO a_4	$1.0758 \ln\left(\frac{Q^2}{\mu^2_{F(GPD)}}\right) - 4.5 \ln\left(\frac{Q^2}{\mu^2_R}\right) - 4.0444 \ln\left(\frac{Q^2}{\mu^2_{F(DA)}}\right) + 22.9987$

numerical values in Table C.4.
Let us also mention that we presented only the results of the subtraction terms for the asymptotic form and the even Gegenbauer coefficients. This is due to the fact that the odd Gegenbauer coefficients are only important for exclusive kaon production. We have discussed this process at LO in detail in Sect. 3.2 where we also investigated the influence of the odd Gegenbauer coefficient a_1. For our NLO analysis in Chapter 4 we do not need the odd coefficients because we concentrate on the production of neutral vector mesons.

C.3 High energy expansion

For the high energy behavior of the amplitude discussed in Sect. 4.4 it is necessary to know the expansion of real and imaginary parts of the polylogarithmic functions $Li_2(1-y)$ and $Li_3(1-y)$ for large negative arguments in powers of $1/y$. Because we found no proper description of this limites in the literature we did the expansion by our own. In this appendix we give our results for the expansions we used to describe the high energy limit of the amplitude in a simple way.
We want to start with the well known expression of the simple logarithmic function for which

Table C.4. Subtraction constants $\mathcal{C}_{Re}^{q(sym)}$ and $\mathcal{C}_{Im}^{q(sym)}$ for real and imaginary part of the symmetric quark convolution.

	$\mathcal{C}_{Re}^{q,sym}$
LO	1.09861
NLO asy.	$8.5662 \ln\left(\frac{Q^2}{\mu^2_{F(GPD)}}\right) - 4.9438 \ln\left(\frac{Q^2}{\mu_R^2}\right) - 7.9031$
NLO a_2	$8.5662 \ln\left(\frac{Q^2}{\mu^2_{F(GPD)}}\right) - 4.9438 \ln\left(\frac{Q^2}{\mu_R^2}\right) - 3.0517 \ln\left(\frac{Q^2}{\mu^2_{F(DA)}}\right) - 13.9378$
NLO a_4	$8.5662 \ln\left(\frac{Q^2}{\mu^2_{F(GPD)}}\right) - 4.9438 \ln\left(\frac{Q^2}{\mu_R^2}\right) - 4.4432 \ln\left(\frac{Q^2}{\mu^2_{F(DA)}}\right) - 17.7761$
	$\mathcal{C}_{Im}^{q,sym}$
LO	1
NLO asy.	$1.0758 \ln\left(\frac{Q^2}{\mu^2_{F(GPD)}}\right) - 4.5 \ln\left(\frac{Q^2}{\mu_R^2}\right) + 6.2980$
NLO a_2	$1.0758 \ln\left(\frac{Q^2}{\mu^2_{F(GPD)}}\right) - 4.5 \ln\left(\frac{Q^2}{\mu_R^2}\right) - 2.7777 \ln\left(\frac{Q^2}{\mu^2_{F(DA)}}\right) + 15.8676$
NLO a_4	$1.0758 \ln\left(\frac{Q^2}{\mu^2_{F(GPD)}}\right) - 4.5 \ln\left(\frac{Q^2}{\mu_R^2}\right) - 4.0444 \ln\left(\frac{Q^2}{\mu^2_{F(DA)}}\right) + 22.6508$

the expansion is given by

$$\ln(1-y) = \ln(-y) - \sum_{n=1}^{\infty} \frac{1}{n\, y^n}\,, \tag{C.44}$$

for $y \to -\infty$. The situation is a little more difficult for the polylogarithmic functions. We demonstrate how one can obtain the expansion on the example of the function $Li_2(y)$ for $y \to -\infty$. One finds for the expansion

$$\begin{aligned}
Li_2(y) &= -\int_0^y dt\, \frac{\ln(1-t)}{t} = -\int_0^{-y} dt\, \frac{\ln(1+t)}{t} \\
&= -\int_0^1 dt\, \frac{\ln(1+t)}{t} - \int_1^{-y} dt\, \frac{\ln(1+t)}{t} \\
&= -\frac{\pi^2}{12} - \int_1^{-y} dt\, \frac{\ln(t)}{t} - \int_1^{-y} dt\, \frac{1}{t} \ln\left(1+\frac{1}{t}\right) \\
&= -\frac{\pi^2}{6} - \frac{1}{2}\ln^2(-y) + \int_{-y}^{\infty} dt\, \frac{1}{t} \ln\left(1+\frac{1}{t}\right)
\end{aligned}$$

$$= -\frac{\pi^2}{6} - \frac{1}{2}\ln^2(-y) + \int_{-y}^{\infty} dt \sum_{n=1}^{\infty} (-1)^{n+1} \frac{t^{-(n+1)}}{n}$$
$$= -\frac{\pi^2}{6} - \frac{1}{2}\ln^2(-y) - \sum_{n=1}^{\infty} \frac{y^{-n}}{n^2}\,. \tag{C.45}$$

We also need the expansion of $Li_2(y)$ in the limit $y \to \infty$ but in this region we are only interested in the real part of the function, which is then given by

$$\mathrm{Re}(Li_2(y)) = \frac{\pi^2}{3} - \frac{1}{2}\ln^2(y) - \sum_{n=1}^{\infty} \frac{y^{-n}}{n^2}\,.$$

The imaginary part of the function $Li_2(y)$ for large positive arguments is just given by the logarithmic expression (C.36) and has therefore no explicit expansion in powers of $1/y$. For the function $Li_3(y)$ and the same two limits as for $Li_2(y)$ we find the expansion

$$Li_3(y) = -\frac{\pi^2}{6}\ln(-y) - \frac{1}{6}\ln^3(-y) + \sum_{n=1}^{\infty} \frac{1}{n^3\, y^3} \tag{C.46}$$

for $y \to -\infty$ and

$$\mathrm{Re}(Li_3(y)) = \frac{\pi^2}{3}\ln(y) - \frac{1}{6}\ln^3(y) + \sum_{n=1}^{\infty} \frac{1}{n^3\, y^n} \tag{C.47}$$

for $y \to \infty$. The imaginary part is again just given by (C.36) with no explicit expansion.

D

Evolutions kernels for GPDs

As explained in Section 2.3 the GPDs show a different evolution behavior than the ordinary PDFs. In this appendix we want to give the evolution kernels for the GPDs. We also want to demonstrate how the evolution of the amplitude with respect to the factorization scale can help to check the correctness of parts of the hard scattering kernels and how this procedure helps to distinguish between the factorization scales of the GPDs and the meson distribution amplitude.

D.1 Evolution kernels for generalized parton distributions

We give now a set of evolution kernels for the GPDs which fulfills the correct energy momentum relation and reproduce in the limit $\xi \to 0$ the well known DGLAP evolution kernels for the usual PDFs.
We want start with reminding the evolution equation for the unpolarized GPDs explained in some detail in Sect. 2.3. For the non-singlet GPD combination it is given by

$$\mu^2 \frac{d}{d\mu^2} F^{q(-)}(x,\xi,t) = \int_{-1}^{1} dx' \, \frac{1}{|\xi|} V_{NS}\left(\frac{x}{\xi}, \frac{x'}{\xi}\right) F^{q(-)}(x',\xi,t)\,, \tag{D.1}$$

and for the singlet combination it is

$$\mu^2 \frac{d}{d\mu^2} \begin{pmatrix} F^{(+)}(x,\xi,t) \\ F^g(x,\xi,t) \end{pmatrix} = \int_{-1}^{1} \frac{dx'}{|\xi|} \begin{pmatrix} V^{qq}\left(\frac{x}{\xi},\frac{x'}{\xi}\right) & \frac{1}{\xi}V^{qg}\left(\frac{x}{\xi},\frac{x'}{\xi}\right) \\ \xi V^{gq}\left(\frac{x}{\xi},\frac{x'}{\xi}\right) & V^{gg}\left(\frac{x}{\xi},\frac{x'}{\xi}\right) \end{pmatrix} \begin{pmatrix} F^{(+)}(x',\xi,t) \\ F^g(x',\xi,t) \end{pmatrix} . \tag{D.2}$$

The evolution kernels in (D.1) and (D.2) are now given by

$$\begin{aligned} V_{NS}(x,y) &= V^{qq}(x,y) \\ &= \frac{\alpha_s\, C_F}{4\pi} \left[\rho(x,y) \frac{1+x}{1+y} \left(1 + \frac{2}{y-x} \right) + \{x \to -x, y \to -y\} \right]_+ , \end{aligned} \tag{D.3}$$

$$\begin{aligned} V^{qg}(x,y) = -\frac{\alpha_s\, C_F}{4\pi}\, T_f N_f \Big[& \rho(x,y) \frac{2(1+x)}{(1+y)^2} (1 - 2x + y(1-x)) \\ & - \{x \to -x, y \to -y\} \Big] , \end{aligned} \tag{D.4}$$

$$\begin{aligned} V^{gq}(x,y) = \frac{\alpha_s}{4\pi} 2 C_F \Big[& \rho(x,y) \left(\frac{1}{2}(2-x)(1+x)^2 - \frac{(1+x)^2}{2(1+y)} \right) \\ & - \{x \to -x, y \to -y\} \Big] , \end{aligned} \tag{D.5}$$

$$\begin{aligned} V^{gg}(x,y) = \frac{\alpha_s}{4\pi} \Big[& C_A \Big\{ \rho(x,y) \frac{(1+x)^2}{(1+y)^2} (1 + 2(y-x) - xy) + \\ & \left[\rho(x,y) \frac{(1+x)^2}{(1+y)^2} \left(2 + \frac{2}{y-x} \right) \right]_+ + \{x \to -x, y \to -y\} \Big\} \\ & + \delta\left(\frac{x-y}{2} \right) \left(\frac{\beta_0}{2} - \frac{7}{3} C_A \right) \Big] . \end{aligned} \tag{D.6}$$

The "+"- prescription used in (D.3) and (D.6) is defined by

$$[f(x,y)]_+ = f(x,y) - \delta(x-y) \int dz\, f(z,y) . \tag{D.7}$$

The function $\rho(x,y)$ appearing in the evolution kernels (D.3)-(D.6) is responsible for the support region of the evolution kernels in the (x,y)-plane and is given by

$$\rho(x,y) = \theta\left(\frac{1+x}{1+y} \right) \theta\left(1 - \frac{1+x}{1+y} \right) sgn\left(\frac{1+y}{2} \right) , \tag{D.8}$$

with the usual step function $\theta(x)$.
Performing the limit $\xi \to 0$ in the following way

$$\lim_{\xi\to 0} \frac{1}{|\xi|} \begin{pmatrix} V^{qq} & \frac{1}{\xi} V^{qg} \\ \xi V^{gq} & V^{gg} \end{pmatrix} \left(\frac{z}{\xi}, \frac{1}{\xi}\right) , \tag{D.9}$$

one obtains the usual DGLAP evolution kernels.
A second consistency check for the evolution kernels is the energy momentum relation. The kernels have to obey the relation

$$\frac{d}{d\mu^2} \int_{-1}^{1} dx \left[x\, F^{(+)}(x,\xi,t) + F^g(x\xi,t) \right] = 0 , \tag{D.10}$$

which can be easily checked for our set of evolution kernels.

We also want to give the evolution kernels for the polarized GPDs for completeness. The polarized GPDs $\tilde{F}(x,\xi,t)$ have similar evolution equations for their singlet and non-singlet combinations as the unpolarized ones. For completeness we also want to give the evolution equation and kernels for the polarized GPDs. The evolution equation is given for the non-singlet GPD by

$$\mu^2 \frac{d}{d\mu^2} \tilde{F}^{q(-)}(x,\xi,t) = \int_{-1}^{1} dx' \, \frac{1}{|\xi|} \Delta V_{NS} \left(\frac{x}{\xi}, \frac{x'}{\xi}\right) \tilde{F}^{q(-)}(x',\xi,t) , \tag{D.11}$$

where

$$\tilde{F}^{q(-)}(x,\xi,t) = \tilde{F}^q(x,\xi,t) - \tilde{F}^q(-x,\xi,t) . \tag{D.12}$$

For the singlet combination

$$\tilde{F}^{(+)}(x,\xi,t) = \sum_q \left(\tilde{F}^q(x,\xi,t) - \tilde{F}^q(-x,\xi,t) \right) , \tag{D.13}$$

the evolution equation is given by

$$\mu^2 \frac{d}{d\mu^2} \begin{pmatrix} \tilde{F}^{(+)}(x,\xi,t) \\ \tilde{F}^g(x,\xi,t) \end{pmatrix} = \int_{-1}^{1} dx' \, \frac{1}{|\xi|} \begin{pmatrix} \Delta V^{qq}\left(\frac{x}{\xi}, \frac{x'}{\xi}\right) & \frac{1}{\xi} \Delta V^{qg}\left(\frac{x}{\xi}, \frac{x'}{\xi}\right) \\ \xi \Delta V^{gq}\left(\frac{x}{\xi}, \frac{x'}{\xi}\right) & \Delta V^{gg}\left(\frac{x}{\xi}, \frac{x'}{\xi}\right) \end{pmatrix} \begin{pmatrix} \tilde{F}^{(+)}(x',\xi,t) \\ \tilde{F}^g(x',\xi,t) \end{pmatrix} . \tag{D.14}$$

Now the evolution kernels are defined by

$$\Delta V_{NS}(x,y) = \Delta V^{qq}(x,y) = V^{qq}(x,y) , \tag{D.15}$$

$$\Delta V^{qg}(x,y) = -\frac{\alpha_s\, C_F}{4\pi}\, T_f N_f \left[\rho(x,y) \frac{2(1+x)}{(1+y)^2} - \{x \to -x, y \to -y\} \right] , \tag{D.16}$$

$$\Delta V^{gq}(x,y) = \frac{\alpha_s}{4\pi} 2C_F \left[\rho(x,y)\frac{(1+x)^2}{2(1+y)} - \{x \to -x, y \to -y\}\right], \tag{D.17}$$

$$\Delta V^{gg}(x,y) = \frac{\alpha_s}{4\pi}\left[C_A\left\{\left[\rho(x,y)\frac{(1+x)^2}{(1+y)^2}\left(2+\frac{2}{y-x}\right)\right]_+ + \{x \to -x, y \to -y\}\right\} + \delta\left(\frac{x-y}{2}\right)\left(\frac{\beta_0}{2} - \frac{7}{3}C_A\right)\right]. \tag{D.18}$$

For the polarized GPDs there is no check of the evolution kernels as the relation (D.10) but taking the limit $\xi \to 0$ as described in (D.9) one obtains again the well known DGLAP kernels for the polarized forward PDFs.

D.2 Evolution of the NLO vector meson amplitude

In this section we want to demonstrate how one can use the evolution equations to check the correctness of the scattering kernels. A nice additional feature is that within the following procedure one can distinguish between the factorization scale of the GPDs and the meson DA which was not done in the original calculation of the scattering kernel at NLO [99].

Before we can proceed we need in addition to the evolution equation of the GPDs, specified in the previous section, the evolution equation of the meson DA. It is governed by the ERBL equation which is given by

$$\mu^2 \frac{d}{d\mu^2}\phi(u,\mu) = \int_{-1}^{1} du'\, V_V(u,u')\phi(u',\mu)\,, \tag{D.19}$$

with the evolution kernel

$$V_V(u,u') = \frac{\alpha_s\, C_F}{4\pi}\left[\frac{1+u}{1+u'}\left(1+\frac{2}{u'-u}\right)\rho(u,u') + \{u \to -u, u' \to -u'\}\right]_+ . \tag{D.20}$$

In the above definition of the kernel we used the same definition of the '+'-prescription as in (D.7). We also want to mention that we changed the variable of the meson DA in the following way

$$z \to \frac{1+u}{2} \tag{D.21}$$

because now the variable has the same support region as the variable x of the GPDs.
To take now the derivative of the amplitude with respect to the factorization scale it is easier to go back to go the original definition of the amplitude given in [99]

$$\mathcal{M}_{\gamma_L^* N \to V_L N} = \frac{\pi\sqrt{4\pi\alpha} f_V}{N_c\, Q\, \xi}\int_{-1}^{1} du\, \phi_V(u) \int_{-1}^{1} dx \Big[\sum_q e_q^V T_q(u,x) F^{q(+)}(x,\xi,t) + Q_V\left(T_g(u,x)F^g(x,\xi,t) + T_{(+)}(u,x)F^{(+)}(x,\xi,t)\right)\Big]. \tag{D.22}$$

Taking now the derivative with respect to μ_F and keep only terms up to the order α_s^2 we obtain

$$\frac{d}{d\,\ln(\mu_F^2)} \equiv \frac{d}{dL}\mathcal{M} = \tag{D.23}$$

$$\frac{\pi\sqrt{4\pi\alpha}f_V}{N_c Q\xi}\int\limits_{-1}^{1}du\int\limits_{-1}^{1}dx\Bigg\{\underbrace{Q_V\,T_g^{(0)}(u,x)F^g(x,\xi)\int\limits_{-1}^{1}du' V_V(u,u')\phi_V(u')}_{\mathcal{A}}$$

$$+\sum_q e_q^V\underbrace{T_q^{(0)}(u,x)F^{q(+)}(x,\xi)\int\limits_{-1}^{1}du' V_V(u,u')\phi_V(u')}_{\mathcal{B}}+\underbrace{Q_V\,F^g(x,\xi)\phi_v(u)\frac{d}{dL}T_g^{(1)}(u,x)}_{\mathcal{C}}$$

$$+\underbrace{Q_V\,F^{(+)}(x,\xi)\phi_V(u)\frac{d}{dL}T^{(+)}(u,x)}_{\mathcal{D}}+\sum_q e_q^V\underbrace{F^{q(+)}(x,\xi)\phi_V(u)\frac{d}{dL}T_q^{(1)}(u,x)}_{\mathcal{E}}$$

$$\underbrace{+Q_V\,T_g^{(0)}(x,\xi,t)\phi_V(u)\int\limits_{-1}^{1}dx'\frac{1}{|\xi|}\left[\xi V^{gq}\left(\frac{x}{\xi},\frac{x'}{\xi}\right)F^{(+)}(x',\xi)+V^{gg}\left(\frac{x}{\xi},\frac{x'}{\xi}\right)F^g(x',\xi)\right]}_{\mathcal{F}}$$

$$\underbrace{+\sum_q e_q^V\,T_q^{(0)}(x,u)\phi_V(u)\int\limits_{-1}^{1}dx'\frac{1}{|\xi|}\left[V^{qq}\left(\frac{x}{\xi},\frac{x'}{\xi}\right)F^{q(+)}(x',\xi)+\frac{1}{N_f\xi}V^{qg}\left(\frac{x}{\xi},\frac{x'}{\xi}\right)F^g(x',\xi)\right]}_{\mathcal{G}}\Bigg\}$$

$$\stackrel{!}{=}0\,,$$

where $T_g^{(0)}(u,x)$ and $T_q^{(0)}(x,u)$ denote the pure LO gluon and quark scattering kernel and $T_g^{(1)}(u,x)$ and $T_q^{(1)}(u,x)$ the pure NLO gluon and quark scattering kernel which are given in (C.1) and (C.11). We have suppressed the t dependence of the GPDs for simplicity in the above equation. With the help of the above expression we can make the distinction of the two different types of factorization scales $\mu_{F(DA)}$ and $\mu_{F(GPD)}$. We do not want to repeat the complete calculation but only want to say in which terms of (D.23) the different contributions appear. It is clear that the responsible terms can only be found in the NLO parts of the gluon and quark scattering kernel because they are the only terms which depend on μ_F. The singlet scattering kernel $T^{(+)}(u,x)$ also depends on μ_F but if one looks carefully at the calculation it is clear that for that scattering kernel we cannot expect to be dependent on $\mu_{F(DA)}$ and $\mu_{F(GPD)}$ because a dependence on $\mu_{F(DA)}$ would be of order α_s^3 which we will not consider here. In order to find the $\mu_{F(DA)}$ dependence of the gluon and quark scattering kernel one has to evaluate the term $\mathcal{A}$ and $\mathcal{C}$ for the gluon and $\mathcal{B}$ and $\mathcal{E}$ for the quark scattering kernel. Summing up these terms we immediately find the terms which cancel each

other. These terms then correspond to the $\mu_{F(DA)}$ dependent parts of the scattering kernel, and some remaining terms corresponding to the $\mu_{F(FPD)}$ dependent parts of the scattering kernels.

Bibliography

[1] O. C. S. I. Estermann and O. Stern, "The magnetic moment of the proton," *Phys. Rev.* **52** (1937) 535 – 545.

[2] M. Gell-Mann, "A schematic model of baryons and mesons," *Phys. Lett.* **8** (1964) 214–215.

[3] G. Zweig, "An su(3) model for strong interaction symmetry and its breaking. 2,". CERN-TH-412.

[4] D. J. Gross and F. Wilczek, "Ultraviolet behavior of non-abelian gauge theories," *Phys. Rev. Lett.* **30** (1973) 1343–1346.

[5] H. D. Politzer, "Reliable perturbative results for strong interactions?," *Phys. Rev. Lett.* **30** (1973) 1346–1349.

[6] S. B. Libby and G. Sterman, "Jet and lepton pair production in high-energy lepton - hadron and hadron - hadron scattering," *Phys. Rev.* **D18** (1978) 3252.

[7] R. K. Ellis, H. Georgi, M. Machacek, H. D. Politzer, and G. G. Ross, "Perturbation theory and the parton model in qcd," *Nucl. Phys.* **B152** (1979) 285.

[8] R. K. Ellis, H. Georgi, M. Machacek, H. D. Politzer, and G. G. Ross, "Factorization and the parton model in qcd," *Phys. Lett.* **B78** (1978) 281.

[9] D. Amati, R. Petronzio, and G. Veneziano, "Relating hard qcd processes through universality of mass singularities," *Nucl. Phys.* **B140** (1978) 54.

[10] G. Curci, W. Furmanski, and R. Petronzio, "Evolution of parton densities beyond leading order: The nonsinglet case," *Nucl. Phys.* **B175** (1980) 27.

[11] J. C. Collins, D. E. Soper, and G. Sterman, "All order factorization for drell-yan cross-sections," *Phys. Lett.* **B134** (1984) 263.

[12] J. Pumplin *et al.*, "New generation of parton distributions with uncertainties from global qcd analysis," *JHEP* **07** (2002) 012, hep-ph/0201195.

[13] M. Gluck, E. Reya, and A. Vogt, "Dynamical parton distributions revisited," *Eur. Phys. J.* **C5** (1998) 461–470, hep-ph/9806404.

[14] **European Muon** Collaboration, J. Ashman *et al.*, "An investigation of the spin structure of the proton in deep inelastic scattering of polarized muons on polarized protons," *Nucl. Phys.* **B328** (1989) 1.

[15] J. C. Collins, L. Frankfurt, and M. Strikman, "Factorization for hard exclusive electroproduction of mesons in qcd," *Phys. Rev.* **D56** (1997) 2982–3006, hep-ph/9611433.

[16] J. C. Collins and A. Freund, "Proof of factorization for deeply virtual compton scattering in QCD," *Phys. Rev.* **D59** (1999) 074009, hep-ph/9801262.

[17] F. M. Dittes, D. Mueller, D. Robaschik, B. Geyer, and J. Horejsi, "The altarelli-parisi kernel as asymptotic limit of an extended brodsky-lepage kernel," *Phys. Lett.* **B209** (1988) 325–329.

[18] V. N. Gribov and L. N. Lipatov, "Deep inelastic e p scattering in perturbation theory," *Sov. J. Nucl. Phys.* **15** (1972) 438–450.

[19] A. P. Bukhvostov, L. N. Lipatov, and N. P. Popov, "Parton distribution functions in perturbation theory," *Yad. Fiz.* **20** (1974) 532–548.

[20] L. N. Lipatov, "The parton model and perturbation theory," *Sov. J. Nucl. Phys.* **20** (1975) 94–102.

[21] G. Altarelli and G. Parisi, "Asymptotic freedom in parton language," *Nucl. Phys.* **B126** (1977) 298.

[22] Y. L. Dokshitzer, "Calculation of the structure functions for deep inelastic scattering and e^+ e^- annihilation by perturbation theory in quantum chromodynamics. (in russian)," *Sov. Phys. JETP* **46** (1977) 641–653.

[23] A. V. Efremov and A. V. Radyushkin, "Factorization and asymptotical behavior of pion form-factor in qcd," *Phys. Lett.* **B94** (1980) 245–250.

[24] V. L. Chernyak, A. R. Zhitnitsky, and V. G. Serbo, "Asymptotic hadronic form-factors in quantum chromodynamics," *JETP Lett.* **26** (1977) 594–597.

[25] G. R. Farrar and D. R. Jackson, "The pion form-factor," *Phys. Rev. Lett.* **43** (1979) 246.

[26] G. P. Lepage and S. J. Brodsky, "Exclusive processes in perturbative quantum chromodynamics," *Phys. Rev.* **D22** (1980) 2157.

[27] D. Mueller, D. Robaschik, B. Geyer, F. M. Dittes, and J. Horejsi, "Wave functions, evolution equations and evolution kernels from light-ray operators of QCD," *Fortschr. Phys.* **42** (1994) 101, hep-ph/9812448.

[28] K. Watanabe, "Elastic scattering and hadron dynamics at short distances," *Prog. Theor. Phys.* **66** (1981) 1003.

[29] X.-D. Ji, "Gauge invariant decomposition of nucleon spin," *Phys. Rev. Lett.* **78** (1997) 610–613, hep-ph/9603249.

[30] A. V. Radyushkin, "Scaling limit of deeply virtual compton scattering," *Phys. Lett.* **B380** (1996) 417–425, hep-ph/9604317.

[31] X.-D. Ji, "Deeply-virtual compton scattering," *Phys. Rev.* **D55** (1997) 7114–7125, hep-ph/9609381.

[32] A. V. Radyushkin, "Asymmetric gluon distributions and hard diffractive electroproduction," *Phys. Lett.* **B385** (1996) 333–342, hep-ph/9605431.

[33] M. Burkardt, "Impact parameter dependent parton distributions and off- forward parton distributions for $\zeta \to 0$," *Phys. Rev.* **D62** (2000) 071503, hep-ph/0005108.

[34] M. Diehl, W. Kugler, A. Schafer, and C. Weiss, "Exclusive channels in semi-inclusive production of pions and kaons," *Phys. Rev.* **D72** (2005) 034034, hep-ph/0506171.

[35] X.-D. Ji, "Off-forward parton distributions," *J. Phys.* **G24** (1998) 1181–1205, hep-ph/9807358.

[36] A. V. Radyushkin, "Generalized parton distributions," hep-ph/0101225.

[37] K. Goeke, M. V. Polyakov, and M. Vanderhaeghen, "Hard exclusive reactions and the structure of hadrons," *Prog. Part. Nucl. Phys.* **47** (2001) 401–515, hep-ph/0106012.

[38] M. Diehl, "Generalized parton distributions," *Phys. Rept.* **388** (2003) 41–277, hep-ph/0307382.

[39] A. V. Belitsky and A. V. Radyushkin, "Unraveling hadron structure with generalized parton distributions," *Phys. Rept.* **418** (2005) 1–387, hep-ph/0504030.

[40] A. V. Radyushkin, "Nonforward parton distributions," *Phys. Rev.* **D56** (1997) 5524–5557, hep-ph/9704207.

[41] B. Melic, B. Nizic, and K. Passek, "Complete next-to-leading order perturbative QCD prediction for the pion form factor," *Phys. Rev.* **D60** (1999) 074004, hep-ph/9802204.

[42] M. Burkardt, "Impact parameter space interpretation for generalized parton distributions," *Int. J. Mod. Phys.* **A18** (2003) 173–208, hep-ph/0207047.

[43] M. Burkardt, "Impact parameter dependent parton distributions and transverse single spin asymmetries," *Phys. Rev.* **D66** (2002) 114005, hep-ph/0209179.

[44] L. V. Gribov, E. M. Levin, and M. G. Ryskin, "Semihard processes in qcd," *Phys. Rept.* **100** (1983) 1–150.

[45] A. D. Martin and M. G. Ryskin, "The effect of off-diagonal parton distributions in diffractive vector meson electroproduction," *Phys. Rev.* **D57** (1998) 6692–6700, hep-ph/9711371.

[46] A. V. Belitsky and D. Mueller, "Next-to-leading order evolution of twist-two conformal operators: The abelian case," *Nucl. Phys.* **B527** (1998) 207–234, hep-ph/9802411.

[47] A. V. Belitsky and D. Mueller, "Broken conformal invariance and spectrum of anomalous dimensions in QCD," *Nucl. Phys.* **B537** (1999) 397–442, hep-ph/9804379.

[48] A. V. Belitsky, D. Mueller, and A. Freund, "Reconstruction of non-forward evolution kernels," *Phys. Lett.* **B461** (1999) 270–279, hep-ph/9904477.

[49] A. V. Belitsky and D. Mueller, "Exclusive evolution kernels in two-loop order: Parity even sector," *Phys. Lett.* **B464** (1999) 249–256, hep-ph/9906409.

[50] A. V. Belitsky, A. Freund, and D. Mueller, "Evolution kernels of skewed parton distributions: Method and two-loop results," *Nucl. Phys.* **B574** (2000) 347–406, hep-ph/9912379.

[51] A. Manashov, M. Kirch, and A. Schafer, "Solving the leading order evolution equation for gpds," *Phys. Rev. Lett.* **95** (2005) 012002, hep-ph/0503109.

[52] M. Kirch, A. Manashov, and A. Schafer, "Evolution equation for generalized parton distributions," *Phys. Rev.* **D72** (2005) 114006, hep-ph/0509330.

[53] A. V. Vinnikov, "Code for prompt numerical computation of the leading order gpd evolution," hep-ph/0604248.

[54] A. Freund and M. McDermott, "A detailed next-to-leading order qcd analysis of deeply virtual compton scattering observables," *Eur. Phys. J.* **C23** (2002) 651–674, hep-ph/0111472.

[55] X.-D. Ji, W. Lu, J. Osborne, and X.-T. Song, "One-loop factorization of the nucleon g_2 structure function in the non-singlet case," *Phys. Rev.* **D62** (2000) 094016, hep-ph/0006121.

[56] A. Chodos, R. L. Jaffe, K. Johnson, C. B. Thorn, and V. F. Weisskopf, "A new extended model of hadrons," *Phys. Rev.* **D9** (1974) 3471–3495.

[57] S. Scopetta and V. Vento, "Generalized parton distributions in constituent quark models," *Eur. Phys. J.* **A16** (2003) 527–535, hep-ph/0201265.

[58] P. A. M. Guichon, L. Mosse, and M. Vanderhaeghen, "Pion production in deeply virtual compton scattering," *Phys. Rev.* **D68** (2003) 034018, hep-ph/0305231.

[59] L. Mankiewicz, G. Piller, and A. Radyushkin, "Hard exclusive electroproduction of pions," *Eur. Phys. J.* **C10** (1999) 307–312, hep-ph/9812467.

[60] M. Penttinen, M. V. Polyakov, and K. Goeke, "Helicity skewed quark distributions of the nucleon and chiral symmetry," *Phys. Rev.* **D62** (2000) 014024, hep-ph/9909489.

[61] V. Y. Petrov *et al.*, "Off-forward quark distributions of the nucleon in the large n_c limit," *Phys. Rev.* **D57** (1998) 4325–4333, hep-ph/9710270.

[62] M. Gockeler *et al.*, "Nucleon structure from generalized parton distributions in lattice qcd," *Nucl. Phys. Proc. Suppl.* **153** (2006) 146–153, hep-lat/0512011.

[63] R. G. Edwards *et al.*, "Nucleon structure in the chiral regime with domain wall fermions on an improved staggered sea," hep-lat/0610007.

[64] M. V. Polyakov and C. Weiss, "Skewed and double distributions in pion and nucleon," *Phys. Rev.* **D60** (1999) 114017, hep-ph/9902451.

[65] I. V. Musatov and A. V. Radyushkin, "Evolution and models for skewed parton distributions," *Phys. Rev.* **D61** (2000) 074027, hep-ph/9905376.

[66] L. Mankiewicz, G. Piller, and T. Weigl, "Hard leptoproduction of charged vector mesons," *Phys. Rev.* **D59** (1999) 017501, hep-ph/9712508.

[67] L. L. Frankfurt, P. V. Pobylitsa, M. V. Polyakov, and M. Strikman, "Hard exclusive pseudoscalar meson electroproduction and spin structure of a nucleon," *Phys. Rev.* **D60** (1999) 014010, hep-ph/9901429.

[68] **HERMES** Collaboration, A. Airapetian *et al.*, "Quark helicity distributions in the nucleon for up, down, and strange quarks from semi-inclusive deep-inelastic scattering," *Phys. Rev.* **D71** (2005) 012003, hep-ex/0407032.

[69] **HERMES** Collaboration, A. Airapetian *et al.*, "Single-spin asymmetries in semi-inclusive deep-inelastic scattering on a transversely polarized hydrogen target," *Phys. Rev. Lett.* **94** (2005) 012002, hep-ex/0408013.

[70] A. Szczurek, V. Uleshchenko, and J. Speth, "anti-d anti-u asymmetry and semi-inclusive production of pions in dis," *Phys. Rev.* **D63** (2001) 114005, hep-ph/0009318.

[71] V. Uleshchenko and A. Szczurek, "Nonpartonic effects in pion electroproduction in the hermes kinematical region," *Acta Phys. Polon.* **B33** (2002) 3299–3304, hep-ph/0207049.

[72] **HERMES** Collaboration, A. Airapetian *et al.*, "Exclusive leptoproduction of ρ^0 mesons from hydrogen at intermediate virtual photon energies," *Eur. Phys. J.* **C17** (2000) 389–398, hep-ex/0004023.

[73] **HERMES** Collaboration, A. B. Borissov *Nucl. Phys. Proc. Suppl.* **A99** (2001) 156.

[74] **HERMES** Collaboration, A. B. Borissov *Procs. of the 9th International Workshop on High-Energy Spin Physics (SPIN01), Dubna, Russia, Aug. 2001, DESY-HERMES-01-60.*

[75] M. Tytgat, "Doctoral thesis, univeristeit gent, 2000,".

[76] G. L. Ragness, "Doctoral thesis, doctoral thesis, univerity of coloradi at boulder, 2000,".

[77] **CLAS** Collaboration, C. Hadjidakis *et al.*, "Exclusive ρ^0 meson electroproduction from hydrogen at clas," *Phys. Lett.* **B605** (2005) 256–264, hep-ex/0408005.

[78] L. N. Hand, "Experimental investigation of pion electroproduction," *Phys. Rev.* **129** (1963) 1834–1846.

[79] M. Diehl, B. Pire, and L. Szymanowski, "Probing the partonic structure of pentaquarks in hard electroproduction," *Phys. Lett.* **B584** (2004) 58–70, hep-ph/0312125.

[80] M. Beneke and M. Neubert, "Qcd factorization for $b \to p\,p$ and $b \to p\,v$ decays," *Nucl. Phys.* **B675** (2003) 333–415, hep-ph/0308039.

[81] I. V. Anikin, B. Pire, L. Szymanowski, O. V. Teryaev, and S. Wallon, "On blm scale fixing in exclusive processes," *Eur. Phys. J.* **C42** (2005) 163–168, hep-ph/0411408.

[82] M. Diehl, T. Feldmann, R. Jakob, and P. Kroll, "Generalized parton distributions from nucleon form factor data," *Eur. Phys. J.* **C39** (2005) 1–39, hep-ph/0408173.

[83] L. Frankfurt, M. Strikman, and C. Weiss, "Dijet production as a centrality trigger for p p collisions at lhc," *Phys. Rev.* **D69** (2004) 114010, hep-ph/0311231.

[84] **LHPC** Collaboration, LHPC *et al.*, "Transverse structure of nucleon parton distributions from lattice qcd," *Phys. Rev. Lett.* **93** (2004) 112001, hep-lat/0312014.

[85] **H1** Collaboration, C. Adloff *et al.*, "Elastic electroproduction of rho mesons at hera," *Eur. Phys. J.* **C13** (2000) 371–396, hep-ex/9902019.

[86] M. Diehl and A. V. Vinnikov, "Quarks vs. gluons in exclusive rho electroproduction," *Phys. Lett.* **B609** (2005) 286–290, hep-ph/0412162.

[87] L. L. Frankfurt, M. V. Polyakov, M. Strikman, and M. Vanderhaeghen, "Hard exclusive electroproduction of decuplet baryons in the large n(c) limit," *Phys. Rev. Lett.* **84** (2000) 2589–2592, hep-ph/9911381.

[88] W. Koepf, L. L. Frankfurt, and M. Strikman, "The nucleon's virtual meson cloud and deep inelastic lepton scattering," *Phys. Rev.* **D53** (1996) 2586–2598, hep-ph/9507218.

[89] M. Diehl, P. Kroll, and C. Vogt, "The annihilation of virtual photons into pseudoscalar mesons," *Eur. Phys. J.* **C22** (2001) 439–450, hep-ph/0108220.

[90] A. P. Bakulev, S. V. Mikhailov, and N. G. Stefanis, "Cleo and e791 data: A smoking gun for the pion distribution amplitude?," *Phys. Lett.* **B578** (2004) 91–98, hep-ph/0303039.

[91] A. Khodjamirian, T. Mannel, and M. Melcher, "Kaon distribution amplitude from qcd sum rules," *Phys. Rev.* **D70** (2004) 094002, hep-ph/0407226.

[92] V. M. Braun and A. Lenz, "On the su(3) symmetry-breaking corrections to meson distribution amplitudes," *Phys. Rev.* **D70** (2004) 074020, hep-ph/0407282.

[93] E. Leader, A. V. Sidorov, and D. B. Stamenov, "Polarized parton densities in the nucleon," *Phys. Rev.* **D58** (1998) 114028, hep-ph/9807251.

[94] J. Blumlein and H. Bottcher, "Qcd analysis of polarized deep inelastic scattering data and parton distributions," *Nucl. Phys.* **B636** (2002) 225–263, hep-ph/0203155.

[95] T. Feldmann, "Quark structure of pseudoscalar mesons," *Int. J. Mod. Phys.* **A15** (2000) 159–207, hep-ph/9907491.

[96] A. D. Martin, R. G. Roberts, W. J. Stirling, and R. S. Thorne, "Nnlo global parton analysis," *Phys. Lett.* **B531** (2002) 216–224, hep-ph/0201127.

[97] A. D. Martin, R. G. Roberts, W. J. Stirling, and R. S. Thorne, "Uncertainties of predictions from parton distributions. i: Experimental errors. ((t))," *Eur. Phys. J.* **C28** (2003) 455–473, hep-ph/0211080.

[98] S. Alekhin, "Parton distributions from deep-inelastic scattering data," *Phys. Rev.* **D68** (2003) 014002, hep-ph/0211096.

[99] D. Y. Ivanov, L. Szymanowski, and G. Krasnikov, "Vector meson electroproduction at next-to-leading order," *JETP Lett.* **80** (2004) 226–230, hep-ph/0407207.

[100] L. Frankfurt, W. Koepf, and M. Strikman, "Hard diffractive electroproduction of vector mesons in qcd," *Phys. Rev.* **D54** (1996) 3194–3215, hep-ph/9509311.

[101] B. Lehmann-Dronke, P. V. Pobylitsa, M. V. Polyakov, A. Schafer, and K. Goeke, "Hard diffractive electroproduction of two pions," *Phys. Lett.* **B475** (2000) 147–156, hep-ph/9910310.

[102] N. Kivel, M. V. Polyakov, and M. Vanderhaeghen, "Dvcs on the nucleon: Study of the twist-3 effects," *Phys. Rev.* **D63** (2001) 114014, hep-ph/0012136.

[103] P. Schweitzer, S. Boffi, and M. Radici, "Polynomiality of off-forward distribution functions in the chiral quark soliton model," *Phys. Rev.* **D66** (2002) 114004, hep-ph/0207230.

[104] M. Vanderhaeghen, P. A. M. Guichon, and M. Guidal, "Deeply virtual electroproduction of photons and mesons on the nucleon: Leading order amplitudes and power corrections," *Phys. Rev.* **D60** (1999) 094017, hep-ph/9905372.

[105] S. V. Goloskokov and P. Kroll, "Vector meson electroproduction at small bjorken-x and generalized parton distributions," *Eur. Phys. J.* **C42** (2005) 281–301, hep-ph/0501242.

[106] A. B. Borissov, "private communications,".

[107] **CLAS** Collaboration, K. Lukashin *et al.*, "Exclusive electroproduction of phi mesons at 4.2-gev," *Phys. Rev.* **C63** (2001) 065205, hep-ex/0101030.

[108] **CLAS** Collaboration, L. Morand *et al.*, "Deeply virtual and exclusive electroproduction of omega mesons," *Eur. Phys. J.* **A24** (2005) 445–458, hep-ex/0504057.

[109] **The Jefferson Lab F(pi)** Collaboration, J. Volmer *et al.*, "New results for the charged pion electromagnetic form- factor," *Phys. Rev. Lett.* **86** (2001) 1713–1716, nucl-ex/0010009.

[110] C. J. Bebek *et al.*, "Electroproduction of single pions at low epsilon and a measurement of the pion form-factor up to $q^2 = 10\,\mathrm{GeV}^2$," *Phys. Rev.* **D17** (1978) 1693.

[111] R. Jakob, P. Kroll, and M. Raulfs, "Meson - photon transition form-factors," *J. Phys.* **G22** (1996) 45–58, hep-ph/9410304.

[112] **HERMES** Collaboration, C. Hadjidakis, D. Hasch, and E. Thomas, "Exclusive π^+ production at hermes," *Int. J. Mod. Phys.* **A20** (2005) 593–595, hep-ex/0405078.

[113] C. Hadjidakis, "private communications,".

[114] S. Kretzer, "Fragmentation functions from flavour-inclusive and flavour- tagged e^+ e^- annihilations," *Phys. Rev.* **D62** (2000) 054001, hep-ph/0003177.

[115] **HERMES** Collaboration, B. Maiheu, "The fragmentation process at hermes," *AIP Conf. Proc.* **792** (2005) 776–779.

[116] S. V. Goloskokov and P. Kroll, "The longitudinal cross section of vector meson electroproduction," hep-ph/0611290.

[117] A. V. Belitsky, D. Mueller, L. Niedermeier, and A. Schafer, "Deeply virtual compton scattering in next-to-leading order," *Phys. Lett.* **B474** (2000) 163–169, hep-ph/9908337.

[118] A. Freund and M. F. McDermott, "A next-to-leading order qcd analysis of deeply virtual compton scattering amplitudes," *Phys. Rev.* **D65** (2002) 074008, hep-ph/0106319.

[119] D. Mueller, "Next-to-next-to leading order corrections to deeply virtual compton scattering: The non-singlet case," *Phys. Lett.* **B634** (2006) 227–234, hep-ph/0510109.

[120] K. Kumericki, D. Mueller, K. Passek-Kumericki, and A. Schafer, "Deeply virtual compton scattering beyond next-to-leading order: The flavor singlet case," hep-ph/0605237.

[121] A. V. Belitsky and D. Mueller, "Hard exclusive meson production at next-to-leading order," *Phys. Lett.* **B513** (2001) 349–360, hep-ph/0105046.

[122] D. Y. Ivanov, A. Schafer, L. Szymanowski, and G. Krasnikov, "Exclusive photoproduction of a heavy vector meson in qcd," *Eur. Phys. J.* **C34** (2004) 297–316, hep-ph/0401131.

[123] **H1** Collaboration, A. Kreisel, "Exclusive vector meson production at hera," hep-ex/0208013.

[124] J. A. Crittenden, "Exclusive production of neutral vector mesons at the electron proton collider hera," hep-ex/9704009.

[125] **ZEUS** Collaboration, S. Chekanov *et al.*, "Exclusive photoproduction of j/ψ mesons at hera," *Eur. Phys. J.* **C24** (2002) 345–360, hep-ex/0201043.

[126] **H1** Collaboration, A. Aktas *et al.*, "Elastic j/ψ production at hera," *Eur. Phys. J.* **C46** (2006) 585–603, hep-ex/0510016.

[127] S. J. Brodsky, G. P. Lepage, and P. B. Mackenzie, "On the elimination of scale ambiguities in perturbative quantum chromodynamics," *Phys. Rev.* **D28** (1983) 228.

[128] A. Freund and M. F. McDermott, "Next-to-leading order evolution of generalized parton distributions for hera and hermes," *Phys. Rev.* **D65** (2002) 056012, hep-ph/0106115.

[129] V. M. Braun *et al.*, "Moments of pseudoscalar meson distribution amplitudes from the lattice," *Phys. Rev.* **D74** (2006) 074501, hep-lat/0606012.

[130] A. P. Bakulev, S. V. Mikhailov, and N. G. Stefanis, "Tagging the pion quark structure in qcd," *Phys. Rev.* **D73** (2006) 056002, hep-ph/0512119.

[131] "Zeus collaboration, paper 594 submitted to the international europhysics conference on high energy physics (eps 2001), july 2001, budapest, hungary, available from http://www-zeus.desy.de,".

[132] **ZEUS** Collaboration, J. Breitweg *et al.*, "Exclusive electroproduction of ρ^0 and j/ψ mesons at hera," *Eur. Phys. J.* **C6** (1999) 603–627, hep-ex/9808020.

[133] K. Schilling and G. Wolf, "How to analyze vector meson production in inelastic lepton scattering," *Nucl. Phys.* **B61** (1973) 381–413.

[134] A. Devoto and D. W. Duke, "Table of integrals and formulae for feynman diagram calculations," *Riv. Nuovo Cim.* **7N6** (1984) 1–39.

[135] D. Diakonov, V. Y. Petrov, and P. V. Pobylitsa, "A chiral theory of nucleons," *Nucl. Phys.* **B306** (1988) 809.

[136] A. D. Martin, R. G. Roberts, W. J. Stirling, and R. S. Thorne, "Physical gluons and high-e(t) jets," *Phys. Lett.* **B604** (2004) 61–68, hep-ph/0410230.

[137] L. Frankfurt, W. Koepf, and M. Strikman, "Diffractive heavy quarkonium photo- and electroproduction in qcd," *Phys. Rev.* **D57** (1998) 512–526, hep-ph/9702216.

[138] V. M. Braun, A. Khodjamirian, and M. Maul, "Pion form factor in qcd at intermediate momentum transfers," *Phys. Rev.* **D61** (2000) 073004, hep-ph/9907495.

[139] A. P. Bakulev, A. V. Radyushkin, and N. G. Stefanis, "Form factors and qcd in spacelike and timelike regions," *Phys. Rev.* **D62** (2000) 113001, hep-ph/0005085.

[140] N. G. Stefanis, W. Schroers, and H.-C. Kim, "Analytic coupling and sudakov effects in exclusive processes: Pion and $\gamma^*\gamma \to \pi^0$ form factors," *Eur. Phys. J.* **C18** (2000) 137–156, hep-ph/0005218.

Acknowledgments

At this point I want to thank all the people who made this work possible. First of all I want to thank my advisor Prof. Dr. Andreas Schäfer who gave me the possibility to work in this very interesting field, for his interest in my work and his support in many respects. Especially I am grateful to him for giving me the chance to do part of the work in the theory group of DESY Hamburg, where I found a very stimulating and friendly atmosphere.

Special thanks goes to Dr. Markus Diehl from the DESY theory group for taking over part of my advise in Hamburg. I am very grateful for his enormous effort in answering my uncountable questions and his never-ending support through very interesting discussions and ideas for this work.

I also want to thank Dr. Christian Weiss and Dr. Dmitri Ivanov for very fruitful and interesting discussions during different stages of this work. For very illuminating discussion about the experimental side of the covered field I want to thank Elke-Caroline Aschenauer and Alexander Borissov from the HERMES group. I also want to thank Dr. Alessandro Bacchetta for his interest in my work and his useful suggestions when finishing this work.

I also want to thank my colleagues Daniela Amrath, Birgit Eberele and Alexander Westphal for the cheerful atmosphere in our office and the rest of the DESY theory group for the open, friendly and encouraging period at DESY.

Personally I want to thank my parents, they provided an admirable support during my studies and the period of my PhD thesis.

Finally I want to thank Birgit for her never-ending understanding and for her courage to move with me into a “foreign” land.